A comparative study of the antioxidant properties of chalcone derivatives through the Fe chelation mechanism

Kemoabetswe Rakgadi Nototi Serobatse

BSc Hons in Chemistry (North-West University)
BSc in Chemistry (North-West University)

Student number 23301570

Dissertation submitted in fulfilment of the requirements for the degree Master of Science in Chemistry at the Mafikeng Campus of the North-West University.

Supervisor: Dr. Kabanda Mwombeki Mwadham
Department of Chemistry, North-West University (Mafikeng Campus), South Africa

NORTH-WEST UNIVERSITY
YUNIBESITI YA BOKONE-BOPHIRIMA
NOORDWES-UNIVERSITEIT

September 2016

DECLARATION

I, Kemoabetswe Rakgadi Nototi Serobatse, hereby declare that this dissertation is a presentation of my original research work for the degree MSc Chemistry, and has not been submitted to this institution or any other South African institution of higher learning. Every contribution of others involved in this dissertation has been acknowledged. All sources used have been referenced. The work was done under the supervision of Dr. M. M. Kabanda of the Chemistry Department at the North-West University, Mafikeng Campus.

Signature: ..... Date: .....

Student Number: 23301570

Signature…….. Date……

Supervisor : Dr. Mwadham M Kabanda

ABSTRACT

This dissertation reports the results of a theoretical investigation on the conformational and antioxidant properties of four chalcone derivatives, namely butein, homobutein, kanakugiol and pedicellin, through their Fe coordination ability. Chalcone derivatives have been reported to possess various biological activities such as anticancer, antimalarial and antioxidant. The antioxidant activities of chalcone derivatives have been investigated extensively from an experimental approach and from a theoretical approach using the hydrogen atom and electron transfer mechanism. However, there is scarce information on the metal chelation ability of these compounds as pertaining to their antioxidant properties; therefore, the study reported here investigated the Fe^{n+} chelation ability of four chalcone derivatives. The selection of the Fe^{n+} cations is based on the fact that they have been utilised extensively in the experimental investigation of antioxidant activity of biologically active molecules. The conformers of the isolated chalcone derivatives were investigated with the aim of understanding factors influencing their stability and as starting point for obtaining the lowest-energy conformer(s) that can be utilised in the study involving the Fe^{n+} cations. The ligand···Fe^{n+} complexes were investigated with the objective of elucidating the nature of the complexes, Fe···ligand stabilities, metal ion affinities and electronic properties of the cations before and after complexation. The study was performed *in vacuo* and in water solution by utilising the DFT/B3LYP and DFT/BP86 methods. The 6-31+G(d,p) basis set was utilised to describe the C, H, O atoms and the LANL2DZ basis set was selected to describe the Fe^{n+} cations. Final energies were obtained by running single point calculations on the optimised geometries using the 6-311+G(2d,p) basis set.

The results suggest that conformational stability of the selected chalcone derivatives is influenced by the presence of intramolecular hydrogen bonds, arrangement of the 2-propen-1-one aliphatic chain and in the cases of homobutein, kanakugiol and pedicellin, the orientation of the methoxy groups. The stability of the ligand···Fe^{n+} complexes is influenced by the media (the relative energy values in water are dampened relative to those obtained *in vacuo*), the nature of the Fe^{n+} cation and the nature of the ligand···Fe^{n+} interactions; the binding energies depend on the media (they are higher *in vacuo* than in water solution), the site for coordination of the Fe^{n+} cation as well as the nature of the cation. The reducing ability of the chalcone derivatives were assessed by the reduction of charge on the Fe^{n+} cation after complexation. All the selected chalcone derivatives exhibited the ability to reduce the Fe^{n+} cation, which indicates that all the investigated chalcone derivatives may play an important role as antioxidant molecules.

Keywords: Antioxidant, DFT, chalcone derivatives, metal ion affinity, AIM analysis

PUBLICATIONS

The results of this work have been published or accepted for publication in the following journal articles:

1. **Kemoabetswe R. N. Serobatse**, Mwadham M. Kabanda. A theoretical study on the antioxidant properties of methoxy-substituted chalcone derivatives: a case study of kanakugiol and pedicellin through their Fe (II and III) coordination ability. *Journal of Theoretical and Computational Chemistry;* doi: 10.1142/S0219633616500486.
2. **Kemoabetswe R. N. Serobatse**, Mwadham M. Kabanda. Antioxidant and antimalarial properties of butein and homobutein based on their ability to chelate iron (II and III) cations: A DFT study in vacuo and in solution. *European Food Research and Technology*, 242 (**2016**) 71–90.

The following publication is also closely related to the work presented in this dissertation.

1. Tshepiso J. Tsiepe, Mwadham M. Kabanda, **Kemoabetswe R. N. Serobatse**. Antioxidant properties of kanakugiol revealed through the hydrogen atom transfer, electron transfer and M^{2+} (M^{2+} = Cu(II) or Co(II) ion) coordination ability mechanisms. A DFT study *in vacuo* and in solution. *Food biophysics*, 10 (**2015**) 342–359.

ACKNOWLEDGMENTS

First and foremost I would like to thank my heavenly Father, God Almighty for the strength, wisdom and patience he has granted me throughout the duration of this project. If it was not of the Lord who was on my side I would not have made it this far.

My sincere and heartfelt gratitude goes to my supervisor Dr. M. M Kabanda of the Department of Chemistry, North-West University, Mafikeng Campus, who has not only been a good supervisor but a great mentor. I would like to thank him for his continuous support and constructive criticism, his advice and correction has contributed greatly in making my research project a success. Thank you for pushing me beyond my limits and for your guidance and advice throughout this project.

I would also like to express my gratitude to my sponsors the NWU Mafikeng Campus, Sasol Inzalo Foundation and the South African National Research Foundation (NRF), (Grant UID 95578), for their financial assistance. Opinions expressed and conclusions arrived at are those of the author and are not necessarily to be attributed to the NRF or Sasol Inzalo Foundation.

I would like to thank the contribution made by the Department of Chemistry of the North-West University (Mafikeng Campus) for providing computational facilities. I would also wish to express my gratitude to Prof Eno Ebenso and Mr Francis Lugayizi of the North-West University (Mafikeng Campus) for providing extra computational facilitates that has made the completion of this work possible.

To everyone whom I have not mentioned by name but have contributed in some way or the other to the success of this project, thank you. To all my friends and family for your support and your prayers, I am very grateful.

LIST OF ABBREVIATIONS

ACF	Adiabatic connection formula
AIP	Adiabatic ionization potential
AIM	Atoms in molecules
AM1	Austin model 1
B3LYP	Becke three parameter Lee-Yang-Parr
BCP	Bond critical point
BDE	Bond dissociation enthalpy
BP86	Perdew 86 (P86)
CAM	Coulomb attenuated method
CDS	Cavity-dispersion solvent
CNDO	Complete neglect of differential overlap approximation
CP	Critical point
CCP	Cage critical point
DDOA	Diatomic differential overlap approximation
DFT	Density functional theory
ECP	Effective core potential
ET	Electron transfer
ETE	Electron transfer enthalpy
GGA	Generalized gradient approximations
GTO	Gaussian type orbital
HAT	Hydrogen atom transfer
HF	Hartree–Fock
IEF	Integral equation formalism
INDO	Intermediate neglect of differential overlap approximation
LCAO	Linear combination of atomic orbitals
LDA	Local density approximations
LSDA	Local spin density approximation
MIA	Metal ion affinity
MINDO	Modified intermediate neglect of differential overlap
MP	Møller–Plesset
NBO	Natural bond order
NDDO	Neglect of diatomic differential overlap approximation
NPA	Natural population analysis

NCP	Nuclear critical point
PBE	Perdew, Burke and Ernzerhof
PDE	Proton dissociation enthalpy
PM3	Parametric method version 3
RCP	Ring critical point
RHF	Restricted Hartree-Fock
RNA	Ribonucleic acid
RNS	Reactive nitrogen species
ROS	Reactive oxygen species
SCF	Self-consistent field
SCRF	Self consistent reaction field
SET	Single electron transfer
SET-PT	Single electron transfer followed by proton transfer
SMD	Solvation model density
SPLET	Sequential proton loss electron transfer
STO	Slater type orbital
UHF	Unrestricted Hartree-Fock
UV	Ultraviolet
VDW	Van der Waals
ZINDO	Zerner intermediate neglect of differential overlap

LIST OF FIGURES

LIST OF TABLES

TABLE OF CONTENT

CHAPTER 1

INTRODUCTION

1.1. Significance of the study of molecules with antioxidant activity

Antioxidants are substances that are able to either scavenge excess reactive species (e.g., reactive oxygen species (ROS) and reactive nitrogen species (RNS)) or chelate excess free (i.e., non-protein bound) transition metal ions present in biological systems, thereby preventing damage to biological components. Examples of ROS include the superoxide, hydrogen peroxide and hydroxyl radicals; examples of reactive nitrogen species include hormone nitric oxide and peroxinitrite [1]. ROS and RNS may be present in the atmosphere as pollutants; they can be generated during exposure to radiation (e.g., UV light, X-rays and gamma rays), metal-catalysed reactions and mitochondria-catalysed electron transport reactions [2]. When reactive species are produced in excess in the biological systems such that the cell's antioxidant defence system cannot regulate their production, the excess reactive species may oxidise all types of cellular components (e.g., deoxyribose nucleic acid, RNA and mitochondria), which in turn may lead to the onset of various diseases such as degenerative diseases (e.g., Parkinson's disease, Alzheimer and aging), cancer, cardiovascular, and diabetes [3]. When the body's antioxidant defence is not able to regulate the production of excess reactive species, it becomes important to supplement the body with antioxidant molecules from natural sources (e.g., plant material, fruits and vegetables) or those that are synthetically produced [4,5]. Synthetically produced antioxidants are often preferred in the food and pharmaceutical industries, however, they have several side effects, including toxicity towards the body cells; as a consequence, there is currently a strong trend to search for easily available, and efficient antioxidants from natural sources to replace the synthetic ones, thus minimising damage to our body cells [6–8]. The study presented in this dissertation focuses on the investigation of the antioxidant properties of chalcone molecules derived from plant sources.

Antioxidants are known to exert their effect through several mechanisms, including free radical scavenging, lipid peroxidation inhibition, stimulation of the natural protective mechanisms and the metal chelation [9]. The most investigated mechanism is the ability of antioxidants to scavenge free radical species either through the hydrogen transfer or the single electron transfer

mechanism [10–15]. This study aims to investigate the ability of antioxidants to chelate transition metal ions. The metal chelation has been selected for this study because of the scarcity of information from theoretical perspective on this type of antioxidant mechanism [16–18]; the study aims to provide theoretical data on the antioxidant properties of the selected chalcone derivatives that might enhance the understanding of the metal chelation mechanism in general and specifically for the chalcone derivatives.

The objectives of the overall work are to

- investigate the conformational preference of each of the chalcone derivative (isolated ligand),
- determine the stability of the metal···ligand complexes,
- determine the metal ion affinities to the selected ligand molecules (i.e., butein, homobutein, kanakugiol and pedicellin),
- determine the geometric and electronic properties (e.g., partial atomic charges and spin density) on the metal ions in the isolated and in the complexed state,
- investigate the simultaneous interaction of the metal ions with the C=C double bond in the 2-propen-1-one aliphatic chain and the neighbouring methoxy group,
- investigate the preferred aromatic ring for interaction with the metal ion.

1.2. Chalcone derivatives and their role as antioxidants

Chalcone (Figure 1.1) is a moiety made up of two benzene rings joined by a 2-propen-1-one aliphatic chain [19, 20]. The aromatic ring closest to the *keto* group is conventionally referred to as A and the aromatic ring closest to the C=C group is conventionally referred to as B [21]. Multitudes of functional groups are often appended on either of the aromatic rings giving rise to chalcone derivatives; for instance, polyphenol chalcone derivatives are derived from appending the chalcone moiety with multiple OH functional groups and methoxy-substituted chalcone derivatives are obtained when the phenolic H atom on the polyphenol chalcone derivatives is substituted by the methyl group. Polyphenol and methoxy-substituted chalcone derivatives are derived from various natural sources such as plant materials, fruits and vegetables [22–24]; they have been shown to exhibit a number of useful biological activities including antibacterial [25, 26], antimalarial [27], antifungal [28], antioxidant [29, 30], anti-viral [31], anti-cancer [24, 32] and anti-diabetic [33].

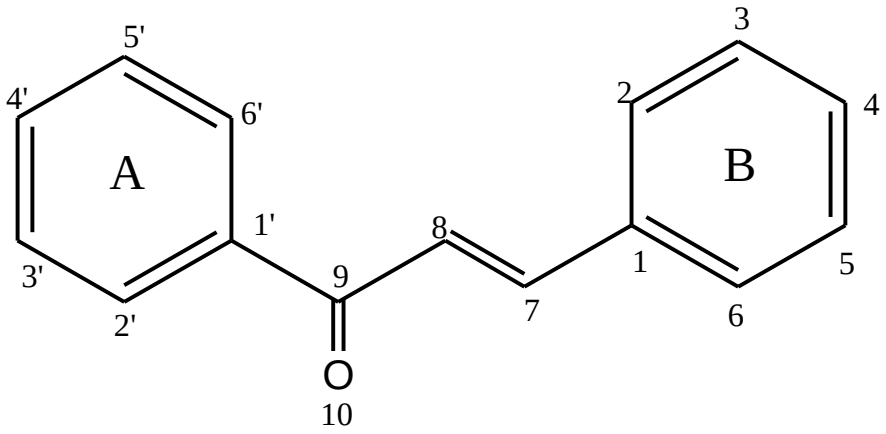

Figure 1.1 A schematic representation of a chalcone moiety together with atom numbering.

The antioxidant property of polyphenol chalcone derivatives is related to the number of the phenolic hydroxyl groups present in a given antioxidant molecule [34], the type of substituent present on the aromatic rings (i.e., hydroxyl or methoxy group[21]) the presence of the 2-propen-1-one chain [35] and the presence of the *keto* group [36]. For instance, studies have shown that the higher the number of phenolic OH groups, the higher is the expected antioxidant activity [37]. Several experimental studies have also confirmed the antioxidant activity of methoxy-substituted chalcone derivatives [36, 38–40]. For instance, the antioxidant activity of curcumin is related to the presence of the phenolic and methoxy groups on the phenyl ring as well as the presence of the 1,3-diketone system [36]; 2,4,5-trimethoxy chalcones and analogues from asaronaldehyde were found to possess greater nitric oxide scavenging activity than standard antioxidants such as ascorbic acid and α-tocopherol [38]. An experimental finding established that among the compounds with multiple *o*-methoxy substituents, for which the antioxidant activity is weaker than in the case of compounds with high number of phenolic OH substituents, the metal chelation mechanism is the preferred mode for controlling oxidative stress [41]. The current study focuses on four selected chalcone derivatives possessing only phenolic OH substituents, only methoxy substituent or a combination of both phenolic OH and methoxy substituents, with the objective of comparing their antioxidant properties.

1.3. Chalcone derivatives selected for the study

The four chalcone derivatives selected for the study (Figure 1.2) are butein (2′,4′,3,4-tetrahyroxychalcone), homobutein (3-methoxy-2′,4′,4-trihyroxychalcone), kanakugiol (2′-hydroxy-3′,4′,5′,6′-tetramethoxychalcone) and pedicellin (2′,3′, 4′, 5′, 6′-pentamethoxychalcone). These compounds have been isolated from plant materials; for instance, butein is isolated from *Dalbergia odorifera* [42] and *Butea frondosa* [43]; homobutein is isolated from *Erythrina abyssinica* [44], *Trifolium fruticosa* [45], and *Iryanthera polyneura* [46], kanakugiol is isolated from *Lindera Erythrocarpa* Makino plant [47], *Lindera Lucida* [48] and *Fissistigma polyanthum* plant species [32] and pedicellin is isolated from *Didymocarpus Pedicellatus* [49–51].

Butein and homobutein are structurally similar with the difference being in ring B; in ring A, both compounds have hydroxyl (OH) substituents at the *para* and *ortho* positions; in ring B, butein possess the phenolic OH group at the *meta* position while homobutein possess the methoxy group at the *meta* position. Kanakugiol and pedicellin can also be considered to be structurally similar with a difference at the C2′ substitution; in kanakugiol, the C2′ position is substituted with the phenolic OH group while for pedicellin the C2′ position is substituted with the methoxy group. The major reason for selecting kanakugiol and pedicellin for the study is to obtain information on the antioxidant properties of compounds with neighbouring methoxy groups (i.e., methoxy–methoxy reactive sites) in the aromatic rings and compounds in which the metal ion may interact simultaneously with the *keto* group and the neighbouring methoxy group (methoxy–*keto* reactive site). Furthermore, the outcome of this study is expected to form a basic foundation for understanding the antioxidant activity of other chalcone derivatives in which the methyl of the methoxy groups may be substituted by a much larger group such as a glycone, which would be computationally expensive to investigate. Therefore both kanakugiol and pedicellin may serve as model structures for elucidating the antioxidant properties of chalcone glycosides [52–54].

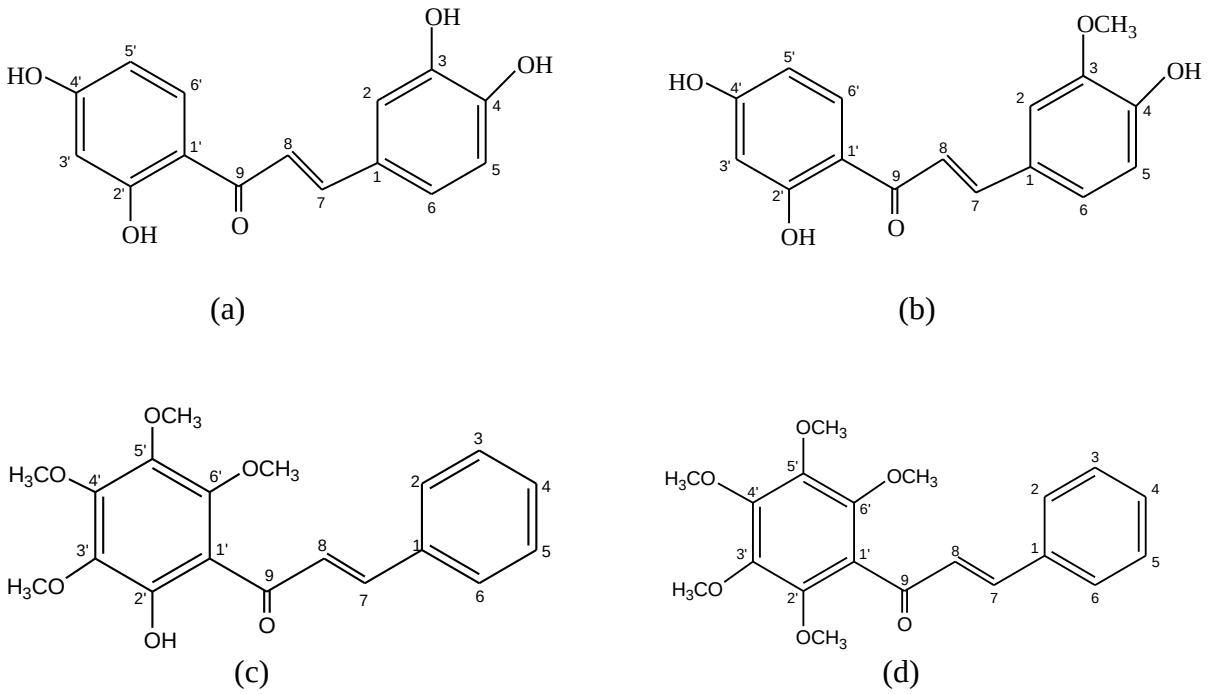

Figure 1.2 A schematic representation, together with atom numbering, of a) butein, b) homobutein, c) kanakugiol and (d) pedicellin. The atom attached directly to the ring is numbered with the same number as the C atom to which it is attached on the ring. The atom directly attached to the O atom linked to the ring is numbered with the same number of the O atom but with the double prime symbol (″) next to the number.

Butein has 7 rotatable single bonds; they include two O–H bonds present in ring A, two O–H bonds present in ring B and three C−C bonds in the 2-propen-1-one chain, homobutein has 7 rotatable single bonds; they include two O–H bonds present in ring A, one O–H bond and one C–O bond present in ring B and three C−C bonds in the 2-propen-1-one chain, kanakugiol has 8 rotatable single bonds; which include five C−O bonds present in ring A and three of which are the C−C bonds in the 2-propen-1-one chain and pedicellin similarly has 8 rotatable single bonds; five C−O bonds present in ring A and three C−C bonds in the 2-propen-1-one chain. The presence of the 2-propen-1-one aliphatic chain in chalcone derivatives suggests that the compounds can exist as *E* and *Z* geometric isomers. The *E* configuration of chalcone derivatives is considered to be the most thermodynamically as well as biologically favourable form [21]. More importantly, the isolated compounds of butein, homobutein [23], kanakugiol and pedicellin are reported to be of the *E* form [32, 51]. For this reason, the study reported here focuses only on the *E* geometric isomer of these compounds.

1.4. Metal ions selected for the investigation

The Fe^{2+} and Fe^{3+} cations have been selected for the investigation mainly because studies have shown that an increase in the concentration of free (non-protein-bound) iron is associated with oxidative stress in humans [55]. Excess free Fe (II and III) cations are also implicated in degenerative diseases (such as Alzheimer's and Parkinson's diseases) and cancer [56]. Several experimental studies have shown the ability of polyphenol derivatives to chelate intracellular non-protein bound iron [34, 37, 56, 57]. It is therefore important from a theoretical perspective to investigate the polyphenol binding ability of Fe^{n+} cations with the aim of elucidating the origin of the antioxidant properties of such compounds. The selection of the Fe^{n+} cations is also based on the fact that butein has been confirmed (through both experimental [58] and theoretical methods [59]) to chelate Fe (II), thereby playing a crucial role as a powerful antioxidant against lipid and low density lipoprotein peroxidation by its iron (II) chelation [58]. The selection of the ferric and ferrous forms of Fe is based on the fact that a comparison of the affinity of the selected chalcone derivatives can be assessed for coordination with the different oxidation states of the Fe^{n+} cations.

1.5. Overview of the dissertation arrangement

This work is organised in six chapters. Chapter two provides a detailed description of the theoretical background; this includes the methods that are utilised for the study of molecular properties, approaches to conformational analysis and geometry optimisation, information about the metal chelation mechanism and population analysis. Chapter 3 provides information on the specific methods utilised in the current study; this information includes the method utilised and the reasons for the selected method, basis set selected and the criteria for their selection. Chapter 4 provides information on the results and discussion for the isolated butein and homobutein ligands and their iron-complexes. Chapter 5 presents results and discussion on the isolated kanakugiol and pedicellin ligands and their iron-complexes. The two chapters are separated such that the first chapter (chapter 4) discusses the simplest chalcones selected for the study while the second (chapter 5) describes the results for the more substituted chalcone derivatives. Chapter 6 provides conclusions to the overall study as well as recommendations for further studies.

CHAPTER 2

THEORETICAL BACKGROUND

2.1. Theoretical methods for the study of molecules

The study of molecular structures is often performed using either one of the two major approaches: molecular mechanics or quantum mechanics.

2.1.1. Molecular mechanics

Molecular mechanics is based on the laws of classical physics [60, 61] which means that a molecule is considered as a collection of atoms (made up of nuclei) connected by springs, which represent chemical bonds (Figure 2.1). The energy of the molecular system is considered to be due to potential energy contribution and is estimated by considering the ability of the molecule to resist distortion from an ideal geometry; such distortions can be a result of bond stretching, bond bending, torsional motion and non-bonded interactions caused by steric effect due to atom crowding [60, 61]. This implies that changes in the bond lengths and bond angles, rotations about single bonds as well as changes in the non-bonded interactions, such as van der Waals and Coulombic interaction, directly lead to the change in the energy of the molecular system.

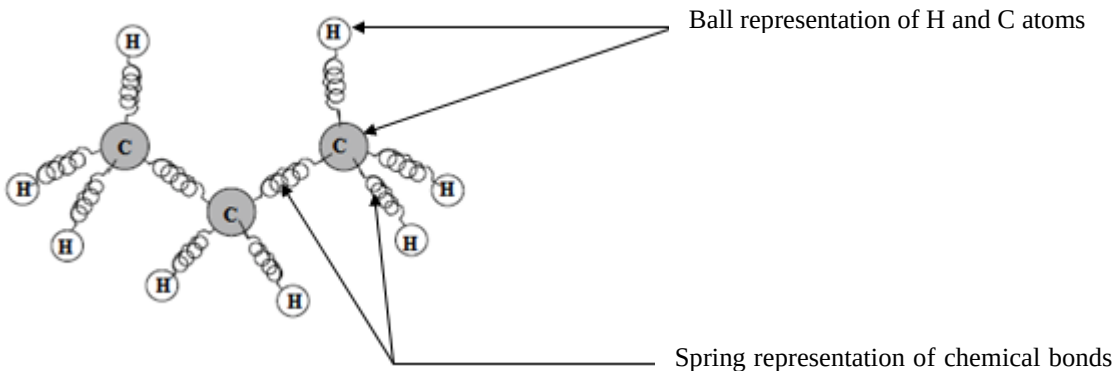

Figure 2.1 A schematic representation of a molecular system, where the atoms in the molecule are connected by springs which represent the chemical bonds.

Mathematically, the contribution to the energy of the system as a result of bond stretching, bond bending and steric effects due to atom crowding can be expressed through the equation [60, 61]:

$$E = \sum_{bonds} E_{stretch} + \sum_{angles} E_{bend} + \sum_{dihedrals} E_{torsion} + \sum_{pairs} E_{non-bonded}, \quad (2.1)$$

where $E_{stretch}$, E_{bend}, $E_{torsion}$ and $E_{non\text{-}bonded}$ are energy contributions from bond stretching, angle bending, torsional motion, and interactions between atoms or groups which are non-bonded, respectively. In this way, energy obtained using this expression corresponds to the minimum-energy geometry or, to the various possible potential energy surface minima. The energy expression as written in equation 2.1 is referred to as a forcefield. The $E_{stretch}$ and E_{bend} terms can be estimated by considering Hooke's law, which states that the potential energy of a system is directly proportional to the square distance between two points when a spring is either stretching or bending [62]. Mathematically, $E_{stretch}$ and E_{bend} terms can be written as

$$E_{stretch}(\mathrm{r}) = \frac{1}{2} k_{stretch}(r - r_{eq})^2, \quad (2.2)$$

$$E_{bend}(\alpha) = \frac{1}{2} k_{bend}(\alpha - \alpha_{eq})^2, \quad (2.3)$$

where r and α are the bond distances and bond angles after the stretching and bending effects, r_{eq} and α_{eq} are the equilibrium bond lengths and bond angles respectively; $k_{stretch}$ and k_{bend} are the force constants corresponding to stretching and bending motions respectively. The torsion contribution term takes into consideration the fact that molecules with single bonds may undergo rotations. The rotation of single bonds may repeat after 360° so that the energy of the molecule may vary with the dihedral angle in a sine or cosine function forms. To take into consideration the fact that the torsion angle repeats itself after 360° implies inclusion of periodicity. A general expression for the torsion contribution term to the potential energy, that includes the periodicity factor, has the form [61]

$$E_{torsion} = \mathrm{k}_0 + \sum_{r=1}^{n} k_r \left[1 + \cos(r\theta)\right] \quad (2.4)$$

The non-bonded terms which contribute to the potential energy include the van der Waals (VDW) and Coulombic type of interactions.

$$E_{non-bonded}(\mathrm{r}) = \mathrm{E}_{\mathrm{VDW}}(\mathrm{r}) + E_{Coulombic}(\mathrm{r}) \tag{2.5}$$

Van der Waals interactions consist of the attractive forces (e.g., hydrogen bond) and repulsive forces (e.g., dipole-dipole interactions or dispersive interactions) between two molecules or between atoms within a molecule. The potential energy for the VDW interactions can be expressed through the Lennard Jones (12, 6) potential equation (Figure 2.2, [63]):

$$E_{VDW}(r) = 4\varepsilon\left[\left(\frac{r_0}{r}\right)^{12} - \left(\frac{r_0}{r}\right)^{6}\right], \tag{2.6}$$

where r is the non-bonded distance, ε is the depth of the well of the potential (i.e., it is the lowest energy on the potential surface) and r_0 is the separation (between atomic or molecular entities) at which energy is minimum (i.e., $E_{VDW}(r) = 0$). The first term represents repulsions and the second term attractions. At long range the interactions between separated atoms are attractive, and are represented by the negative term (i.e., a decrease in the potential energy). At close range the interactions between separated atoms are repulsive and there is sharp rise in the potential energy, represented by the positive term (Figure 2.2).

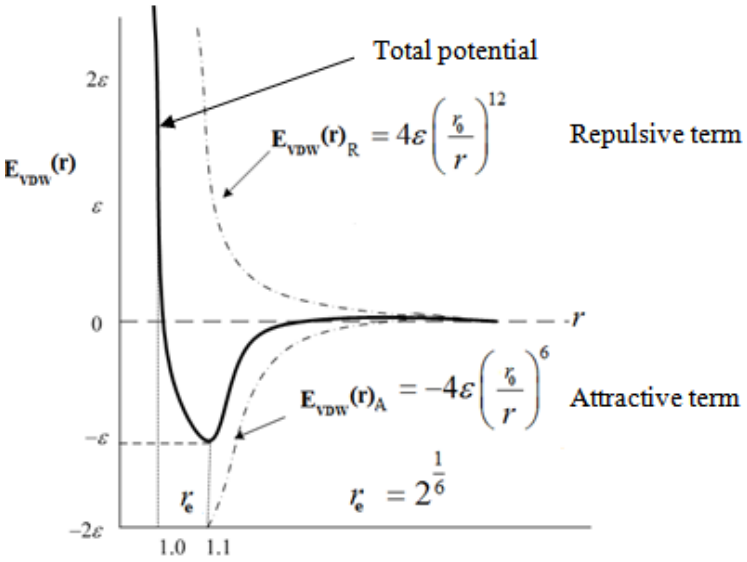

Figure 2.2 A graphical representation of the Lennard−Jones potential, and the parameters which relate the curve to the Lennard-Jones expression.

The Coulombic term takes into consideration the interactions between charged particles. If we consider a particle (e.g., an atom) of charge q and another particle of charge q' separated by a distance r, then the Coulomb potential has the form:

$$E_{Coulombic}(r) = \frac{qq'}{4\pi\varepsilon r}, \tag{2.7}$$

where ε is the dielectric constant (permittivity) in space or in the media of interest, for a neutral molecule, the sum of the atomic charges needs to be equal to the total charge of the molecule (i.e., the charges must be 0 if a neutral molecule is being considered).

A combination of equations 2.2–2.5 provides a force field for a given molecular system. In this way, the overall potential energy of a molecular system is found by developing a relevant forcefield describing the motions of atoms within that particular molecular entity. Since molecular mechanics does not consider the fact that molecules are made up of electrons moving about stable nuclei configurations, this results in its inability to describe some features of molecular systems [60, 61]. For instance, molecular mechanics cannot describe the reaction mechanism that involves forming and breaking of bonds. In such chemical reactions, it is necessary to have information related to the transfer of electrons. It is also not able to provide a proper description of systems in excited states because such systems are formed through promotion of an electron or pair of electrons [60, 61].

Despite a number of limitations, molecular mechanics has been found to provide a good description for a number of ground state systems, for instance [60]:

- those requiring less of computation time than quantum mechanical methods;
- those that are very rapid when calculating molecules containing atoms of 1000-2000 and more. This is because it does not have to calculate the terms associated with electronic integrals.

2.1.2. Electronic structure methods

Electronic structure methods such as quantum chemical methods are such methods that consider a molecular system as a collection of stable nuclei and electrons and describe the properties of molecular systems by taking into account the effects caused by electronic distribution. In this way, much of the molecular properties are better described by electronic structure methods. Among the different electronic structure methods, quantum mechanics is the preferred approach for the study of molecular systems, provided that the size of the molecule allows for computation [60–62]. This study utilises electronic structure methods because of the need to take into consideration the electronic effects, which are important in describing the antioxidant properties of biologically active molecules. Since the work reported in this dissertation utilises quantum chemical approaches, it is considered useful that the next section (section 2.2) provides detailed information on the foundation and fundamental basis in the development of such methods and on how such methods are utilised to obtain various molecular properties.

2.2. Quantum mechanical approach to the study of molecules

The basis of electronic structure methods is the assumption that all chemistry can be described in terms of the interactions between electronic charges within molecules. Quantum mechanical approaches are based on the solution of the Schrödinger equation for the molecule considered. All properties of the molecule (e.g., geometry, energies, and electronic properties) are considered to be derived from the solutions of the Schrödinger equation [60, 64, 65].

2.2.1. The Schrödinger equation

The Schrödinger equation related to the motion of a particle of mass m moving in space at time t and experiencing an external potential V has the form

$$\hat{H}\,\Psi(r, t) = i\,\hbar \frac{\partial}{\partial t}\,\Psi(r, t), \tag{2.8}$$

where Ψ is the wavefunction that describes the state of the system and $\hat{H}$ is the energy operator, called the *Hamiltonian operator*. Usually this is a more complete form of the Schrödinger

equation, however, for simplicity sake, the time-independent equation is often considered. When the system is studied without explicit consideration of time-dependence, the time-independent Schrödinger equation is written as follows

$$\hat{H}\,\Psi\,(r) = E\Psi, \tag{2.9}$$

where E is the energy of the system. The Hamiltonian operator is built as a sum of all the contributions to the energy of the particle (e.g., kinetic and potential energy contributions) and it has the general form;

$$\hat{H} = \frac{-\hbar^2}{2m}\left(\frac{\partial^2}{\partial x^2} + \frac{\partial^2}{\partial y^2} + \frac{\partial^2}{\partial z^2} \right) + V\,(x, y, z) \tag{2.10}$$

The first term on the right is the kinetic energy operator, while the second term is the potential energy operator for the particle. When a system consists of many particles, the Hamiltonian operator includes all the energy terms for each of the particles. For instance, consider a system with *r* nuclei and *s* electrons to develop the corresponding Hamiltonian operator; we need the kinetic energies for both the nuclei and the electrons and the potential energies for the nuclei and electrons. The kinetic energy of the nuclei can be written as

$$E_{k,\,nuclei} = \frac{-\hbar^2}{2m_N}\nabla_j^2, \tag{2.11}$$

where m_N is the mass of the nuclei and ∇_j^2 is the Laplace operator for the nuclei.

If we consider a total of *r* nuclei we can sum up the total kinetic energy term of all the nuclei;

$$E_{k,\,nuclei} = \sum_{j=1}^{r} \frac{-\hbar^2}{2m_N}\nabla_j^2, \tag{2.12}$$

Similarly the kinetic energy for the *s* electrons, each with mass *m*, can be written as

$$E_{k,\,electrons} = \sum_{i=1}^{s} \frac{-\hbar^2}{2m_e}\nabla_i^2, \tag{2.13}$$

where m_e is the mass of the electrons and ∇_i^2 is the Laplace operator for the electrons. The total kinetic energy term is the sum of the kinetic energy of the electrons and the kinetic energy of the nuclei

$$E_k = E_{k,\,\text{nuclei}} + E_{k,\,\text{electrons}},$$

which in terms of the Hamiltonian operator can be written as

$$E_k = \sum_{j=1}^{r} \frac{-\hbar^2}{2m_N}\nabla_j^2 + \sum_{i=1}^{s} \frac{-\hbar^2}{2m_e}\nabla_i^2, \tag{2.14}$$

The potential energy term considers the interaction between nuclei, interaction between electrons and interactions between the nuclei and the electrons. If we consider that the total potential energy is V, then this potential energy is the sum of the electron-electron repulsion, nuclear-nuclear repulsion and electron-nuclear attraction.

Potential energy between any two particles is usually written as

$$V = \frac{1}{4\pi\varepsilon_0}\frac{Qq}{r}, \tag{2.15}$$

where Q and q are separate charged systems and r is the distance between them. If we consider two electrons (i and i′) and each having a charge of *e* and separated by a distance $r_{ii'}$, then the repulsion potential energy (V_{ee}) between them is

$$V_{ee} = \frac{1}{4\pi\varepsilon_0}\frac{e^2}{r_{ii'}} \tag{2.16}$$

If we consider two nuclei (j and j′) and each having a charge of *Ze* and separated by a distance $r_{jj'}$, then the repulsion potential energy (V_{NN}) between them is

$$V_{NN} = \frac{1}{4\pi\varepsilon_0}\frac{Z_j e Z_{j'} e}{r_{jj'}} = \frac{1}{4\pi\varepsilon_0}\frac{Z_j Z_{j'} e^2}{r_{jj'}} \tag{2.17}$$

If we consider an electron i and a nucleus j, each having a charge of *e* and Z*e* respectively, separated by a distance r_{ij}, then the attractive potential energy (V_{eN}) between them is

$$V_{eN} = \frac{1}{4\pi\varepsilon_0}\frac{eZ_j e}{r_{ij}} = \frac{1}{4\pi\varepsilon_0}\frac{Z_j e^2}{r_{ij}} \tag{2.18}$$

The total potential energy for the system is the sum of equation 2.16–2.18

$$V_{total} = \sum_{i,i'} \frac{1}{4\pi\varepsilon_0}\frac{e^2}{r_{ii'}} + \sum_{j,j'} \frac{1}{4\pi\varepsilon_0}\frac{Z_j Z_{j'} e^2}{r_{jj'}} + \sum_{i,j} \frac{1}{4\pi\varepsilon_0}\frac{Z_j e^2}{r_{ij}} \tag{2.19}$$

The total Hamiltonian term includes the total kinetic energy term (equation. 2.14) and the total potential energy term (equation. 2.19)

$$\left.\begin{aligned} H = \sum_{j=1}^{r} \frac{-\hbar^2}{2M}\nabla_j^2 + \sum_{i=1}^{s} \frac{-\hbar^2}{2m}\nabla_i^2 + \sum_{i,i'} \frac{1}{4\pi\varepsilon_0}\frac{e^2}{r_{ii'}} + \\ \sum_{j,j'} \frac{1}{4\pi\varepsilon_0}\frac{Z_j Z_j e^2}{r_{jj'}} + \sum_{i,j} \frac{1}{4\pi\varepsilon_0}\frac{Z_j e^2}{r_{ij}} \end{aligned}\right\} \tag{2.20}$$

The solution of the Schrödinger equation is the wavefunction Ψ and the corresponding energy values, E. Both the Hamiltonian operator and the wavefunction depend on the coordinates of all the particles constituting the system; therefore, for a molecule, they depend on the coordinates of all the nuclei and all the electrons [60, 64, 65] (equation. 2.20). However, it is not possible to obtain solutions of the Schrödinger equation for systems with more than one moving particle. In order to solve the Schrödinger equation, as given in equation 2.20, there is a need to introduce approximation procedures. The first approximation is to consider that the motion of the nuclei and the electrons are separated by assuming the nuclei to be stationary and electrons moving about the nucleus. This approximation is known as the Born-Oppenheimer approximation [66] and it is described in brief in the next section.

2.2.2. The Born-Oppenheimer approximation

The Born-Oppenheimer approximation simplifies the Schrödinger equation for molecular systems by assuming that the nuclei are not moving with respect to the motion of the electrons (i.e., the motion of electrons is considered with respect to a fixed framework of nuclei). This assumption is based on the high ratio between nuclei and electronic masses [60−62]; the motion of electrons is much faster than the motion of nuclei, because of the much heavier mass of the nuclei. The approximation therefore makes the assumption that changes in electronic distribution occurs with no nuclei disturbance. The total wavefunction is the product of the electronic wavefunction and the wavefunction of the nuclei [60−62]:

$$\Psi_{total}(x, y) = \psi_{electrons}(x)\,\psi_{nuclei}(y), \tag{2.21}$$

where x represents the coordinates of the electrons and y represents the coordinates of the nuclei. The total energy of the system is the sum of the potential and kinetic energies of the electrons and repulsion potential energies of the nuclei:

$$E_{total} = E_{electrons} + E_{nuclei} \tag{2.22}$$

Electronic calculations are performed for different frameworks of fixed nuclei. Different frameworks correspond to different energy values. Frameworks corresponding to minimal energy values are the *equilibrium geometries* of the molecule.

2.2.3. The Hartree Fock (HF) approximation

This is another approximation method for the solution of the Schrödinger equation related to the multi-electron nature of molecular systems [60, 67, 68]. The HF approximation assumes that the simplest way of writing the wavefunction for a multi-electron system is by considering the electrons as being independent. This means that the motion of one electron is not influenced by the motion of the other electrons [60]. According to Pauli's Exclusion Principle each molecular orbital (φ) can take a maximum of two electrons. Furthermore, electrons have intrinsic spin; therefore it is appropriate for each electron to have both the space coordinates (molecular orbital) and the spin coordinates (spin orbital). The overall molecular orbital is known as the *molecular*

spin orbital, and is hereby denoted as ψ. Then, the total wavefunction can be written as a product of functions (ψ), each of them depending on the coordinates of one electron.

$$\Psi = \psi_1 (1)\, \psi_2 (2) \ldots \psi_N (N), \tag{2.23}$$

where electron 1 occupies molecular spin orbital ψ_1 and electron 2 occupies molecular spin orbital ψ_2. It is essential that the molecular spin orbital follows the anti-symmetric condition, i.e., for any system with N-electrons, the sign of the wavefunction must change when the electrons are exchanged.

For instance, if we have a wavefunction having the coordinates of two or more electrons, the signs should change if we switch their positions; as a result of the change in the signs the molecule is said to be unsymmetrical (equation 2.24); in the case where the signs don't change the molecule is considered to be symmetric (equation 2.25)

$$\psi (1, 2) = -\psi (2, 1) \tag{2.24}$$

$$\psi (1, 2) = \psi (2, 1) \tag{2.25}$$

Once all the possible exchanges of particles (permutations) are considered, a better anti-symmetric wavefunction (corresponding to equation 2.23) is obtained when the total wavefunction is a linear combination of permutations [65, 66];

$$\Psi_{total}(1,2,.....n) = \frac{1}{\sqrt{n!}} \sum (-1)^p \psi_1(k_1)\, \psi_2(k_2) \ldots . \psi_n(k_n) \tag{2.26}$$

where p is the number of transpositions performed on the starting $\psi_1(1)\, \psi_2(2) \ldots \psi_n(N)$ to obtain the given term in the linear combination; k_1, k_2..., k_n are the coordinates resulting after the permutations and $\frac{1}{\sqrt{n!}}$ is the normalization factor. The factor $(-1)^p$ ensures that the wavefunction does not change sign for an even number of transpositions, but only changes sign for an odd number of transpositions.

Another approximation that is related to the Hartree-Fock approximation involves the replacement of the many-electron Hamiltonian operator with an effective one-electron Hamiltonian called the *Fock operator*. The Fock operator contains all the one-electron terms of the Hamiltonian operator (kinetic energy and nuclei-electron attraction potential terms), and considers an effective potential perceived by one electron as a result of Z-1 electrons around it. A problem that arises in considering an average value of the potential due to the presence of the other (Z-1) electrons is that one needs to know the electron distribution in order to evaluate that potential energy accurately, but the electron distribution can be known only after solving the Schrödinger equation. This demands an iteration procedure for the solution of the Schrödinger equation, commonly called the *Self Consistent Field* (SCF) procedure.

The SCF procedure is applied both to the study of atoms and to the study of molecules. This method is ideal for use in computational analysis because it can be written as an algorithm. Initially, a "guess" average potential is utilised in the Hamiltonian operator, and the Schrödinger equation is solved, the solutions obtained are then used to evaluate the average potential energy. If this differs significantly from the initial guess value, the new value is utilised to write the Schrödinger equation. This equation is then solved and the solutions are used to evaluate the average potential energy. The values are compared and if they differ extensively the procedure is repeated. The procedure is repeated until the difference between the value found at the end of a cycle and the value utilised at the beginning of that cycle is less than a pre-fixed value called the *cut-off value*. This is the meaning of an iterative procedure, commonly called the *Self Consistent Field* (SCF) procedure

2.2.4. Linear combination of atomic orbitals (LCAO) approximation

To perform a molecular-orbital theory calculation, one needs to determine each of the molecular orbitals, ψ_i present in equation 2.26 as well as calculate the energy associated with the total wavefunction. The standard procedure for determining the molecular orbitals and their associated energies is to express the molecular orbitals as a linear combination of atomic orbitals (LCAO) and then determine the coefficients in the LCAO by a self-consistent field method. The linear combination of atomic orbitals (LCAO) approximation is based on the assumption that molecular orbitals can be constructed by the combination of simpler functions, such as the atomic wavefunction from which the molecule is made up. Consider for instance an electron

found in an atomic orbital belonging to atom X and also in an atomic orbital belonging to atom Y, the overall wavefunction is a superposition of the two atomic orbitals:

$$\psi_{\pm} = N(X \pm Y), \tag{2.27}$$

where N is the normalisation factor. A common term for superposition expressed in this equation is linear combination of atomic orbital. Wavefunctions (e.g., atomic wavefuntions) that are combined to give a molecular function are known as basis functions. A set of basis functions from which a molecular function is constructed is known as a basis set [69]. An approximate molecular orbital from a linear combination of atom orbitals is called the LCAO-MO. When more than two basis functions are utilised to generate a molecular orbital, it is more appropriate to utilise the equation

$$\psi_{\pm} = \sum_i c_i \chi_i \ , \tag{2.28}$$

where χ are the basis functions (usually centred on atoms) and c_i are the expansion coefficients. Generally, basis sets are formed from atomic orbitals, for instance, in the case of the H_2 molecule, the molecular orbital can be formed as a linear combination of the sigma (*S*) atomic orbital on one H atom (H_A) and the sigma atomic orbital on the other H atom (H_B). In this way, the molecular orbital (ψ) for the hydrogen molecule can be written as:

$$\psi \approx 1S_{H_A} + 1S_{H_B} \tag{2.29}$$

The larger the number of basis functions selected to form molecular orbitals the more accurate is the approximations to the molecular orbitals. It is important to note however that the selection of a suitable basis set is dependent on the size of the molecule being considered for the study.

Usually the basis functions are formed from the Slater-type functions (STO) and the Gaussian-type functions (GTO, [69]).

The Slater-type function (Figure 2.3a) has the mathematical form:

$$\chi^{STO}(x\ y,\ z) = N\ x^a\ y^b\ z^c\ e^{-\zeta\ r}\ , \tag{2.30}$$

while the Gaussian- type functions (Figure 2.3b) has the mathematical form:

$$\chi^{GTO}(x\ y,\ z) = N\ x^a\ y^b\ z^c\ e^{-\zeta\ r^2}\ , \tag{2.31}$$

where N is the normalization constant, a, b and c are parameters that control the angular momentum, ζ controls the width of the orbital (i.e., the large ζ gives tight function and smaller ζ gives diffuse function). STO are better for computations than the GTO's because for a large value of r, the GTO (which are exponential in r^2), decays much faster than the STO [61]. Another advantage of the STO orbitals is that at the nucleus (r = 0) an STO orbital has a cusp (corresponding to zero slope) similar to hydrogen-like atomic orbitals. GTO, on the other hand, is differential at r = 0, indicating that it does not have a cusp. Because of these characteristics, STO orbitals are likely to provide correct descriptions for the short-range and long-range behavior of a molecular system. However, STO is much more computationally expensive. In order to overcome the problem of computational affordability, the STO-type orbitals are approximated by linear combination of GTOs, forming what is referred to as contracted Gaussian basis function. Basis sets may be classified into different types depending on the number of GTO's utilised to emulate an STO. These include hydrogen like orbitals, minimal basis set, split valance basis sets and diffuse basis set [60, 69–72]. Some of these basis sets are described in the next paragraphs, giving information on their applicability and weaknesses.

Slater-type 1s orbital (a)

Gaussian-type 1s Orbital (b)

Figure 2.3 Graphical representation of the Slater-type orbital and the Gaussian-type orbital.

Minimal basis set: This type of basis set describes only the most basic aspects of the orbitals, one basis function for each atomic orbital angular momentum component. It has the minimum number of basis functions (χ) that is needed to describe the ground states of the component atoms in a molecule. An ammonia molecule (NH_3) would require eight basis functions (either STO or GTO types) in place of the eight atomic functions present in the ammonia molecule which include, three 1s orbitals for each of the hydrogen atoms plus a 1s, 2s, $2p_x$, $2p_y$ and $2p_z$ atomic orbitals for the nitrogen atom. In a similar manner, the carbon dioxide (CO_2) molecule would require 15 basis functions in place of the 15 atomic functions present in the molecule. A Slater type orbital may also be approximated by a combination of two or more Gaussian type orbitals leading to such basis functions as STO-2G, STO-3G, etc. [60, 69–72].

All minimal basis sets however have some weakness including the fact that all the basis functions are either themselves spherical or come in sets that when taken together describe a sphere. This means that minimal basis sets are suited to describing molecular systems with spherical molecular environment and are not suitable for description of atoms with aspherical molecular environment. The second weakness of minimal basis sets is that the basis functions are atom centred instead of being between atoms [60, 69–72]. This shortcoming implies that the minimal basis sets are not able to describe accurately the electron distribution between nuclei (i.e., a chemical bond), which is a major factor in chemical systems.

Double zeta basis sets: These basis sets are formed in such a way that each atomic orbital within a molecule is expressed as the sum (linear combination) of two Slater-type orbitals [60, 69–72]. For instance, the case of water, which has seven atomic orbitals, the double zeta basis set is built in such a way that there are 14 basis functions, with two basis functions describing each of the atomic orbitals in the water molecule. The addition of two Slater-type functions to describe the molecular orbital is meant to add flexibility in the molecular orbital so as to be able to describe the electron distribution within the molecule [73] (e.g., atoms with positive charge can be described with a contracted type of orbital while atoms with negative charge can be described using diffuse type of orbitals). In order to achieve a better description of the different molecular environments, the two Slater-type functions employed in the basis set (to represent each atomic orbital) do not have to have the same size because they are constructed from different ζ orbital exponents [73]. For instance, a 2s function can be constructed by means of linear combination of two STO functions, with orbital exponents ζ_1 and ζ_2:

$$\chi_{2s}(\mathrm{r}) = \chi_{2s}^{STO}(r,\zeta_1) + d\chi_{2s}^{STO}(r,\zeta_2), \tag{2.32}$$

where the constant *d* accounts for the contribution of the second STO in the constructed basis function. Since the two atomic orbitals may be of different size, the double zeta basis set has to some extent reduced spherical character which can be described as having anisotropy character with respect to minimal basis sets [60, 70–73].

Split valence basis set: In a split-valence basis set the inner-shell atomic orbitals are represented by one basis function and the valence orbitals are represented by two or more basis functions [60, 72]. For example, the 3-21G basis set has one contracted Gaussian function that describes the inner core orbital (1s). This contracted Gaussian function is formed as a linear combination of three primitive Gaussian functions [72]. In the valence atomic orbitals we distinguish between the inner (2s) and the outer (2p) valence atomic orbitals; the inner valence atomic orbital is described by one contracted Gaussian function which is a linear combination of two primitive Gaussians; the outer valence atomic orbital is described by one primitive Gaussian function [60, 72]. For instance, in the case of the O atom, the inner core orbital is a 1s and is described by linear combination of three primitive Gaussian functions, the inner valence atomic orbital is the 2s and is described by linear combination of two primitive Gaussian functions and the outer valence orbitals are the $2p_x$, $2p_y$ and $2p_z$, each is described by one primitive Gaussian function. Therefore the overall basis set for the O atom is made up of eight primitive Gaussian functions. The 6-31G basis set informs that each inner-core orbital is represented by one contracted Gaussian function that is a linear combination of six primitive Gaussian functions and each valence orbital is represented by two basis functions, one contracted Gaussian function that is a linear combination of three primitive Gaussians describing the inner valence electrons and one primitive Gaussian function describing the outer valence electrons [60, 69–72].

Polarization functions: Both minimal basis sets and spit-valence basis set functions are atom centred, which means that they cannot provide a good description of the region between atoms [69, 72]. This implies that the increase in the number of contracted Gaussian functions per atomic orbital does not necessarily result in a good quality basis set. A better description of chemical bonds requires that other types of basis functions be included in the construction of the overall basis set. Usually, polarised basis functions are utilised to account for the region

between atoms [69]. Polarization refers to the distortion of an electron cloud of a system as a result of the neighbouring species. Therefore contracted Gaussian functions that take into account the fact that the electron cloud of chemical species can be distorted need to be selected and included in the basis set meant to describe molecular systems. Such contracted Gaussian functions are called polarisation functions and are constructed by adjusting the angular momentum parameters (equations 2.30 and 2.31). The polarisation basis functions are represented by the asterisk (*) at the end of the notation of the basis set, for instance, the 6-31G* (also denoted as 6-31(d)) represents that polarisation functions of the *d* type that are added for each of the heavy atoms. When the polarisation functions are also added on the H atoms the basis set is denoted as 6-31G** (also denoted as 6-31G(d,p)), where the second * represents the *p* functions added on the H atom [69]. These types of functions are important in describing various phenomena such as hydrogen bonding where the orbitals on the H atom are not necessarily spherical but are distorted because of the electron cloud of the neighbouring O atom.

Diffuse functions: Diffuse functions are constructed to take into account the fact that in some cases (e.g., anionic systems) the electron distribution may be further away from the nucleus. In order to take into account the features which are away from the nucleus, diffuse functions are needed. These functions are formed by adding very small zeta exponents to a basis set. These basis sets are represented by the + signs. One + sign means that diffuse functions are added on orbitals of the heavy atoms [69], while ++ signals implies that diffuse functions are also added to the s orbitals of the H atom. For instance consider the 6-31G(d) basis set; when the diffuse functions are added to the s and p atomic functions, to describe the character of heavy atoms, the basis set is denoted as 6-31+G(d); when diffuse functions are also added to the s orbital on hydrogen atom, the basis function is denoted as 6-31++G(d) [69].

Effective core potentials (ECP) basis set: The basis sets described so far are suitable for description of molecules containing main group elements, where the number of core electrons is not sufficiently large. When the number of core electrons is very large, as is a case with transition metal atoms (e.g., Fe, Co, Cu, etc.,) the utilisation of such basis sets becomes computationally unaffordable. In order to overcome the limitation of standard basis sets in describing transition metal atom/ions, basis sets that use an effective potential to describe the nucleus and core electrons/orbitals and pseudo-potentials to describe the valence electrons are often utilised for description of transition metal atoms/ions. The justification for utilisation of such basis sets is based on the fact that core (inner) orbitals are in most cases not affected

significantly by changes in chemical bonding. These basis sets, while mimicking the presence of the core electrons by means of an effective potential, treat explicitly only the valence electrons or the two outermost electron shells of the atom [60, 74]. The valence orbitals are replaced by pseudo-orbitals, which are smooth and node-less orbitals capable of reproducing the correct behaviour in the valence region [75]. The fact that the core electrons are not computed explicitly provides an explanation for the reduction in computational time for the calculation of systems containing transition metal atoms [74–76]. Another useful feature of ECP basis sets is that they include relativistic effects, which are important for description of heavy atoms such as transition metal atoms and thus cannot be neglected for accurate investigations.

Unlike standard basis sets, ECP basis sets are not considered as orbitals but rather as modifications to the effective Hamiltonian. An issue related with the ECP basis sets is their inability to eliminate electron density in the core region, although they are able to remove the density due to core orbitals, and replace the core-region density of the true core orbitals by the core-region density of the pseudovalence orbitals (i.e., these are node-less valance orbitals determined in the presence of an ECP and the absence of the explicit core orbitals [74]).

When studying a molecular entity that contains main group elements as well as transition metal ions, thereby forming a coordinated complex, it is often preferred to utilise a mixed basis set of standard basis sets, for the description of main group elements and ECP basis set, for the description of transition metal atoms/ions. Some examples of the ECP basis sets include the Los-Alamos National Laboratory 1 double zeta basis set (LANL1DZ), Los-Alamos National Laboratory 2 double zeta basis set (LANL2DZ), the multi-configuration-Dirac–Hartree–Fock (MDF10) in which only 10 core electrons are replaced by the ECP and the Stuttgart/Dresden (SDD) ECP basis set [74–77]. Since the work that is reported in this dissertation considers the formation of complexes involving the Fe^{n+} ions with selected chalcone derivatives, a mixed type of basis set is used for the optimisation of the complexes; where the metal ion is described by the LANL2DZ basis set and the ligand molecule is described by the 6-31+G(d,p) standard basis set. Further description on the selection of the basis sets specifically for the work reported in this dissertation is given in Chapter 3.

2.2.5. Roothaan-Hall equation and the Hartree-Fock Method

The development of the Roothaan-Hall equations is based on the fact that for the description of the spherical nature of atoms the HF approximation has to be solved numerically for the spin-orbitals; however these numerically solutions cannot be attained in sufficient computational time for the description of molecular properties. The Roothaan-Hall equations are modifications of the HF approximation and were developed by the application of the Hartree-Fock together with the LCAO approximations to the electronic Schrödinger equation [60, 78]. The Hartree-Fock equations on which the procedure is based are obtainable if we consider the Hamiltonian operator of the form [78]

$$\hat{\mathrm{H}} = \sum_i h + \frac{1}{2}\sum_{ii'}{}' \frac{e^2}{4\pi\varepsilon_0 r_{ii'}}, \tag{2.33}$$

where *h* is a hydrogenic Hamiltonian (called the core Hamiltonian) for electron *i* in the field of a bare nucleus of charge Z*e*. The factor of $\frac{1}{2}$ in the double sum is meant to prevent the double counting of interactions. The prime on the summation is meant to exclude the terms for which *i* = *i′* as electrons are considered not to interact with each other. The Hartree-Fock equation can then be developed for a space orbital (ψ_a) that is occupied by one electron

$$\left\{h_1 + \sum_u \left(2J_u - K_u\right)\right\}\psi_a(1) = \varepsilon_a \psi_a(1), \tag{2.34}$$

where the sum is over all occupied spatial wavefunctions, J_u is the Coulomb operator, K_u is the exchange operator and ε_a is the one-electron orbital energy. The coulomb operator (J_u) representing the Coulomb interaction of electron 1 with electron 2 in the orbital ψ_u and is defined as

$$J_u\psi_a(1) = \left\{\int \psi_u^*(2)\left(\frac{e^2}{4\pi\varepsilon_0 r_{12}}\right)\psi_u(2)d\tau_2\right\}\psi_a(1) \tag{2.35}$$

The exchange operator (K_r) is defined similarly

$$K_u\psi_a(1) = \left\{\int \psi_u^*(2)\left(\frac{e^2}{4\pi\varepsilon_0 r_{12}}\right)\psi_a(2)d\tau_2\right\}\psi_u(1) \tag{2.36}$$

Let us for a moment consider equation 2.34 for the spatial function and write it such that

$$f_1\psi_a(1) = \varepsilon_a\psi_a(1), \tag{2.37}$$

where f_1 is the Fock operator expressed in terms of the spatial wavefunctions

$$f_1 = h_1 + \sum_u \left(2J_u(1) - K_u(1)\right).$$

Next we make use of a set of *M* basis functions χ_i (equation 2.28)

$$\psi_n = \sum_{i=1}^{M} c_{in}\chi_i \ , \tag{2.38}$$

where *n* is the number of molecular orbitals developed from *i* number of basis functions orbitals. From a set of *M* basis functions we can obtain *M* linearly independent spatial functions. Since the nature of the *M* basis wavefunctions is known (taken either as Gaussian-type functions or Slater-type functions), the problem of calculating the wavefunctions transforms to one of computing for the coefficients c_{in}. We can substitute equation 2.38 into equation 2.37, taking note of the fact that in equation 2.37, *n* = *a*, and write

$$f_1 \sum_{i=1}^{M} c_{ia}\chi_i(1) = \varepsilon_a \sum_{i=1}^{M} c_{ia}\chi_i(1). \tag{2.39}$$

Multiplying on both sides of equation 2.39 by the conjugate of another set of basis function $\chi_n^*(1)$ acting on electron 1, and integration over space function d$\mathbf{r}_1$, we can write

$$\sum_{i=1}^{M} c_{ia} \int \chi_n^*(1) f_1\chi_i(1)\, \mathrm{d}\mathbf{r}_1 = \varepsilon_a \sum_{i=1}^{M} c_{ia} \int \chi_n^*(1)\chi_i(1)\, \mathrm{d}\mathbf{r}_1. \tag{2.40}$$

The term on the right hand-side can be replaced by the overlap matrix **S** (which is not in general a unit matrix because the basis functions are not necessary orthogonal) with elements

$$S_{ni} = \int \chi_n^*(1)\chi_i(1)\,\mathrm{d}\mathbf{r}_1, \tag{2.41}$$

and the term on the left hand-side can be replaced by the Fock matrix (***F***), which is the matrix formed from the *Fock* operator [45]

$$F_{ni} = \int \chi_n^*(1) f_1 \chi_i(1)\,\mathrm{d}\mathbf{r}_1, \tag{2.42}$$

Substituting equation 2.41 and 2.42 into equation 2.40 we get

$$\sum_{i=1}^{M} c_{ia}\ F_{ni} = \varepsilon_a \sum_{i=1}^{M} c_{ia}\ S_{ni} \tag{2.43}$$

This expression is one in a set of *M* simultaneous equations (one for each value of *n*) that are known as the Roothaan-Hall equations. The entire set of equations can be written as a single matrix equation [73]

$$FC = SC\varepsilon\,, \tag{2.44}$$

where C is an *M* x *M* matrix composed of elements c_{ia} and ε is a diagonal *M* x *M* matrix of the orbital energies ε_a. The results obtained here correspond to the Hartree-Fock method for consideration of molecular systems. Hartree-Fock (HF) calculations must also specify the treatment of electron spin, that is, whether the molecule can be described using an open-shell or a closed shell model. Most molecules have singlet electronic ground states because they contain an even number of electrons, which can be formally assigned to orbitals in pairs of opposite spins. The model for these cases is referred to as *closed shell Hartree-Fock* model. However, several cases, which require explicit consideration of unpaired electrons, are better described by open-shell, spin-unrestricted models that generate separate molecular orbitals for the electrons with different spin (α or β).

HF procedures utilised for open shell calculations can be of Restricted (RHF) or Unrestricted (UHF) type; the open shell RHF or UHF methods [79] are used for:

- molecules with odd number of electrons;
- excited states;
- molecules with triplet or higher-spin ground states (e.g., O_2);
- processes that separate electron pairs (e.g., bond dissociation);
- delocalisation orbitals for resonant system.

2.2.6. The Variational Principle

The orbital energies (expressed in equation 2.44) can be obtained by considering the variational principle. The variational principle states that the energy value for a trial wavefunction (molecular system) is always higher or equal to the true energy of the exact solution [73]. To show this, we consider the ground state of some arbitrary molecular system of wavefunction ψ_0 and energy E_0. The corresponding Schrödinger equation for the system is given by the equation

$$\hat{H}\psi_0 = E_0\psi_0 \tag{2.45}$$

Multiplying equation 2.45 by the conjugate of the function we obtain

$$\psi_0^* \hat{H}\psi_0 = \psi_0^* E_0\psi_0 \tag{2.46}$$

If this expression is integrated overall space we obtain

$$\int \psi_0^* \hat{H}\psi_0 \, d\tau = \int \psi_0^* E_0\psi_0 \, d\tau \tag{2.47}$$

Since E_0 is a constant, it can be taken out of the integral sign and then set as a subject of a formula

$$E_0 = \frac{\int \psi_0^* \hat{H}\psi_0 d\tau}{\int \psi_0^* \psi_0 d\tau}, \tag{2.48}$$

where dτ represent the appropriate volume element. This energy value is termed the expectation value for a given wavefunction ψ_0. Now consider that we have a trial wavefunction ϕ, the expectation value for such wavefunction is given by the equation

$$E_\phi = \frac{\int \psi_\phi^* \hat{\mathrm{H}} \psi_\phi \mathrm{d}\tau}{\int \psi_\phi^* \psi_\phi \mathrm{d}\tau} \tag{2.49}$$

According to the variational principle the relationship between the two energy values is such that

$$E_\phi \geq E_0, \tag{2.50}$$

where the equality holds only if $\phi = \psi_0$.

2.2.7. Ab initio and semi-empirical methods

Ab initio is a Latin word meaning "from the beginning". This term is used to describe the methods which are based on solving the Schrödinger equation directly, without inclusion of experimental data. The *ab initio* methods are therefore very rigorous and tend to be quite expensive in comparison to methods that introduce some experimental values. Different *ab initio* methods are distinguished based on the way in which the approach is applied to solve the Schrodinger equation. Semi-empirical methods follow directly from the Hartree-Fock method. These methods do not solve the Schrödinger equation directly but rather neglect or replace some integrals in the Schrödinger equation with empirical/experimental parameters. Examples of the integral terms that are neglected include the differential overlap integrals, equation 2.41. The remaining integrals can be [80]:

- Used to determine the functional form of atomic orbitals;
- Converted into parameters and given values on the basis of few experimental data;
- Made into parameters and given values based on the fitting to many experimental values.

Different semi-empirical methods are formulated based on the type of neglect of differential overlap. The three types of neglect of differential overlap that are often utilised include the Neglect of Diatomic Differential Overlap Approximation (NDDO), Complete Neglect of Differential Overlap Approximation (CNDO) and Intermediate Neglect of Differential Overlap Approximation (INDO). Some semi-empirical methods developed based on the NDDO algorithm include the AM1 (Austin model 1, [81]), PM3 (Parametric method version 3 [82]); semi-empirical methods developed based on the INDO algorithm include the modified intermediate neglect of differential overlap (MINDO, [83]) and Zerner intermediate neglect of differential overlap (ZINDO, [84]).

Because of the neglect of some integrals in the Schrödinger equation, semi-empirical methods are quicker and less accurate than *ab initio* method [67, 68]. However, when considering large molecular systems, they are the only options for providing reasonable results. When describing systems with small to medium-size molecules, it is possible to use methods that go beyond the HF decscription. There methods that take into account electronic correlation effects are known as Post HF methods.

2.2.8. Correlation effects and Post HF methods

The Hartree-Fock method solves the electronic Schrödinger equation by considering the motion of the multi-electrons as being independent of each other; it assumes that the wavefunction can be written as one Slater determinant and that each electron interacts with an average charge distribution due to the other electrons (i.e., it replaces the electron-electron repulsion potential energy with an average electron charge cloud). The first assumption introduces errors in the wavefunction and the second assumption introduces errors in the energy of the molecular system. The error in the energy is called the correlation energy. The correlation energy is defined as the difference between the true energy (where the interactions between the electrons is taken into account) and the Hartree-Fock energy (where the interactions between electrons are neglected) in a complete basis [73]:

$$E_{correlation} = E_{exact} - E_{HF}. \quad (2.51)$$

Electron correlation effects are necessary for describing many molecular properties [60, 67, 68] and therefore it is necessary to consider methods beyond HF method that can take into consideration these effects. Such methods are referred to as post Hartree-Fock methods and include the Møller–Plesset (MP) perturbation theory method and the Density Functional Theory

(DFT) method [60, 61, 67–69], configuration interaction [78] and multi-configuration methods [78]. For the purpose of this work, we provide an explanation of how the Møller–Plesset second

order (MP2) perturbation theory method and Density Functional Theory (DFT) methods take into account the electron correlation effect. The MP2 method is explained here because, like HF, it is a wavefunction based method and therefore can provide a good comparison with HF method. However, because the molecules investigated in this dissertation are medium-sized molecules, it is not computationally feasible to utilise the MP2 method for calculations. DFT method is used throughout the study and it is therefore necessary that a detailed explanation of the method is provided.

2.2.9. Møller–Plesset second order (MP2) perturbation theory

The Møller–Plesset perturbation theory is formulated on an attempt to find approximate solutions of the Schrödinger equation for a system with Hamiltonian $\hat{H}$ for which it is difficult to find exact solutions. We can write the Schrödinger equation for this system as [73, 85]

$$\hat{\mathrm{H}}\psi_{\mathrm{n}} = E_n\psi_n . \tag{2.52}$$

We assume that we know the exact solution $\psi_n^{(0)}$ for a simpler system of Hamiltonian $\hat{H}^{(0)}$, which is not very different from $\hat{H}$;

$$\hat{H}^{(0)}\psi_n^{(0)} = E_n^{(0)}\psi_n^{(0)}. \tag{2.53}$$

We also take into consideration the assumption that the states $\psi_n^{(0)}$ are non-degenerate, which implies that

$$E_n^{(0)} \neq E_k^{(0)} \text{ if } \mathrm{n} \neq \mathrm{k}. \tag{2.54}$$

The small difference in the two Hamiltonians ($\hat{H}$ and $\hat{H}^{(0)}$) is considered as a perturbation on $\hat{H}^{(0)}$ such that all quantities of the system described by $\hat{H}$ can be expanded as a Taylor series

starting from the unperturbed quantities of the wavefunction with Hamiltonian $\hat{H}^{(0)}$. The Taylor series expansion is done in terms of a parameter λ.

$$\hat{H} = \hat{H}^{(0)} + \lambda\hat{H}^{(1)} + \lambda^2\hat{H}^{(2)} + \lambda^3\hat{H}^{(3)} + ... \quad (2.55)$$

The corresponding wavefunction and energies have the form

$$\psi_n = \psi_n^{(0)} + \lambda\psi_n^{(1)} + \lambda^2\psi_n^{(2)} + \lambda^3\psi_n^{(3)} + ... \quad (2.56)$$

$$E_n = E_n^{(0)} + \lambda E_n^{(1)} + \lambda^2 E_n^{(2)} + \lambda^3 \mathrm{E}_\mathrm{n}^{(3)}. \quad (2.57)$$

The superscript refers to the order of the perturbation theory. The term $\psi_n^{(1)}$ is called the first order correction to the wavefunction and term $E_n^{(1)}$ is called the first order correction to the energy. The term $\psi_n^{(2)}$ is called the second order correction to the wavefunction and term $E_n^{(2)}$ is called the second order correction to the energy and so on. The purpose of perturbation theory is to approximate the energies and wavefunctions of the systems of interest by calculating corrections up to a given order, in our case, the second order. If equation 2.55 and equation 2.56 are substituted on the left hand side of equation 2.52, and equation 2.56 and equation 2.57 are substituted on the right hand side of equation 2.52 we get (considering only up to third order terms)

$$(\hat{H}^{(0)} + \lambda\hat{H}^{(1)} + \lambda^2\hat{H}^{(2)} + \lambda^3\hat{H}^{(3)})(\psi_n^{(0)} + \lambda\psi_n^{(1)} + \lambda^2\psi_n^{(2)} + \lambda^3\psi_n^{(3)}) =$$
$$(E_n^{(0)} + \lambda E_n^{(1)} + \lambda^2 E_n^{(2)} + \lambda^3 E_n^{(3)})(\psi_n^{(0)} + \lambda\psi_n^{(1)} + \lambda^2\psi_n^{(2)} + \lambda^3\psi_n^{(3)}). \quad (2.58)$$

Let us consider the left hand side of equation 2.58 and simplify it to the second order term

$$(\hat{H}^{(0)} + \lambda\hat{H}^{(1)} + \lambda^2\hat{H}^{(2)} + \lambda^3\hat{H}^{(3)})(\psi_n^{(0)} + \lambda\psi_n^{(1)} + \lambda^2\psi_n^{(2)} + \lambda^3\psi_n^{(3)}) =$$
$$\hat{H}^{(0)}\psi_n^{(0)} + \lambda\hat{H}^{(0)}\psi_n^{(1)} + \lambda^2\hat{H}^{(0)}\psi_n^{(2)} + \lambda^3\hat{H}^{(0)}\psi_n^{(3)} + \lambda\hat{H}^{(1)}\psi_n^{0} + \lambda^2\hat{H}^{(1)}\psi_n^{(1)} +$$
$$\lambda^3\hat{H}^{(1)}\psi_n^{(2)} + \lambda^4\hat{H}^{(1)}\psi_n^{(3)} + \lambda^2\hat{H}^{(2)}\psi_n^{(0)} + \lambda^3\hat{H}^{(2)}\psi_n^{(1)} + \lambda^4\hat{H}^{(2)}\psi_n^{(2)} + \lambda^5\hat{H}^{(2)}\psi_n^{(3)}$$
$$+ \lambda^3\hat{H}^{(3)}\psi_n^{(0)} + \lambda^4\hat{H}^{(3)}\psi_n^{(1)} + \lambda^5\hat{H}^{(3)}\psi_n^{(2)} + \lambda^6\hat{H}^{(3)}\psi_n^{(3)}.$$

Grouping like terms on the left-hand side we can write

$$(\hat{H}^{(0)} + \lambda\hat{H}^{(1)} + \lambda^2\hat{H}^{(2)} + \lambda^3\hat{H}^{(3)})(\psi_n^{(0)} + \lambda\psi_n^{(1)} + \lambda^2\psi_n^{(2)} + \lambda^3\psi_n^{(3)}) =$$

$$\hat{H}^{(0)}\psi_n^{(0)} + \lambda(\hat{H}^{(0)}\psi_n^{(1)} + \hat{H}^{(1)}\psi_n^{(0)}) + \lambda^2(\hat{H}^{(0)}\psi_n^{(2)} + \hat{H}^{(1)}\psi_n^{(1)} + \hat{H}^{(2)}\psi_n^{(0)}) + ... \quad (2.59)$$

We now consider the right hand side of equation 2.58 and simplify it to the second order term

$$(E_n^{(0)} + \lambda E_n^{(1)} + \lambda^2 E_n^{(2)} + \lambda^3 E_n^{(3)})(\psi_n^{(0)} + \lambda\psi_n^{(1)} + \lambda^2\psi_n^{(2)} + \lambda^3\psi_n^{(3)}) =$$

$$E_n^{(0)}\psi_n^{(0)} + E_n^{(0)}\psi_n^{(0)} + \lambda E_n^{(0)}\psi_n^{(1)} + \lambda^2 E_n^{(0)}\psi_n^{(2)} + \lambda^3 E_n^{(0)}\psi_n^{(3)} + \lambda E_n^{(1)}\psi_n^{(0)} + \lambda^2 E_n^{(1)}\psi_n^{(1)} + \lambda^3 E_n^{(1)}\psi_n^{(2)} +$$

$$\lambda^4 E_n^{(1)}\psi_n^{(3)} + \lambda^2 E_n^{(2)}\psi_n^{(0)} + \lambda^3 E_n^{(2)}\psi_n^{(1)} + \lambda^4 E_n^{(2)}\psi_n^{(2)} + \lambda^5 E_n^{(2)}\psi_n^{(3)} + \lambda^3 E_n^{(3)}\psi_n^{(0)} + \lambda^4 E_n^{(3)}\psi_n^{(1)}$$

$$\lambda^5 E_n^{(3)}\psi_n^{(2)} + \lambda^6 E_n^{(3)}\psi_n^{(3)}.$$

Collecting the like-terms we can write

$$\left.\begin{aligned}(E_n^{(0)} + \lambda E_n^{(1)} + \lambda^2 E_n^{(2)} + \lambda^3 E_n^{(3)})(\psi_n^{(0)} + \lambda\psi_n^{(1)} + \lambda^2\psi_n^{(2)} + \lambda^3\psi_n^{(3)}) &= \\ E_n^{(0)}\psi_n^{(0)} + \lambda(E_n^{(0)}\psi_n^{(1)} + E_n^{(1)}\psi_n^{(0)}) + \lambda^2(E_n^{(0)}\psi_n^{(2)} + E_n^{(1)}\psi_n^{(1)} + E_n^{(2)}\psi_n^{(0)}) + ...\end{aligned}\right\} \quad (2.60)$$

Combining these two sides of equation 2.58 (i.e., equation 2.59 and 2.60) we obtain

$$\left.\begin{aligned}\hat{H}^{(0)}\psi_n^{(0)} + \lambda(\hat{H}^{(0)}\psi_n^{(1)} + \hat{H}^{(1)}\psi_n^{(0)}) + \lambda^2(\hat{H}^{(0)}\psi_n^{(2)} + \hat{H}^{(1)}\psi_n^{(1)} + \hat{H}^{(2)}\psi_n^{(0)}) + ..= \\ E_n^{(0)}\psi_n^{(0)} + \lambda(E_n^{(0)}\psi_n^{(1)} + E_n^{(1)}\psi_n^{(0)}) + \lambda^2(E_n^{(0)}\psi_n^{(2)} + E_n^{(1)}\psi_n^{(1)} + E_n^{(2)}\psi_n^{(0)}) + ...\end{aligned}\right\} \quad (2.61)$$

In order for equation 2.61 to be true for all values of λ, it is necessary that the coefficients of λ on both sides of the equation be equal

$$\hat{H}^{(0)}\psi_n^{(0)} = E_n^{(0)}\psi_n^{(0)}. \quad (2.62)$$

$$(\hat{H}^{(0)}\psi_n^{(1)} + \hat{H}^{(1)}\psi_n^{(0)}) = (E_n^{(0)}\psi_n^{(1)} + E_n^{(1)}\psi_n^{(0)}). \quad (2.63)$$

$$(\hat{H}^{(0)}\psi_n^{(2)} + \hat{H}^{(1)}\psi_n^{(1)} + \hat{H}^{(2)}\psi_n^{(0)}) = (E_n^{(0)}\psi_n^{(2)} + E_n^{(1)}\psi_n^{(1)} + E_n^{(2)}\psi_n^{(0)}). \quad (2.64)$$

Rearranging equation 2.63 by collecting like terms

$$\hat{H}^{(0)}\psi_n^{(1)} - E_n^{(0)}\psi_n^{(1)} = E_n^{(1)}\psi_n^{(0)} - \hat{H}^{(1)}\psi_n^{(0)}.$$

and taking a common factor on each term, we can write

$$\psi_n^{(1)}(\hat{H}^{(0)} - E_n^{(0)}) = \psi_n^{(0)}(E_n^{(1)} - \hat{H}^{(1)}). \tag{2.65}$$

Rearranging equation 2.64 and collecting like terms

$$\hat{H}^{(2)}\psi_n^{(0)} - E_n^{(2)}\psi_n^{(0)} + \hat{H}^{(1)}\psi_n^{(1)} - E_n^{(1)}\psi_n^{(1)} = E_n^{(0)}\psi_n^{(2)} - \hat{H}^{(0)}\psi_n^{(2)}.$$

and taking a common factor on each term, we can write

$$\psi_n^{(0)}(\hat{H}^{(2)} - E_n^{(2)}) + \psi_n^{(1)}(\hat{H}^{(1)} - E_n^{(1)}) = \psi_n^{(2)}(E_n^{(0)} - \hat{H}^{(0)}). \tag{2.66}$$

Combining equation 2.62, 2.65 and 2.66 we can write

$$\left.\begin{aligned} &\hat{H}^{(0)}\psi_n^{(0)} + \psi_n^{(1)}(\hat{H}^{(0)} - E_n^{(0)}) + \psi_n^{(0)}(\hat{H}^{(2)} - E_n^{(2)}) + \psi_n^{(1)}(\hat{H}^{(1)} - E_n^{(1)}) = \\ &E_n^{(0)}\psi_n^{(0)} + \psi_n^{(0)}(E_n^{(1)} - \hat{H}^{(1)}) + \psi_n^{(2)}(E_n^{(0)} - \hat{H}^{(0)}) \end{aligned}\right\} \tag{2.67}$$

The first terms on each side of equation 2.67 cancel because of the condition in equation 2.53, so that the remaining terms can be written as

$$\left.\begin{aligned} &\psi_n^{(1)}(\hat{H}^{(0)} - E_n^{(0)}) + \psi_n^{(0)}(\hat{H}^{(2)} - E_n^{(2)}) + \psi_n^{(1)}(\hat{H}^{(1)} - E_n^{(1)}) = \\ &\psi_n^{(0)}(E_n^{(1)} - \hat{H}^{(1)}) + \psi_n^{(2)}(E_n^{(0)} - \hat{H}^{(0)}). \end{aligned}\right\} \tag{2.68}$$

The first term on each side of the equation corresponds to first order correction and the second term on each side corresponds to second order correction to the energy and wavefunction. First we consider the first order correction terms (assuming the second order terms negligible) and write

$$\psi_n^{(1)}(\hat{H}^{(0)} - E_n^{(0)}) = \psi_n^{(0)}(E_n^{(1)} - \hat{H}^{(1)}). \tag{2.69}$$

Multiply both sides of equation 2.69 by $\psi_n^{(0)*}$ and integrate overall space we get:

$$\int (\psi_n^{(0)*}(\hat{H}^{(0)} - E_n^{(0)})\psi_n^{(1)}) \, d\tau = \int (\psi_n^{(0)*}(E_n^{(1)} - \hat{H}^{(1)})\psi_n^{(0)}) \, d\tau.$$

$$\int \psi_n^{0*}\hat{H}^{(0)}\psi_n^{(1)}d\tau - \int \psi_n^{0*}E_n^{(0)}\psi_n^{(1)}d\tau = \int \psi_n^{0*}E_n^{(1)}\psi_n^{(0)}d\tau - \int \psi_n^{0*}\hat{H}^{(1)}\psi_n^{(0)}d\tau . \qquad (2.70)$$

The integral in the first term on the right hand side of equation 2.70 is unity because $\psi_n^{(0)}$ is taken to be normalised, i.e., for any normalised function ψ

$$N\int_{-\infty}^{\infty}\psi^*\psi\,dx = 1.$$

More importantly, the first term on the left side of equation 2.70 is zero, as shown below;

$$\begin{aligned}\int \psi_n^{0*}\hat{H}^{(0)}\psi_n^{(1)}d\tau - \int \psi_n^{0*}E_n^{(0)}\psi_n^{(1)}d\tau &= \int \psi_n^{0*}\hat{H}^{(0)}\psi_n^{(1)}d\tau - E_n^{(0)}\int \psi_n^{0*}\psi_n^{(1)}d\tau \\ &= E_n^{0}\int \psi_n^{0*}\psi_n^{(1)}d\tau - E_n^{(0)}\int \psi_n^{0*}\psi_n^{(1)}d\tau \\ &= 0.\end{aligned}$$

If we substitute the known information in equation 2.70 we can write

$$0 = E_n^{(1)} - \int \psi_n^{0*}\hat{H}^{(1)}\psi_n^{(0)}d\tau ,$$

which we can rearranged to

$$E_n^{(1)} = \int \psi_n^{0*}\hat{H}^{(1)}\psi_n^{(0)}d\tau .$$

We now consider the second order correction terms (assuming the first order terms negligible). First we write the first order wavefunction and second order wavefunction as a linear combination of ground state of other functions

$$\psi_n^{(1)} = \sum_m a_m\psi_m^0 . \qquad (2.71)$$

$$\psi_n^{(2)} = \sum_m b_m\psi_m^0 . \qquad (2.72)$$

Substituting equation 2.72 on the right hand side of equation 2.66, we can write

$$\psi_n^{(0)}(\hat{H}^{(2)} - E_n^{(2)}) + \psi_n^{(1)}(\hat{H}^{(1)} - E_n^{(1)}) = \sum_m b_m \psi_m^0 \ (E_n^{(0)} - \hat{H}^{(0)}), \text{ which simplifies to}$$

$$\psi_n^{(0)}(\hat{H}^{(2)} - E_n^{(2)}) + \psi_n^{(1)}(\hat{H}^{(1)} - E_n^{(1)}) = \sum_m (b_m \psi_m^0 E_n^0 - b_m \hat{H}^{(0)} \psi_m^0).$$

Since $\hat{H}^{(0)}\psi_m^0 = \mathrm{E}^0\psi_\mathrm{m}^0$,

we can write

$$\psi_n^{(0)}(\hat{H}^{(2)} - E_n^{(2)}) + \psi_n^{(1)}(\hat{H}^{(1)} - E_n^{(1)}) = \sum_m (b_m \psi_m^0 E_n^0 - b_m E_0 \psi_m^0).$$

Collecting like terms on the right hand side, we write

$$\psi_n^{(0)}(\hat{H}^{(2)} - E_n^{(2)}) + \psi_n^{(1)}(\hat{H}^{(1)} - E_n^{(1)}) = \sum_m b_m (E_n^0 - E_0)\psi_m^0. \qquad (2.73)$$

If we now substitute equation 2.71 in the second term on the left hand side of equation 2.73 we can write

$$\psi_n^{(0)}(\hat{H}^{(2)} - E_n^{(2)}) + \sum_m a_m \psi_m^0 \ (\hat{H}^{(1)} - E_n^{(1)}) = \sum_m b_m (E_n^0 - E_0)\psi_m^0, \text{ which simplifies to}$$

$$\psi_n^{(0)}(\hat{H}^{(2)} - E_n^{(2)}) + \sum_m a_m (\hat{H}^{(1)} - E_n^1)\psi_m^0 = \sum_m b_m (E_n^0 - E_0)\psi_m^0. \qquad (2.74)$$

If we multiply both sides of equation 2.74 by $\psi_n^{(0)*}$ and integrate overall space we get:

$$\left.\begin{aligned} &\int \psi_n^{(0)}(\hat{H}^{(2)} - E_n^{(2)})\ \psi_n^{(0)*}\, \mathrm{d}\tau + \int \sum_m a_m \psi_m^0 \ (\hat{H}^{(1)} - E_n^{(1)})\psi_n^{(0)*}\ \mathrm{d}\tau = \\ &\int \sum_m b_m (E_n^0 - E_0)\psi_m^0\ \psi_n^{(0)*}\ \mathrm{d}\tau. \end{aligned}\right\} \qquad (2.75)$$

We can expand this expression such that

$$\left.\begin{aligned} &\int \psi_n^{(0)} \hat{H}^{(2)} \psi_n^{(0)*} d\tau - E_n^{(2)} \int \psi_n^{(0)} \psi_n^{(0)*} d\tau \; + \\ &\sum_m a_m \int \psi_m^0 \hat{H}^{(1)} \psi_n^{0*} d\tau - \sum_m a_m \int \psi_m^0 E_n^{(1)} \psi_n^{0*} d\tau \; = \\ &\sum_m b_m (E_n^0 - E_0) \int \psi_m^0 \psi_n^{0*} \, \mathrm{d}\tau, \end{aligned}\right\} \tag{2.76}$$

and taking $E_n^{(1)}$ and $E_n^{(2)}$ outside the integration sign we can further write

$$\left.\begin{aligned} &\int \psi_n^{(0)} \hat{H}^{(2)} \psi_n^{(0)*} d\tau - E_n^{(2)} \int \psi_n^{(0)} \psi_n^{(0)*} d\tau + \sum_m a_m \int \psi_m^0 \hat{H}^{(1)} \psi_n^{0*} d\tau \; - \\ &\sum_m a_m E_n^{(1)} \int \psi_m^0 \psi_n^{0*} d\tau \; = \sum_m b_m (E_n^0 - E_0) \int \psi_m^0 \psi_n^{0*} \, \mathrm{d}\tau. \end{aligned}\right\} \tag{2.77}$$

If we simplify this expression by considering that ψ is normalised and that the different wavefuntions are orthonormal, and therefore satisfy orthonormality condition,

$$\int \psi_m^0 \psi_n^{0*} d\tau \; = \delta_{nm} . \tag{2.78}$$

we note that the right hand side of equation 2.77 can be equated to zero

$$\int \psi_n^{(0)} \hat{H}^{(2)} \psi_n^{(0)*} d\tau - E_n^{(2)} + \sum_m a_m \int \psi_m^0 \hat{H}^{(1)} \psi_n^{0*} d\tau - \sum_m a_m E_n^{(1)} \int \psi_m^0 \psi_n^{0*} d\tau \; = 0,$$

from which, if we apply the orthonormality condition, we can write

$$E_n^{(2)} = \int \psi_n^{(0)} \hat{H}^{(2)} \psi_n^{(0)*} d\tau + \sum_m a_m \int \psi_m^0 \hat{H}^{(1)} \psi_n^{0*} d\tau - \sum_m a_m E_n^{(1)} \delta_{nm} , \tag{2.79}$$

which simplifies to

$$E_n^{(2)} = \int \psi_n^{(0)} \hat{H}^{(2)} \psi_n^{(0)*} d\tau - \sum_m a_m (E_n^{(1)} \delta_{nm} - \int \psi_m^0 \hat{H}^{(1)} \psi_n^{0*} d\tau). \quad (2.80)$$

We let the first term on the right be equal to $\hat{H}_{nn}^2$ and consider only the case when n ≠ m

$$E_n^{(2)} = \hat{H}_{nn}^2 + \sum_{m}{}' a_m \int \psi_m^0 \hat{H}^{(1)} \psi_n^{(0*)} d\tau . \quad (2.81)$$

The prime on the summation sign indicates the omission of the state with n = m

The coefficient a_m is given by the equation [78];

$$a_m = \frac{\hat{H}_{mn}^{(1)}}{E_n - E_m} . \quad (2.82)$$

If we substitute equation 2.82 into equation 2.81 and write the integral term on the right as $\hat{H}_{mn}^1$

$$E_n^{(2)} = \hat{H}_{nn}^2 + \sum_{m}{}' \frac{\hat{H}_{mn}^{(1)}}{E_n - E_m} \hat{H}_{mn}^{(1)}, \quad (2.83)$$

which simplifies to

$$E_n^{(2)} = \hat{H}_{nn}^2 + \sum_{m}{}' \frac{(\hat{H}_{mn}^{(1)})^2}{E_n - E_m}, \quad (2.84)$$

which is the expression for the second order correction to the energy. It is possible in a similar manner to derive the corresponding first and second order correction terms for the wavefunction. However, in this work, we restrict ourselves to the derivation of the first and second order correction terms corresponding to the energy of the system.

2.2.10. Density Functional Theory (DFT)

Density functional theory considers the ground state electron density as the main property to consider in the Schrödinger equation, rather than the wavefunction. The "functional" part of the

name comes from the fact that the energy (E) of the molecule is a function of the electron density (ρ) and the

density is a function of position; in mathematics, a function of a function is known as a functional. Electron density is the measure of the probability density of an electron being present at a specific location and is given through the equation;

$$\rho(r) = \sum_{i=1}^{n} |\psi_i(r)|^2 \ , \tag{2.85}$$

where n is the number of electrons and ψ_i are the wavefunctions (orbitals) of the system of interest. If the summation of the electron density is done overall occupied molecular orbitals the probability density is written as

$$\rho(r) = 2\sum_{i=1}^{n} |\psi_i(r)|^2 \ . \tag{2.86}$$

Electron density determines the Hamiltonian operator, and thus all the properties of the system [86–88]. The overall equation for the energy of the system of an n electron molecule can also be considered to be derived from the Hartree-Fock energy. The Hartree-Fock energy (section 2.2.5) is the sum of kinetic energy (E_T), electron-nucleus attractive potential energy term (E_V) and two terms arising from the electron-electron repulsion terms, which are Coulomb potential energy term of interaction between the charges (E_J) and the exchange energy term (E_k), which is a quantum mechanical correction to the Coulomb energy [78]:

$$E^{HF} = E_T + E_V + E_J + E_k. \tag{2.87}$$

The DFT energy is differs from the HF energy on the last term only, in which the exchange energy term (E_k) is replaced by the exchange/correlation energy term (E_{XC}). In this way, the DFT energy can be written as

$$E^{DFT} = E_T + E_V + E_J + E_{XC}. \tag{2.88}$$

With the exception of the kinetic energy term (that depends on the position), all other terms depend on the total electron density [69]. The kinetic energy term has the form;

$$E_T = \sum_{\mu}^{basis\ functions} \sum_{\nu} \int \phi_\mu(\mathbf{r}) \left[-\frac{1}{2}\nabla^2 \right] \phi_\nu(\mathbf{r})\, d\mathbf{r}\,, \tag{2.89}$$

where $\phi_\mu(\mathbf{r})$ and $\phi_\nu(\mathbf{r})$ are the atomic spinorbitals associated with a single electron and $-\frac{1}{2}\nabla^2$ is the kinetic energy operator. The electron-nucleus attractive potential energy term (E_V) present in equation 2.88 is given by the expression

$$E_V = \sum_{\mu}^{basis\ functions} \sum_{\nu} P_{\mu\nu} \sum_{A}^{nuclei} \int \phi_\mu(\mathbf{r}) \left[-\frac{Z_A e^2}{4\pi\varepsilon_0 \,|\, \mathbf{r} - \mathbf{R_A} \,|} \right] \phi_\nu(\mathbf{r})\, d\mathbf{r}\,, \tag{2.90}$$

where $P_{\mu\nu}$ is the electron density matrix, whose elements involve a product of two molecular orbital coefficients:

$$P_{\mu\nu} = 2 \sum_{i}^{occupied\ molecular\ orbitals} c_{\mu i} c_{\nu i}\ . \tag{2.91}$$

The $\left[-\frac{Z_A e^2}{4\pi\varepsilon_0 \,|\, \mathbf{r} - \mathbf{R_A} \,|} \right]$ term in equation 2.90 is the potential energy operator, with Z being the nuclear charge and $\mathbf{r}$-$\mathbf{R_A}$ is the distance between the nucleus and the electron.

The two-electron Coulomb energy term (which is a measure of the repulsion between two electrons in regions of space defined by a basis set), present in equation 2.88, is given through the expression

$$E_J = \frac{1}{2} \sum_{\mu}^{basis\ functions} \sum_{\nu} \sum_{\lambda} \sum_{\sigma} P_{\mu\nu} P_{\lambda\sigma}\ (\mu\nu \,|\, \lambda\sigma), \tag{2.92}$$

where $(\mu\nu \mid \lambda\sigma)$ are the two-electron integrals ($\phi_\mu(\mathbf{r})$ and $\phi_\nu(\mathbf{r})$ are the atomic orbitals associated with electron 1; $\phi_\lambda(\mathbf{r})$ and $\phi_\sigma(\mathbf{r})$ are the atomic orbitals associated with electron 2), which can be expressed as:

$$(\mu\nu \mid \lambda\sigma) = \iint \phi_\mu(1)\,\phi_\nu(1)\left[\frac{1}{r_{12}}\right]\phi_\lambda(2)\,\phi_\sigma(2)\,d\tau_1\,d\tau_2, \tag{2.93}$$

where $\left[\frac{1}{r_{12}}\right]$ is the repulsion potential energy operator. The last term (E_{XC}) in equation 2.88 is the sum of the exchange $E_X(\rho(\mathbf{r}))$ and correlation functional $E_C(\rho(\mathbf{r}))$ terms;

$$E_{XC}\,(\rho(\mathbf{r})) = E_X(\rho(\mathbf{r})) + E_C(\rho(\mathbf{r})). \tag{2.94}$$

$E_{XC}\,(\rho(\mathbf{r}))$, which is the exchange-correlation energy per particle of a uniform electron gas of density ρ(r), is a function of the electron density ($\rho(\mathbf{r})$) and the gradient of the electron density ($\nabla\rho(\mathbf{r})$);

$$E_{XC}\,(\rho(\mathbf{r})) = \int f(\rho(\mathbf{r}), \nabla\rho(\mathbf{r})...)\,d\mathbf{r}\,. \tag{2.95}$$

It is this term that differentiates the energy obtained from DFT methods from the energy obtained from HF methods. However, this term cannot be evaluated exactly because the form of the functional *f* is not known and therefore it has to be approximated. Different approaches have been developed to solve for the exchange-correlation energy term. The approach utilised to obtain the approximate functional for the exchange-correlation term characterise the type of the DFT method [87, 89]. Below is a brief description of the local density, generalised gradient and hybrid approximation functional methods.

Local Density Approximations (LDA) functionals: The local density approximation (LDA) is the basis of all approximate exchange-correlation functional. This type of approximation makes the assumption that the electronic density slowly varies and that the inhomogeneous density of a solid or molecule can be calculated using the homogeneous electron gas functional model [90]. For the LDA approximation E_{XC} can be written as:

$$E_{XC}[\rho] = \int \rho(r)\ \varepsilon_{\mathrm{XC}}[\rho(r)]\,\mathrm{dr}\,, \tag{2.96}$$

where $\varepsilon_{XC}[\rho(r)]$ is the exchange-correlation energy per electron in a homogenous electron gas of constant density. This equation represents an approximation because in real systems, neither the nuclei nor the electronic charges are uniformly distributed. This type of method can be improved by including the gradient of the density into the functional (because the original definition of the functional f (equation 2.95) includes the gradient of the density); an example of the LDA functionals is the Local Spin Density Approximation (LSDA) functional [91].

Generalized Gradient Approximations (GGA) functionals: This approximation considers the variations in the density by not only accounting for the local density but also by inclusion of the gradient of the density (i.e., first derivative of the density with respect to position) in the functional;

$$\varepsilon_{XC}^{GGA}[\rho(r)] = \varepsilon_{XC}^{LSD}[\rho(r)] + \Delta\varepsilon_{XC}\left[\frac{|\nabla\rho(\mathbf{r})|}{\rho^{4/3}(\mathbf{r})}\right], \tag{2.97}$$

where the second term is a dimensionless reduced gradient and indicates that the density is not uniform but varies slowly. $\varepsilon_{XC}^{GGA}[\rho(r)]$ is usually split into its exchange and correlation contributions which are then approximated separately;

$$\varepsilon_{XC}^{GGA}[\rho(r)] = \varepsilon_{X}^{GGA}[\rho(r)] + \varepsilon_{C}^{GGA}[\rho(r)]\,. \tag{2.98}$$

Some of the earlier gradient exchange functionals such as the Becke exchange (B88, [92]), Coulomb attenuated method (CAM, [86]) and Perdew and Wang's 1991 (PW91, [93]) functionals were developed by having a mathematical form that could correctly reproduce the behaviour of the systems at long range for the energy density and were further developed by in-cooperating a single empirical parameter, the value of which was optimised by fitting the exact known exchange energies of the six noble gas atoms [94]. Some examples of the correlation functionals that are, for instance, stored in Gaussian 09, include the Perdew 86 (P86), Perdew, Burke and Ernzerhof (PBE) functional of 1996 [95] and the correlation functional of Lee, Yang, and Parr (LYP), which includes both local and non-local terms [96]. BP86 functional is an

example of a functional that has both the exchange component and the correlation component (as given in equation 2.98). This functional is a GGA functional combining the Becke 1988 functional and the Perdew 86 correlation functional [97].

Hybrid functionals: Hybrid functionals are formed by mixing the exact (single-determinant) exchange, Ex (obtained from HF calculations) and the approximate E_c contributions from Kohn-Sham orbitals (i.e., from DFT method). Mathematically this can be written as [72];

$$E_{XC\ Hybrid} = E_X^{exact} + E_X^{KS}. \quad (2.99)$$

The link between these two terms of the exchange correlation term is called the adiabatic connection formula (ACF)

$$E_{XC}[\rho] = \int_0^1 E_{ncl}^{\lambda}[\rho]\, d\lambda, \quad (2.100)$$

where λ is the coupling strength parameter and its values range between 0 and 1; E_{ncl} is the non-classical contribution to the electron-electron interaction for the different values of λ. Some examples of the hybrid functionals include the Becker three parameter Lee,Yang and Parr (B3LYP) exchange correlation functional [98], the hybrid functional of Truhlar and Zhao (M06 [99] and M062X [100]).

2.3. Computational study of molecules in solution

The significance of performing calculations in solution is based on the fact that most biological activities are exhibited in physiological media (e.g., polar or non-polar media). The presence of a solvent is important for the functioning of biological systems both directly, by actively participating in biological processes and indirectly, by stabilizing biologically active conformations of proteins and nucleic acid [101]. The properties of the molecule, such as the geometic properties (e.g., bond lengths, bond angles, torsion angles, possible hydrogen bonds) and electronic properties (e.g., charges on the atoms and dipole moments) are not expected to be similar in different media. Therefore it is important to know the properties of the molecule in both *vacuum* and in solvent media. The influence of the solvent on the solute geometry can be

determined by comparing the geometic parameters of the solute molecule *in vacuo* and in the solvent medium. In the next sections, the discussion of the solvation process as well as the possible solvation models that are utilised to study molecules are described in detail.

2.3.1. The solvation process

Solvation is a process in which a solute molecule is transferred from the gas phase to the condensed phase. The insertion of the solute within a solvent necessitates a significant change in the energy of the system overall and on the energy of the individual solute and solvent molecules. Within the isolated solute system, there are solute···solute interactions and within a solvent medium there are solvent···solvent interactions. When the solute is transferred into the solvent medium, the geometry of the solute as well as the geometry of the nearby solvent molecules polarise each other. The polarisation of the solute molecule implies distortion of the geometry of the solute from the optimum gas phase geometry (e.g., lengthening of the bond length and significant changes in some torsion angles within a molecule), implying that the internal energy of the solute is increased with respect to the internal energy of the solute *in vacuo*. Furthermore, some of the solute···solute and solvent···solvent interactions should be broken to allow for the formation of the solute···solvent interactions. The nature and the strength of solute···solvent interactions depend on the nature of both the solute and the solvent [102]. The solute···solvent interactions are electrostatic and non-electrostatic in nature. The electrostatic contribution to the solute···solvent interactions is a result of the interaction between the solute charge distribution and the electric polarization field of the solvent minus the energy contribution due to the cost of polarizing the solute and the solvent [103]. The non-electrostatic nature of the interactions arises from two components; the first component is the van der Waals interactions which can include induction (also known as polarization i.e., which is the attractive interaction between a permanent multipole on one molecule with an induced multipole on another) and dispersion and hydrogen bonding [104, 105]. The dispersion interactions may be a result of favourable dipole···dipole interactions between the solute and the surrounding solvent molecules as well as interactions between induced dipoles in adjacent solvent molecules. When the solute···solvent interactions overcome the solute···solute and solvent···solvent interactions, the structure is considered to be completely relaxed (i.e., the solute is completely dissolved in a solvent). The second component to the non-electrostatic interactions is the cavitation energy, which is the energy required to create a cavity for the insertion of a solute molecule within the solvent medium [102, 106–109]. The solvation process implies an increase in the entropy of the

system whose major contributing factor is the local changes in the arrangement of the solvent molecules as a result of the insertion of the solute molecules [110].

The solvation free energy (ΔG_{solv}) is then expressed as the sum of electrostatic contributions (ΔG_{ele}) and the non-electrostatic contributions ($\Delta G_{non\text{-}ele}$);

$$\Delta G_{solv} = \Delta G_{ele} + \Delta G_{non\text{-}ele}. \quad (2.101)$$

The electrostatic term (ΔG_{ele}) is the difference between the electrostatic potential term in solution (which is a sum of the potential energy between the nuclei and electrons within the solute and the potential energy as a result of polarisation of the solvent and solute) and the electrostatic term of the isolated solute;

$$\Delta G_{ele} = \Delta G_{ele,\,soln} - \Delta G_{ele,\,vac}. \quad (2.102)$$

The non-electrostatic term ($\Delta G_{non\text{-}ele}$) is a sum of dispersion (ΔG_{dis}), repulsion (ΔG_{rep}) and cavitation energy (ΔG_{cav}) terms. If we substitute these terms into equation 2.101, we can write it as

$$\Delta G_{solv} = \Delta G_{ele} + \Delta G_{dis} + \Delta G_{rep} + \Delta G_{cav}. \quad (2.103)$$

2.3.2. Modelling solvent effect: explicit solvation models

The most realistic way to model the solvent effect is to surround the solute with sufficiently large number of solvent molecules in order to get information on bulk solvent effects. However, modelling such a system at a quantum mechanical level requires large computational efforts. In order to overcome this shortcoming, two approaches have been developed to describe the solvation process; explicit solvation models and implicit solvation models.

Explicit solvation models provide a discreet representation of the solvent molecule, where the molecular details of each solvent molecule are considered individually [111, 112]. In this approach, a limited number of solvent molecules are added to specific regions of the molecule in order to simulate the effect of the solvent on the specific regions of the molecular system. For instance, when studying metal···ligand systems, it is necessary that explicit solvent molecules are

included in the coordination sphere because the metal ions are not expected to be "naked" [113, 114]. The number of solvent molecules that can be added depends on the size of the molecule and the specific site of interest on the molecule which is being investigated. The system formed by adding solvent molecules to the central molecules is known as a supermolecular or adduct structure (hence the approach is also sometimes referred to as supermolecular approach). Once the supermolecular structure is prepared, the Schrödinger equation is then solved in order to obtain information on its most favourable geometrical arrangements (i.e., the favourable arrangement of the central solute molecule as well as the most favourable geometrical arrangements of the solvent molecules around the solute molecule). Explicit solvation models give a better description of various aspects such as the explicit solute···solvent interactions [115, 116], for instance the type of hydrogen bond involved (i.e., whether it is intramolecular or intermolecular hydrogen bonding, [102]). However the explicit consideration of the solvent molecules increases the number of atoms present in the system under study, consequently causing an increase in computational time [102, 112].

2.3.3. Modelling solvent effect: implicit solvation models

Implicit solvation models simulates the effect of the solvent on the solute molecule without considering individual solvent molecules, but by considering an overall effect called the *bulk solvent effect*. In these models, the solvent is replaced by a continuum dielectric medium (i.e., a polarisable non-conducting medium); the solute is considered to polarise the dielectric medium and the solvent in turn polarises the solute [117]. The consideration of the solvent molecule as a dielectric medium keeps computational time affordable [118]. There are various models that can be utilized to study solute···solvent effects in a continuum medium. These models include the Onsager models [119], the conductor like screening model [120], the polarizable continuum model [119, 103], isodensity polarizable continuum model [119] and solvation model density (SMD, [103]), The models differ in a number of aspects including [121]:

- size and shape of the solute cavity,
- method of calculating the cavity creation and the dispersion contributions,
- how the charge distribution of solute model is represented,
- whether the solute model is described classically or quantum mechanically.

The paragraphs that follow describe only the features of the SMD model because it is the model that is selected for the study reported in this dissertation.

Continuum solvation model density (SMD) is based on interaction of the charge density of a solute molecule with a continuum description of a solvent molecule [103]. The "D" in the name of the model stands for density to show that the full solute electron density is utilized and the "continuum" explains that the solvent molecule in this model is not considered explicitly but rather as a dielectric medium [103]. In the SMD model, the free energy of interaction between a solute molecule and a solvent molecule is separated into two components, the first component being the bulk-electrostatic contributions and the second component being the non-electrostatic contribution comprising of the cavity-dispersions terms [70, 122].

The bulk-electrostatic contributions to the free energy of solvation in the SMD arise from a self-consistent reaction field (SCRF) treatment which involves the solution of the non-homogenous Poisson equation for electrostatic terms [103, 123], as outlined in the basic integral equation formalism (IEF [124]). The homogenous Poisson equation (inside the cavity) and the Laplacian equation (outside the cavity) for electrostatic term has the form

$$\Delta V = -4\pi\rho, \qquad \text{inside the cavity} \qquad (2.104i)$$

$$\Delta V = 0, \qquad \text{outside the cavity} \qquad (2.104ii)$$

The non-homogeneous Poisson equation as implemented in the IEF approach has the form

$$L_i\, V = -4\pi\rho_{M,} \qquad \text{inside the cavity} \qquad (2.105i)$$

$$L_e\, V = 0, \qquad \text{outside the cavity} \qquad (2.105ii)$$

$$[V] = 0, \qquad \text{on the cavity surface} \qquad (2.105iii)$$

$$[\partial_L\, V] = 0, \qquad \text{on the cavity surface} \qquad (2.105iv)$$

where ρ_M is the charge density of the solute, V is the total electrostatic potential, L is the operator, which is defined with a subscript *i* inside the cavity and subscript *e* outside the cavity. Equation 2.105i corresponds to the non-homogenous Poisson equation.

The SMD model defines the cavity for the solute by superpositions of nuclear-centred spheres and by the use of semi-empirical surface tensions that are utilised to determine the non-electrostatic terms such as cavitation and dispersion-repulsion energies [103]. The non-electrostatic component terms are collectively referred to as the cavity-dispersion solvent-structure term (CDS) and arise from short-range interactions between the solute molecule and the solvent molecule in the first solvation shell.

2.4. Conformational analysis and geometry optimisation

2.4.1. Isolated molecule

The first stage in the study of the molecular properties of a given molecule (both *in vacuo* and in solution) is to identify its conformations. Molecular conformations are the different nuclear arrangements which a molecule can be transformed into by the rotation of one or more geometric parameters (i.e., bond length, bond angle and torsion angles). Conformations play an important role in prediction of not just physico-chemical properties [125–129] but also the biological activity of compounds [129–133]. Different conformers have different energies on the molecular potential energy surface. A molecular potential energy surface is a plot of energy versus the spatial degrees of freedom of the molecule (i.e., x, y and z coordinates in a Cartesian coordinate system or the bond length, bond angle and torsion angle in an internal coordinate system). The different energies of the molecular system are obtained by varying the geometric parameters of the molecule, (i.e., bond lengths, bond angles and torsion angles [126]). The potential energy surface has maxima, minima and saddle points (Figure 2.4). All these points on a potential energy surface are collectively referred to as *stationary points*. A stationary point is one at which the first derivative of the potential energy with respect to each geometric parameter is zero [62]:

$$\frac{\partial E}{\partial R_1} = \frac{\partial E}{\partial A_1} = \frac{\partial E}{\partial D_1} = ... = 0, \tag{2.106}$$

where R represents the bond length parameter, A represents the bond angle parameter and D represents the torsion angle parameter. The partial derivatives are written here rather than the ordinary differential derivatives to emphasize that each derivative is with respect to just one of the variables of which E is a function.

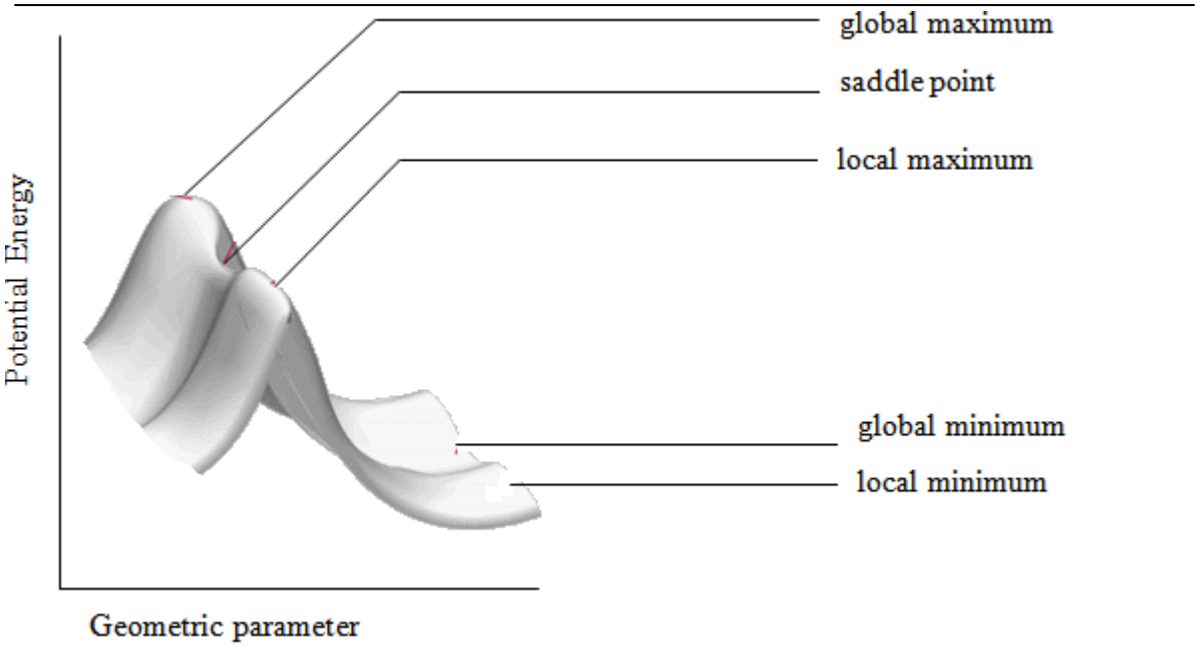

Figure 2.4 Illustration of the stationary points on the molecular potential energy surface [119]. The geometric parameter can be bond length, bond angle or torsion angle.

The minima points correspond to the most stable geometries of the molecule. They are identified through geometry optimisation [119]. Geometry optimisation is the process of finding the arrangement of nuclei for which the potential energy is a minimum (i.e., it is a process of locating local or global minimum for a given molecular system). The optimised input structure(s) are referred to as geometries/conformations of the molecule.

Geometry optimisation analysis on a molecule can only be performed once a basis set has been selected. The procedure initially determines the wavefunctions and the energy corresponding to the given arrangement. It then proceeds to a new geometry, most likely to give a lower energy. The alterations in the conformer continue until a lowest-energy possible geometry, relative to the starting one, is obtained.

Different molecular conformations (geometries) of a given molecule may have different molecular properties and, therefore, they may have different biological activities. The biological activities of a molecule are often associated with the lowest-energy conformers because these are the conformations that the molecule exists in for most of the time. Therefore, it is important to identify all the energetically preferred conformations for the molecular system of interest.

2.4.2. Ligand···metal complex

Once the conformations of a given molecular system are determined, the conformers with relatively low energy are utilized in the preparation of the metal···ligand complexes. The conformer corresponding to the lowest-energy is not necessarily the only conformer associated with the biological activity which is why conformers which may be populated are considered [102], because these are conformers with relative energy of approximately 3.5 kcal/mol. Considering relative energy of ≈ 3.5 kcal/mol ensures that no conformer which might be populated is overlooked.

Once all the conformers that might be populated are determined, the next step is to identify all the electron density (charge density) rich sites in a given conformer. Electron density rich sites are often all the sites in a ligand molecule where there is a high electron density and include such regions as the aromatic rings, multiple bonds (e.g., C=C double bonds and C≡C triple bonds) and lone pair of electrons on heteroatoms (e.g., O or N atoms). The aromatic rings are electron rich centres as a result of the presence of π electrons above and below the ring. The multiple bonds are electron rich centres also because of the presence of π electrons. The heteroatoms are electron rich centres because of the presence of lone pair of electrons that are considered to be further away from the nucleus and therefore can easily be donated to the metal ion.

Transition metal ions are more likely to bind at the electron rich sites of the ligand because they are electron deficient species; they have vacant or partially-filled *d* orbitals. In order to determine the preferred complex, the input structures should be prepared in such a way that the transition metal ion is arranged in the vicinity of the available electron rich sites. Each input structure should have a single metal ion on a given electron rich site. The prepared input structures should then be optimised separately to determine the preferred complex. The preferred complex is the one with the lowest total energy. A comparison of the stability of the different complexes can be determined by estimating the relative energy values with respect to the lowest-energy complex.

2.5. Hydrogen bonding

2.5.1. Relevance of hydrogen bonds in biological systems

A hydrogen bond is an electrostatic attraction between a highly electronegative atom and a hydrogen atom attached to a relatively electronegative atom [134, 135]. It is denoted using the symbol X–H···A, in which the functional group X-H is an electronegative atom (usually oxygen, nitrogen, fluorine etc.) referred to as the 'donor', the dotted sign (···) represents the hydrogen bond and A denotes the 'acceptor' atom.

Hydrogen bonds are known to influence many biological processes [136, 137] and to play a significant role in determining conformational stability of biological molecules [138–140], molecular complexes [141] and crystal structures [142]. In biological systems, hydrogen bonding is responsible for structural features like protein folding or the bonds between the two strands of DNA; the influence of hydrogen bonds on biological activities may range from molecular recognition [143–145], to antitumor activity [146], antioxidant activity [147, 148] and selective binding [145, 149]. Hydrogen bonds also influence physico-chemical properties like chemical shifts, vibrational frequencies, density, dielectric constants and vaporization enthalpy.

Hydrogen bonds are classified into two groups; intramolecular and intermolecular (Figure 2.5). In intramolecular hydrogen bonds, the X and A atoms pertain to the same molecule, while in intermolecular hydrogen bonds the X and A atoms pertain to different molecules of the same or different compounds. Intramolecular hydrogen bonds are important in the stabilisation of the individual conformers of molecules, while intermolecular hydrogen bonds are important in the stabilisation of the condensed phases of pure substances [150] as well as interactions between solvent and solute molecules capable of forming them [151]. Intermolecular and intramolecular hydrogen bonds have also been observed to occur simultaneously, both in solution and in the solid state, for several systems [152].

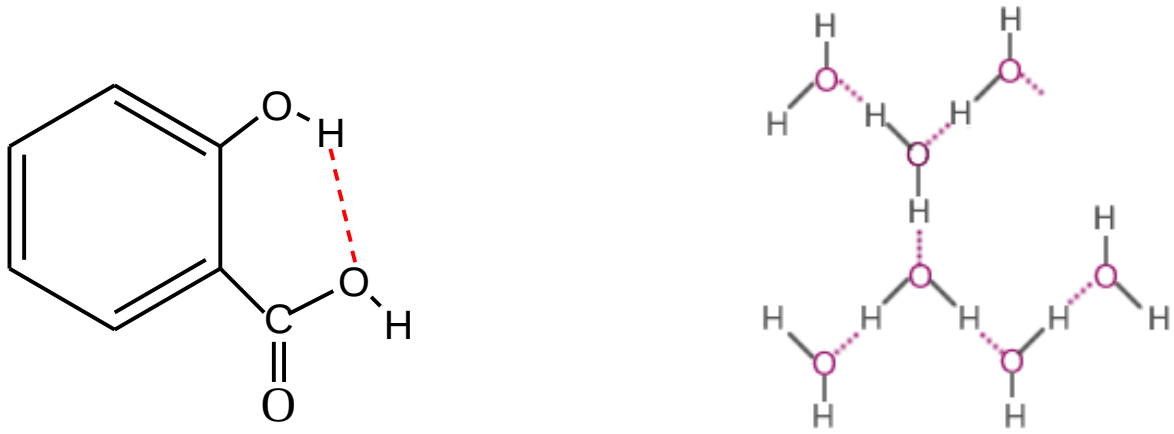

(a) (b)

Figure 2.5 Schematic representations of a) intramolecular hydrogen bond in salicylic acid and b) intermolecular hydrogen bonds between the water molecules. The hydrogen bond is denoted with the dotted lines.

2.5.2. Strong, moderate and weak hydrogen bonds

The energy of hydrogen bonds spans a broad range of values [153], to an extent that there are hydrogen bonds that are so strong that they resemble covalent bonds in most of their properties, others that are so weak that their energy is close to the range of van der Waals interactions and a variety of intermediate situations. For this reason, the classification of the hydrogen bonds as strong, moderate and weak does not imply sharp borderlines between the various categories, but it rather has "border regions" and, therefore, it should not be taken as a restrictive one [153, 154]. Strong hydrogen bonds have energies ranging from 15 kcal/mol and above, with the H-bond length being 1.2–1.5 Å [155]. Moderate hydrogen bonds have energy ranging between 4 and 15kcal/mol and bond length 1.5–2.2 Å [155]. Weak hydrogen bonds have energy less than 4kcal/mol and the bond length is 2.2–3.2 Å [155]; their directionality is less marked than for strong hydrogen bonds; they include some bifurcated and multi-centred hydrogen bonds as well as unconventional hydrogen bonds. For instance, the typical strength of π-hydrogen bonds is ≤ 5kcal/mol [156].

2.5.3. Unconventional hydrogen bonds

Unconventional hydrogen bonds are examples of weak hydrogen bonds involving less polar groups. These include [157]:

- hydrogen bonds with unconventional hydrogen donors like C–H, or unconventional acceptors such as π charge distributions. In both cases, the H atom plays the role of the electron acceptor.
- dihydrogen bonds involving two H atoms, one of which accepts electrons and the other provides them. The bond is denoted as X–H·····H–Y, where X–H is the proton donating bond and Y is usually boron or a transition metal. The hydrogen bonded to X donates electrons; while the H atom bonded to Y accept electrons.
- inverse hydrogen bonds, i.e., hydrogen bonds in which the H atom is partially negative. This occurs in particular complexes involving hydrides with highly electron deficient atoms, such as LiH, or BeH_2. Then the H atom acts as a bridge between two partially positive atoms.

The most relevant types of unconventional hydrogen bonds in the selected chalcone derivatives are the one involving unconventional hydrogen donors like C–H. C–H···O unconventional hydrogen bonds are known to play significant roles (which may sometimes become dominant [158–161]) in determining molecular conformations, in several chemical and biological processes [138] including molecular recognition [162], in the stabilization of inclusion complexes [163, 164] and in the activity of biological macromolecules [165].

2.6. Population analysis

Systems containing metal complexes usually have distribution of charge density between the central ligand molecule and the metal cation. One approach that is often utilised in the understanding of the distribution of the charge density within the metal-ligand complex system is the use of the population analysis schemes [94, 166]. The principle of population analysis studies is to accurately model the magnitude of the partial charge and its location within a molecule [94, 166]. There are various methods that are utilized in population analysis; these methods include the popular Mulliken analysis, the Löwdin population analysis, the natural bond order (NBO) analysis and the atom in molecules (AIM) analysis [167, 168] schemes.

The subsections that follow will provide more information on these methods, reflecting on how these methods function and some of their advantages and disadvantages.

2.6.1. Mulliken and Löwdin population analysis schemes

The Mulliken analysis method is one of the oldest methods utilised in the study of molecular charge distribution and is a default method for estimation of partial atomic charges in several quantum chemical software programs, such as Gaussian program, Spartan [169] and Mutliwfn [170]. This method is based on the linear combination of atomic orbitals obtained from wavefunction of a given system [171, 172]:

$$N_{\mathrm{A}} = \sum_{\mu \in A} N_{\mu}^{A} \ , \tag{2.107}$$

where N_{μ}^{A} is the atomic orbital contributions to the molecular orbital.

The Mulliken analysis is advantageous for utilisation in the determination of charge distribution in molecular systems because [30, 94, 166]:

- it is computationally affordable;
- it works well for comparing changes in partial charge between two different geometries when the same size basis set is used.

However, the Mulliken population analysis scheme has several caveats that include the strong dependence of the results from the level of theory (basis sets or kind of calculation method selected) and the occurrence of inappropriate occupation numbers [80, 171]. As a result of these limitations, other alternative methods are explored which are able to improve on some of the shortcomings of the Mulliken analysis method.

The Löwdin population analysis method is constructed with the objective of improving upon the weaknesses of the Mulliken method (i.e., to correct the instability of predicted charges with increasing the basis set size). The correction is achieved by transforming the atomic orbital basis functions (equations 2.107) into an orthonormal set of basis functions prior to the population analysis. The transformation of atomic basis functions into orthonormal basis functions guarantees that they do not overlap (i.e., the overlap integral for the orthonormal wavefuntions is zero, [173]). The Löwdin population analysis scheme is more stable than the Mulliken population analysis with changes in the basis set, although with very large basis sets it may also have problems [174].

2.6.2. Natural Bond Orbital (NBO)

NBO analyses transpose the quantum-mechanical wavefunction into a more natural Lewis structure. This approach introduces the concept of natural orbitals and occupation-based symmetric orthogonalization [175–177]. In this scheme, the total density is differentiated into localized contributions associated with individual atoms giving rise to natural charges and further into 1-center (lone pairs) and two-center (bonds) pieces. NBO also allows one to determine hybridization of the atomic orbitals contributing to a particular bond.

The NBO analysis has been incorporated into quantum chemical packages like Gaussian, Gamess, Q-Chem, Spartan, etc. In the Gaussian program calculation of NBO include the command "pop=nbo". This command gives information about the natural population analysis (NPA) and the atomic-atomic spin densities. The advantages of the NBO include [175, 177]:

- ability to differentiate between the orbitals that will overlap to form a bond and those that are too near the core of an atom to be involved in bonding,
- smaller dependence on the basis set in comparison to Mulliken analysis

The disadvantages of the NBO population analysis include [175, 177]:

- being more computationally expensive than both Mulliken population analysis and Löwdin population analysis,
- predicting larger charges than several other population analysis methods, so like Mulliken charges NPA is best used for comparing differences rather than determining absolute atomic charges.

2.6.3. Atoms in molecule (AIM) analysis scheme

The atom in molecules (AIM) analysis is a population analysis scheme which provides a universal partitioning of the electron density function (ρ (r)) into fragments of the molecule [178, 179]. This population analysis scheme is often utilised to assess the formation of intermolecular interactions such as hydrogen bonds and such weak interactions as dative bonding and metal–ligand interactions [180–184]. The AIM analysis scheme is based on the topological analysis of the electron density distribution [180]. It is therefore a method in which chemically significant information is obtained from the electron density [185]. In topological analysis, the critical points (CP) are those points where the first derivative of the electron density with respect

to position is zero [186]. The characteristics of these points are determined by the second derivative of ρ and the Hessian matrix of ρ [187]. The Hessian is the (3 x 3) symmetric matrix of partial second derivatives.

$$\begin{vmatrix} \frac{\partial^2 \rho}{\partial x^2} & \frac{\partial^2 \rho}{\partial x \partial y} & \frac{\partial^2 \rho}{\partial x \partial z} \\ \frac{\partial^2 \rho}{\partial y \partial x} & \frac{\partial^2 \rho}{\partial y^2} & \frac{\partial^2 \rho}{\partial y \partial z} \\ \frac{\partial^2 \rho}{\partial z \partial x} & \frac{\partial^2 \rho}{\partial z \partial x} & \frac{\partial^2 \rho}{\partial z^2} \end{vmatrix} \qquad (2.108)$$

In order to obtain the three principal axis of curvature (i.e., the second derivative of ρ), the Hessian matrix is diagonalised, which results in setting the off-diagonal terms to zero. The sum of the diagonal terms is called the Laplacian of ρ and denoted as $\nabla^2(\rho)$;

$$\nabla^2(\rho) = \frac{\partial^2 \rho}{\partial x^2} + \frac{\partial^2 \rho}{\partial y^2} + \frac{\partial^2 \rho}{\partial z^2} . \qquad (2.109)$$

At a critical point, the eigenvalues of the Hessian matrix are all non-zero real values. Each critical point is characterised by two parameters, namely the *rank* and the *signature*; the rank is defined as the number of non-zero eigenvalues at a given critical point and the signature is defined as the total sum of the signs of the eigenvalues. For topologically stable critical points, the rank has a value of 3 [179, 186]. This means that there are four possible critical points [187], namely the nuclear critical point (3, -3), ring critical point (3, +1), bond critical point (3, -1) and the cage critical point (3, +3). In the (3, −3) nuclear critical point (NCP), all three eigenvalues of the Hessian matrix are negative. This point corresponds to a local maximum. The ring critical point (RCP) has only one eigenvalue of the Hessian matrix negative, and two eigenvalues of the Hessian matrix being positive. The bond critical point (BCP) has two negative eigenvalues for the Hessian matrix and one positive value for the Hessian matrix [188]. The cage critical point (CCP) point cage point has all its eigenvalues for the Hessian matrix positive.

The number of critical points (CP) found for a particular molecular system must be in agreement with the Poincare–Hopf rule, which states that the total number of the nuclear critical points (*n*), the bond critical points (*b*), the ring critical points (*r*) and cage critical points (*c*) is equal to 1 and can be represented mathematically as [186];

$$n - b + r - c = 1. \tag{2.110}$$

Beside the valuable information from bond critical point properties, AIM analysis provides information on the local energy density properties (potential, kinetic and total density energies) for the bonded interactions. Such information can be obtained if we consider the ground state energy of a molecular system of interest. The potential energy density, V(**r**), is the average effective potential field experienced by a single electron at point *r* in a multi-electron system [189]. If we consider that the antisymmetric many-electron wavefunction is represented as Ψ, then the gradient kinetic energy density (G(**r**)) is given by the expression

$$\mathrm{G}(\mathbf{r}) = \frac{\hbar^2}{2m} N \int \nabla\Psi^* \cdot \nabla\Psi d\tau \ . \tag{2.111}$$

The Laplacian of the charge density is related to the local contributions to the total energy through the expression [178]

$$\frac{\hbar^2}{4m} \nabla^2 \rho(\mathbf{r}) = 2\, G(\mathbf{r}) + V(\mathbf{r}). \tag{2.112}$$

The kinetic energy term is always positive while the potential energy term is always negative, taking these precautions into consideration it can be seen from equation 2.112 that at the BCP, interactions for which $\nabla^2\rho < 0$ are dominated by a local reduction of the potential energy and interactions for which $\nabla^2\rho > 0$ are dominated by a local excess in the kinetic energy. In chemical systems, $\nabla^2\rho(r)$ provides a measure of the local charge concentration (indication of bond formation) or depletion. The Laplacian ($\nabla^2\rho$) of the electron density provides information on the type of bond formed between the atoms of interest in a given molecular system. For instance, in the case of metal···ligand complexes, $\nabla^2\rho$ provides information on the type of bonding (e.g., covalent, ionic or dative bonding) between a given atom of the central ligand molecule and the metal cation. A negative value of the Laplacian indicates that the bonds between a given atom in

the ligand molecule and the cation are covalent in nature while a positive value indicates closed-interactions such as hydrogen bonds or dative bonds [190, 191].

Equation 2.112 does not show a clear representation of the relationship between the total energy and the individual contributions. A better comparison of the kinetic and potential energy densities contributions to the total energy is provided by the Cremer and Kraka expression [192];

$$H_{BCP} = G_{BCP} + V_{BCP}. \tag{2.113}$$

The values of H and its components (i.e., G and V) provide valuable information on the nature of the chemical bond. For instance, these parameters are often utilised to determine the strength of a particular bond [193, 194]. For stronger bonds such as the covalent bonds V is usually negative and relatively large, while G is positive and H is negative. In such systems, both interacting atoms are sharing electrons, which are considerably localized in the inter-nuclear space between the atoms of interest. Strong bonds are characterised by negative values of $\nabla^2\rho$ and are referred to as shared interactions. Weak bonds, such as H-bonding interactions, are characterised as closed-shell interactions. In this type of bonding, H has a positive value and is close to zero, G has positive value and V has negative value. However, the positive value of G predominates over the negative value of V, since the electrons are energetically less stable in the region between two closed-shell systems.

The relationship between the electron density at BCP and the bond strength has been found for strong bonds (e.g., covalent bonds), and for weak interactions, such as metal–ligand interactions and hydrogen bonding [193, 195]. The potential energy density estimated in BCP has large values because the electrons are relatively stable energetically in the inter-nuclear region. Closed-shell interactions are also accompanied by $\nabla^2\rho > 0$ estimated at the corresponding BCP. The metal-ligand interaction has characteristics that represent the mixture of shared and closed-shell interactions. For instance, the value of H is usually negative and close to zero, as found for shared interactions, but with a positive value of $\nabla^2\rho$, as found for closed-shell interactions.

2.7. Antioxidant properties: a theoretical perspective

Antioxidants are molecules that are able to slow down or alternatively prevent the oxidation of macromolecules (e.g., DNA) in biological systems. In the oxidation process, free radicals may be produced which start chain reactions that damage cells; antioxidants act as the body's protective mechanism by terminating these chain reactions through their ability to remove free radical intermediates [196]. Antioxidants are found in various natural sources including plant roots [197–199], stem [200–202] and leaves [203–205] and in foods such as fruits, vegetables and meats [196, 206]. There are various mechanisms which antioxidants utilise as a mode of action in the biological processes; these include [207–210]:

- free radical scavenging,
- lipid peroxidation inhibition;
- metal chelation.

2.7.1 Free radical scavenging

Free radicals are species with unpaired electrons and are unstable and highly reactive. In order to attain stability, free radicals tend to react with other species which are able to provide electrons to the radicals. When they react with cellular components in biological systems they are likely to cause damage, which results in several degenerative diseases such as cancer, aging, neurodegenerative diseases, heart-attacks etc. The free radical scavenging mechanism is often discussed through four mechanisms, the hydrogen atom transfer (HAT, [211−213]), the single electron transfer (SET, [214]), the single electron transfer followed by proton transfer (SET-PT, [215]) and the sequential proton loss electron transfer (SPLET, [216]) mechanisms. The HAT, SET-PT and SPLET mechanisms depend on the presence of free phenolic OH group(s). The HAT mechanism is related to the ability of the molecule to donate its phenolic H atom to the radical species:

$$R^{\bullet} + ArOH \rightarrow RH + ArO^{\bullet} \qquad (2.114)$$

The termination of further chain reactions depends on the stability of the neutral radical intermediates ($ArO^{\bullet}$ radical species) formed. This means that factors enhancing the stability of the $ArO^{\bullet}$ radical species, such as the resonance delocalisation of the electron within the aromatic ring and the formation of the quinine structure, increase the antiradical activity. The ability of phenolic antioxidants to donate a hydrogen atom is mainly governed by the homolytic O−H bond dissociation enthalpy (BDE).

The SET mechanism is governed by the capacity of an antioxidant compound to transfer an electron and reduce any other compound including metal ions and radical species. In the case of antioxidant reactions involving radical species, the antioxidant compound (ArOH) transfers a single electron to the radical species ($R^{\bullet}$):

$$R^{\bullet} + ArOH \rightarrow ArOH^{\bullet+} + R^{-} \quad (2.115)$$

Relative reactivity in SET mechanism is primarily determined by adiabatic ionisation potential (AIP) value [217, 218] of the reactive functional group. The lower the AIP value, the more favourable the electron transfer reaction [213, 219].

The single electron transfer followed by proton transfer (SET-PT, [214]) is a two-step reaction mechanism. In the first step a phenolic antioxidant molecule reacts with the free radical giving rise to the cationic radical form of the phenolic antioxidant and an anionic form of the radical.

$$R^{\bullet} + ArOH \rightarrow ArOH^{\bullet+} + R^{-} \quad (2.116)$$

This reaction is a thermodynamically significant step of this two-step mechanism. In the second step the cationic radical form of the phenolic antioxidant decomposes into a phenolic radical and a proton.

$$ArOH^{\bullet+} \rightarrow ArO^{\bullet} + H^{+} \quad (2.117)$$

The numerical parameters related with the SET-PT mechanism are the Adiabatic Ionization Potential (AIP) for the first step and Proton Dissociation Enthalpy (PDE) for the second step.

The sequential proton loss electron transfer reaction is also a two-step reaction mechanism. In the first step the phenolic antioxidant dissociates into an anionic form and proton,

$$ArOH \rightarrow ArO^{-} + H^{+} \quad (2.118)$$

In the second step, the ions created in the first reaction react with the free radical giving rise to the radical form of the phenolic antioxidant as well as a neutral molecule.

$$ArO^- + X^\bullet + H^+ \rightarrow ArO^\bullet + XH \quad (2.119)$$

The numerical parameters related with this mechanism are the Proton Affinity (PA), for the first reaction step, and Electron Transfer Enthalpy (ETE) for the second step.

2.7.2. Lipid peroxidation inhibition

Lipid peroxidation is the radical chain oxidation of unsaturated fatty acids, sterols and their esters in biological systems. Studies have found that lipid peroxidation is a consequence of toxic metabolites (e.g. CCl_4) that produce highly reactive radical species, disruption of the intracellular membranes and cellular damage [220]. Lipid peroxidation proceeds by a free-radical mediated chain reaction that includes initiation, propagation and termination reactions. If we denote a lipid molecule as R-H and the reactive radical species as $ln^\bullet$, the various stages of lipid peroxidation can be written as;

Initiation	$R\text{-}H + ln^\bullet \rightarrow R^\bullet + lnH$
Propagation	$R^\bullet + O_2 \rightarrow ROO^\bullet$
	$ROO^\bullet + R\text{-}H \rightarrow ROOH + R^\bullet$
Termination	$R^\bullet + R^\bullet \rightarrow$ non-radical products

The termination stage is achieved when two free radicals conjugate each other (mutual termination) or by addition of chain-breaking antioxidant. In this way, lipid peroxidation mechanism is governed by the ability of the antioxidant molecule to inhibit a free radical from extracting electrons from the cell membrane of lipids (e.g., unsaturated fatty acids) in biological systems [221].

2.7.3. Metal chelation mechanism

The metal chelation mechanism is governed by the ability of the antioxidant molecule to reduce the transition metal ion (by donating electrons to the metal cation) and forming a stable metal-ligand complex. This process can be represented by the expression:

$$M^{n+} + L \leftrightarrows [M^{(n-1)+} \cdots L^{\bullet+}] \quad (2.120)$$

The formation of the complex structure, as a result of the interaction of the antioxidant with the transition metal ion, prevents the metal ion (e.g., Fe(II), Fe(III), Cu(II),..) from participating in free radical generation. While the metal ions could be toxic in nature, their complexes with chelating agents may be less toxic in nature.

The interaction between the metal ion and the ligand can be described in terms of the number of positions for which the metal is binding to the ligand, what is referred to as dentate attachment (Figure 2.6). The metal ion can have a single position of attachment to the ligand and this is referred to as monodentate arrangement, an example of a monodentate ligand is ammonia. The ligand can have two interaction sites with the metal, and this is referred to as bidentate; an example of a bidentate ligand is ethylenediamine, where the metal may have several positions for interaction with the ligand molecule – this is referred to as multi- or poly-dentate attachment. An example of a multidentate ligand with tridentate attachment is tripyridyl.

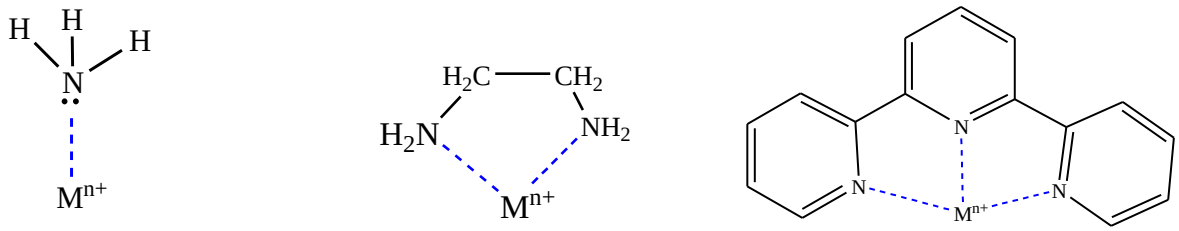

monodentate ligand **bidentate ligand** **multi-dentate ligand**

Figure 2.6 Illustration of the formation of metal···ligand complexes through the mono, bi and tridentate ligands.

Metal ions have the ability to induce reactive oxygen species resulting in the depletion of antioxidant cell defences and this has a consequence in the disruption of the pro-oxidant/antioxidant balance in tissue, modifications to DNA bases, enhanced lipid peroxidation, and changes in calcium and sulphydryl homeostasis [222]. Some examples of biological reactions through which metal ions are known to cause the generation of free radical species is the Fenton reaction and the Haber–Weiss cycle reactions. The metal ions (e.g., Fe(II) and Cu(II) ions) catalyse the Fenton reaction to produce hydroxyl radicals [223]:

$$Fe^{2+}(Cu^{+}) + H_2O_2 \leftrightarrows \quad Fe^{3+}(Cu^{2+}) + OH^{-} + {}^{\bullet}OH \tag{2.121}$$

$$Fe^{3+}(Cu^{2+}) + AscH^{-} \rightarrow Fe^{2+}(Cu^{+}) + Asc^{\bullet-} + H^{+} \tag{2.122}$$

The $Fe^{3+}(Cu^{2+})$ ions, which are biologically inactive forms of the ions, can be recycled back to $Fe^{2+}(Cu^{+})$ through interaction with cellular reductants such as ascorbate ($AscH^{-}$) and NADH (equation 2.118). Therefore, in the presence of excess biological peroxides (such as H_2O_2, which form naturally during cellular respiration [224]), the reaction can be considered catalytic, leading to the production of excess free OH radicals which can result in lipid peroxidation, protein modification and DNA damage [67]. The chelating agents may sequestrate metal ions and potentially inhibit the biologically metal-dependent Fenton reactions.

Superoxide ($O_2^{-\bullet}$) radicals are able to reduce aqueous Fe^{3+} or Cu^{2+} to Fe^{2+} or Cu^{+} ions;

$$O_2^{-\bullet} + Fe^{3+}(Cu^{2+}) \rightarrow O_2 + Fe^{2+}(Cu^{+}) \tag{2.123}$$

the reduced form of Fe^{3+} or Cu^{2+} ions are then available for reactions with hydrogen peroxide (H_2O_2) in a Fenton reaction (equation 2.117). A combination of the Fenton reaction and the reduction of Fe^{3+} or Cu^{2+} by superoxide (equation 2.119) give rise to the net Haber–Weiss cycle reaction;

$$O_2^{-\bullet} + H_2O_2 \rightarrow \quad O_2 + OH^{-} + {}^{\bullet}OH \quad . \tag{2.124}$$

The Haber–Weiss reaction is therefore associated with the generation of toxic free hydroxyl radicals from the less reactive superoxide and hydrogen peroxide that could be generated enzymatically [223].

Transition metal ions (i.e., the Fe(II) and Fe(III) cations) are present at low concentration levels in biological systems and it has been suggested that the Haber–Weiss reaction may account for the *in vivo* generation of the highly reactive •OH [225].

One of the approaches that is utilised to prevent metal ions from inducing oxidative damage to body cells or tissues is by increasing the cells antioxidant defences through endogenous supplementation of antioxidant molecules [226]. Most natural phenolic compounds are known to have high antioxidant activities and are increasingly utilised as antioxidant supplements. One of the reasons for their utilisation as antioxidant is because of their ability to chelate/coordinate free transition metal ions found in biological systems, thereby preventing metal ions from participating in free radical generation [227–230].

CHAPTER 3

COMPUTATIONAL APPROACHES

3.1. Selection of the computational method

This chapter provides an explanation of the computational approaches utilised in the investigation of the antioxidant property of selected chalcone derivatives. As described in chapter 2, the study of molecular systems requires a selection of suitable basis sets, suitable functionals and suitable computational methods, which are expanded enough to take into consideration the important features of the molecular system under study. The different computationally methods have been discussed in section 2.2 of chapter 2. These methods include the Hartree-Fock method, post–Hartree Fock methods such as the Møller–Plesset perturbation theory (MP2) and the density functional theory (DFT). The criteria in the selection of the method utilised is based on the fact that the selected method has to give a good compromise in being both computationally available and giving significantly accurate results (i.e., results that are comparable with studies that have already been reported for similar biological systems). For this reason the Hartree-Fock and MP2 methods were considered not suitable for this work, because the Hartree-Fock methods do not take into consideration electron correlation effects [60]. Although they are computationally affordable, their lack of consideration of electron correlation makes them unsuitable for use in the work reported in this dissertation; the description of the interaction between a ligand and a metal ion requires inclusion of electron correlation effects. The use of MP2 method, which is known to include correlation effects [60, 61], in this study is also not feasible because these methods are computationally expensive for investigations of medium to large size molecules (i.e., molecules with more than 20 atoms). Therefore, to have a better assessment of the antioxidant property of the selected chalcone derivatives, the DFT method was utilised throughout this study; the selection of the DFT method is based on two reasons [60]:

- it is less expensive because it scales better than both HF and MP2 methods,
- it includes correlation effects and can describe well many features of complex molecules, including the geometry and the electronic properties.

3.2. Preparation of the input structures for the isolated ligands

Input structures of the isolated ligands (butein, homobutein, kanakugiol and pedicellin) were prepared using GaussView5 program and the schematic representations were drawn using the ChemOffice package in the UltraChem 2010 version [231] for both the neutral and deprotonated species. The π-conjugation of the C7=C8 double bond to benzene ring B requires that the aliphatic chain lies on the same plane as the plane of benzene ring B; the conjugation of C7=C8 double bond to the carbonyl C=O group requires that the C=O lie on the same plane as the plane of the C7=C8 double bond. Therefore, although the selected ligands have a number of rotatable single bonds (i.e., butein and homobutein both have 7 rotatable bonds while kanakugiol and pedicellin both have 8 rotatable bonds respectively); the number of possible rotations leading to low-energy conformers is limited to such arrangements as can result in the formation of intramolecular hydrogen bonds, minimisation of steric effects between neighbouring OCH_3 groups and planar arrangement in accordance with the π conjugation nature of aromatic ring A and ring B, C7=C8 double bond and C=O group in the 2-propen-1-one aliphatic chain. Therefore, the preparation of the input structures took into consideration these three factors. For all four ligands, input structures were prepared in which the number of possible intramolecular hydrogen bonds present were maximised and steric hindrances between neighbouring OCH_3 groups (in kanakugiol and pedicellin) were minimised. In order to maximise the number of intramolecular hydrogen bonds and to minimise the steric effects, input structures were prepared by rotation of the C–O bonds in the aromatic rings and the rotation of the C1′–C9 bond. Input structures corresponding to the rotation of the C1′-C9 were meant to determine the preferred orientation of the O9 carbonyl atom with respect to the plane of ring A.

Inputs structures corresponding to the rotation of the C–O bonds in butein were prepared considering the rotation of the C2′–O2′ bond (corresponding to the C3′–C2′–O2′–H2″ torsion angle), the C4′–O4′ bond (corresponding to the C3′–C4′–O4′–H4″ torsion angle), the C4–O4 bond (corresponding to the C3–C4–O4–H4″ torsion angle) and the C3–O3 bond (corresponding to the C2–C3–O3–H3″ torsion angle). Similarly, input structures for homobutein were prepared through rotation of the C2′–O2′ bond (corresponding to the C3′–C2′–O2′–H2″ torsion angle), the C4′–O4′ bond (corresponding to the C3′–C4′–O4′–H4″ torsion angle), the C4–O4 bond (corresponding to the C3–C4–O4–C4″ torsion angle) and the C3–O3 bond (corresponding to the C2–C3–O3–C3″ torsion angle). Preparation of the kanakugiol input structures involved the rotation of the C2′–O2′ (corresponding to the C3′–C2′–O2′–H2″ torsion angle), C3′–O3′ bond

(corresponding to the C4′–C3′–O3′–C3″ torsion angle), the C4′–O4′ bond (corresponding to the C5′–C4′–O4′–C4″ torsion angle), the C5′–O5′ bond (corresponding to the C6′–C5′–O5′–C5″ torsion angle) and the C6′–O6′ bond (corresponding to the C5′–C6′–O6′–C6″ torsion angle) and pedicellin input structures were prepared by rotation of similar bonds as in kanakugiol.

Inputs structures corresponding to the rotation of the C–C bond in the 2-propen-1-one aliphatic chain corresponded to the rotation of the C9–C8 bond (C1′–C9–C8–C7 torsion angle); two types of input structures were generated as a result of this rotation, structures with the bent chain (C1′–C9–C8–C7 torsion angle of ≈ 0) and structures with the non-bent chain (C1′–C9–C8–C7 torsion angle of ≈180).

The input structures for the deprotonated species considered the optimised conformer of the neutral species as the starting structure. Each input structure was prepared by removal of a single phenolic proton before optimisation. Previous studies have shown that metal chelation mechanism is more effective situations in which multidendate coordiantion is achieved. Therefore, it is interesting to consider sites at which a removal of the proton will still results in multidendate coordianation of the Fe^{n+} ion. In line with this, butein has three phenolic OH protons that can be deprotonated, which are H2′, H3″ and H4″ protons. Homobutein has two phenolic OH protons, which are H2′ and H4″. The deprotonation of kanakugiol corresponds to the removal of the phenolic H2′ proton.

3.3. Optimisation of the input structures for the isolated ligands

Geometry optimisations on the isolated ligands were carried out without consideration of the symmetry constraints. The 6-31+G(d,p) basis set was utilised for the geometry optimisations while the 6-311+G(2d,p) basis set was utilised for single points calculations on already optimised conformers. The single point calculations were performed with the aim of improving final energies on all optimised conformers. The selection of the 6-31+G(d,p) basis set is based on the fact that it is considered a standard basis set and is therefore able to describe main group elements efficiently. The calculations were performed utilising the DFT/B3LYP and DFT/BP86 method. The two functionals were selected for this work because they have been utilised in many theoretical investigations of molecular systems [232–235]. Frequency calculations were performed, at the same level of calculations as the geometry optimisation, on fully optimised conformers, to determine the nature of the stationary points. The study was performed *in vacuo*

and in water solution. Similar computational methods were considered for the study in water solution as to those *in vacuo*. The study in water was meant to mimic the environment in biological systems, where these compounds are likely to interact with biological free transition metal ions. Solvent effects on the optimised conformers were described using continuum solvation model density SMD model (section 2.3.3). Geometry optimisation calculations on the input structures were performed using the Gaussian09 program [236].

3.4. Input structures for the ligand···Fe^{n+} complexes

The lowest-energy conformers (for either the neutral or deprotonated species) of the selected chalcone derivatives were utilised in the preparation of the inputs for the ligand···Fe^{n+} complexes. The preparation of the inputs took into consideration possible sites on the ligands where interactions with the Fe^{n+} cation would be likely to occur; the possible sites on the ligand are known as the electron rich centres. The electron rich centres on the ligands were identified as the *keto* group (because of the presence of lone pair of electrons on the O9 atom), the O2′H2′ hydroxyl group, the π system of the two aromatic ring A and B, the methoxy groups (because of the presence of lone pair of electrons on these centres) and the C7=C8 multiple bond. Each Fe^{n+} cation was then coordinated between two neighbouring electron rich centres in order to form a bidentate or multi-dentate complex; the coordination positions for the Fe(II) and Fe(III) cations on the ligand are referred to as reactive sites. The possible reactive sites (section 1.3) include the hydroxyl–*keto* site, methoxy–*keto* site, hydroxyl–methoxy site, methoxy–methoxy site, methoxy–α,β-unsaturated site and the aromatic rings site.

Input structures for the micro-hydrated complexes of butein and homobutein were prepared from the corresponding optimised non-hydrated ligand···Fe complex (in which the ligand is the deprotonated species). The four water molecules were added in the vicinity of the coordinated Fe^{n+} cations in order to complete the octahedral arrangement requirement for the hydrated Fe^{n+} cations [113]. This investigation was performed only for butein and homobutein because the calculation with explicit water molecules on kanakugiol and pedicellin were considered to be too computationally expensive to be affordable by our current computational capability. It is however envisaged that the results of the study on butein and homobutein may be considered transferrable to other chalcone derivatives.

3.5. Optimisation of the ligand···Fe^{n+} complexes

Geometry optimisation on the ligand···Fe^{n+} input structures were performed without considering symmetry constraints. The main group elements; C, H and O atom were described using the 6-31+G(d,p) basis set (as a reasonable compromise between result accuracy and computational affordability) and the Fe^{n+} cations were described using the LANL2DZ basis set. The "6-31+G(d,p) + LANL2DZ" combination has been extensively utilised and found efficient in the assessment of the energetic properties of various ligand–metal complexes [113, 227, 230].

The B3LYP and BP86 functionals were selected together for the study of the complexes because they have been utilised in the study of the isolated ligand. The selection of the B3LYP and BP86 functionals was also meant to assess the ability of the hybrid and non-hybrid density functional based methods in the estimation of the antioxidant properties for the selected chalcone derivatives. These functionals have been found to provide adequate information in the study of other metal–ligand complexes with implication on the antioxidant properties [113, 227, 228, 230, 237].

Single point calculations on the optimised complexes were performed using the 6-311+G(2d,p) basis set (on all the atoms of the complex molecule) with the aim of improving final energies of the complexes. Solvent effects on the properties of the geometries and energies were considered using the continuum solvation model density (SMD). All calculations were performed with Gaussian09 and optimised isolated conformers as well as ligand···metal complexes were drawn using GaussView5 program.

3.6. Estimation of the interaction energies

The ligand···Fe^{n+} interaction energy with the bare Fe^{n+} cation was estimated using the equation:

$$E_{inter} = E_{L\cdots M}{}^{n+} - E_M{}^{n+} - E_{L,\,iso} \qquad (3.1)$$

where $E_{L\cdots}M^{n+}$ is the total energy of the optimised complex, $E_M{}^{n+}$ is the total energy of the isolated Fe^{n+} cations, and $E_{L,\,iso}$ is the total energy of the isolated ligand molecule.

The interaction energy for the complexes involving the hydrated Fe^{n+} cation was estimated using the equation:

$$E_{inter} = E_{L\cdots}M^{n+} - (E_{L,\,iso} + E_M{}^{n+}{}_{,\,iso} + E_{4aq,\,iso}) \quad (3.2)$$

where $E_{L\cdots}M^{n+}$ is the total energy of the optimised complex, $E_M{}^{n+}$ is the total energy of the isolated Fe^{n+} cations, and $E_{L,\,iso}$ is the total energy of the isolated ligand molecule and $E_{4aq,\,iso}$ is the total energy of four isolated water molecules.

The binding energy of the complexes is then estimated as the negative of the interaction energy estimated in equation 3.1 and equation 3. 2.

$$\Delta E_{binding} = -\Delta E_{inter} \quad (3.3)$$

However, after complexation the conformer utilised in the preparation of the complexes undergoes deformation. Therefore, the binding energy estimated using equation 3.3 contains deformation energy (E_{def}) of the ligand molecule. E_{def} was estimated as the energy difference between the energy of the ligand in the complex ($E_{L,\,complex}$) minus the energy of the isolated ligand (i.e., optimised conformer ($E_{L,\,iso}$)).

$$E_{def} = E_{L,\,com} - E_{L,\,iso} \quad (3.4)$$

$E_{L,\,com}$ for each complex was estimated by removing the Fe^{n+} cation and running single point energy calculation on the ligand structure [227, 238]. In this way, the binding energy that is free of deformation energy is estimated as

$$\Delta E'_{binding,} = -(E_{inter} - E_{def}) \quad (3.5)$$

The greater the computed value of the binding energy, the stronger the affinity of Fe^{n+} cation to bind to the ligand [227, 238]. All energies obtained were converted from Hartree to kcal/mol using the 1 Hartree = 627.509 kcal/mol conversion factor.

3.7. NBO and AIM population analysis

Natural Bond order (NBO) analysis and atom in molecule (AIM) population analysis schemes were utilised in the investigation of the electron density transfer, the spin density, the strength of the bonds and the type of bonding between the metal and the ligand in the ligand···Fe^{n+} complexes. Natural population analysis (NPA) charges were determined from the NBO calculations, using the "pop=nbo" keywords in the route section during the optimisation procedure with the Gaussian09 program.

The atom in molecules (AIM) analysis was performed using the AIMAll program [239]. The number of critical points (CP) for the systems under study has to be in agreement with the Poincare–Hopf rule (which is explained in chapter 2). The following parameters of the bond critical point (BCP) were analysed, the electron density (ρ) and its Laplacian ($\nabla^2\rho$), the total energy density of electrons (H), and its two components, the Lagrangian kinetic electron density (G) and the potential electron density (V). The total energy density, H, was estimated as the sum of the kinetic electron density and potential energy density [192]:

$$H_{BCP} = G_{BCP} + V_{BCP}. \quad (3.6)$$

CHAPTER 4

RESULTS AND DISCUSSION: ANTIOXIDANT PROPERTIES OF BUTEIN AND HOMOBUTEIN

4.1. Introduction

This chapter provides results and discussion on the antioxidant properties (from the metal chelation perspective) of butein and homobutein, the two simplest chalcone derivatives selected in this study. The results *in vacuo* are presented first followed by the results in water solution. The results *in vacuo* are reported first because they provide valuable information necessary for further steps of the study. Within each media, the results on the isolated butein and homobutein ligands, for both the neutral and deprotonated species are reported first followed by the results of the complexes of the ligands with the Fe^{n+} cations. The results of the isolated ligands are reported first because the study on the complexes depends on the information obtained from the study of the isolated ligands (i.e., isolated conformers of the ligands were used in the preparation of the complexes). The results on butein are reported before the results on homobutein because by presenting butein first it becomes easier to investigate the influence of the methoxy substituent in homobutein on the antioxidant property. The study on the two compounds is inter-related, a comparison of the results on the complexes of butein and homobutein with either Fe(II) or Fe(III) cations is discussed in the text, where necessary, without introducing a specific section. At the end of the chapter a section is given where a comparison is made between the results obtained with the different computational approaches selected for this work.

Conformational stability is discussed in terms of the relative energy (ΔE, kcal/mol) among the conformers of a given ligand. The stability of the complexes of butein···Fe^{n+} and homobutein···Fe^{n+} are also discussed in terms of the relative energy; the ability of the ligand to coordinate the Fe^{n+} cations is discussed in terms of metal ion affinity (MIA). Final energies were obtained by running single point calculations on the already optimised conformers and complexes therefore, results obtained with the 6-311+G(2d,p) basis set are utilised for discussions throughout the chapter.

The results reported in this chapter (and in the next chapter) also include the geometrical properties (e.g., metal···ligand bond distances) and electronic properties (e.g., partial atomic charges and spin density). The discussion on the partial charges on the atoms provides information on the oxidation state of the Fe^{n+} cation in the complexes. Data from spin density and orbital occupancy are expected to provide information on the nature of the electronic distribution in the complex molecule. The discussion on the differences in the bond lengths between the Fe(II) and the Fe(III) as well as the discussion on the electron density and related properties (such as Laplacian of the electron density) may provide information on the type of interaction involved between the ligand and the cation (i.e., whether the interactions are covalent or ionic in nature). The presentation of the results on the geometrical properties will be discussed where necessary throughout the chapter without introducing a specific section. All the bond lengths, charges, spin densities and electron density properties reported in the text are obtained from DFT/B3LYP calculation results with the 6-31+G(d,p) basis set unless indicated otherwise.

Naming of the conformers and complexes: The naming for the conformers of butein and homobutein is such that the letters B and hB are utilised to denote butein and homobutein respectively, followed by the Arabic number to indicate the different conformers. Conformers that do not have the first hydrogen bond (i.e., the H-bond involving the O9 atom and the O2′ atom) are denoted with the acronym noHB1 while conformers that do not have the second hydrogen bond (i.e., the H-bond at the catechol moiety) are denoted as noHB2. The same pattern utilised for the neutral species is adopted for the deprotonated species, however the acronym "an" is used to indicate deprotonation and the Arabic number is utilised to indicate the different possible conformers. The naming of the complexes of the ligands with the Fe^{n+} cations involves the name of the conformer from which it was obtained followed by the atom(s) to which the Fe^{n+} cation is coordinated, with the oxidation state of the cation indicated in round brackets. For instance, the B-1noHB1-O2′-Fe(II)-O9 complex implies that the B-1noHB1 conformer was utilised in the preparation of the complex and that the Fe^{n+} cation of oxidation state +2 is coordinated at the O2′ and O9 reactive site. The naming pattern utilised for complexes with neutral butein and homobutein ligands has been adopted in the naming of the deprotonated species however the acronym “an” is utilised to denote deprotonation.

4.2. Results *in vacuo*

4.2.1. Conformational stability and geometries for the butein conformers

The *in vacuo* optimised conformers are shown in Figure 4.1 and their corresponding relative energy values (ΔE, kcal/mol) are reported in Table 4.1. A total of 12 conformers were obtained. The lowest-energy conformers are those stabilised by the presence of intramolecular hydrogen bonds (i.e., B-1, B-2 and B-3); this result is in agreement with the fact that intramolecular hydrogen bonding plays a crucial role in stabilising conformations (Chapter 2). The results further imply that conformers are better stabilised by the presence of both the first intramolecular hydrogen bond and the second intramolecular hydrogen bond as opposed to the presence of only one intramolecular hydrogen bond (i.e., the higher the number of intramolecular hydrogen bonds the greater is the stability of the conformer). For instance, the ΔE gap between B-1 and B-1-noHB2 pair of conformers corresponds to 3.931 kcal/mol which supports the fact that the more intramolecular hydrogen bonds present in a conformer the better the conformational stability. Among the first three conformers of butein (i.e., B-1, B-2 and B-3) the ΔE gap between the conformers is negligibly small (< 1 kcal/mol) and in all these conformers both intramolecular hydrogen bonds are present. The minimal difference in the ΔE value of these conformers suggests that they may be considered to co-exist *in vacuo*. The major difference in the geometric features of the first three conformers is related to the orientation of the hydroxyl groups which suggests the orientation of the substituent group has minimal effect on conformational stability. A comparison of the B-3 and B-3noHB1 conformers suggests that the removal of the first intramolecular hydrogen bond corresponds to relative energy of 14.454 kcal/mol. This result further suggests the latter conformer cannot be considered to exist *in vacuo* (because its energy is too high for the conformer to be considered populated). Conformers which corresponds to the removal of either the first or the second intramolecular hydrogen corresponds to large relative energies such that these conformers are considered to not exist *in vacuo*. Removal of the first intramolecular bond corresponds to an energy range of 14.454–14.964 kcal/mol and the removal of the second intramolecular hydrogen bond corresponds to 3.931–4.503 kcal/mol.

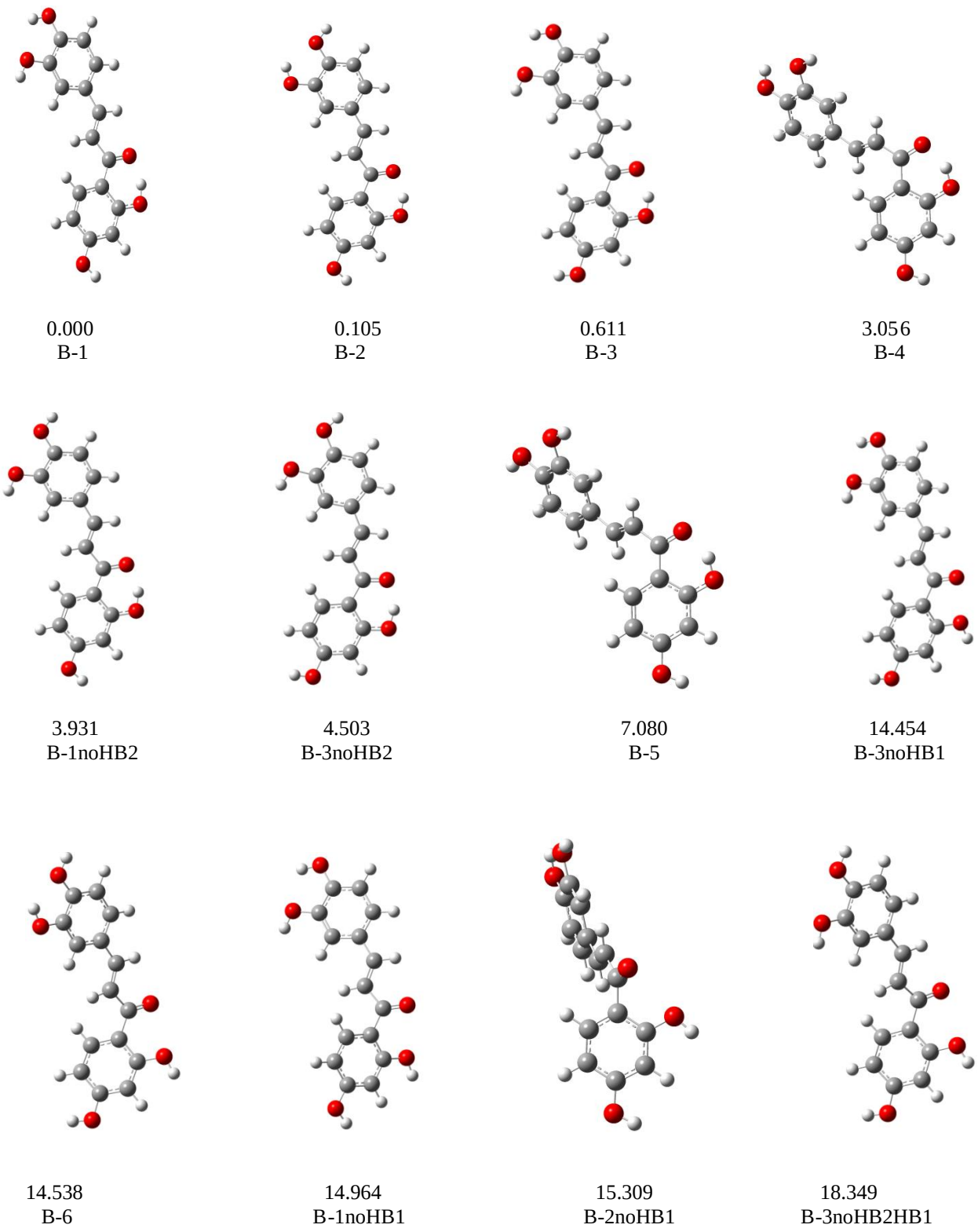

Figure 4.1 B3LYP/6-31+G(d,p) optimised conformers for neutral butein arranged in order of increasing relative energy (ΔE, kcal/mol). B3LYP/6-311+G(2d,p)//B3LYP/6-31+G(d,p) relative energy results. Similar geometries were obtained using the BP86/6-31+G(d,p) calculation method.

Table 4.1 *In vacuo* relative energy values (ΔE, kcal/mol) for the neutral conformers of butein

Conformer	*A*[a]		*B*[b]	
	total energy (Hartree)	ΔE (kcal/mol)	total energy (Hartree)	ΔE (kcal/mol)
DFT/B3LYP results				
B-1	-955.0038798	0.000	-955.2415803	0.000
B-2	-955.0037070	0.108	-955.2414131	0.105
B-3	-955.0027050	0.737	-955.2406068	0.611
B-4	-954.9988635	3.148	-955.2367096	3.056
B-1noHB2	-954.9972074	4.186	-955.2353167	3.931
B-3noHB2	-954.9961008	4.881	-955.2344050	4.503
B-5	-954.9920295	7.436	-955.2302970	7.080
B-3noHB1	-954.9802830	14.807	-955.2185461	14.454
B-6	-954.9801423	14.895	-955.2184122	14.538
B-1noHB1	-954.9794951	15.301	-955.2177333	14.964
B-2noHB1	-954.9787955	15.741	-955.2171858	15.309
B-3noHB2HB1	-954.9736717	18.955	-955.2123389	18.349
DFT/BP86 results				
B-1	-955.0104938	0.000	-955.2502046	0.000
B-2	-955.0100632	0.270	-955.2498194	0.242
B-3	-955.0093082	0.744	-955.2492520	0.598
B-4	-955.0055362	3.111	-955.2453590	3.041
B-1noHB2	-955.0041888	3.956	-955.2442717	3.723
B-3noHB2	-955.0030678	4.660	-955.2433538	4.299
B-5	-954.9920295	11.587	-955.2302970	12.492
B-3noHB1	-954.9839196	16.676	-955.2242155	16.308
B-6	-954.9835380	16.915	-955.2238623	16.530
B-1noHB1	-954.9831456	17.161	-955.2234042	16.817
B-2noHB1	-954.9824361	17.606	-955.2227718	17.214
B-3noHB2HB1	-954.9776762	20.593	-955.2183383	19.996

[a] Results obtained using the 6-31+G(d,p) basis set
[b] Single point results using the 6-311+G(2d,p) basis set, starting from the optimised geometries.

B-4, B-5 and B-2noHB1 are formed as a result of the rotation of the C7–C8 bond in B-1, B-1noHB2 and B-1noHB1 respectively, so that the C1′–C7–C8–C9 torsion angle is nearly 0°. The results suggest that the orientation in which the C1′–C7–C8–C9 torsion angle is nearly 180° is favoured compared to the orientation in which the C1′–C7–C8–C9 torsion angle is nearly 0°. Moreover, the energy difference among the pair of conformers suggests that it is higher (≈ 3 kcal/mol) when the first intramolecular hydrogen bond is present, as seen in the B-1 & B-4 and B-1noHB2 & B-5 pairs, than when the first intramolecular hydrogen bond is absent, as seen in the B-1noHB1 and B-2noHB1 pair (where the energy difference is 0.345 kcal/mol). The energy difference between B-1 and B-4 conformers and between B-1noHB2 and B-5 conformers may be related to the off-plane arrangement of the O9 atom in the conformer in which the C1′–C9–C8–C7 torsion angle is nearly 0°; for instance, the C2′–C1′–C9–O9 torsion angle is ≈ 0° in B-1 and −13.1° in B-4.

The off-plane arrangement of the O9 atom implies significant elongation in the first intramolecular hydrogen bond (it is 1.591 Å in B-1 and 1.635 Å in B-4).

The optimised conformers of the deprotonated butein ligand are shown in Figure 4.2 and the corresponding relative energies are reported in Table 4.2. Butein has three possible sites for deprotonation, namely H2′, H3″ and H4″. The lowest-energy conformer (B-2-an) corresponds to the deprotonation at the O4 site. It is characterised by the formation of the intramolecular hydrogen bond between the deprotonated O4 atom and the neighbouring O3H3″ phenolic group.

It is also possible to assess the ease with which the proton can be removed from butein by investigating the deprotonation energy (i.e., the energy required to remove a proton from the starting conformer); the higher the deprotonation energy the more difficult it is to remove the proton at a particular site and the lower the protonation energy, the easier it is to remove that proton from a particular site. If for simplicity sake we consider that the electronic energy of the proton to be zero (i.e., a proton does not contain an electron), then we can estimate the protonation energy as the energy difference between the deprotonated and the neutral butein. The protonation energy (kcal/mol) as a result of the removal of the H2′, H3″ and H4″ protons in B-1noHB1, B-1 and B-2 conformers is 341.696, 329.128 and 322.029 respectively, which indicates that the phenolic proton that is easily removed is H4″ in B-2. Therefore, both the deprotonation energy and the relative energy values indicate that O4 is the preferred site for deprotonation.

The ΔE energy gap between B-2-an and the rest of the deprotonated conformers of butein is significantly large (with energy range of 6.994–36.292 kcal/mol). Application of the Boltzmann population analysis to the relative energy of all the deprotonated conformers suggests that all other deprotonated conformers, with the exception of B-2-an, may not exist *in vacuo*.

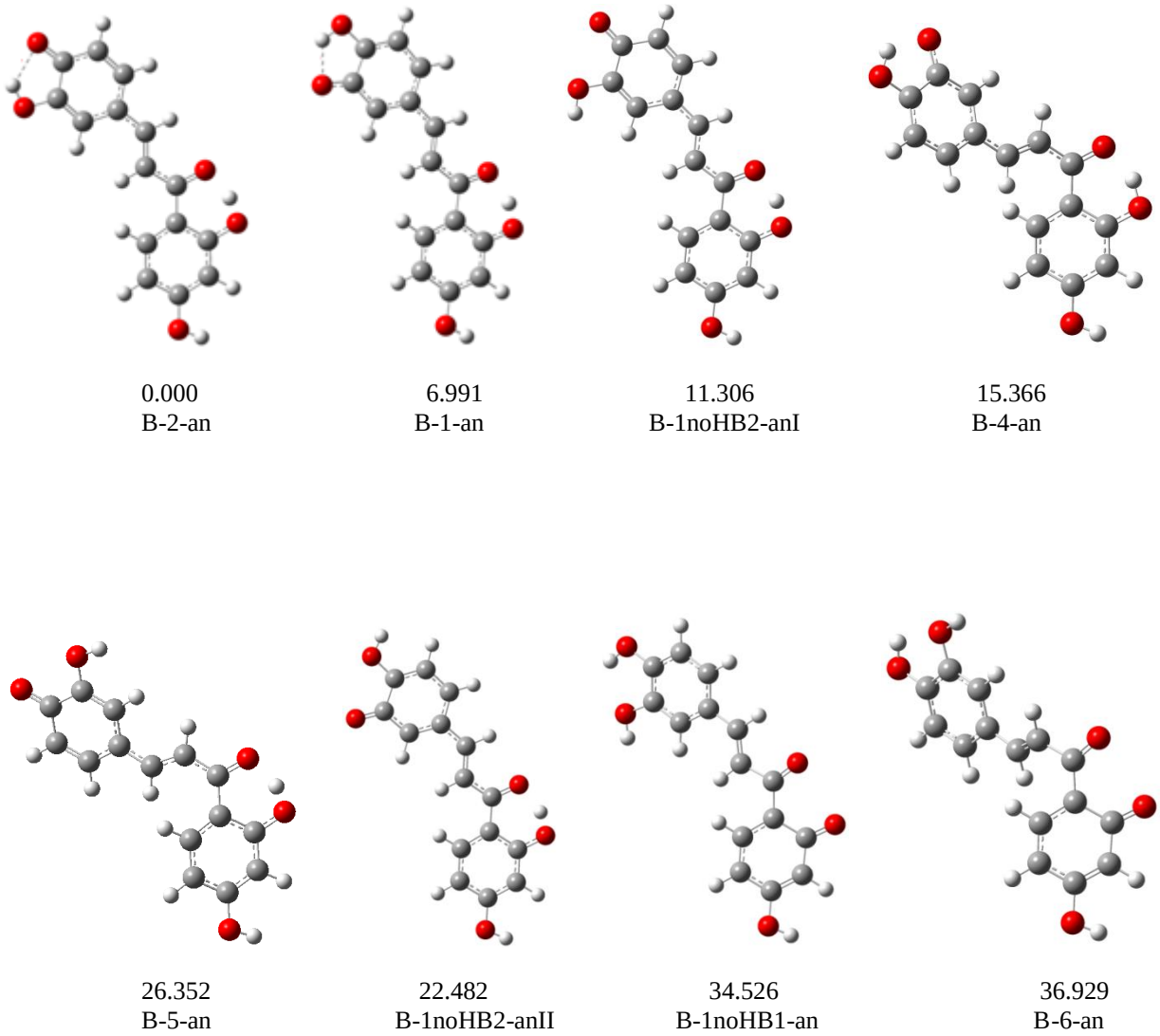

Figure 4.2 B3LYP/6-31+G(d,p) optimised conformers for deprotonated butein arranged in order of increasing relative energy (ΔE, kcal/mol). B3LYP/6-311+G(2d,p)//B3LYP/6-31+G(d,p) results. Similar geometries were obtained using the BP86/6-31+G(d,p) calculation method.

Table 4.2 *In vacuo* relative energy values (ΔE, kcal/mol) for the deprotonated conformers of butein

Conformer	*A*[a]		*B*[b]	
	total energy (Hartree)	ΔE (kcal/mol)	total energy (Hartree)	ΔE (kcal/mol)
DFT/B3LYP results				
B-2-an	-954.4907948	0.000	-954.7282262	0.000
B-1-an	-954.4796480	6.995	-954.7170805	6.994
B-1noHB2-anI	-954.4726196	11.405	-954.7102082	11.306
B-4-an	-954.4660713	15.514	-954.7037386	15.366
B-1noHB2-anII	-954.4546761	22.665	-954.6923995	22.482
B-5-an	-954.4483095	26.660	-954.6862199	26.359
B-1noHB1-an	-954.4356455	34.607	-954.6732052	34.526
B-6-an	-954.4328948	36.333	-954.6703918	36.292
DFT/BP86 results				
B-2-an	-954.5065722	0.000	-954.7458832	0.000
B-1-an	-954.4969017	6.068	-954.7362142	6.067
B-1noHB2-anI	-954.4876032	11.903	-954.7269364	11.889
B-4-an	-954.4815315	15.713	-954.7208277	15.732
B-1noHB2-anII	-954.4699756	22.965	-954.7095033	22.829
B-5-an	-954.4639083	26.772	-954.7035148	26.587
B-1noHB1-an	-954.4450458	38.608	-954.6845026	38.517
B-6-an	-954.4424430	40.242	-954.6818259	40.197

[a] Results obtained using the 6-31+G(d,p) basis set
[b] Single point results using the 6-311+G(2d,p) basis set, starting from optimised geometries

4.2.2. Relative stability and binding energies for butein···Fe^{n+} complexes formed from neutral butein and bare Fe^{n+} cations

The optimised structures of the butein···Fe^{n+} complexes are shown in Figure 4.3 for the DFT/B3LYP method and Figure 4.4 for the DFT/BP86 method; the corresponding relative energy values (ΔE, kcal/mol) are reported in Table 4.3. The stability of the chelate ring formed usually follows the order 4<< 5 > 6 > 7 or larger [240], however, when the ring formed contains conjugated double bonds, the six-member ring may be more stable than the five member ring. Among the butein···Fe^{n+} complexes with the neutral butein ligand the most preferred coordination site for the Fe^{n+} cation is the hydroxyl–*keto* site (the complexes are B-1noHB1-O2′-Fe(II)-O9 and B-1noHB1-O2′-Fe(III)-O9). The stability of the lowest-energy complexes may be related to the formation of the six membered chelate ring. The bond distance (Å) values between the Fe^{n+} cation and the ligand in the lowest-energy complex is 1.836 and 1.821 for O9···Fe^{2+} and O9···Fe^{3+} bonds respectively and 2.045 and 2.067 for O2′···Fe^{2+} and O2′···Fe^{3+} respectively.

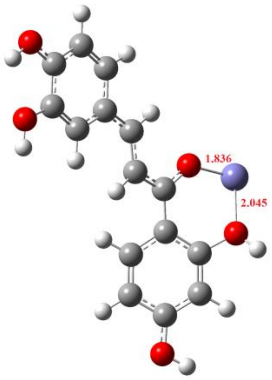

0.000
B-1noHB1-O2′-Fe(II)-O9

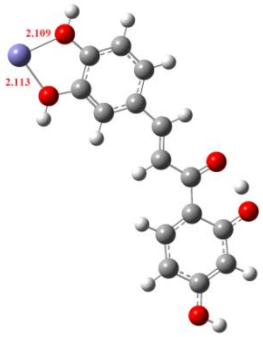

13.449
B-1noHB2-O3-Fe(II)-O4

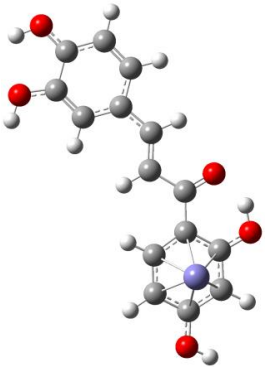

17.106
B-1-ring-Fe(II)-A

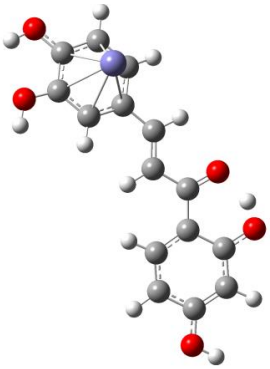

23.584
B-1-ring-Fe(II)-B

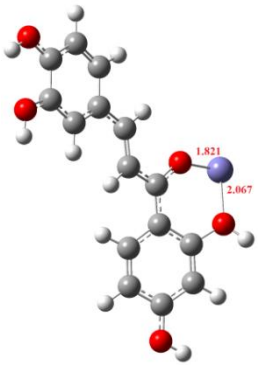

0.000
B-1noHB1-O2′-Fe(III)-O9

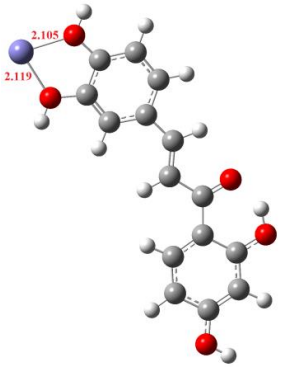

30.174
B-1noHB2-O3-Fe(III)-O4

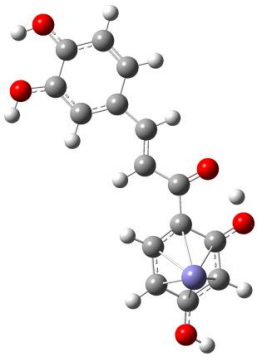

38.118
B-1-ring-Fe(III)-A

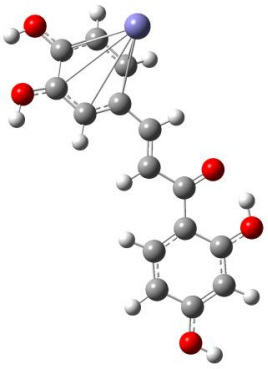

40.676
B-1-ring-Fe(III)-B

Figure 4.3 B3LYP/6-31+G(d,p) optimised butein···Fe^{n+} complexes (arranged in order of increasing relative energy (ΔE, kcal/mol)) formed from neutral butein and bare Fe^{n+} cations B3LYP/6-311+G(d,p)//B3LYP/6-31+G(d,p) results *in vacuo*. The bond length between the cation and the ligand are reported in Å.

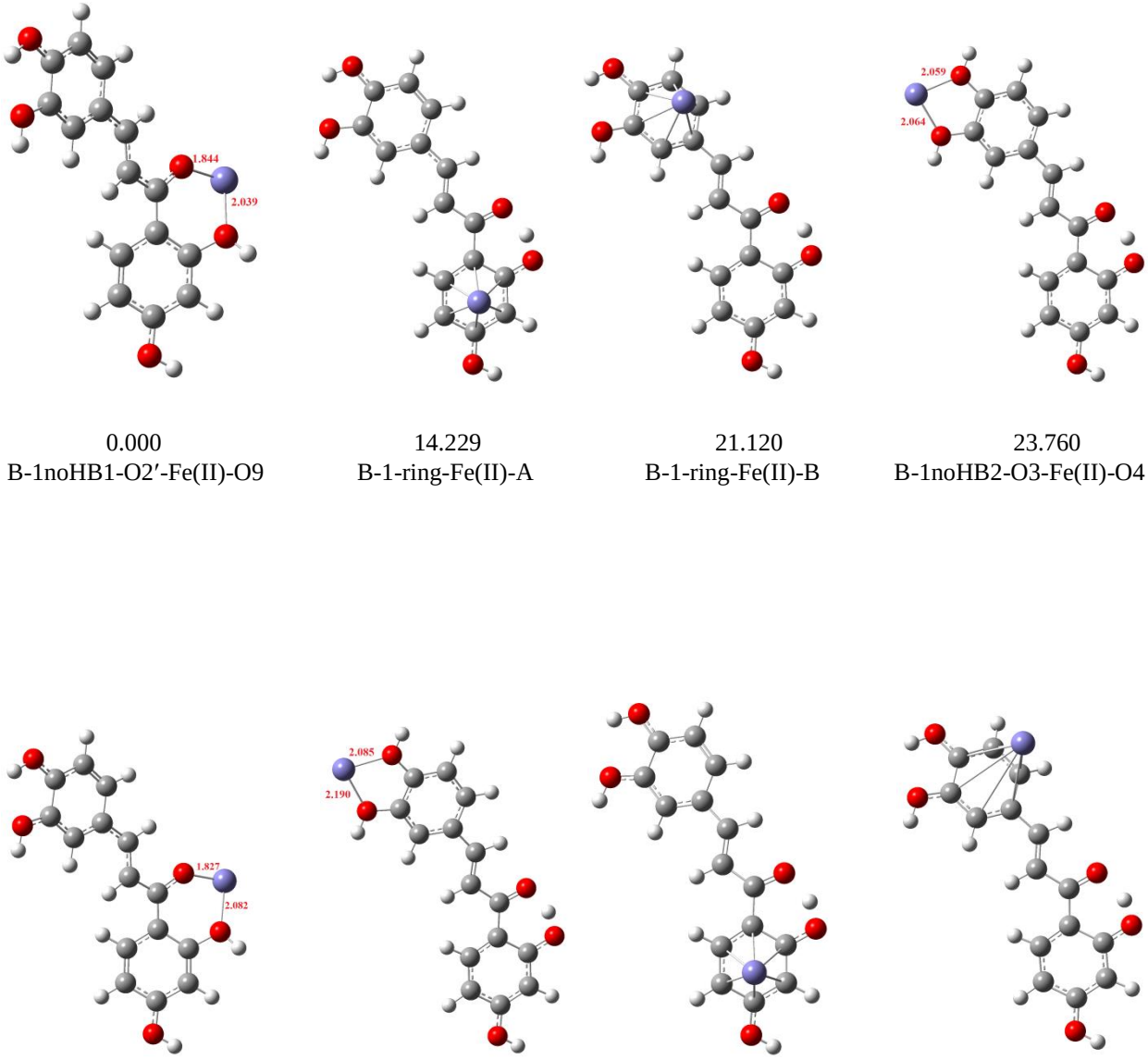

0.000
B-1noHB1-O2′-Fe(II)-O9

14.229
B-1-ring-Fe(II)-A

21.120
B-1-ring-Fe(II)-B

23.760
B-1noHB2-O3-Fe(II)-O4

0.000
B-1noHB1-O2′-Fe(III)-O9

22.377
B-1noHB2-O3-Fe(III)-O4

27.831
B-1-ring-Fe(III)-A

33.677
B-1-ring-Fe(III)-B

Figure 4.4 BP86/6-31+G(d,p) optimised butein···Fe^{n+} complexes (arranged in order of increasing relative energy (ΔE, kcal/mol)) formed from neutral butein and bare Fe^{n+} cations. BP86/6-311+G(d,p)//BP86/6-31+G(d,p) results *in vacuo*. The bond length between the cation and the ligand are reported in Å.

Table 4.3 *In vacuo* relative energy values (ΔE, kcal/mol) for butein···Fe^{n+} complexes formed from neutral butein and bare Fe^{n+} cations

Complex	*A*[a]		*B*[b]	
	total energy (Hartree)	ΔE (kcal/mol)	total energy (Hartree)	ΔE (kcal/mol)
DFT/B3LYP results				
B-1noHB1-O2′-Fe(II)-O9	-1077.8397264	0.000	-2218.3550216	0.000
B-1noHB2-O3-Fe(II)-O4	-1077.8137107	16.325	-2218.3335900	13.449
B-1-ring-Fe(II)-A	-1077.8014735	24.004	-2218.3277611	17.106
B-1-ring-Fe(II)-B	-1077.7909802	30.589	-2218.3174382	23.584
B-1noHB1-O2′-Fe(III)-O9	-1077.3550959	0.000	-2217.8820544	0.000
B-1noHB2-O3-Fe(III)-O4	-1077.3199125	22.080	-2217.8339687	30.174
B-1-ring-Fe(III)-A	-1077.2932584	38.804	-2217.8213100	38.118
B-1-ring-Fe(III)-B	-1077.2924209	39.329	-2217.8172335	40.676
DFT/BP86 results				
B-1noHB1-O2′-Fe(II)-O9	-1077.9168098	0.000	-2218.5384232	0.000
B-1-ring-Fe(II)-A	-1077.8890892	17.395	-2218.5157475	14.229
B-1-ring-Fe(II)-B	-1077.8781043	24.288	-2218.5047658	21.120
B-1noHB2-O3-Fe(II)-O4	-1077.8849576	19.988	-2218.5005595	23.760
B-1noHB1-O2′-Fe(III)-O9	-1077.4264736	0.000	-2218.0474547	0.000
B-1noHB2-O3-Fe(III)-O4	-1077.3966673	18.704	-2218.0117948	22.377
B-1-ring-Fe(III)-A	-1077.3771007	30.982	-2218.0031037	27.831
B-1-ring-Fe(III)-B	-1077.3745201	32.601	-2217.9937869	33.677

[a] Results obtained using the 6-31+G(d,p) basis set

[b] Single point results using the 6-311+G(2d,p) basis set, starting from optimised geometries

The second-lowest energy complex (B-1noHB2-O3-Fe(II)-O4 and B-1noHB2-O3-Fe(III)-O4) corresponds to the coordination of the Fe^{n+} cation at the hydroxyl–hydroxyl reactive site (i.e., catechol site) with bond distance values of 2.113 Å and 2.119 Å for the O3···Fe^{2+} and the O3···Fe^{3+} bonds respectively and 2.109 Å and 2.105 Å for the O4···Fe^{2+} and the O4···Fe^{3+} bonds respectively. However, the energy gap between the lowest-energy complex and the second energy complex is significantly large such that it is possible to consider that the Fe^{n+} cation is less likely to bind at the catechol site. Moreover, the relative energy values for complexes in which the Fe^{n+} cation is coordinated at other sites (e.g., the π system of the aromatic rings) are above 13 kcal/mol for Fe(II) cation and above 30 kcal/mol for the complexes with the Fe(III) cation; this result implies that only the coordination of the Fe^{n+} cation at the O2′∪O9 reactive site is probable to observe *in vacuo*. The coordination of the Fe^{n+} cations at the π system of the aromatic rings is the least preferred, which indicates that the cation···lone pair interactions are preferred to the cation···π pair interactions.

The binding energies ($\Delta E'_{binding}$, kcal/mol) for the butein$\cdots Fe^{n+}$ complexes with the neutral butein ligand are reported in Table 4.4. The energy values for the complexes are influenced by a number of factors which include the site of coordination, the nature of the cation, the media and the nature of the ligand. Among the complexes of butein with the Fe(II) cation the highest binding energy value (257.816 kcal/mol) corresponds to the coordination of the Fe^{n+} cation at the hydroxyl–*keto* reactive site. Similar results have been reported on the interaction between flavones (e.g., quercetin and oxovitisin) and Fe (II), where the preferred binding site is that between the hydroxyl group and the adjacent 4-carbonyl group [113, 241, 242]. The coordination of the Fe(II) cation to the hydroxyl–hydroxyl reactive site corresponds to binding strength of 224.575 kcal/mol. The weakest binding corresponds to the coordination of the Fe^{n+} cation to the π system of the aromatic ring and has binding energy of 220.375 and 213.254 kcal/mol for the B-1-ring-Fe(II)-A and the B-1-ring-Fe(II)-B complexes respectively; these results are in agreement with the results of the relative energies where coordination to the π system of the aromatic rings has large relative energies such that the complexes are not considered populated *in vacuo*.

Among the butein$\cdots Fe^{3+}$ complexes, the strongest binding corresponds to the coordination of the Fe(III) cation to the hydroxyl–*keto* site with binding strength of 695.053 kcal/mol in the B-1noHB1-O2′-Fe(III)-O9 complex. For complexes with the Fe(III) cation, the coordination at the π system of aromatic ring A has higher metal ion affinity (MIA) than coordination at the catechol moiety; a trend that is different for the complexes with the coordination of the Fe(II) cation. The weakest binding energy value corresponds to the coordination of the Fe(III) cation at the π system of aromatic ring B which has a value of 636.433 kcal/mol, these results are in agreement with the results reported for the relative energies in that coordination at aromatic ring B results in the least preferred complex. The butein$\cdots Fe^{n+}$ complexes appear to be thermodynamically favoured as reflected by the positive $\Delta E'_{binding}$ values reported in Table 4.4.

A comparison of the $\Delta E'_{binding}$ values among the Fe(II) and the Fe(III) cations, for a given coordination site, shows that Fe(III) cation has stronger affinity to the butein ligand than Fe(II) cation. The ability of the Fe(III) cation to bind to butein better than the Fe(II) cation is related to the high charge on the Fe(III) cation as compared to the charge on the Fe(II) cation. In terms of the antioxidant, the implication of the results reported here is that butein may play a greater role as an antioxidant when chelating Fe(III) cation than the Fe(II) cation.

Table 4.4 Binding energy values ($\Delta E'_{binding,}$ kcal/mol) for butein···Fe^{n+} complexes formed from neutral butein and bare Fe^{n+} cations *in vacuo*. The complexes are arranged in order of decreasing $\Delta E'_{binding}$ values

Complex	*A*[a]			*B*[b]		
	$\Delta E_{inter,}$ kcal/mol	ΔE_{def} kcal/mol	$\Delta E'_{binding,}$ kcal/mol	$\Delta E_{inter,}$ kcal/mol	ΔE_{def} kcal/mol	$\Delta E'_{binding,}$ kcal/mol
DFT/B3LYP results						
B-1noHB1-O2′-Fe(II)-O9	–237.980	14.627	252.607	–242.387	15.429	257.816
B-1noHB2-O3-Fe(II)-O4	–210.540	6.413	216.953	–217.904	6.671	224.575
B-1-ring-Fe(II)-A	–198.674	9.269	207.943	–210.317	10.058	220.375
B-1-ring-Fe(II)-B	–192.089	8.632	200.721	–203.839	9.415	213.254
B-1noHB1-O2′-Fe(III)-O9	–676.457	19.985	696.442	–674.014	21.039	695.053
B-1-ring-Fe(III)-A	–622.352	20.440	642.792	–620.932	21.438	642.370
B-1noHB2-O3-Fe(III)-O4	–643.265	8.931	652.196	–632.806	9.500	642.306
B-1-ring-Fe(III)-B	–621.827	17.163	638.990	–618.374	18.059	636.433
DFT/BP86 results						
B-1noHB1-O2′-Fe(II)-O9	–257.424	11.921	269.345	–271.798	12.614	284.412
B-1-ring-Fe(II)-A	–222.867	9.127	231.994	–240.752	10.031	250.783
B-1-ring-Fe(II)-B	–215.974	7.894	223.868	–233.861	8.7768	242.638
B-1noHB2-O3-Fe(II)-O4	–224.231	4.969	229.200	–234.944	5.224	240.186
B-1noHB1-O2′-Fe(III)-O9	–698.207	16.215	714.422	–698.333	17.235	715.568
B-1-ring-Fe(III)-A	–650.064	13.285	663.349	–653.685	18.433	672.118
B-1noHB2-O3-Fe(III)-O4	–666.299	7.763	674.062	–662.862	8.415	671.277
B-1-ring-Fe(III)-B	–648.445	14.657	663.102	–647.839	15.664	663.503

[a] Results obtained using the 6-31+G(d,p) basis set
[b] Single point results using the 6-311+G(2d,p) basis set, starting from optimised geometries

4.2.3. Relative stability and binding energies for butein···Fe^{n+} complexes formed from deprotonated butein and bare Fe^{n+} cations

The optimised butein···Fe^{n+} complexes with the deprotonated butein are shown in Figure 4.5 for DFT/B3LYP results and Figure 4.6 for DFT/BP86; the corresponding relative energy values (ΔE, kcal/mol) are reported in Table 4.5. The lowest-energy complex corresponds to the coordination of the Fe^{n+} ion at the O2′∪O9 reactive site (B-1noHB1-an-O2′-Fe(II)-O9 and the B-1noHB1-an-O2′-Fe(III)-O9 complexes). The high stability of the complex in which the Fe^{n+} cation is coordinated at the O2′∪O9 reactive site may be related to the fact that both O2′ and O9 atoms act as *keto* groups and therefore the two oxygen atoms have ample lone pairs of electrons (i.e., high electron density) to donate to the Fe^{n+} cations. The second lowest-energy complex corresponds to the coordination of the Fe^{n+} cation at the O3∪O4H4″ reactive site and the least preferred complex corresponds to the coordination of the Fe^{n+} cation at the O3H3″∪O4 reactive site.

The ΔE gap between the lowest-energy complexes and the remaining complexes for both Fe(II) and Fe(III) cations are relatively large such that the coordination of the cations at the O2′∪O9 reactive site is the only complex that may be considered to exist *in vacuo*. The stability of these complexes may also be accounted for by the nature of the chelate ring formed upon coordination of the cations; a six membered chelate ring involving the Fe^{n+} cation and the C1′, C2′, O2′, O9, and C9 atoms while the coordination of the cation between O3 and O4 results in a five-member ring involving the Fe^{n+} cation, C3, O3, O4 and C4 atoms.

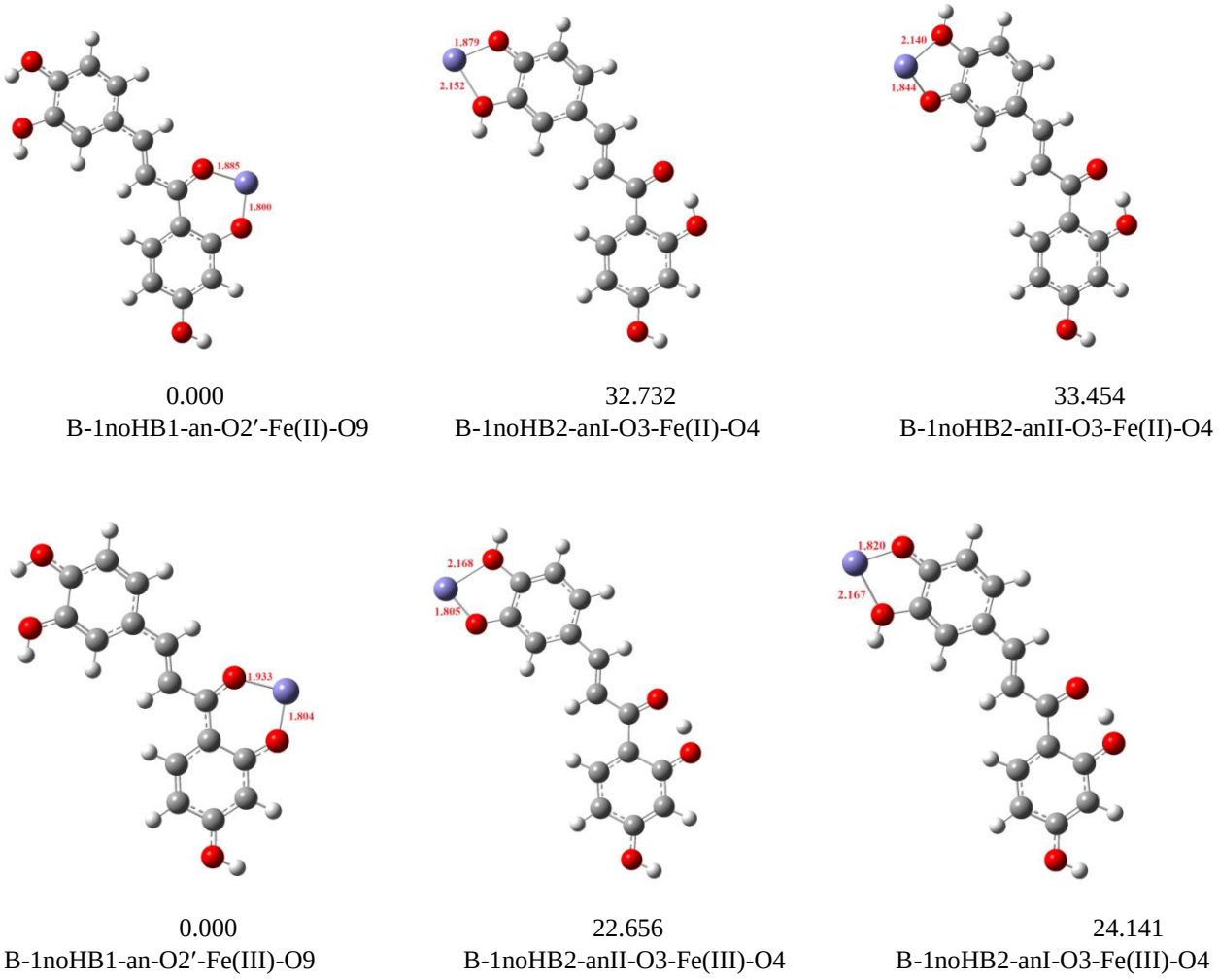

0.000
B-1noHB1-an-O2′-Fe(II)-O9

32.732
B-1noHB2-anI-O3-Fe(II)-O4

33.454
B-1noHB2-anII-O3-Fe(II)-O4

0.000
B-1noHB1-an-O2′-Fe(III)-O9

22.656
B-1noHB2-anII-O3-Fe(III)-O4

24.141
B-1noHB2-anI-O3-Fe(III)-O4

Figure 4.5 B3LYP/6-31+G(d,p) optimised butein···Fe^{n+} complexes (arranged in order of increasing relative energy (ΔE, kcal/mol)) formed from deprotonated butein and bare Fe^{n+} cation, B3LYP/6-311+G(2d,p)//B3LYP/6-31+G(d,p) results *in vacuo*. The bond length between the cation and the ligand are reported in Å.

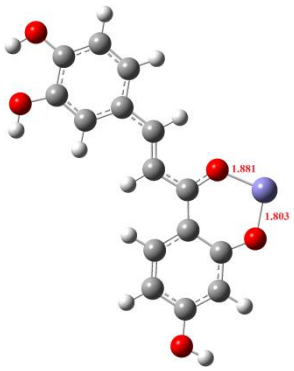

0.000
B-1noHB1-an-O2′-Fe(II)-O9

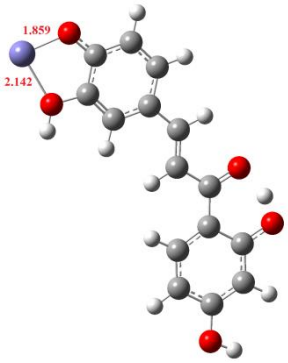

25.410
B-1noHB2-anI-O3-Fe(II)-O4

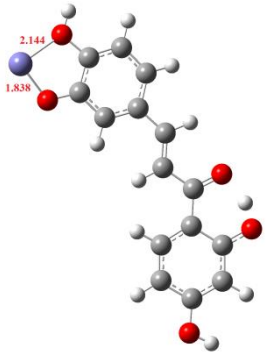

26.196
B-1noHB2-anII-O3-Fe(II)-O4

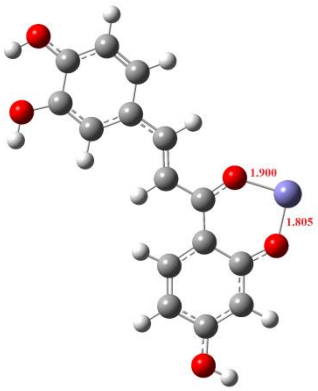

0.000
B-1noHB1-an-O2′-Fe(III)-O9

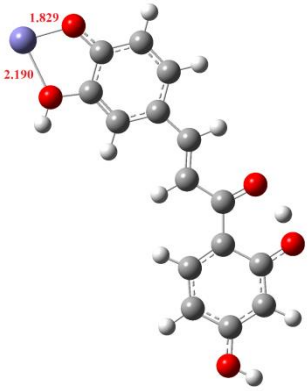

24.153
B-1noHB2-anI-O3-Fe(III)-O4

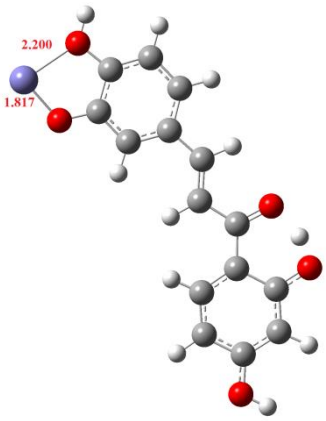

24.991
B-1noHB2-anII-O3-Fe(III)-O4

Figure 4.6 BP86/6-31+G(d,p) optimised butein···Fe^{n+} complexes (arranged in order of increasing relative energy (ΔE, kcal/mol)) formed from deprotonated butein and bare Fe^{n+} cation. BP86/6-311+G(2d,p)//BP86/6-31+G(d,p) results *in vacuo*. The bond length between the cation and the ligand are reported in Å.

Table 4.5 *In vacuo* relative energy values (ΔE, kcal/mol) for butein···Fe^{n+} complexes formed from deprotonated butein and bare Fe^{n+} cation

Complex	*A*[a]		*B*[b]	
	total energy (Hartree)	ΔE (kcal/mol)	total energy (Hartree)	ΔE (kcal/mol)
DFT/B3LYP results				
B-1noHB1-an- O2′-Fe(II)-O9	-1077.6071065	0.000	-2218.1400787	0.000
B-1noHB2-anI-O3-Fe(II)-O4	-1077.5641984	26.925	-2218.0879132	32.734
B-1noHB2-anII-O3-Fe(II)-O4	-1077.5602664	29.393	-2218.0866212	33.545
B-1noHB1-an-O2′-Fe(III)-O9	-1077.2376533	0.000	-2217.7686282	0.000
B-1noHB2-anII-O3-Fe(III)-O4	-1077.2056250	20.098	-2217.7325233	22.656
B-1noHB2-anI-O3-Fe(III)-O4	-1077.2006854	23.198	-2217.7301568	24.141
DFT/BP86 results				
B-1noHB1-an-O2′-Fe(II)-O9	-1077.6831808	0.000	-2218.3091025	0.000
B-1noHB2-anI-O3-Fe(II)-O4	-1077.6476897	22.271	-2218.2686095	25.410
B-1noHB2-anII-O3-Fe(II)-O4	-1077.6454444	23.680	-2218.2673560	26.196
B-1noHB1-an-O2′-Fe(III)-O9	-1077.3157007	0.000	-2217.9421503	0.000
B-1noHB2-anII-O3-Fe(III)-O4	-1077.2828374	20.622	-2217.9036593	24.153
B-1noHB2-anI-O3-Fe(III)-O4	-1077.2814289	21.506	-2217.9023250	24.991

[a] Results obtained using the 6-31+G(d,p) basis set
[b] Single point results using the 6-311+G(2d,p) basis set, starting from optimised geometries

The binding energy values ($\Delta E'_{binding}$, kcal/mol) for the complexes formed from the deprotonated butein and Fe^{n+} cations are reported in Table 4.6. The highest binding energy value (465.182 and 963.337 kcal/mol for Fe(II) and Fe(III) respectively) corresponds to the coordination of the Fe^{n+} cation to the O2′∪O9 reactive site. These results are in agreement with the relative energy values in that the most preferred coordination is at the O2′∪O9 reactive site. Coordination of the Fe^{n+} cation at the O3H3″∪O4 reactive site is preferred to its coordination at the O3∪O4H4″ reactive site. The results obtained for coordination of the Fe(II) cation at the O2′⁻∪O9 and the O3H3″∪O4 reactive site are similar to the values reported in other works, for the coordination of the Fe(II) ion to the butein ligand [59]. The O3∪O4H4″ reactive site corresponds to the weakest binding for complexes with the Fe(III) cation, while O3H3″∪O4 reactive site corresponds to the weakest binding for complexes with the Fe(II) cation.

A comparison of the Fe(II) and Fe(III) complexes suggests that Fe(III) cation binds stronger to the deprotonated butein ligand than Fe(II) cation; similar trends are observed for the complexes with the neutral ligand. The deformation energy values also indicate that the coordination of the Fe(III) cation to the butein ligand results in greater deformation than the coordination of the Fe (II) cation.

Table 4.6 Binding energy values ($\Delta E'_{binding,}$ kcal/mol) for butein···Fe^{n+} complexes formed from deprotonated butein and bare Fe^{n+} cation results *in vacuo*. The complexes are arranged in order of decreasing $\Delta E'_{binding}$ values

Complex	*A*[a]			*B*[b]		
	$\Delta E_{inter,}$ kcal/mol	ΔE_{def} kcal/mol	$\Delta E'_{binding,}$ kcal/mol	$\Delta E_{inter,}$ kcal/mol	ΔE_{def} kcal/mol	$\Delta E'_{binding,}$ kcal/mol
DFT/B3LYP results						
B-1noHB1-an-O2′-Fe(II)-O9	–433.279	15.353	448.632	–449.205	15.977	465.182
B-1noHB2-anII-O3-Fe(II)-O4	–391.945	8.767	400.712	–403.615	8.577	412.192
B-1noHB2-anI-O3-Fe(II)-O4	–383.152	8.867	392.019	–393.251	8.737	401.988
B-1noHB1-an-O2′-Fe(III)-O9	–944.032	18.135	962.167	–944.534	18.803	963.337
B-1noHB2-anI-O3-Fe(III)-O4	–911.991	13.433	925.424	–909.834	13.426	923.260
B-1noHB2-anII-O3-Fe(III)-O4	–897.632	14.899	912.531	–897.173	14.945	912.118
DFT/BP86 results						
B-1noHB1-an-O2′-Fe(II)-O9	–448.482	12.950	461.432	–466.063	13.441	479.504
B-1noHB2-anII-O3-Fe(II)-O4	–409.158	8.182	417.340	–424.179	8.046	432.225
B-1noHB2-anI-O3-Fe(II)-O4	–399.506	8.199	407.705	–414.026	8.105	422.131
B-1noHB1-an-O2′-Fe(III)-O9	–966.359	15.881	982.240	–970.420	16.498	986.918
B-1noHB2-anI-O3-Fe(III)-O4	–930.093	11.048	941.141	–930.578	11.083	941.661
B-1noHB2-anII-O3-Fe(III)-O4	–918.147	11.317	929.464	–918.801	11.394	930.195

[a] Results obtained using the 6-31+G(d,p) basis set
[b] Single point results using the 6-311+G(2d,p) basis set starting from optimised geometries

4.2.4. Relative stability and binding energies for butein···Fe^{n+} complexes formed from deprotonated butein and hydrated Fe^{n+} cations

The optimised complexes of butein with hydrated Fe^{n+} are shown in Figure 4.7 and Figure 4.8 for DFT/B3LYP and DFT/BP86 results respectively; the relative energies (ΔE, kcal/mol) are reported in Table 4.7. The lowest-energy complex corresponds to the coordination of the Fe^{n+} cations at the O2′$^{-}$∪O9 reactive site. Among the Fe(II) complexes, the second lowest-energy complex corresponds to the coordination of the Fe^{n+} cation at the O3∪O4H4″ reactive site (B-1noHB2-anII-O3-Fe(II)-O4-4aq complex) with ΔE of 16.053 kcal/mol. Among the Fe(III) complexes, the coordination at the O3H3″∪O4 reactive site in the B-1noHB2-anI-O3-Fe(III)-O4-4aq complex corresponds to the second lowest-energy complex. Although the ΔE gap between the lowest-energy complex and the second lowest-energy complex among the complexes with the Fe(III) cation is reduced with respect to the results of the complexes with the Fe(II) cation, this complex (B-1noHB2-anI-O3-Fe(III)-O4-4aq) is not considered to exist. Coordination at the O3H3″∪O4 reactive site corresponds to ΔE values of 16.053 and 9.907 kcal/mol for Fe(II) and Fe(III) cations respectively. The least preferred complex corresponds to the coordination of the Fe^{n+} cation to the O3H3″∪O4 and O3∪O4H4″ reactive sites for the

Fe(II) and Fe(III) complexes respectively. Coordination at these sites have ΔE of 22.436 Fe(II) cation and 12.477 kcal/mol Fe(III) cation. Overall, it is reasonable to infer that since ΔE gap between the lowest-energy complex and the rest of the complexes is significantly large, only the coordination of the Fe^{n+} cation at the O2′∪O9 reactive site may be probable to observe in nature.

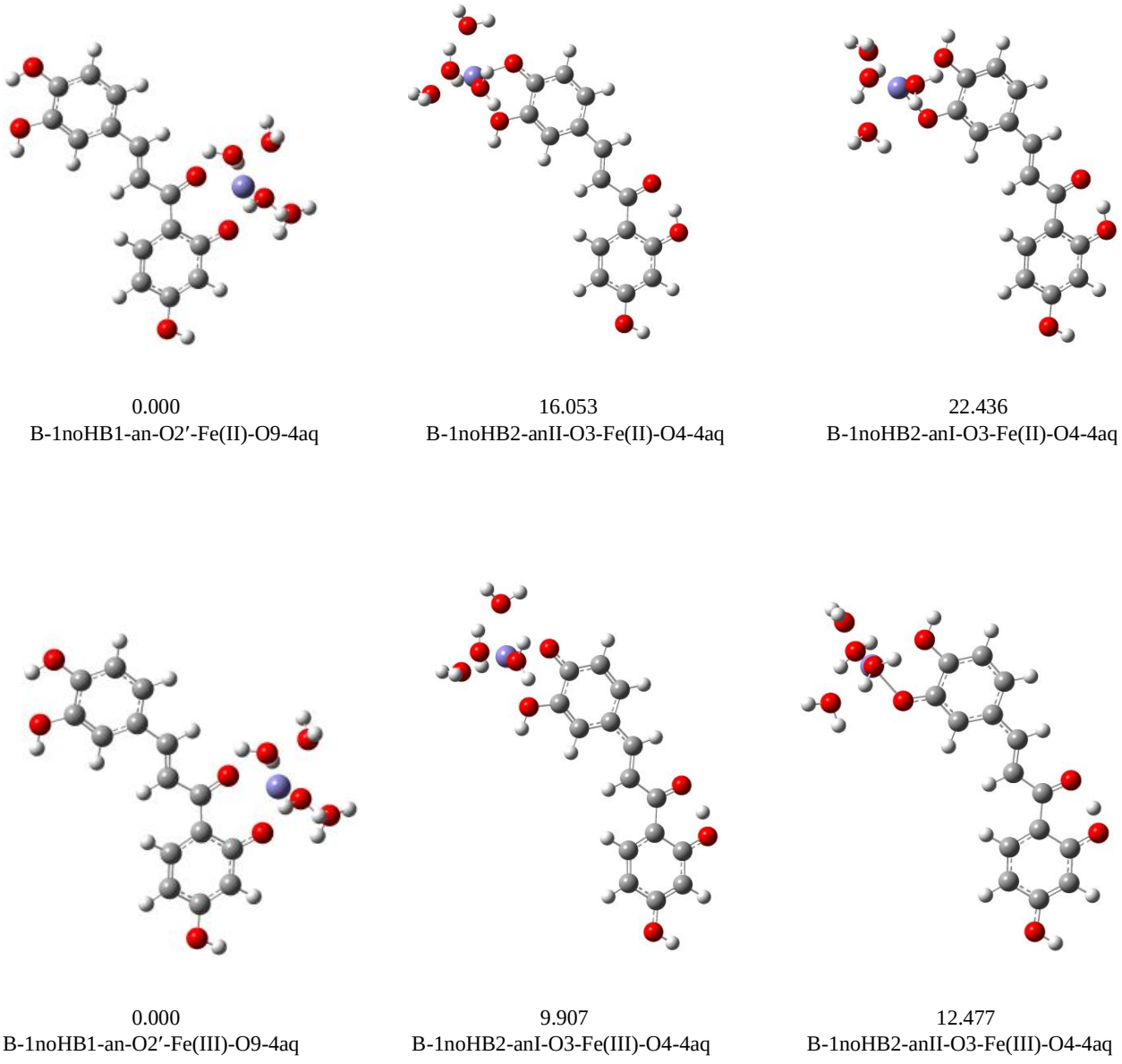

Figure 4.7 B3LYP/6-31+G(d,p) optimised butein···Fe^{n} complexes (arranged in order of increasing relative energy (ΔE, kcal/mol)) formed from deprotonated butein and hydrated Fe^{n+} cation B3LYP/6-311+G(2d,p)//B3LYP/6-31+G(d,p) results *in vacuo*.

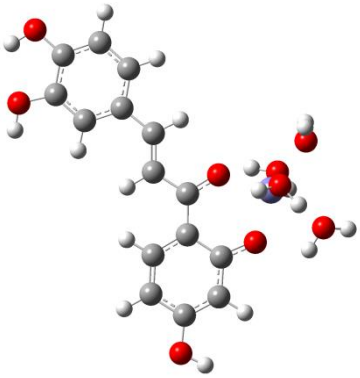

0.000
B-1noHB1-an-O2′-Fe(II)-O9-4aq

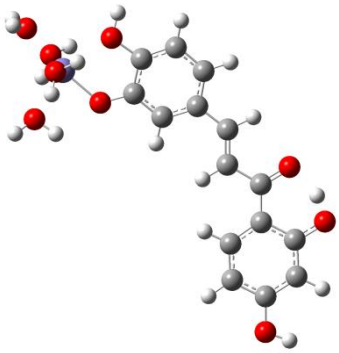

15.825
B-1noHB2-anII-O3-Fe(II)-O4-4aq

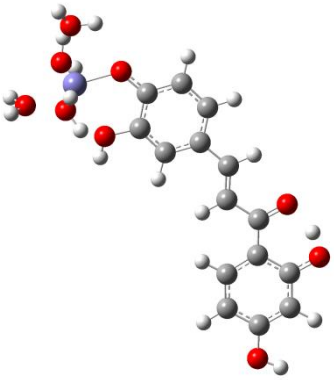

16.801
B-1noHB2-anI-O3-Fe(II)-O4-4aq

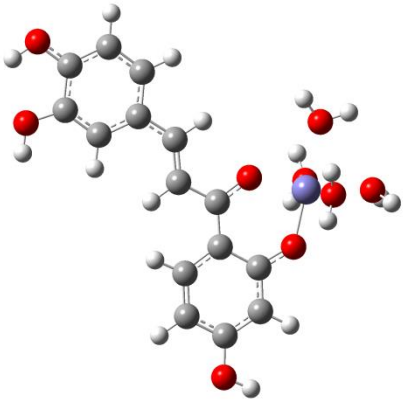

0.000
B-1noHB1-an-O2′-Fe(III)-O9-4aq

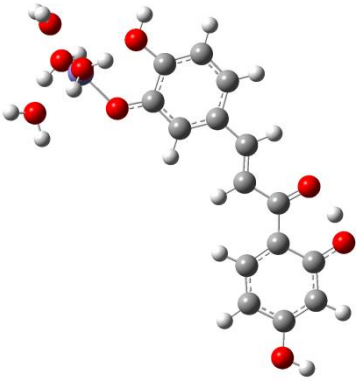

17.872
B-1noHB2-anII-O3-Fe(III)-O4-4aq

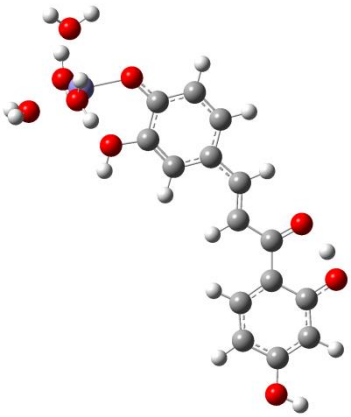

18.226
B-1noHB2-anI-O3-Fe(III)-O4-4aq

Figure 4.8 BP86/6-31+G(d,p) optimised butein···Fe^{n} complexes (arranged in order of increasing relative energy (ΔE, kcal/mol)) formed from deprotonated butein and hydrated Fe^{n+} cation BP86/6-311+G(2d,p)//BP86/6-31+G(d,p) results *in vacuo*.

Table 4.7 *In vacuo* relative energy values (ΔE, kcal/mol) for butein···Fe^{n+} complexes formed from deprotonated butein ligand and hydrated Fe^{n+} cations

Complex	*A*[a]		*B*[b]	
	total energy (Hartree)	ΔE (kcal/mol)	total energy (Hartree)	ΔE (kcal/mol)
DFT/B3LYP results				
B-1noHB1-an-O2′-Fe(II)-O9-4aq	-1383.4865306	0.000	-2524.1101669	0.000
B-1noHB2-anII-O3-Fe(II)-O4-4aq	-1383.4618264	15.502	-2524.0845854	16.053
B-1noHB2-anI-O3-Fe(II)-O4-4aq	-1383.4626941	14.958	-2524.0744122	22.436
B-1noHB1-an-O2′-Fe(III)-O9-4aq	-1383.1461132	0.000	-2523.770596	0.000
B-1noHB2-anI-O3-Fe(III)-O4-4aq	-1383.1326102	8.473	-2523.7548087	9.907
B-1noHB2-anII-O3-Fe(III)-O4-4aq	-1383.1285883	10.997	-2523.7507125	12.477
DFT/BP86 results				
B-1noHB1-an-O2′-Fe(II)-O9-4aq	-1383.5469192	0.000	-2524.2700602	0.000
B-1noHB2-anII-O3-Fe(II)-O4-4aq	-1383.5241515	14.287	-2524.2448407	15.825
B-1noHB2-anI-O3-Fe(II)-O4-4aq	-1383.5225073	15.319	-2524.2432868	16.801
B-1noHB1-an-O2′-Fe(III)-O9-4aq	-1383.2184882	0.000	-2523.9460626	0.000
B-1noHB2-anII-O3-Fe(III)-O4-4aq	-1383.1967199	13.660	-2523.9175811	17.872
B-1noHB2-anI-O3-Fe(III)-O4-4aq	-1383.1950082	14.734	-2523.9170172	18.226

[a] Results obtained using the 6-31+G(d,p) basis set
[b] Single point results using the 6-311+G(2d,p) basis set, starting from optimised geometries

The binding energy values ($\Delta E'_{binding}$, kcal/mol) are reported in Table 4.8. The highest binding energy value corresponds to the coordination of the hydrated Fe^{n+} cations at the O2′∪O9 reactive site, with $\Delta E'_{binding}$ values of 540.676 and 1059.121 kcal/mol for Fe(II) and Fe(III) cations respectively. The coordination of the hydrated cations at the O4∪O3H3″ reactive site results in the binding energy values of 512.399 for Fe(II) cation and 1031.083 kcal/mol for Fe(III) cations. The weakest binding corresponds to the coordination of the Fe^{n+} cations at the O4H4″∪O3 reactive site with $\Delta E'_{binding}$ values of 497.364 and 1022.784 kcal/mol.

A comparison of the results obtained for the complexes formed between the deprotonated ligand and bare Fe^{n+} cations and the complexes formed between the deprotonated ligand and hydrated Fe^{n+} cations suggests in both cases, the preferred binding site for the Fe^{n+} ion is the O2′∪O9 reactive site. However, the binding energy is higher when the Fe^{n+} cation is hydrated than when it is bare, which indicates that the hydration effect favours stronger interactions between ligand the Fe^{n+} cations. The preference for the hydration of the Fe^{n+} cations towards binding to the Fe^{n+} cations may be attributed to the cooperativity effects arising from the interaction between the water molecules and the neighbouring ligand donor atoms.

Table 4.8 Binding energy values ($\Delta E'_{binding,}$ kcal/mol) for butein···Fe^{n+} complexes formed from deprotonated butein ligand and hydrated Fe^{n+} cations results *in vacuo*. The complexes are arranged in order of decreasing $\Delta E'_{binding}$ values

	A[a]			*B*[b]		
Complex	$\Delta E_{inter,}$ kcal/mol	ΔE_{def} kcal/mol	$\Delta E'_{binding,}$ kcal/mol	$\Delta E_{inter,}$ kcal/mol	ΔE_{def} kcal/mol	$\Delta E'_{binding,}$ kcal/mol
DFT/B3LYP results						
B-1noHB1-an-O2′-Fe(II)-O9-4aq	–523.159	8.178	531.337	–532.068	8.608	540.676
B-1noHB2-anI-O3-Fe(II)-O4-4aq	–495.716	8.661	504.377	–503.971	8.428	512.399
B-1noHB2-anII-O3-Fe(II)-O4-4aq	–485.000	11.127	496.127	–486.412	10.952	497.364
B-1noHB1-an-O2′-Fe(III)-O9-4aq	–1052.132	11.237	1063.369	–1047.402	11.719	1059.121
B-1noHB2-anI-O3-Fe(III)-O4-4aq	–1029.193	8.200	1037.393	–1022.880	8.203	1031.083
B-1noHB2-anII-O3-Fe(III)-O4-4aq	–1020.457	8.483	1028.940	–1014.275	8.509	1022.784
DFT/BP86 results						
B-1noHB1-an-O2′-Fe(II)-O9-4aq	–528.772	8.481	537.253	–542.600	8.866	551.466
B-1noHB2-anI -O3-Fe(II)-O4-4aq	–471.810	8.863	480.673	–510.111	8.606	518.717
B-1noHB2-anII-O3-Fe(II)-O4-4aq	–487.780	9.523	497.303	–500.147	9.312	509.459
B-1noHB1-an-O2′-Fe(III)-O9-4aq	–1071.153	12.506	1083.66	–1073.911	13.027	1086.940
B-1noHB2-anI-O3-Fe(III)-O4-4aq	–1040.775	8.061	1048.84	–1039.996	8.028	1048.020
B-1noHB2-anII-O3-Fe(III)-O4-4aq	–1030.787	7.835	1038.62	–1029.411	7.849	1037.260

[a] Results obtained using the 6-31+G(d,p) basis set
[b] Single point results using the 6-311+G(2d,p) basis set, starting from optimised geometries

4.2.5. AIM analysis of the bonding within the butein complexes

The bond critical point (BCP) data for the butein···Fe^{n+} complexes are reported in Table 4.9 for the DFT/B3LYP results and Table 4.10 for the DFT/BP86 results. There are four types of ligand···cation bonding interactions, which are the C_{arom}···Fe^{n+} type of bonding (i.e., which provides information on the interaction between the ligand and the π electrons of the aromatic ring) and three cation···lone pair interactions involving the O atoms, including the C=O···Fe^{n+} bond, the HO···Fe^{n+} bond and O^{-}···Fe^{n+} bond (which is only present at the site of the deprotonation). For the complexes of butein with the neutral ligand the largest value of ρ (e/Å^3) corresponds to the O9···Fe^{n+} bond (B-1noHB1-O2′-Fe(n)-O9) and has values of 0.123 and 0.129 for Fe(II) and Fe(III) cations respectively. This result is in agreement with the ΔE and the $\Delta E'_{binding}$ values where coordination at the O2′∪O9 reactive site results in the most preferred complex and the strongest binding energy. The weakest bond corresponds to the C3′···Fe bond in the B-1-ring-Fe(II)-A complex with ρ value of 0.042 and the O3···Fe bond in the B-1noHB2-O3-Fe(III)-O4 complex with ρ value of 0.056.

Among the complexes with deprotonated butein ligand the largest value of ρ corresponds to the O2′···Fe^{n+} bond (present in B-1noHB1-an-O2′-Fe(II)-O9 and B-1noHB1-an-O2′-Fe(III)-O9 complexes), which has values of 0.142 and 0.139 for Fe(II) and Fe(III) cations respectively. The values of ρ for the complexes with hydrated Fe^{n+} cation is smaller than for the complexes with bare Fe^{n+} cation, which suggests that the effect of hydration weakens the O···Fe and the C_{arom}···Fe bonds. This is despite the fact that the interaction energy is stronger on hydration, a factor that may largely be attributed to coopeativity effect.

The Laplacian of the electron density ($\nabla^2\rho(r)$) provides information on the type of bonding between the Fe^{n+} cations and the butein ligand (section 2.6.3). $\nabla^2\rho$ (e/Å^5) values (Table 4.9) have 0.118–0.729 range for the Fe(II) complexes and 0.106–0.689 range for the Fe(III) complexes with neutral butein ligand and the 0.293–0.716 range for the Fe(II) complexes and 0.274–0.713 range for Fe(III) complexes among the complexes with the deprotonated butein ligand. The positive values of $\nabla^2\rho$ in all cases suggest that the type of interactions between the Fe^{n+} cations and the butein ligand may have dative character. Table 4.10 reports the BCP data with the DFT/BP86 method.

Analysis of the values of *H* and its components (Table 4.9), the kinetic (*G*) and potential (*V*) further supports the fact that the type of interactions between the Fe^{n+} cation and the central butein ligand are dative in nature; *H* has a positive value and is close to zero, *G* has positive value and *V* has negative value. The |V|/G ratio also provides information on the type of chemical bonds formed between the Fe^{n+} cation and the butein ligand. The |V|/G ratio among the complexes of butein (i.e., for both neutral and deprotonated ligand) has a range of 0.982–1.437 range; suggesting that the interactions between the Fe^{n+} cation and the butein ligand are dative interactions as indicated by the analysis of the Laplacian values. However, the positive value of *G* predominates over the negative value of *V*. It is therefore reasonable to infer that the interactions between the Fe^{n+} cations and the butein ligand are dative in nature.

Table 4.9 Bond critical point data for the butein···Fe^{n+} complexes for both the neutral and deprotonated butein UB3LYP/6-31+G(d,p) results *in vacuo*

Complex	Bond type	ρ e/Å^3	$\nabla^2\rho$ e/Å^5	V (Hartree)	G (Hartree)	H (Hartree)	$\frac{\lvert V \rvert}{G}$
B-1noHB1-O2′-Fe(II)-O9	O2′···Fe	0.068	0.405	–0.104	0.103	–0.002	1.015
	O9···Fe	0.123	0.729	–0.243	0.213	–0.030	1.143
B-1noHB2-O3-Fe(II)-O4	O3···Fe	0.057	0.331	–0.082	0.082	0.001	0.994
	O4···Fe	0.057	0.336	–0.083	0.083	0.001	0.994
B-1-ring-Fe(II)-A	C3′···Fe	0.042	0.119	–0.044	0.037	–0.007	1.191
	C6′···Fe	0.054	0.170	–0.062	0.052	–0.010	1.189
B-1-ring-Fe(II)-B	C2···Fe	0.039	0.118	–0.042	0.036	–0.006	1.172
	C5···Fe	0.052	0.161	–0.060	0.050	–0.010	1.195
B-1noHB1-an-O2′-Fe(II)-O9	O2′···Fe	0.142	0.716	–0.272	0.225	–0.046	1.206
	O9···Fe	0.115	0.575	–0.195	0.169	–0.026	1.150
B-1noHB2-anI-O3-Fe(II)-O4	O3···Fe	0.051	0.293	–0.071	0.072	0.001	0.982
	O4···Fe	0.112	0.630	–0.204	0.181	–0.023	1.129
B-1noHB2-anII-O3-Fe(II)-O4	O3···Fe	0.125	0.662	–0.073	0.074	0.001	0.985
	O4···Fe	0.053	0.302	–0.231	0.198	–0.033	1.166
B-1noHB1-an-O2′-Fe(II)-O9-4aq	O2′···Fe	0.093	0.494	–0.149	0.136	–0.013	1.093
	O9···Fe	0.076	0.433	–0.118	0.113	–0.005	1.044
B-1noHB2-anI-O3-Fe(II)-O4-4aq	O3···Fe	0.038	0.170	–0.043	0.043	–4E–04	1.010
	O4···Fe	0.105	0.614	–0.193	0.173	–0.020	1.113
B-1noHB2-anII-O3-Fe(II)-O4-4aq	O3···Fe	0.108	0.558	–0.183	0.161	–0.022	1.135
	O4···Fe	0.037	0.177	–0.043	0.044	0.000	0.990
B-1noHB1-O2′-Fe(III)-O9	O2′···Fe	0.065	0.377	–0.096	0.095	–0.001	1.011
	O9···Fe	0.129	0.689	–0.243	0.208	–0.035	1.171
B-1noHB2-O3-Fe(III)-O4	O3···Fe	0.056	0.321	–0.079	0.079	0.001	0.990
	O4···Fe	0.058	0.333	–0.082	0.082	0.001	0.992
B-1-ring-Fe(III)-A	C5′···Fe	0.072	0.106	–0.068	0.047	–0.021	1.437
	C6′···Fe	0.066	0.142	–0.067	0.051	–0.016	1.312
B-1-ring-Fe(III)-B	C5···Fe	0.069	0.147	–0.072	0.054	–0.018	1.324
	C6···Fe	0.066	0.142	–0.067	0.051	–0.016	1.312
B-1noHB1-an-O2′-Fe(III)-O9	O2′···Fe	0.139	0.713	–0.265	0.222	–0.044	1.196
	O9···Fe	0.101	0.504	–0.161	0.143	–0.017	1.121
B-1noHB2-anI-O3-Fe(III)-O4	O3···Fe	0.050	0.275	–0.067	0.068	0.001	0.984
	O4···Fe	0.133	0.685	–0.249	0.210	–0.039	1.185
B-1noHB2-anII-O3-Fe(III)-O4	O3···Fe	0.139	0.711	–0.067	0.068	0.001	0.985
	O4···Fe	0.050	0.274	–0.265	0.221	–0.044	1.197
B-1noHB1-an-O2′-Fe(III)-O9-4aq	O2′···Fe	0.086	0.493	–0.141	0.132	–0.009	1.067
	O9···Fe	0.083	0.440	–0.126	0.118	–0.008	1.067
B-1noHB2-anI-O3-Fe(III)-O4-4aq	O3···Fe	0.032	0.149	–0.037	0.037	0.000	0.994
	O4···Fe	0.097	0.497	–0.154	0.139	–0.015	1.107
B-1noHB2-anII-O3-Fe(III)-O4-4aq	O3···Fe	0.103	0.534	–0.170	0.152	–0.018	1.120
	O4···Fe	0.031	0.146	–0.036	0.036	0.000	0.994

Table 4.10 Bond critical point data for the butein···Fe^{n+} complexes for both the neutral and deprotonated butein UBP86/6-31+G(d,p) results *in vacuo*

Complex	Bond type	ρ e/Å^3	$\nabla^2\rho$ e/Å^5	V (Hartree)	G (Hartree)	H (Hartree)	$\frac{\lvert V \rvert}{G}$
B-1noHB1-O2′-Fe(II)-O9	O2′···Fe	0.070	0.408	–0.107	0.104	–0.003	1.029
	O9···Fe	0.122	0.657	–0.224	0.194	–0.030	1.155
B-1noHB2-O3-Fe(II)-O4	O3···Fe	0.066	0.375	–0.097	0.095	–0.002	1.021
	O4···Fe	0.067	0.382	–0.099	0.097	–0.002	1.021
B-1-ring-Fe(II)-A	C3′···Fe	0.050	0.127	–0.052	0.042	–0.010	1.238
	C6′···Fe	0.066	0.186	–0.076	0.061	–0.015	1.246
B-1-ring-Fe(II)-B	C2···Fe	0.050	0.135	–0.053	0.043	–0.010	1.233
	C5···Fe	0.063	0.175	–0.071	0.057	–0.014	1.246
B-1noHB1-an-Fe-O2′-Fe(II)-O9	O2′···Fe	0.139	0.709	–0.264	0.221	–0.043	1.195
	O9···Fe	0.112	0.602	–0.198	0.174	–0.024	1.138
B-1noHB2-anI-Fe-O3-Fe(II)-O4	O3···Fe	0.054	0.285	–0.072	0.071	–0.001	1.014
	O4···Fe	0.121	0.614	–0.213	0.183	–0.030	1.164
B-1noHB2-anII-Fe-O3-Fe(II)-O4	O3···Fe	0.128	0.641	–0.230	0.195	–0.035	1.179
	O4···Fe	0.055	0.279	–0.071	0.071	0.000	1.000
B-1noHB1-an-O2′-Fe(II)-O9-4aq	O2′···Fe	0.097	0.498	–0.154	0.139	–0.015	1.108
	O9···Fe	0.087	0.477	–0.139	0.129	–0.010	1.078
B-1noHB2-anI-O3-Fe(II)-O4-4aq	O3···Fe	0.034	0.147	–0.038	0.037	–0.001	1.027
	O4···Fe	0.108	0.558	–0.183	0.161	–0.022	1.137
B-1noHB2-anII-O3-Fe(II)-O4-4aq	O3···Fe	0.112	0.568	–0.189	0.166	–0.023	1.139
	O4···Fe	0.034	0.143	–0.037	0.037	0.000	1.000
B-1noHB1-O2′-Fe(III)-O9	O2′···Fe	0.603	0.352	–0.090	0.089	–0.001	1.011
	O9···Fe	0.128	0.673	–0.236	0.202	–0.034	1.168
B-1noHB2-O3-Fe(III)-O4	O3···Fe	0.060	0.349	–0.088	0.087	–0.001	1.011
	O4···Fe	0.062	0.363	–0.091	0.091	0.000	1.000
B-1-ring-Fe(III)-A	C3′···Fe	0.050	0.095	–0.045	0.034	–0.011	1.324
	C5′···Fe	0.062	0.124	–0.061	0.046	–0.015	1.326
B-1-ring-Fe(III)-B	C5···Fe	0.076	0.174	–0.083	0.063	–0.020	1.317
	C6···Fe	0.077	0.150	–0.079	0.058	–0.021	1.362
B-1noHB1-an-O2′-Fe(III)-O9	O2′···Fe	0.138	0.717	–0.263	0.221	–0.042	1.190
	O9···Fe	0.107	0.572	–0.184	0.164	–0.020	1.122
B-1noHB2-anI-O3-Fe(III)-O4	O3···Fe	0.048	0.248	–0.061	0.062	0.001	0.984
	O4···Fe	0.130	0.657	–0.237	0.200	–0.037	1.185
B-1noHB2-anII-O3-Fe(III)-O4	O3···Fe	0.134	0.676	–0.248	0.208	–0.040	1.192
	O4···Fe	0.048	0.243	–0.060	0.061	0.001	0.984
B-1noHB1-an-O2′-Fe(III)-O9-4aq	O2′···Fe	0.112	0.593	–0.195	0.172	–0.023	1.134
	O9···Fe	0.096	0.491	–0.152	0.137	–0.015	1.109
B-1noHB2-anI-O3-Fe(III)-O4-4aq	O3···Fe	0.031	0.125	–0.033	0.032	–0.001	1.031
	O4···Fe	0.103	0.521	–0.167	0.149	–0.018	1.121
B-1noHB2-anII-O3-Fe(III)-O4-4aq	O3···Fe	0.112	0.573	–0.191	0.167	–0.024	1.144
	O4···Fe	0.034	0.145	–0.037	0.037	0.000	1.000

4.2.6. NPA charges, spin density and orbital occupancies

The oxidation state of the Fe^{n+} ion before and after coordination to the ligand molecule provides information on the effect of its coordination on the ligand. A decrease in the oxidation number provides an indication on the extent of reduction for the Fe^{n+} ions upon complexation. The partial charges and spin density values (calcualted with both methods) for the Fe^{n+} ions in the complexes are reported in Table 4.11. The charge on the free Fe(II) and Fe(III) cations is +2 and +3 respectively. For the Fe(II) cation the charge is reduced from 2 to a 1–1.3 *e* range and from 3 to a 1–1.5 *e* range for Fe(III), indicating that the positive charge is transferred from the Fe^{n+} cations to butein. For the complexes with neutral butein with Fe^{n+} cation the highest amount of charge is transferred with a value of 1.092 and 1.778 *e* for Fe(II) and Fe(III) respectively for coordination at the O2′∪O9 site for Fe(II) and the π system of the aromatic ring for Fe(III). Among the complexes of deprotonated butein ligand with the Fe^{n+} cation, the highest amount of charge transfer corresponds to the coordination of the cation at the O2′∪O9 reactive site (with values of 0.851 and 1.616 *e* for Fe(II) and Fe(III) respectively). The results obtained further suggest that charge transfer is greater for the non-deprotonated ligand than for the deprotonated ligand and that the charge transfer is highest in the Fe(III) complexes than in the Fe(II) complexes.

Table 4.11 NPA charges and spin densities values for the Fe^{n+} cations in the complexes of butein

Complex	charge *(e)*		spin density	
	DFT/B3LYP results	DFT/BP86 results	DFT/B3LYP results	DFT/BP86 results
DFT/B3LYP results				
B-1noHB1-O2′-Fe(II)-O9	1.328	0.550	3.445	3.330
B-1noHB2-O3-Fe(II)-O4	0.908	1.023	2.962	3.102
B-1-ring-Fe(II)-A	0.915	0.554	2.951	3.014
B-1-ring-Fe(II)-B	0.909	0.959	2.942	3.004
B-1noHB1-an-O2′-Fe(II)-O9	1.149	1.206	3.561	3.392
B-1noHB2-anI-O3-Fe(II)-O4	1.227	1.061	3.286	3.251
B-1noHB2-anII-O3-Fe(II)-O4	1.223	1.065	3.377	3.268
B-1noHB1-an-O2′-Fe(II)-O9-4aq	1.203	0.545	3.653	3.524
B-1noHB2-anI-O3-Fe(II)-O4-4aq	1.252	0.549	3.638	3.482
B-1noHB2-anII-O3-Fe(II)-O4-4aq	1.200	0.543	3.640	3.497
B-1noHB1-O2′-Fe(III)-O9	1.521	0.568	3.632	3.478
B-1noHB2-O3-Fe(III)-O4	1.289	1.250	3.347	3.325
B-1-ring-Fe(III)-A	1.324	0.570	3.497	3.353
B-1-ring-Fe(III)-B	1.222	1.173	3.342	3.297
B-1noHB1-an-O2′-Fe(III)-O9	1.384	1.319	3.589	3.459
B-1noHB2-anI-O3-Fe(III)-O4	1.392	1.246	3.519	3.401
B-1noHB2-anII-O3-Fe(III)-O4	1.391	1.251	3.534	3.410
B-1noHB1-an-O2′-Fe(III)-O9-4aq	1.266	1.174	3.718	3.674
B-1noHB2-anI-O3-Fe(III)-O4-4aq	1.252	1.111	3.687	3.571
B-1noHB2-anII-O3-Fe(III)-O4-4aq	1.234	1.114	3.669	3.581

The spin density distribution for the complexes formed from the neutral ligand and bare Fe^{n+} cations are shown in Figure 4.9 while spin density for the complexes formed from deprotonated butein and bare Fe^{n+} cations are shown in Figure 4.10 and spin density for the complexes formed from deprotonated butein and the hydrated Fe^{n+} cations are shown in Figure 4.11. The spin density of both Fe (II) and Fe (III) cations in the isolated state are 4 and 5 respectively. Among the butein···Fe^{n+} complexes, the Fe^{n+} cation has spin density values less than 4 for both Fe(II) and Fe(III) cation. The reduction in the spin density suggests that the transfer of electrons from butein to the Fe^{n+} cations increases the tendency for the electrons in the *d* orbitals to be paired. This phenomenon can be explained by considering that the electrons that are transferred from the ligand molecules occupy the partially-filled *d* orbitals as well as the empty 4s orbital of Fe^{n+} cations. A comparison of the Fe(II) and Fe(III) complexes implies that there is greater spin density delocalisation in the Fe(III) complexes (1.3–1.6) than in the Fe(II) complexes (0.5–1.0), which further supports the fact that Fe(III) binds stronger to the ligand molecule than Fe(II).

A comparison of the occupancy of the isolated Fe^{n+} cations and that of the complexed Fe^{n+} ions also provides better evaluation for the effect of electron transfer from the ligand to the metal cation. Table 4.12 reports the values of the orbital occupancies among the various complexes. The main effect observed upon complexation is the variation in the occupancies of the 4s and the 3d orbitals. The orbital occupancy is dependent on the site at which the Fe^{n+} cations are coordinated; the results of the complexes with the Fe(II) cation; the occupancy for the 4s orbital increases from 0.000 *e* (in the isolated cation) to a range of 0.091–0.164 *e* and 0.092–0.154 *e* for Fe(II) and Fe(III) cations respectively, for complexes with neutral butein. Among Fe^{n+} complexes with deprotonated butein, the occupancy for the 4s orbital increases from 0.000 *e* to 0.120–0.140 *e* in the Fe(II) and 0.108–0.122 *e* in the Fe(III) cation. Analysis of the occupancy of the *d* orbitals shows that for the occupancy of the d_{xy} (3*d*) orbital, there is a transfer of charge density from the Fe(II) cation to the butein ligand (i.e., for cases where the Fe(II) cation is coordinating to both the neutral and deprotonated ligand); this is evident by analysis of the decrease from 1.998 *e* to a range of 1.046–1.998 *e* for both complexes with the neutral and deprotonated ligand. The remaining *d* orbitals occupancy values shows that upon coordination the butein ligand transfers electron density to the Fe^{n+} cations.

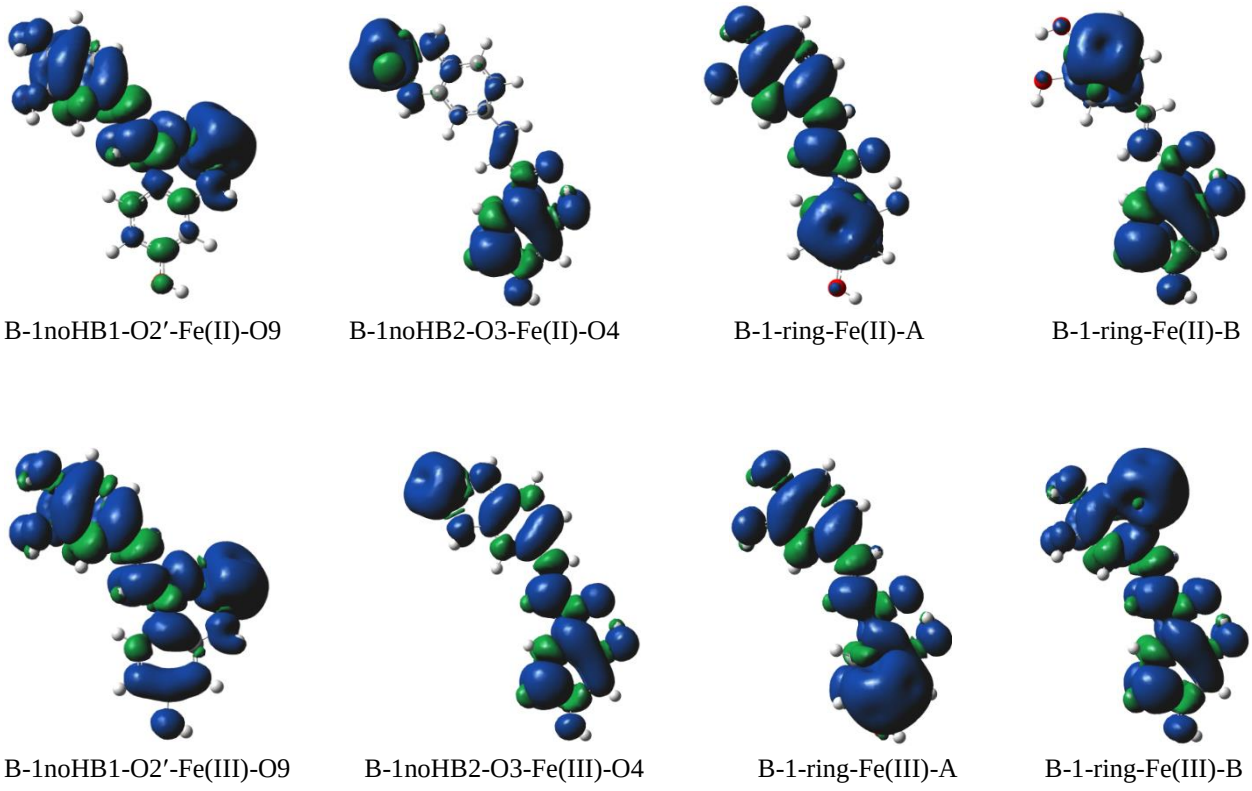

Figure 4.9 Spin density distribution for the butein···Fe^{n+} complexes formed from the interaction of neutral butein and bare Fe^{n+} cations, B3LYP/6-31+G(d,p) results *in vacuo*. The surface isovalue used is 0.0004 au. The blue colour corresponds to positive spin densities and the green colour denotes the negative spin density.

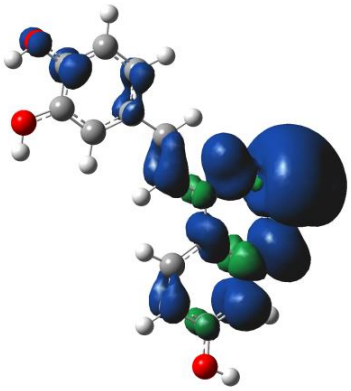

B-1noHB1-an-O2′-Fe(II)-O9

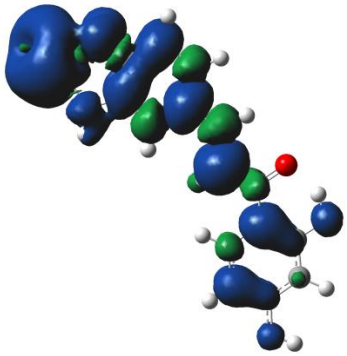

B-1noHB2-anI-O3-Fe(II)-O4

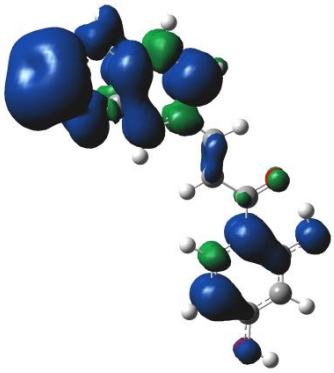

B-1noHB2-anII-O3-Fe(II)-O4

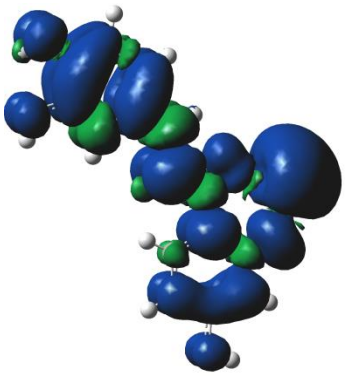

B-1noHB1-an-O2′-Fe(III)-O9

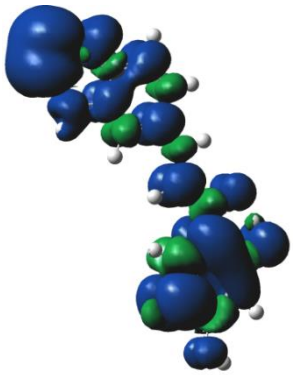

B-1noHB2-anI-O3-Fe(III)-O4

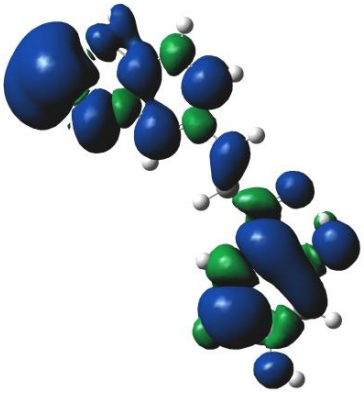

B-1noHB2-anII-O3-Fe(III)-O4

Figure 4.10 Spin density distribution for the butein···Fe^{n+} complexes formed from the interactions of deprotonated butein and bare Fe^{n+} cations, B3LYP/6-31+G(d,p) results *in vacuo*. The surface isovalue used is 0.0004 au. The blue colour corresponds to positive spin densities and the green colour denotes the negative spin density.

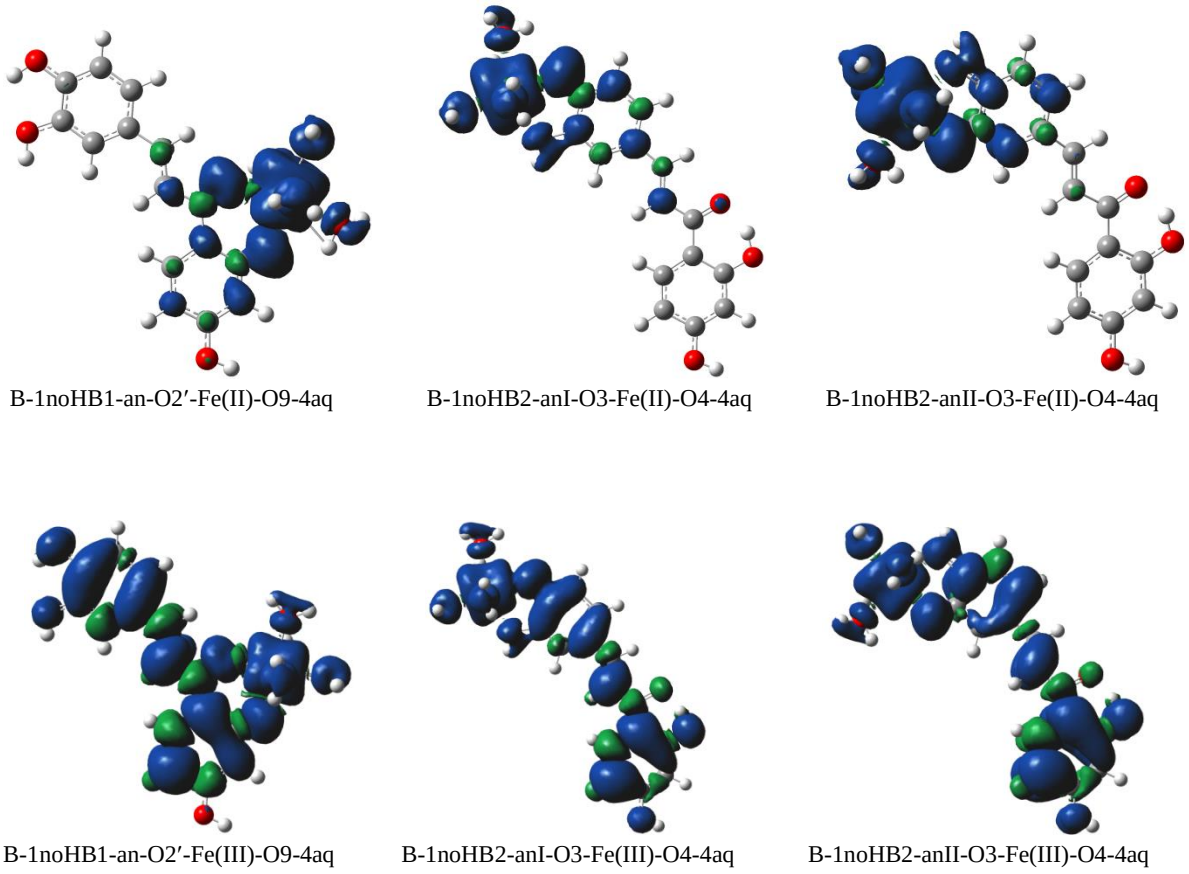

Figure 4.11 Spin density distribution for the butein···Fe^{n+} complexes formed from interactions of deprotonated butein and hydrated Fe^{n+} cation, B3LYP/6-31+G(d,p) results *in vacuo*. The surface isovalue used is 0.0004 au. The blue colour corresponds to positive spin densities and the green colour denotes the negative spin density.

Table 4.12 Natural atomic orbital occupancies for some valence orbitals in the isolated Fe^{n+} cations and in complexes with butein results *in vacuo* with different methods

Isolated and Fe complex	Orbitals and the corresponding natural atomic orbital occupancies					
	S (4s)	d_{xy} (3d)	d_{xz} (3d)	d_{yz} (3d)	$d_{x^2-y^2}$ (3d)	d_{z^2} (3d)
DFT/B3LYP results						
Fe(II)	0.000	1.998	1.000	1.000	1.000	1.000
B-1noHB1-O2′-Fe(II)-O9	0.100	1.188	1.246	1.448	1.494	1.141
B-1noHB2-O3-Fe(II)-O4	0.164	1.240	1.706	1.197	1.491	1.258
B-1-ring-Fe(II)-A	0.088	1.320	1.504	1.578	1.416	1.098
B-1-ring-Fe(II)-B	0.091	1.232	1.296	1.568	1.544	1.285
B-1noHB1-an-O2′-Fe(II)-O9	0.140	1.198	1.306	1.827	1.044	1.023
B-1noHB2-anI-O3-Fe(II)-O4	0.120	1.046	1.823	1.037	1.405	1.365
B-1noHB2-anII-O3-Fe(II)-O4	0.131	1.099	1.061	1.154	1.441	1.830
B-1noHB1-an-O2′-Fe(II)-O9-4aq	0.188	1.133	1.809	1.176	1.053	1.104
B-1noHB2-anI-O3-Fe(II)-O4-4aq	0.183	1.624	1.373	1.116	1.067	1.074
B-1noHB2-anII-O3-Fe(II)-O4-4aq	0.188	1.555	1.253	1.117	1.107	1.268
Fe(III)	0.000	1.000	1.000	1.000	1.000	1.000
B-1noHB1-O2′-Fe(III)-O9	0.092	1.434	1.137	1.240	1.381	1.148
B-1noHB2-O3-Fe(III)-O4	0.050	1.166	1.101	1.280	1.630	1.453
B-1-ring-Fe(III)-A	0.133	1.083	1.832	1.134	1.339	1.102
B-1-ring-Fe(III)-B	0.154	1.145	1.613	1.111	1.352	1.388
B-1noHB1-an-O2′-Fe(III)-O9	0.118	1.182	1.599	1.508	1.059	1.024
B-1noHB2-anI-O3-Fe(III)-O4	0.122	1.069	1.066	1.362	1.670	1.280
B-1noHB2-anII-O3-Fe(III)-O4	0.108	1.469	1.286	1.148	1.158	1.391
B-1noHB1-an-O2′-Fe(III)-O9-4aq	0.188	1.133	1.750	1.187	1.046	1.090
B-1noHB2-anI-O3-Fe(III)-O4-4aq	0.183	1.624	1.373	1.116	1.067	1.074
B-1noHB2-anII-O3-Fe(III)-O4-4aq	0.183	1.506	1.276	1.111	1.107	1.273
DFT/BP86 results						
Fe(II)						
B-1noHB1-O2′-Fe(II)-O9	0.119	1.225	1.270	1.502	1.431	1.203
B-1noHB2-O3-Fe(II)-O4	0.133	1.249	1.694	1.203	1.398	1.26
B-1-ring-Fe(II)-A	0.115	1.361	1.432	1.554	1.345	1.135
B-1-ring-Fe(II)-B	0.117	1.250	1.258	1.528	1.501	1.3
B-1noHB1-an-O2′-Fe(II)-O9	0.156	1.230	1.437	1.809	1.057	1.022
B-1noHB2-anI-O3-Fe(II)-O4	0.183	1.175	1.599	1.189	1.370	1.367
B-1noHB2-anII-O3-Fe(II)-O4	0.210	1.158	1.418	1.079	1.463	1.549
B-1noHB1-an-O2′-Fe(II)-O9-4aq	0.206	1.193	1.834	1.176	1.071	1.116
B-1noHB2-anI-O3-Fe(II)-O4-4aq	0.209	1.554	1.450	1.163	1.114	1.172
B-1noHB2-anII-O3-Fe(II)-O4-4aq	0.211	1.582	1.305	1.133	1.168	1.252
Fe(III)						
B-1noHB1-O2′-Fe(III)-O9	0.105	1.418	1.219	1.322	1.366	1.168
B-1noHB2-O3-Fe(III)-O4	0.063	1.132	1.105	1.271	1.676	1.471
B-1-ring-Fe(III)-A	0.125	1.346	1.751	1.226	1.109	1.162
B-1-ring-Fe(III)-B	0.181	1.392	1.452	1.21	1.227	1.349
B-1noHB1-an-O2′-Fe(III)-O9	0.127	1.236	1.737	1.399	1.089	1.029
B-1noHB2-anI-O3-Fe(III)-O4	0.128	1.346	1.634	1.121	1.214	1.268
B-1noHB2-anII-O3-Fe(III)-O4	0.130	1.275	1.148	1.258	1.295	1.599
B-1noHB1-an-O2′-Fe(III)-O9-4aq	0.217	1.236	1.554	1.217	1.104	1.133
B-1noHB2-anI-O3-Fe(III)-O4-4aq	0.202	1.580	1.394	1.163	1.094	1.138
B-1noHB2-anII-O3-Fe(III)-O4-4aq	0.204	1.446	1.308	1.138	1.144	1.322

4.2.7. Conformational stability and geometries for the homobutein conformers

The optimised conformers for homobutein are shown in Figure 4.12 and their corresponding relative energies (ΔE, kcal/mol) are reported in Table 4.13. The lowest-energy conformers are those stabilised by the presence of the intramolecular hydrogen bond and the higher the number of intramolecular hydrogen bonds is, the greater is the stability of the conformers; a similar trend was observed for the conformers of butein. The ΔE gap between the first lowest-energy conformer and the second lowest-energy conformer is 0.624kcal/mol, suggesting that both of these conformers may exist *in vacuo*. The difference in the energy between the two conformers is related to the difference in the orientation of the O4′H4′ group. The ΔE gap between the lowest-energy conformer and the rest of the conformers (i.e., excluding the second lowest-energy conformer) has a range of 4.311−20.216 kcal/mol, which suggests that these conformers may not be considered to exist in nature (i.e., they are minimally populated). A comparison of the hB-1 and hB-1-noHB2 pair suggests that the removal of the second intramolecular hydrogen bond corresponds to energy increase of ≈ 4.311 kcal/mol, which is similar to energy range for the removal of the H-bond from the catechol unit [140]. The removal of the first intramolecular hydrogen bond in the hB-2 to form hB-2-noHB1 results in energy increase of 14.460 kcal/mol; these results suggest that the second intramolecular hydrogen bond is weaker than the first intramolecular hydrogen, so that the first intramolecular hydrogen bond has greater stabilising role than the second intramolecular hydrogen bond. Similar trends are observed for the conformers of butein, where the second intramolecular hydrogen bond, formed at the catechol unit, is weaker than the first intramolecular hydrogen bond.

Conformers hB-4, hB-5 and hB-6 were obtained through rotation of the C7−C8 bond in hB-1, hB-1-noHB2 and hB-1-noHB1 respectively so that the C1–C7–C8–C9 torsion angle is nearly 0°. The energy difference between the conformer with the bent aliphatic chain and the conformer with the non-bent aliphatic chain is 6.297 kcal/mol (in the hB-1 & hB-4 conformers), where both the first intramolecular hydrogen bond and the second intramolecular hydrogen bond are present, and a difference of 0.271 kcal/mol for the hB-1noHB1 & hB-6 pair, where only the first intramolecular hydrogen bond is absent. An overall comparison of the conformers with non-bent chain and the corresponding conformers with the bent aliphatic chain suggests that the bent chain arrangement is preferred to the non-bent arrangement.

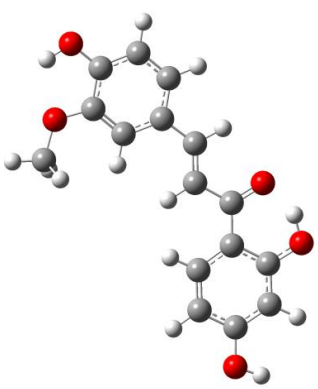

0.000
hB-1

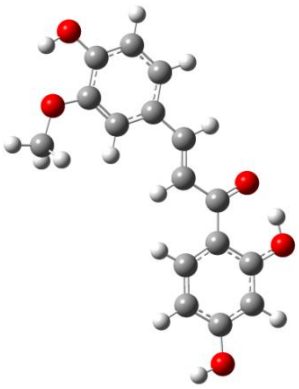

0.624
hB-2

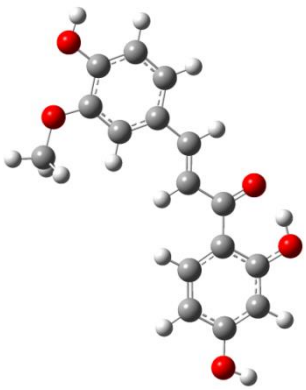

4.311
hB-1noHB2

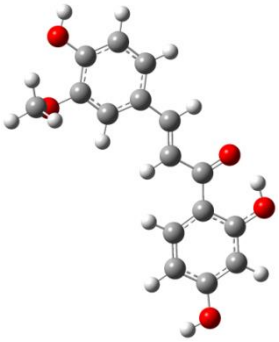

6.309
hB-3

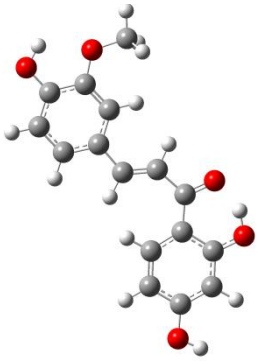

6.297
hB-4

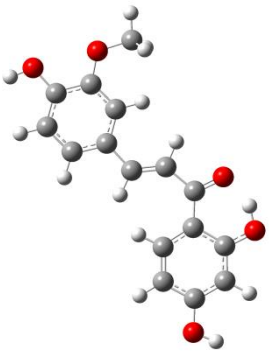

14.295
hB-5

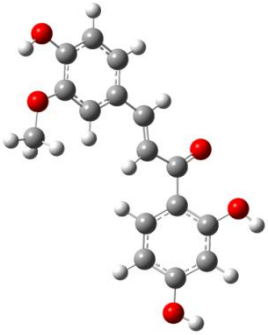

15.084
hB-1noHB1

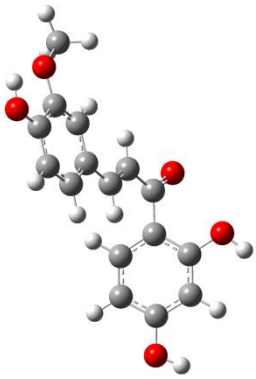

15.355
hB-6

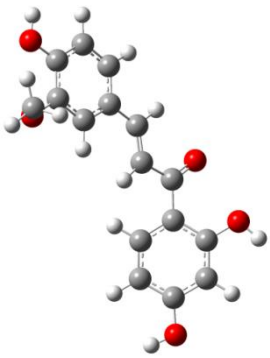

20.216
hB-3noHB1

Figure 4.12 B3LYP/6-31+G(d,p) optimised conformers for neutral homobutein arranged in order of increasing relative energy (ΔE, kcal/mol) B3LYP/6-311+G(2d,p)//B3LYP/6-31+G(d,p) results *in vacuo*. Similar geometries were obtained using the BP86/6-311+G(2d,p)//BP86/6-31+G(d,p) calculation method.

Table 4.13 *In vacuo* relative energy values (ΔE, kcal/mol) for the neutral conformers of homobutein

Conformer	*A*[a]		*B*[b]	
	total energy (Hartree)	ΔE (kcal/mol)	total energy (Hartree)	ΔE (kcal/mol)
DFT/B3LYP results				
hB-1	-994.3084711	0.000	-994.5530655	0.000
hB-2	-994.3072586	0.761	-994.5520710	0.624
hB-1noHB2	-994.3011406	4.600	-994.5461952	4.311
hB-3	-994.2982447	6.417	-994.5430110	6.309
hB-4	-994.2979633	6.594	-994.5430305	6.297
hB-5	-994.2832858	15.804	-994.5302852	14.295
hB-1noHB1	-994.2838856	15.428	-994.5290274	15.084
hB-6	-994.2906174	11.203	-994.5285960	15.355
hB-3noHB1	-994.2754070	20.750	-994.5208487	20.216
DFT/BP86 results				
hB-1	-994.3114432	0.000	-994.5582217	0.000
hB-2	-994.3102363	0.757	-994.5572329	0.620
hB-1noHB2	-994.3044615	4.381	-994.5516191	4.143
hB-3	-994.3021267	5.846	-994.5489516	5.817
hB-4	-994.2997457	7.340	-994.5469494	7.074
hB-6	-994.2993013	7.619	-994.5465726	7.310
hB-5	-994.2838663	17.305	-994.5311851	16.966
hB-1noHB1	-994.2832643	17.683	-994.5306706	17.289
hB-3noHB1	-994.2742514	23.338	-994.5218438	22.827

[a] Results obtained using the 6-31+G(d,p) basis set
[b] Single point results using the 6-311+G(2d,p) basis set, starting from the optimised geometries

The optimised deprotonated conformers of homobutein are shown in Figure 4.13 and the corresponding relative energy values (ΔE, kcal/mol) are reported in Table 4.14. Homobutein has two possible sites where a proton can be removed, H2′ and H4″. The lowest-energy conformer corresponds to the removal of the H4″ proton, a result which is consistent with the results obtained for the deprotonated butein (section 4.2.1). The ΔE gap between the lowest-energy conformer and the second lowest-energy conformer is 4.112 kcal/mol. The high relative energy values for hB-6-an and hB-1noHB1-an indicate that it is not a preferred action to remove a proton that is engaged in intramolecular hydrogen bonding.

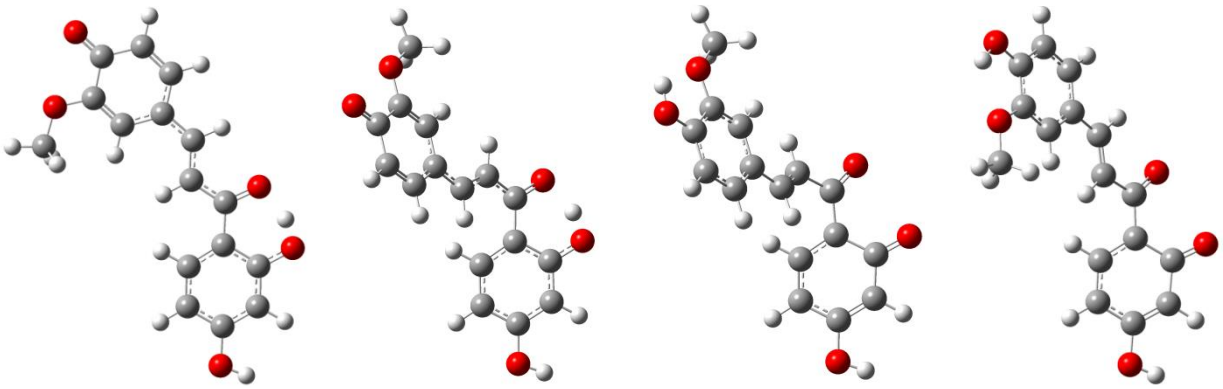

0.000
hB-1noHB2-an

4.112
hB-4-an

20.400
hB-6-an

23.256
hB-1noHB1-an

Figure 4.13 B3LYP/6-31+G(d,p) optimised conformers of the deprotonated isolated homobutein arranged in order of increasing relative energy (ΔE, kcal/mol) B3LYP/6-311+G(2d,p)// B3LYP/6-31+G(d,p) results *in vacuo*. Similar geometries were obtained using the BP86/6-311+G(2d,p)// BP86/6-31+G(d,p) calculation method.

Table 4.14 *In vacuo* relative energy values (ΔE, kcal/mol) for deprotonated conformers of homobutein

Conformer	*A*[a]		*B*[b]	
	total energy (Hartree)	ΔE (kcal/mol)	total energy (Hartree)	ΔE (kcal/mol)
DFT/B3LYP results				
hB-1noHB2-an	-993.7758992	0.000	-994.0205417	0.000
hB-4-an	-993.7692462	4.175	-994.0139887	4.112
hB-6-an	-993.7362190	24.900	-993.9880318	20.400
hB-1noHB1-an	-993.7389862	23.163	-993.9834814	23.256
DFT/BP86 results				
hB-1noHB2-an	-993.7872307	0.000	-994.0337530	0.000
hB-4-an	-993.7810815	3.857	-994.0275787	3.874
hB-6-an	-993.7420610	28.344	-993.9885109	23.390
hB-1noHB1-an	-993.7447025	26.687	-993.9912435	26.675

[a] Results obtained using the 6-31+G(d,p) basis set
[b] Single point results using the 6-311+G(2d,p) basis set, starting from optimised geometries

4.2.8. Relative stability and binding energies for homobutein···Fe^{n+} complexes formed from neutral homobutein and bare Fe^{n+} cations

The optimised structures for the homobutein···Fe^{n+} complexes are shown in Figure 4.14 and Figure 4.15 for the DFT/B3LYP results and DFT/BP86 results respectively; the corresponding relative energy values (ΔE, kcal/mol) are reported in Table 4.15. The lowest-energy complexes (hB-1noHB1-O2′-Fe(II)-O9 and hB-1noHB1-O2′-Fe(III)-O9) correspond to the coordination of the cation at the hydroxyl–*keto* reactive site. The ΔE gap between the lowest-energy complex and the second lowest-energy complex is 21.865 and 27.241 kcal/mol for the Fe(II) and Fe(III) cations respectively, which suggest that only coordination at the O2′∪O9 reactive site is the most probable to observe *in vacuo*. The formation of the six membered chelate ring on the hB-1noHB1-O2′-Fe(n)-O9 complexes may account for the preference of the cation to coordinate at the O2′∪O9 reactive site.

The second lowest-energy complex corresponds to the coordination of the cation at the methoxy–hydroxyl reactive site. Coordination of the cations at the π system of the aromatic ring A and B suggests that among the Fe(II) complexes the coordination at ring A is preferred over coordination at ring B while for complexes with the Fe(III) cation coordination at ring B is preferred over coordination at ring A. The results obtained suggest that cation···lone pair interactions are stronger (and therefore have greater role in stabilising the complexes) than cation···π interactions. The relative energy trend obtained here is also in agreement with the trend observed for butein.

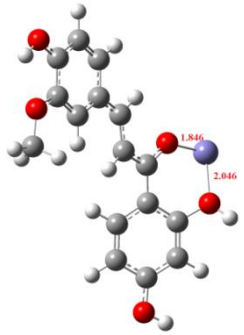

0.000
hB-1noHB1-O2′-Fe(II)-O9

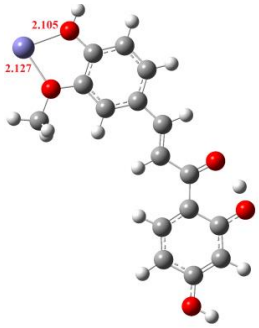

21.865
hB-1noHB2-O3-Fe(II)-O4

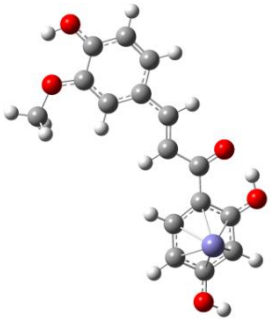

22.545
hB-1-ring-Fe(II)-A

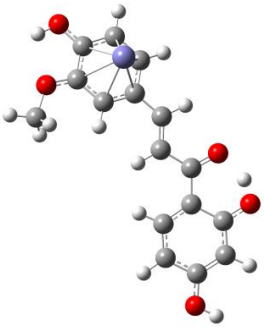

30.639
hB-1-ring-Fe(II)-B

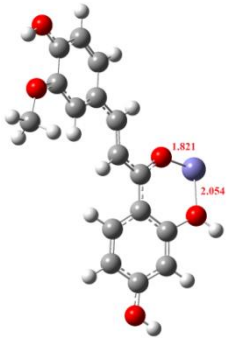

0.000
hB-1noHB1-O2′-Fe(III)-O9

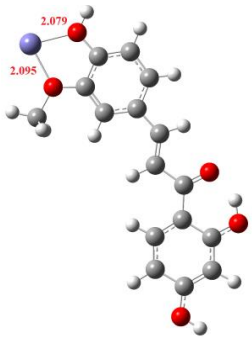

27.241
hB-1noHB2-O3-Fe(III)-O4

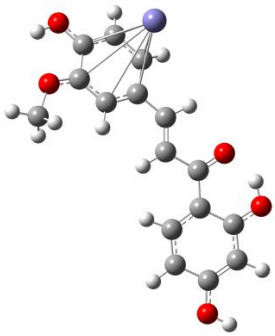

38.313
hB-1-ring-Fe(III)-B

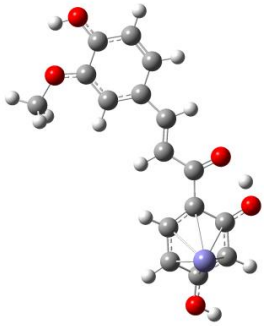

40.027
hB-1-ring-Fe(III)-A

Figure 4.14 B3LYP/6-31+G(d,p) optimised homobutein···Fe^{n+} complexes (arranged in order of increasing relative energy (ΔE, kcal/mol)) formed from neutral homobutein with bare Fe^{n+} cation, B3LYP/6-311+G(2d,p)//B3LYP/6-31+G(d,p) results *in vacuo*. The bond distances between the ligand and the Fe^{n+} cation are reported in Å.

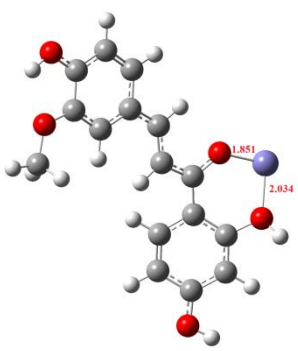

0.000
hB-1noHB1-O2′-Fe(II)-O9

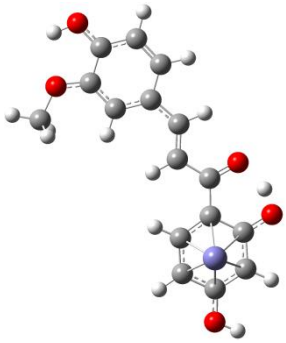

13.476
hB-1-ring-Fe(II)-A

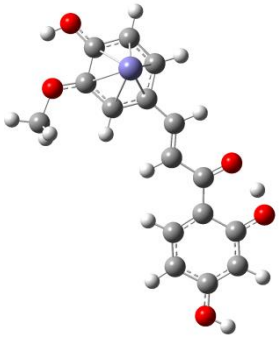

20.747
hB-1-ring-Fe(II)-B

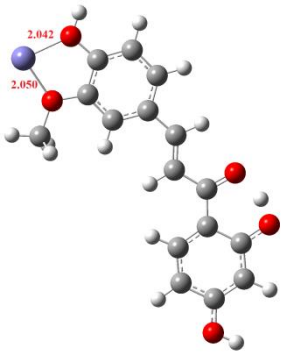

24.282
hB-1noHB2-O3-Fe(II)-O4

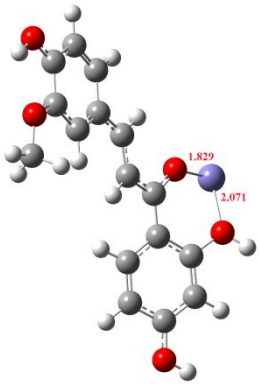

0.000
hB-1noHB1-O2′-Fe(III)-O9

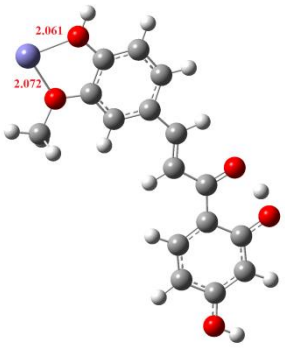

23.889
hB-1noHB2-O3-Fe(III)-O4

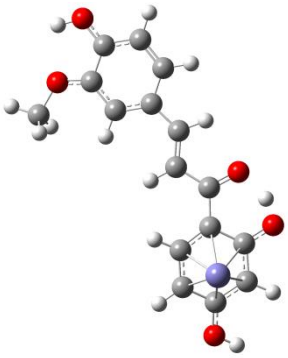

26.825
hB-1-ring-Fe(III)-A

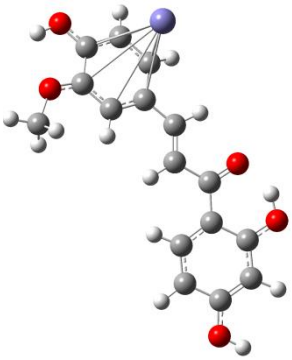

33.402
hB-1-ring-Fe(III)-B

Figure 4.15 BP86/6-31+G(d,p) optimised homobutein···Fe^{n+} complexes (arranged in order of increasing relative energy (ΔE, kcal/mol)) formed from neutral homobutein and bare Fe^{n+} cation, BP86/6-311+G(2d,p)//BP86/6-31+G(d,p) results *in vacuo*. The bond distances between the ligand and the Fe^{n+} cation are reported in Å.

Table 4.15 *In vacuo* relative energy values (ΔE, kcal/mol) for homobutein···Fe^{n+} complexes formed from neutral homobutein and bare Fe^{n+} cations

Complex	*A*[a]		*B*[b]	
	total energy (Hartree)	ΔE (kcal/mol)	total energy (Hartree)	ΔE (kcal/mol)
DFT/B3LYP results				
hB-1noHB1-O2′-Fe(II)-O9	-1117.1488702	0.000	-2257.6829046	0.000
hB-1noHB2-O3-Fe(II)-O4	-1117.1170775	19.950	-2257.6480600	21.865
hB-1-ring-Fe(II)-A	-1117.1130926	22.451	-2257.6469772	22.545
hB-1-ring-Fe(II)-B	-1117.1001259	30.587	-2257.6340780	30.639
hB-1noHB1-O2′-Fe(III)-O9	-1116.6704360	0.000	-2257.2050864	0.000
hB-1noHB2-O3-Fe(III)-O4	-1116.6329094	23.548	-2257.1616749	27.241
hB-1-ring-Fe(III)-B	-1116.6089343	38.593	-2257.1440301	38.313
hB-1-ring-Fe(III)-A	-1116.6081970	39.056	-2257.1412986	40.027
DFT/BP86 results				
hB-1noHB1-O2′-Fe(II)-O9	-1117.2226953	0.000	-2257.8518663	0.000
hB-1-ring-Fe(II)-A	-1117.1962886	16.570	-2257.8303903	13.476
hB-1-ring-Fe(II)-B	-1117.1845432	23.941	-2257.8188046	20.747
hB-1noHB2-O3-Fe(II)-O4	-1117.1893278	20.938	-2257.8131708	24.282
hB-1noHB1-O2′-Fe(III)-O9	-1116.7384608	0.000	-2257.3672520	0.000
hB-1noHB2-O3-Fe(III)-O4	-1116.7057095	20.552	-2257.3291822	23.889
hB-1-ring-Fe(III)-A	-1116.6900251	30.394	-2257.3245041	26.825
hB-1-ring-Fe(III)-B	-1116.6869438	32.327	-2257.3140217	33.402

[a] Results obtained using the 6-31+G(d,p) basis set
[b] Single point results using the 6-311+G(2d,p) basis set, starting from optimised geometries

The binding energy values ($\Delta E'_{binding}$, kcal/mol) are reported in Table 4.16. The strongest binding between the homobutein central ligand and the Fe^{n+} cations corresponds to coordination at the hydroxyl–*keto* reactive site, with MIA values of 267.348 and 702.916 kcal/mol for the coordination of the Fe(II) and Fe(III) cations respectively. This result is in agreement with the relative stability results in that, coordination at the hydroxyl–*keto* reactive site is the most preferred. The coordination of the Fe^{n+} cations at the methoxy–hydroxyl site has MIA values of 226.290 for Fe(II) cation and 653.516 kcal/mol for Fe(III) cation. The weakest binding corresponds to the coordination of the Fe^{n+} cations at the π system of the aromatic rings, similar trends were observed for the relative energy of the complexes. The $\Delta E'_{binding}$ values of the Fe(III) cation are much higher than those of Fe(II) which indicates that homobutein acts as a better antioxidant when chelating Fe(III) than Fe(II) cation.

Table 4.16 Binding energy values ($\Delta E'_{binding,}$ kcal/mol) for homobutein···Fe^{n+} complexes formed from netural homobutein and bare Fe^{n+} cations results *in vacuo*. The complexes are arranged in order of decreasing $\Delta E'_{binding}$ values

	A[a]			*B*[b]		
Complex	$\Delta E_{inter,}$ kcal/mol	ΔE_{def} kcal/mol	$\Delta E'_{binding,}$ kcal/mol	$\Delta E_{inter,}$ kcal/mol	ΔE_{def} kcal/mol	$\Delta E'_{binding,}$ kcal/mol
DFT/B3LYP results						
hB-1noHB1-O2′-Fe(II)-O9	–240.962	13.843	254.805	–252.797	14.551	267.348
hB-1noHB2-O3-Fe(II)-O4	–210.184	5.873	216.057	–220.158	6.132	226.290
hB-1-ring-Fe(II)-A	–203.084	9.492	212.576	–215.168	10.186	225.354
hB-1-ring-Fe(II)-B	–194.947	8.840	203.787	–207.074	9.586	216.660
hB-1noHB1-O2′-Fe(III)-O9	–683.328	20.602	703.930	–681.380	21.536	702.916
hB-1noHB2-O3-Fe(III)-O4	–648.952	9.653	658.605	–643.366	10.150	653.516
hB-1-ring-Fe(III)-A	–628.845	20.890	649.735	–626.268	21.787	648.055
hB-1-ring-Fe(III)-B	–629.308	18.100	647.408	–627.982	18.869	646.851
DFT/BP86 results						
hB-1noHB1-O2′-Fe(II)-O9	–260.664	12.095	272.759	–275.352	12.145	287.497
hB-1-ring-Fe(II)-A	–226.790	9.335	236.125	–244.909	10.184	255.093
hB-1-ring-Fe(II)-B	–219.419	8.191	227.610	–236.639	9.043	245.682
hB-1noHB2-O3-Fe(II)-O4	–226.802	5.193	231.995	–238.247	5.438	243.685
hB-1noHB1-O2′-Fe(III)-O9	–705.277	16.600	721.877	–705.874	17.541	723.415
hB-1-ring-Fe(III)-A	–657.578	17.060	680.140	–662.084	18.185	680.269
hB-1noHB2-O3-Fe(III)-O4	–671.801	8.339	674.638	–669.162	8.900	678.062
hB-1-ring-Fe(III)-B	–655.644	15.460	671.104	–655.605	16.389	671.994

[a] Results obtained using the 6-31+G(d,p) basis set
[b] Single point results using the 6-311+G(2d,p) basis set, starting from optimised geometries

4.2.9. Relative stability and binding energies for homobutein···Fe^{n+} complexes formed from deprotonated homobutein and bare Fe^{n+} cations

The optimised homobutein···Fe^{n+} complexes with deprotonated homobutein ligand are shown in Figure 4.16; the corresponding relative energy values (ΔE, kcal/mol) are reported in Table 4.17. The lowest-energy complex corresponds to coordination of the Fe^{n+} cation at the O2′∪O9 reactive site in hB-1noHB2-an-O2′-Fe(II)-O9 and hB-1noHB2-an-O2′-Fe(III)-O9 complexes. The stability of these complexes may be related to the fact that upon coordination of the Fe^{n+} cation, a six membered chelate ring is formed involving the Fe^{n+} cations and the C1′,C9, O9, O2′ and C2′ atoms. The relative stability of these complexes may furthermore be related to the fact that the O2′ and O9 atom acts as a carbonyls with ample of electrons to donate to the Fe^{n+} cations, thus resulting in relatively stable complexes. The ΔE gap between the complexes obtained through coordination of the Fe^{n+} cation at the two available sites suggests that *in vacuo* only the coordination of the cation at the O2′∪O9 reactive site may be considered to exist. Similar trends were reported for the Fe complexes with the deprotonated butein ligand.

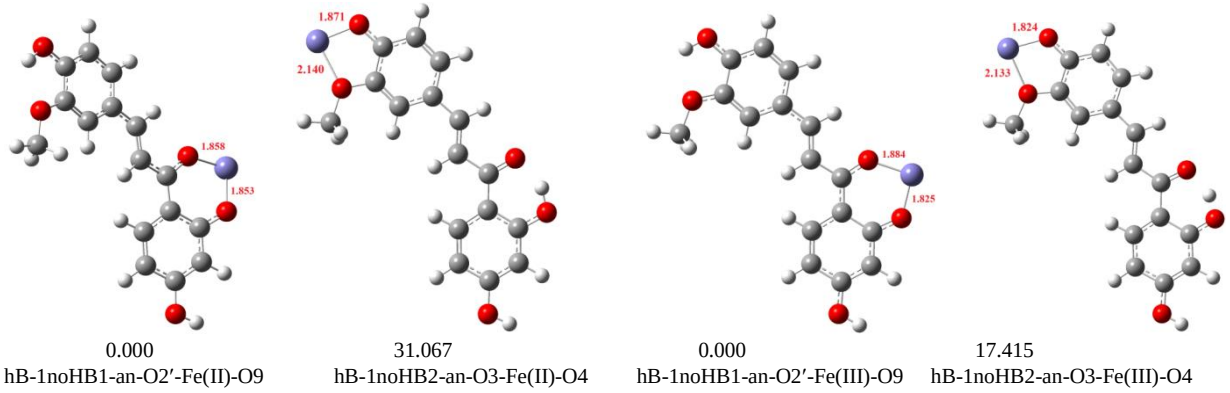

0.000 hB-1noHB1-an-O2′-Fe(II)-O9 | 31.067 hB-1noHB2-an-O3-Fe(II)-O4 | 0.000 hB-1noHB1-an-O2′-Fe(III)-O9 | 17.415 hB-1noHB2-an-O3-Fe(III)-O4

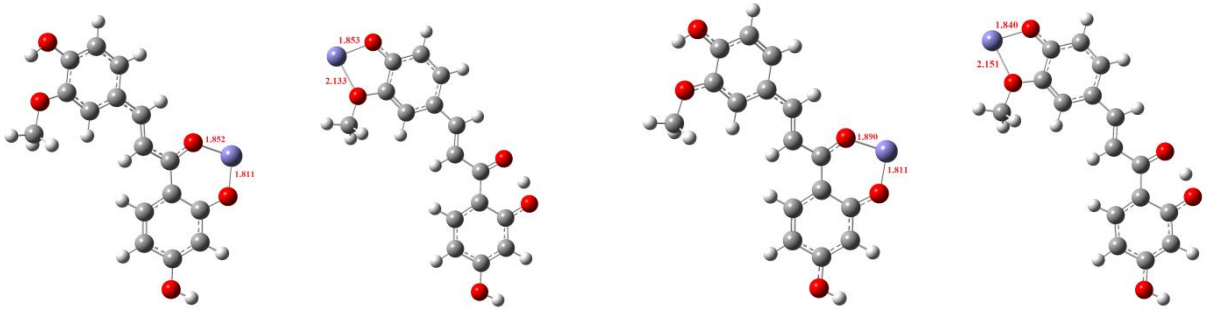

0.000 hB-1noHB1-an-O2′-Fe(II)-O9 | 27.287 hB-1noHB2-an-O3-Fe(II)-O4 | 0.000 hB-1noHB1-an-O2′-Fe(III)-O9 | 26.004 hB-1noHB2-an-O3-Fe(III)-O4

Figure 4.16 Optimised homobutein···Fe^{n+} complexes (arranged in order of increasing relative energy (ΔE, kcal/mol)) formed from deprotonated homobutein and bare Fe^{n+} cation B3LYP/6-31+G(d,p) results are reported in the first row and BP86/6-31+G(d,p) optimised complexes are reported in the second row. The bond length between the cation and the ligand are reported in Å.

Table 4.17 *In vacuo* relative energy values (ΔE, kcal/mol) for homobutein···Fe^{n+} complexes formed from deprotonated homobutein ligand and bare Fe^{n+} cations

Complex	*A*[a]		*B*[b]	
	total energy (Hartree)	ΔE (kcal/mol)	total energy (Hartree)	ΔE (kcal/mol)
DFT/B3LYP results				
hB-1noHB1-an-O2′-Fe(II)-O9	-1116.9047898	0.000	-2257.4530918	0.000
hB-1noHB2-an-O3-Fe(II)-O4	-1116.8705791	21.468	-2257.4035840	31.067
hB-1noHB1-an-O2′-Fe(III)-O9	-1116.5504590	0.000	-2257.0721640	0.000
hB-1noHB2-an-O3-Fe(III)-O4	-1116.5093248	25.812	-2257.0444107	17.415
DFT/BP86 results				
hB-1noHB1-an-O2′-Fe(II)-O9	-1116.9881467	0.000	-2257.6227484	0.000
hB-1noHB2-an-O3-Fe(II)-O4	-1116.9503515	23.717	-2257.5792635	27.287
hB-1noHB1-an-O2′-Fe(III)-O9	-1116.6231196	0.000	-2257.2570445	0.000
hB-1noHB2-an-O3-Fe(III)-O4	-1116.5868179	22.780	-2257.2156049	26.004

[a] Results obtained using the 6-31+G(d,p) basis set
[b] Single point results using the 6-311+G(2d,p) basis set, starting from optimised geometries

The binding energy values ($\Delta E'_{binding}$, kcal/mol) are reported in Table 4.18. The strongest binding corresponds to the coordination at the O2′∪O9 reactive site with the MIA value of 465.519 and 959.927 kcal/mol for the Fe(II) and Fe(III) cations respectively. This result is in agreement with the relative energy values for these complexes in that the O2′∪O9 reactive site is the most preferred site of coordination. The bond distance values at the O2 deprotonated site corresponds to 1.853 and 1.825 Å for complexes with the Fe(II) and Fe(III) cation respectively and to 1.871 and 1.824 Å at the O4 deprotonated site for Fe(II) and Fe(III) cations respectively. The shortened bond distances among the complexes with the Fe(III) cations suggests that the binding of the Fe(III) cation to the homobutein ligand is stronger than that of the Fe(II), this is further supported by the strong binding energy values of the complexes with the Fe(III) cation. A comparison of the binding energy for the non-deprotonated and the corresponding complex in which the proton is removed suggests that the Fe^{n+} cation has greater affinity for the deprotonated species than the neutral chalcone molecule. The implication for this is that in biological systems, the antioxidant properties of chalcone derivatives (in line with their metal chelation ability) are likely to be associated with the deprotonated species of these compounds.

Table 4.18 Binding energy values ($\Delta E'_{binding,}$ kcal/mol) for homobutein···Fe^{n+} complexes formed from deprotonated homobutein ligand and bare Fe^{n+} cations results *in vacuo*. The complexes are arranged in order of decreasing $\Delta E'_{binding}$ values

	A[a]			*B*[b]		
Complex	$\Delta E_{inter,}$ kcal/mol	ΔE_{def} kcal/mol	$\Delta E'_{binding,}$ kcal/mol	$\Delta E_{inter,}$ kcal/mol	ΔE_{def} kcal/mol	$\Delta E'_{binding,}$ kcal/mol
DFT/B3LYP results						
hB-1noHB1-an-O2′-Fe(II)-O9	–429.729	14.033	443.762	–450.922	14.597	465.519
hB-1noHB2-an-O3-Fe(II)-O4	–385.099	9.241	394.340	–396.599	9.091	405.690
hB-1noHB1-an-O2′-Fe(III)-O9	–949.971	19.034	969.005	–940.305	19.622	959.927
hB-1noHB2-an-O3-Fe(III)-O4	–900.995	14.764	915.759	–899.634	14.781	914.415
DFT/BP86 results						
hB-1noHB1-an-O2′-Fe(II)-O9	–451.813	13.691	465.504	–470.396	14.149	484.545
hB-1noHB2-an-O3-Fe(II)-O4	–401.410	8.359	409.769	–416.434	8.246	424.680
hB-1noHB1-an-O2′-Fe(III)-O9	–971.229	16.181	987.410	–975.536	16.725	992.261
hB-1noHB2-an-O3-Fe(III)-O4	–921.763	11.293	933.056	–922.857	11.343	934.200

[a] Results obtained using the 6-31+G(d,p) basis set
[b] Single point results using the 6-311+G(2d,p) basis set, starting from optimised geometries

4.2.10. Relative stability and binding energies for the homobutein···Fe^{n+} complexes formed from deprotonated homobutein and hydrated Fe^{n+} cations

The homobutein···Fe^{n+} complexes with the hydrated Fe^{n+} cations are shown in Figure 4.17 and the corresponding relative energy values (ΔE, kcal/mol) are reported in Table 4.19. The only preferred site for the coordination of the hydrated Fe^{n+} cation is the O2′∪O9 reactive site. Similar trends are observed for the complexes with the bare Fe^{n+} cations; the results furthermore imply that *in vacuo* the presence of explicit solvent molecules does not significantly alter the relative stability of the complexes.

The binding energy values ($\Delta E'_{binding}$ kcal/mol) are reported in Table 4.20. The highest binding energy corresponds to the coordination to the O2′∪O9 reactive site with MIA values of 542.150 and 1062.841 kcal/mol for Fe(II) and Fe(III) cations respectively. The coordination of the Fe^{n+} cation at the O3∪O4 reactive site is 504.562 kcal/mol for Fe(II) cation and 1024.313 kcal/mol for the Fe(III) cation. Inclusion of explicit solvent molecules at the reactive site to which the Fe^{n+} cation is coordinated results in stronger binding energies compared to the binding energy values with the bare Fe^{n+} cations. The results of the complexes with the Fe(III) cation have higher binding energy values than those of the complexes with the Fe(II) cation; implying that homobutein may act as a better antioxidant when chelating the Fe(III) cation than the Fe(II) cation.

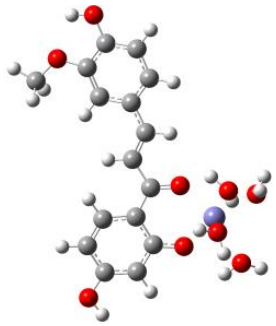

0.000
hB-1noHB1-an-O2′-Fe(II)-O9-4aq

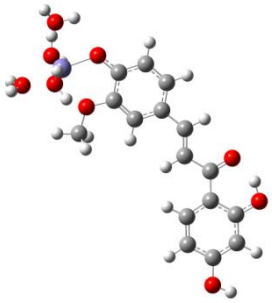

16.404
hB-1noHB2-an-O3-Fe(II)-O4-4aq

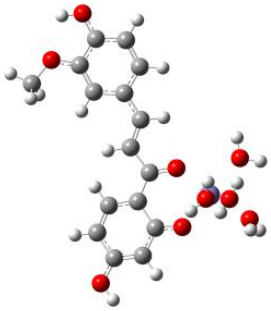

0.000
hB-1noHB1-an-O2′-Fe(III)-O9-4aq

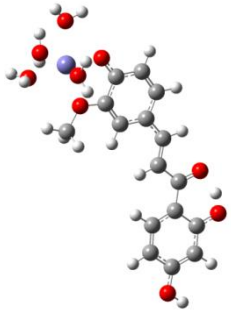

11.700
hB-1noHB2-an-O3-Fe(III)-O4-4aq

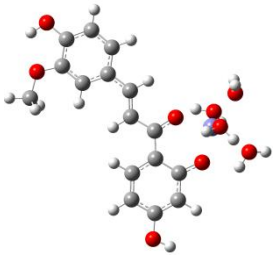

0.000
hB-1noHB1-an-O2′-Fe(II)-O9-4aq

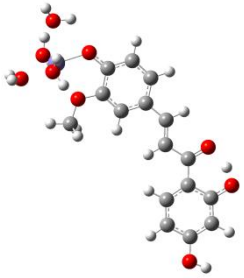

16.555
hB-1noHB2-an-O3-Fe(II)-O4-4aq

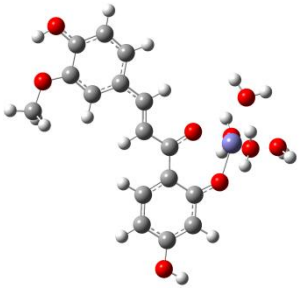

0.000
hB-1noHB1-an-O2′-Fe(III)-O9-4aq

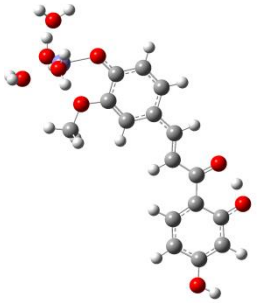

19.177
hB-1noHB2-an-O3-Fe(III)-O4-4aq

Figure 4.17 Optimised homobutein···Fe^{n+} complexes (arranged in order of increasing relative energy (ΔE, kcal/mol)) formed from deprotonated homobutein ligand and hydrated Fe^{n+} cations B3LYP/6-31+G(d,p) results are reported in the first row and BP86/6-31+G(d,p) results are reported in the second row.

Table 4.19 *In vacuo* relative energy values (ΔE, kcal/mol) for homobutein···Fe^{n+} complexes formed from deprotonated homobutein and hydrated Fe^{n+} cations

Complex	*A*[a]		*B*[b]	
	total energy (Hartree)	ΔE (kcal/mol)	total energy (Hartree)	ΔE (kcal/mol)
DFT/B3LYP results				
hB-1noHB1-an-O2′-Fe(II)-O9-4aq	-1422.7914253	0.000	-2563.4226537	0.000
hB-1noHB2-an-O3-Fe(II)-O4-4aq	-1422.7663956	15.706	-2563.3965126	16.404
hB-1noHB1-an-O2′-Fe(III)-O9-4aq	-1422.4546969	0.000	-2563.0866523	0.000
hB-1noHB2-an-O3-Fe(III)-O4-4aq	-1422.4384133	10.218	-2563.0680075	11.700
DFT/BP86 results				
hB-1noHB1-an-O2′-Fe(II)-O9-4aq	-1422.8486005	0.000	-2563.5790368	0.000
hB-1noHB2-an-O3-Fe(II)-O4-4aq	-1422.8243660	15.207	-2563.5526543	16.555
hB-1noHB1-an-O2′-Fe(III)-O9-4aq	-1422.5231965	0.000	-2563.2581912	0.000
hB-1noHB2-an-O3-Fe(III)-O4-4aq	-1422.4991164	15.110	-2563.2276311	19.177

[a] Results obtained using the 6-31+G(d,p) basis set
[b] Single point results using the 6-311+G(2d,p) basis set, starting from optimised geometries

Table 4.20 Binding energy values ($\Delta E'_{binding}$, kcal/mol) for homobutein···Fe^{n+} complexes formed from deprotonated butein ligand and hydrated Fe^{n+} cations results *in vacuo*. The complexes are arranged in order of decreasing $\Delta E'_{binding}$ values

Complex	*A*[a]			*B*[b]		
	ΔE_{inter}, kcal/mol	ΔE_{def} kcal/mol	$\Delta E'_{binding}$, kcal/mol	ΔE_{inter}, kcal/mol	ΔE_{def} kcal/mol	$\Delta E'_{binding}$, kcal/mol
DFT/B3LYP results						
hB-1noHB1-an-O2′-Fe(II)-O9-4aq	–598.683	8.286	606.969	–533.455	8.695	542.150
hB-1noHB2-an-O3-Fe(II)-O4-4aq	–559.813	10.916	570.729	–493.795	10.767	504.562
hB-1noHB1-an-O2′-Fe(III)-O9-4aq	–1056.992	9.832	1066.824	–1051.029	11.812	1062.841
hB-1-noHB2-an-O3-Fe(III)-O4-4aq	–1022.041	8.241	1030.282	–1016.074	8.239	1024.313
DFT/BP86 results						
hB-1noHB1-an-O2′-Fe(II)-O9-4aq	530.042	8.551	538.593	–544.003	8.891	552.894
hB-1noHB2-an-O3-Fe(II)-O4-4aq	488.148	9.084	497.232	–500.773	8.901	509.674
hB-1noHB1-an-O2′-Fe(III)-O9-4aq	1074.322	12.528	1086.850	–1077.291	12.962	1090.253
hB-1noHB2-an-O3-Fe(III)-O4-4aq	1032.525	7.661	1040.190	–1031.439	7.652	1039.091

[a] Results obtained using the 6-31+G(d,p) basis set
[b] Single point results using the 6-311+G(2d,p) basis set, starting from optimised geometries

4.2.11. AIM analysis of the bonding within the homobutein complexes

The bond critical point values for the homobutein···Fe^{n+} complexes are reported in Table 4.21 and Table 4.22 for the DFT/B3LYP and DFT/BP86 results respectively. The strongest bond for the complexes with the neutral homobutein ligand corresponds to the O9···Fe^{n+} bond; which has the highest values (of 0.120 e/$Å^3$ for Fe(II) and 0.130 e/$Å^3$ for Fe(III)). The weakest bond corresponds to the coordination of the cation at the π system of the aromatic rings. The various C···Fe bonds have a range of 0.042–0.054 for the Fe(II) cation and 0.069–0.072 e/$Å^3$ for the Fe(III) cation. Among the complexes with the deprotonated homobutein ligand the largest value of ρ corresponds to the O2′···Fe^{n+} in the hB-1noHB1-an-O2′-Fe(II)-O9 complex with values of 0.124 and 0.128 e/$Å^3$ for Fe(II) and Fe(III) cations respectively. Similar trends are observed for the homobutein···Fe^{n+} complexes to those of the butein···Fe^{n+} complexes in that for the neutral ligand molecule, the strongest bond corresponds to the O9···Fe^{n+} bond and for complexes with the deprotonated ligand the O2′···Fe^{n+} bond is the strongest.

The value of ρ for the complexes with hydrated Fe^{n+} cation is smaller than for the complexes with bare Fe^{n+} cation, which suggests that the effect of hydration weakens the O···Fe bond as well as the C···Fe bond. Analysis of the $\nabla^2\rho$ (e$Å^5$) values among the homobutein···Fe^{n+} complexes shows a range of 0.120–0.673 and 0.107–0.687 e/$Å^5$ for Fe(II) and Fe(III) with the neutral ligand and a 0.342–0.674 and 0.283–0.740 e/$Å^5$ range for complexes with the deprotonated ligand. The positive values of the Laplacian ($\nabla^2\rho$) are an indication of dative interactions, consistent with the results obtained for the butein complexes. Furthermore, the analysis of the *H* and its components, the kinetic (*G*) and potential (*V*) further supports the fact that the interactions between the Fe^{n+} cation and the ligand are dative in nature. The |V|/G ratio with a 0.9–1.4 range also suggests that the interactions are dative in character.

Table 4.21 Bond critical point data for butein···Fe^{n+} complexes for both the neutral and deprotonated butein UB3LYP/6-31+G(d,p) results *in vacuo*

Complex	Bond type	ρ e/Å^3	$\nabla^2\rho$ e/Å^5	V (Hartree)	G (Hartree)	H (Hartree)	$\frac{\lvert V \rvert}{G}$
hB-1noHB1-O2′-Fe(II)-O9	O2′···Fe	0.068	0.407	–0.105	0.103	–0.002	1.014
	O9···Fe	0.120	0.673	–0.225	0.197	–0.029	1.145
hB-1noHB2-O3-Fe(II)-O4	O3···Fe	0.056	0.317	–0.079	0.079	0.000	0.999
	O4···Fe	0.058	0.339	–0.084	0.084	0.001	0.995
hB-1-ring-Fe(II)-A	C3′···Fe	0.042	0.120	–0.044	0.037	–0.007	1.191
	C6′···Fe	0.054	0.170	–0.062	0.052	–0.010	1.189
hB-1-ring-Fe(II)-B	C2···Fe	0.043	0.128	–0.047	0.039	–0.007	1.185
	C5···Fe	0.049	0.151	–0.055	0.046	–0.009	1.185
hB-1noHB1-an-O2′-Fe(II)-O9	O2′···Fe	0.124	0.618	–0.219	0.187	–0.032	1.173
	O9···Fe	0.122	0.621	–0.215	0.185	–0.030	1.161
hB-1noHB2-an-O3-Fe(II)-O4	O3···Fe	0.050	0.342	–0.075	0.080	0.005	0.934
	O4···Fe	0.110	0.674	–0.223	0.196	–0.027	1.139
hB-1noHB1-an-O2′-Fe(II)-O9-4aq	O2′···Fe	0.093	0.494	–0.149	0.136	–0.013	1.093
	O9···Fe	0.076	0.433	–0.118	0.113	–0.005	1.044
hB-1noHB2-an-O3-Fe(II)-O4-4aq	O3···Fe	0.040	0.194	–0.048	0.048	0.000	0.994
	O4···Fe	0.108	0.559	–0.183	0.161	–0.022	1.134
hB-1noHB1-O2′-Fe(III)-O9	O2′···Fe	0.067	0.393	–0.101	0.100	–0.002	1.015
	O9···Fe	0.130	0.687	–0.243	0.207	–0.036	1.172
hB-1noHB2-O3-Fe(III)-O4	O3···Fe	0.061	0.355	–0.089	0.089	–0.000	1.004
	O4···Fe	0.061	0.379	–0.093	0.094	0.001	0.993
hB-1-ring-Fe(III)-A	C5′···Fe	0.072	0.107	–0.067	0.047	–0.020	1.431
hB-1-ring-Fe(III)-B	C5···Fe	0.069	0.153	–0.072	0.055	–0.017	1.308
	C6···Fe	0.069	0.137	–0.069	0.052	–0.018	1.341
hB-1noHB1-an-O2′-Fe(III)-O9	O2′···Fe	0.128	0.740	–0.254	0.219	–0.034	1.155
	O9···Fe	0.109	0.633	–0.201	0.179	–0.021	1.116
hB-1noHB2-an-O3-Fe(III)-O4	O3···Fe	0.059	0.283	–0.074	0.072	–0.002	1.024
	O4···Fe	0.133	0.675	–0.247	0.208	–0.039	1.187
hB-1noHB1-an-O2′-Fe(III)-O9-4aq	O2′···Fe	0.087	0.496	–0.143	0.133	–0.010	1.070
	O9···Fe	0.082	0.438	–0.124	0.117	–0.008	1.064
hB-1noHB2-an-O3-Fe(III)-O4-4aq	O3···Fe	0.035	0.163	–0.041	0.041	-2×10^{-5}	1.000
	O4···Fe	0.097	0.499	–0.155	0.140	–0.015	1.109

Table 4.22 Bond critical point data for butein···Fe^{n+} complexes for both the neutral and deprotonated butein UBP86/6-31+G(d,p) results *in vacuo*

Complex	Bond type	ρ e/Å^3	$\nabla^2\rho$ e/Å^5	V (Hartree)	G (Hartree)	H (Hartree)	$\frac{\lvert V\rvert}{G}$
hB-1noHB1-O2′-Fe(II)-O9	O2′···Fe	0.071	0.414	–0.109	0.106	–0.003	1.028
	O9···Fe	0.120	0.647	–0.218	0.190	–0.028	1.147
hB-1noHB2-O3-Fe(II)-O4	O3···Fe	0.070	0.391	–0.104	0.101	–0.003	1.030
	O4···Fe	0.070	0.401	–0.105	0.103	–0.002	1.019
hB-1-ring-Fe(II)-A	C3′···Fe	0.051	0.130	–0.053	0.043	–0.010	1.233
	C6′···Fe	0.067	0.188	–0.077	0.062	–0.015	1.242
hB-1-ring-Fe(II)-B	C2···Fe	0.053	0.142	–0.057	0.046	–0.011	1.239
	C5···Fe	0.060	0.168	–0.067	0.054	–0.013	1.241
hB-1noHB1-an-O2′-Fe(II)-O9	O2′···Fe	0.139	0.689	–0.258	0.215	–0.043	1.200
	O9···Fe	0.124	0.623	–0.219	0.187	–0.032	1.171
hB-1noHB2-an-O3-Fe(II)-O4	O3···Fe	0.057	0.291	–0.075	0.074	–0.001	1.014
	O4···Fe	0.123	0.623	–0.218	0.187	–0.031	1.166
hB-1noHB1-an-O2′-Fe(II)-O9-4aq	O2′···Fe	0.097	0.497	–0.154	0.139	–0.015	1.108
	O9···Fe	0.087	0.475	–0.138	0.129	–0.009	1.070
hB-1noHB2-an-O3-Fe(II)-O4-4aq	O3···Fe	0.038	0.042	–0.043	0.042	–1E-03	1.024
	O4···Fe	0.109	0.560	–0.184	0.162	–0.022	1.136
hB-1noHB1-O2′-Fe(III)-O9	O2′···Fe	0.065	0.365	–0.094	0.093	–0.001	1.011
	O9···Fe	0.128	0.669	–0.235	0.201	–0.034	1.169
hB-1noHB2-O3-Fe(III)-O4	O3···Fe	0.065	0.371	–0.096	0.095	–0.001	1.011
	O4···Fe	0.065	0.385	–0.098	0.097	–0.001	1.010
hB-1-ring-Fe(III)-A	C3′···Fe	0.049	0.096	–0.045	0.034	–0.011	1.324
	C5′···Fe	0.060	0.134	–0.061	0.047	–0.014	1.298
hB-1-ring-Fe(III)-B	C5···Fe	0.074	0.195	–0.085	0.067	–0.018	1.269
	C6···Fe	0.081	0.146	–0.083	0.060	–0.023	1.383
hB-1noHB1-an-O2′-Fe(III)-O9	O2′···Fe	0.137	0.694	–0.257	0.215	–0.042	1.195
	O9···Fe	0.111	0.574	–0.190	0.167	–0.023	1.138
hB-1noHB2-an-O3-Fe(III)-O4	O3···Fe	0.055	0.277	–0.071	0.070	–1E-03	1.014
	O4···Fe	0.127	0.641	–0.229	0.194	–0.035	1.180
hB-1noHB1-an-O2′-Fe(III)-O9-4aq	O2′···Fe	0.112	0.592	–0.195	0.171	–0.024	1.140
	O9···Fe	0.096	0.489	–0.151	0.136	–0.015	1.110
hB-1noHB2-an-O3-Fe(III)-O4-4aq	O3···Fe	0.035	0.138	–0.037	0.036	–0.001	1.028
	O4···Fe	0.105	0.534	–0.174	0.154	–0.020	1.130

4.2.12. NPA charges, spin density and orbital occupancies

The NPA charges and spin density values for the homobutein···Fe^{n+} complexes are reported in Table 4.23. The initial charge on free Fe(II) and Fe(III) cations is +2 and +3 respectively. For the Fe(II) cation the charge is reduced from 2 to a 1–1.5 *e* range and from 3 to a 1–1.5 *e* range for Fe(III), which indicates the transfer of positive charge from the Fe^{n+} cation to the homobutein ligand. For the complexes of neutral butein with Fe^{n+} cation the highest amount of charge transfer corresponds to a situation where the Fe^{n+} cation is coordinated at the π system of the aromatic ring. This large amount of charge transfer can be explained in terms of the electron cloud that surrounds the benzene ring. The amount of charge transferred correspond to 1.093 and

1.714 *e* for the Fe(II) and Fe(III) cation respectively. Among the complexes of deprotonated homobutein ligand with the Fe^{n+} cations the highest amount of charge transfer corresponds to a situation where the cation is coordinated to the catechol unit (with values of 0.86 and 1.641 *e* for Fe(II) and Fe(III) respectively). The results obtained further suggest that charge transfer is greater for the non-deprotonated ligand than for the deprotonated ligand and that more charge is transferred in the coordination with the Fe(III) cation than with the Fe(II) cation.

Table 4.23 NPA charges and spin density values for the Fe^{n+} cations in the complexes of homobutein

Complex	charge *(e)*		spin density	
	DFT/B3LYP results	DFT/BP86 results	DFT/B3LYP results	DFT/BP86 results
hB-1noHB1-O2′-Fe(II)-O9	1.519	1.182	3.420	3.317
hB-1noHB2-O3-Fe(II)-O4	0.963	1.012	3.027	3.097
hB-1-ring-Fe(II)-A	0.912	0.948	2.948	2.992
hB-1-ring-Fe(II)-B	0.907	0.955	2.944	3.013
hB-1noHB1-an-O2′-Fe(II)-O9	1.397	1.172	3.579	3.359
hB-1noHB2-an-O3-Fe(II)-O4	1.140	1.046	3.290	3.251
hB-1noHB1-an-O2′-Fe(II)-O9-4aq	1.203	1.062	3.653	3.523
hB-1noHB2-an-O3-Fe(II)-O4-4aq	1.191	1.020	3.633	3.475
hB-1noHB1-O2′-Fe(III)-O9	1.519	1.355	3.634	3.474
hB-1noHB2-O3-Fe(III)-O4	1.286	1.236	3.353	3.321
hB-1-ring-Fe(III)-A	1.210	1.195	3.486	3.324
hB-1-ring-Fe(III)-B	1.317	1.204	3.336	3.296
hB-1noHB1-an-O2′-Fe(III)-O9	1.418	1.292	3.563	3.445
hB-1noHB2-an-O3-Fe(III)-O4	1.359	1.219	3.506	3.387
hB-1noHB1-an-O2′-Fe(III)-O9-4aq	1.261	1.169	3.713	3.668
hB-1noHB2-an-O3-Fe(III)-O4-4aq	1.244	1.101	3.684	3.568

The spin density on the isolated Fe^{n+} cations is 4 and 5 for Fe(II) and Fe(III) cations respectively. Among the homobutein···Fe^{n+} complexes, the Fe(n) cation has spin density values which fall in the 3.027–3.684 range for both complexes with both the neutral and deprotonated homobutein ligand. The reduction in the spin density suggests that the transfer of electrons from homobutein to the metal ions increases the tendency for the electrons in the *d* orbitals to be paired. The spin density distributions are shown in Figure 4.18 and Figure 4.19 for the complexes formed between neutral ligand and bare Fe^{n+} cations, deprotonated ligand and bare Fe^{n+} cations as well as deprotonated ligand with hydrated Fe^{n+} cations respectively. The results clearly suggest that there is significant reduction in the delocalisation of the spin density distribution between the results corresponding to the bare Fe^{n+} cations and the results corresponding to the hydrated Fe^{n+} cations. For instance, it is observed that the spin density is largely localised on the Fe^{n+} cation among the complexes with explicit water molecules, consistent with the data on spin density values reported in Table 4.23.

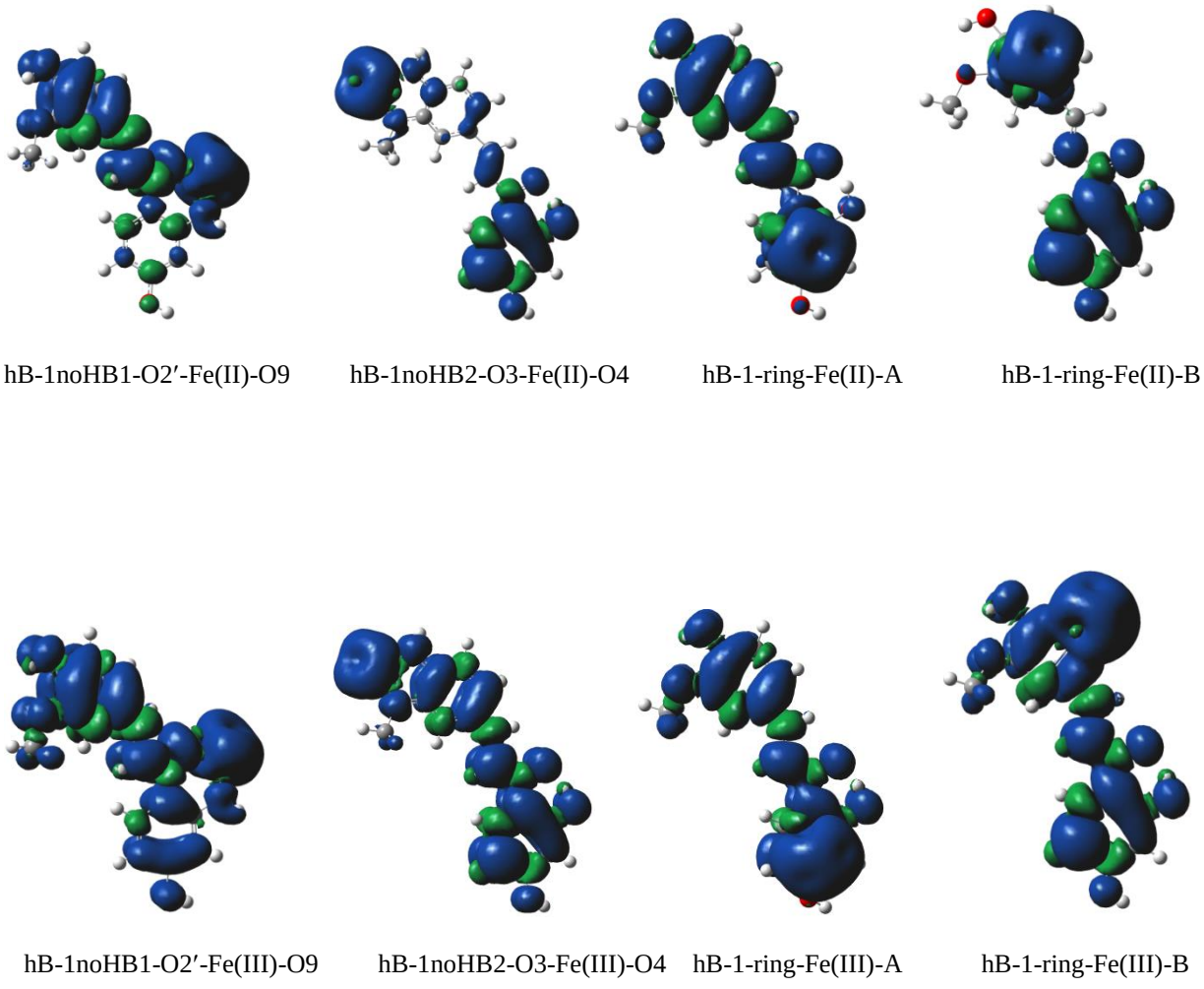

Figure 4.18 Spin density distribution for the homobutein···Fe^{n+} complexes formed from interactions of neutral homobutein and bare Fe^{n+} cations, B3LYP/6-31+G(d,p) results *in vacuo*. The surface isovalue used is 0.0004 au. The blue colour corresponds to positive spin densities and the green colour denotes the negative spin density.

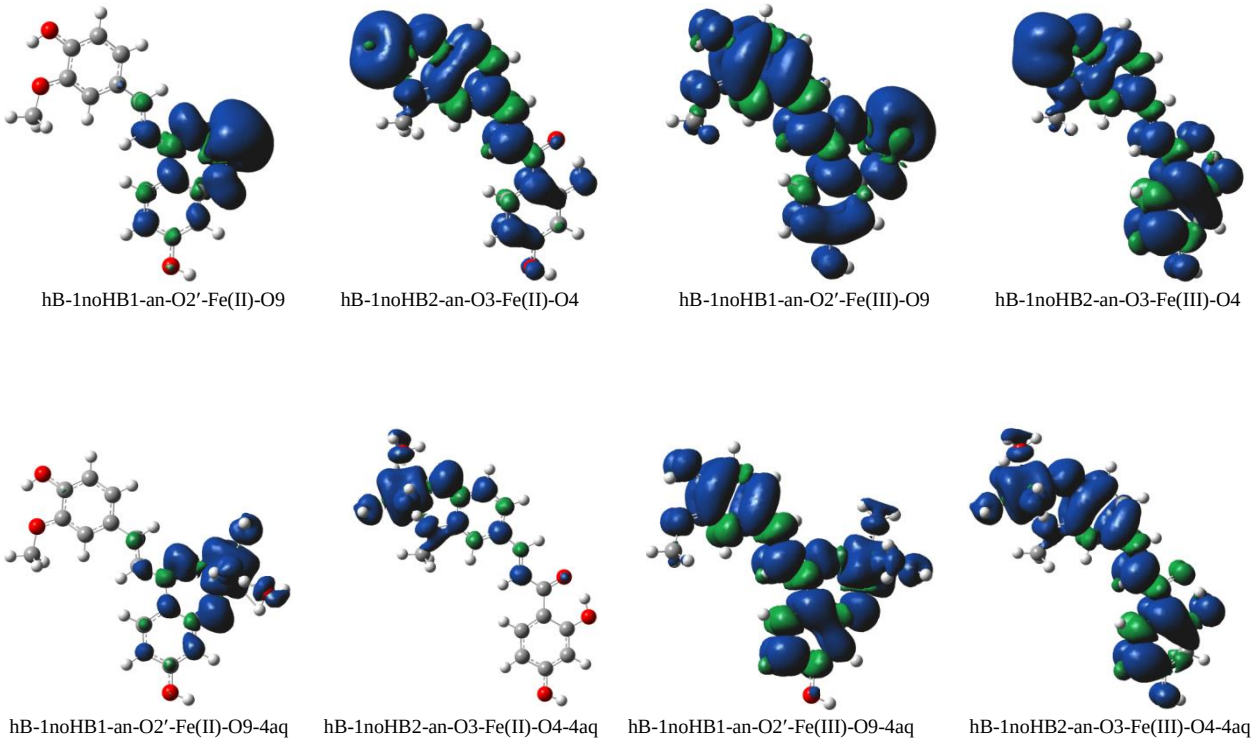

Figure 4.19 Spin density distribution for the homobutein···Fe^{n+} complexes, B3LYP/6-31+G(d,p) results *in vacuo*; the complexes formed from the interactions of deprotonated homobutein and the bare Fe^{n+} cation are represented in the first row and complexes formed from the deprotonated homobutein and the hydrated Fe^{n+} cation are represented in the second row. The surface isovalue used is 0.0004 au. The blue colour corresponds to positive spin densities and the green colour denotes the negative spin density.

Table 4.24 reports the values of the orbital occupancies of the Fe^{n+} cation before and after complexation. The occupancy of the 4s orbital increases from 0.000*e* to a 0.065–0.099 *e* and a range of 0.058–0.158 *e* for Fe(II) and Fe(III) cations with neutral homobutein ligand respectively. For the complexes with the deprotonated homobutein ligand the occupancy of the 4s orbital increases from 0.000 to a range of 0.131–0.139 for Fe(II) cation and 0.134–0.173 *e* for the Fe(III) cation. The occupancy of the *d* orbitals suggests that upon coordination the ligand transfers electron density to the Fe^{n+} cations; this is seen in values on Table 4.24.

Table 4.24 Natural atomic orbital occupancies for some valence orbitals in the isolated Fe^{n+} cations and in complexes with homobutein results *in vacuo* with different methods

Isolated cations and complexes	Orbitals and the corresponding natural atomic orbital occupancies					
DFT/B3LYP results						
	S (4s)	d_{xy} (3d)	d_{xz} (3d)	d_{yz} (3d)	$d_{x^2-y^2}$ (3d)	d_{z^2} (3d)
Fe(II)	0.000	1.998	1.000	1.000	1.000	1.000
hB-1noHB1-O2′-Fe(II)-O9	0.099	1.545	1.220	1.348	1.215	1.216
hB-1noHB2-O3-Fe(II)-O4	0.065	1.132	1.088	1.210	1.772	1.728
hB-1-ring-Fe(II)-A	0.088	1.277	1.538	1.532	1.466	1.106
hB-1-ring-Fe(II)-B	0.091	1.186	1.414	1.676	1.535	1.112
hB-1noHB1-an-O2′-Fe(II)-O9	0.139	1.202	1.836	1.078	1.155	1.114
hB-1noHB2-an-O3-Fe(II)-O4	0.131	1.230	1.350	1.782	1.134	1.174
hB-1noHB1-an-O2′-Fe(II)-O9-4aq	0.188	1.132	1.800	1.176	1.054	1.114
hB-1noHB2-an-O3-Fe(II)-O4-4aq	0.190	1.642	1.348	1.131	1.072	1.112
Fe(III)	0.000	1.000	1.000	1.000	1.000	1.000
hB-1noHB1-O2′-Fe(III)-O9	0.094	1.736	1.045	1.255	1.115	1.189
hB-1noHB2-O3-Fe(III)-O4	0.058	1.119	1.077	1.233	1.708	1.483
hB-1-ring-Fe(III)-A	0.131	1.102	1.827	1.158	1.323	1.087
hB-1-ring-Fe(III)-B	0.158	1.167	1.608	1.076	1.348	1.417
hB-1noHB1-an-O2′-Fe(III)-O9	0.173	1.086	1.149	1.430	1.546	1.129
hB-1noHB2-an-O3-Fe(III)-O4	0.134	1.356	1.143	1.171	1.078	1.707
hB-1noHB1-an-O2′-Fe(III)-O9-4aq	0.188	1.133	1.783	1.152	1.047	1.097
hB-1noHB2-an-O3-Fe(III)-O4-4aq	0.187	1.663	1.343	1.109	1.065	1.075
DFT/BP86 results						
Fe(II)						
hB-1noHB1-O2′-Fe(II)-O9	0.120	1.538	1.287	1.421	1.211	1.187
hB-1noHB2-O3-Fe(II)-O4	0.145	1.221	1.718	1.191	1.417	1.254
hB-1-ring-Fe(II)-A	0.115	1.358	1.420	1.573	1.356	1.135
hB-1-ring-Fe(II)-B	0.117	1.203	1.371	1.537	1.510	1.174
hB-1noHB1-an-O2′-Fe(II)-O9	0.239	1.195	1.220	1.216	1.546	1.334
hB-1noHB2-an-O3-Fe(II)-O4	0.193	1.356	1.285	1.596	1.103	1.36
hB-1noHB1-an-O2′-Fe(II)-O9-4aq	0.206	1.192	1.825	1.176	1.072	1.127
hB-1noHB2-an-O3-Fe(II)-O4-4aq	0.209	1.592	1.410	1.165	1.115	1.177
Fe(III)						
hB-1noHB1-O2′-Fe(III)-O9	0.107	1.757	1.059	1.305	1.122	1.251
hB-1noHB2-O3-Fe(III)-O4	0.071	1.114	1.083	1.240	1.718	1.503
hB-1-ring-Fe(III)-A	0.123	1.374	1.667	1.280	1.111	1.178
hB-1-ring-Fe(III)-B	0.171	1.070	1.537	1.099	1.594	1.314
hB-1noHB1-an-O2′-Fe(III)-O9	0.165	1.092	1.256	1.096	1.670	1.364
hB-1noHB2-an-O3-Fe(III)-O4	0.144	1.175	1.326	1.747	1.125	1.216
hB-1noHB1-an-O2′-Fe(III)-O9-4aq	0.217	1.234	1.574	1.207	1.103	1.132
hB-1noHB2-an-O3-Fe(III)-O4-4aq	0.206	1.624	1.349	1.149	1.112	1.139

4.3. Results in water solution

4.3.1. Conformational stability and geometries for the butein conformers

The optimised conformers of butein are shown in Figure 4.20 and the corresponding relative energy values (ΔE, kcal/mol) are reported in Table 4.25. In water solution the relative energy values are significantly dampened with respect to the results *in vacuo* such that six conformers may be considered to co-exist in physiological in conditions. The lowest-energy conformers (i.e., B-1, B-2 and B-3) are the same as those obtained *in vacuo*, confirming that intramolecular hydrogen bonding has significant role in stabilising conformations both *in vacuo* and in water solution. Conformers in which the first intramolecular is absent corresponds to relatively large energy values with the range of 7.191–7.990 kcal/mol. These results are in agreement with the *in vacuo* results where the presence of the first intramolecular bond stabilises conformers better than the presence of the second intramolecular hydrogen bond.

A comparison of the relative energies among conformers in which the aliphatic chain is bent and their corresponding conformers with non-bent aliphatic chain arrangement corresponds to energy difference of ≈3 kcal/mol for cases where the first intramolecular hydrogen bond is present, similar energy values was obtained for the results *in vacuo*. The absence of the first intramolecular hydrogen bond results in an energy difference of 0.785 kcal/mol for the bent and non-bent arrangement of the aliphatic chain. Similar results were obtained for the *in vacuo* conformers. Therefore, the presence of the solvent media has minimal role in influencing the energy difference between conformers obtained by rotation of the C7–C8 bond.

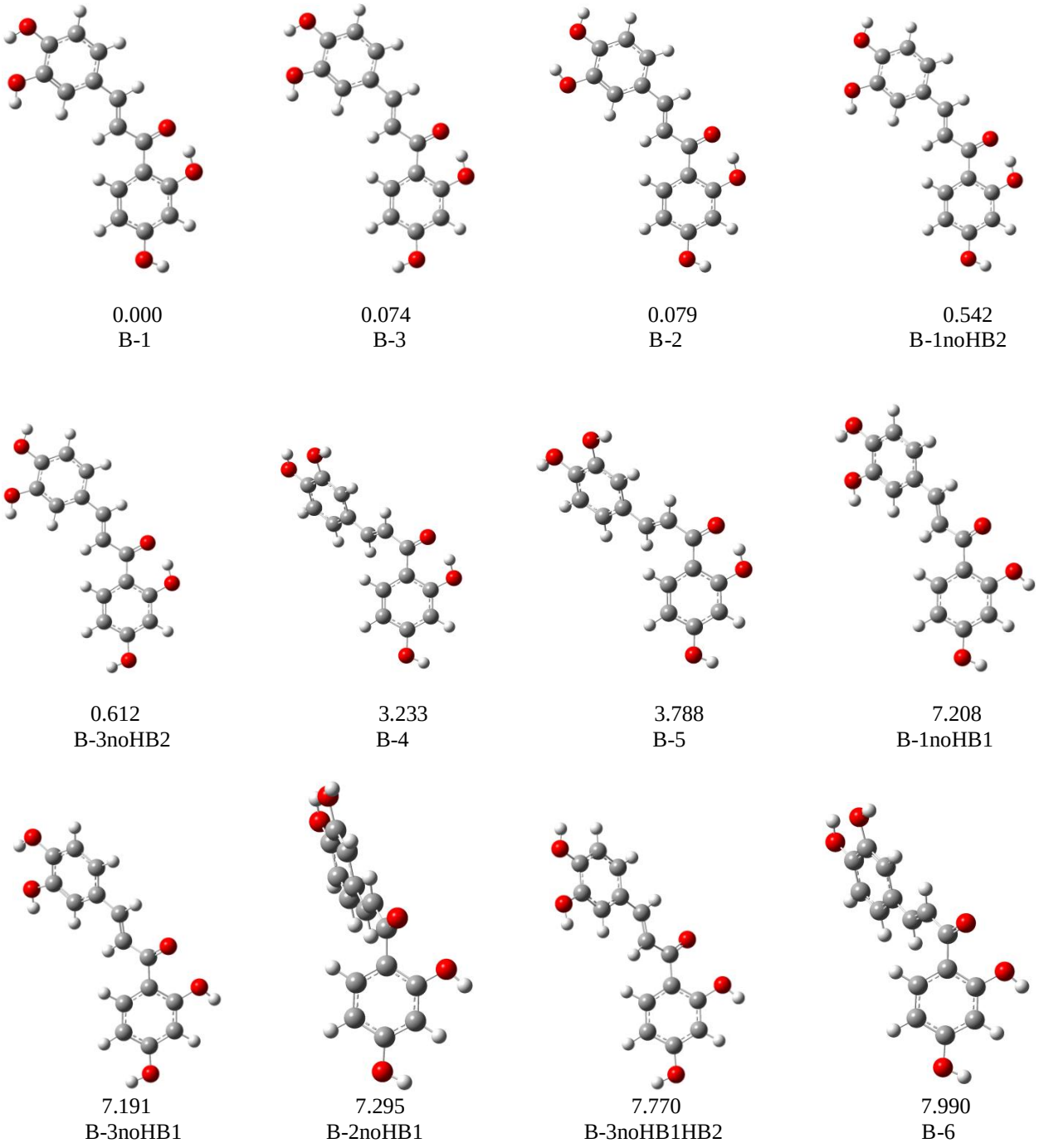

Figure 4.20 B3LYP/6-31+G(d,p) optimised conformers for neutral butein arranged in order of increasing relative energy (ΔE, kcal/mol). B3LYP/6-311+G(2d,p)//B3LYP/6-31+G(d,p) results. Similar geometries were obtained using the BP86/6-31+G(d,p) calculation method.

Table 4.25 Relative energy values (ΔE, kcal/mol) for the neutral conformers of butein in water solution

Conformer	*A*[a]		*B*[b]	
	total energy (Hartree)	ΔE (kcal/mol)	total energy (Hartree)	ΔE (kcal/mol)
DFT/B3LYP results				
B-1	-955.0357072	0.000	-955.2707727	0.000
B-2	-955.0355948	0.071	-955.2706474	0.079
B-3	-955.0355375	0.106	-955.2706549	0.074
B-1noHB2	-955.0349403	0.481	-955.2699085	0.542
B-3noHB2	-955.0347842	0.579	-955.2697974	0.612
B-4	-955.0305708	3.223	-955.2656203	3.233
B-5	-955.0297730	3.724	-955.2647366	3.788
B-1noHB1	-955.0242176	7.210	-955.2592867	7.208
B-3noHB1	-955.0242209	7.208	-955.2593127	7.191
B-2noHB1	-955.0241790	7.234	-955.2591480	7.295
B-3noHB2HB1	-955.0234084	7.718	-955.2583908	7.770
B-6	-955.0229671	7.995	-955.2580391	7.990
DFT/BP86 results				
B-1	-955.0417409	0.000	-955.2788650	0.000
B-3	-955.0415601	0.113	-955.2787324	0.083
B-2	-955.0415541	0.117	-955.2786787	0.117
B-1noHB2	-955.0409474	0.498	-955.2779368	0.582
B-3noHB2	-955.0407800	0.603	-955.2778373	0.645
B-4	-955.0364024	3.350	-955.2734985	3.368
B-5	-955.0355882	3.861	-955.2725645	3.954
B-3noHB1	-955.0272602	9.087	-955.2644452	9.049
B-1noHB1	-955.0272685	9.082	-955.2644304	9.058
B-2noHB1	-955.0271481	9.157	-955.2643257	9.124
B-3noHB2HB1	-955.0264201	9.614	-955.2634712	9.660
B-6	-955.0260601	9.840	-955.2631805	9.842

[a] Results obtained using the 6-31+G(d,p) basis set
[b] Single point results using the 6-311+G(2d,p) basis set, starting from the optimised geometries

The optimised conformers of the deprotonated butein ligand are shown in Figure 4.21 and the corresponding relative energy values (ΔE, kacl/mol) are reported in Table 4.26. The lowest energy conformer corresponds to the removal of the H4″ proton in the B-2-an conformer, where both the first and second intramolecular hydrogen bonds are present. The ΔE gap in water solution is significantly dampened such that the first three conformers (B-2, B-1noHB2-anI and B-1-an) may be considered to co-exist under physiological conditions. The ΔE gap in the B-1noHB2-anI and B-1-an conformers which corresponds to the removal of the H4″ and H3″ proton respectively is 0.248 kcal/mol, what suggests that in the presence of the first intramolecular hydrogen bond there is no preference for removal of either of the protons over the other.

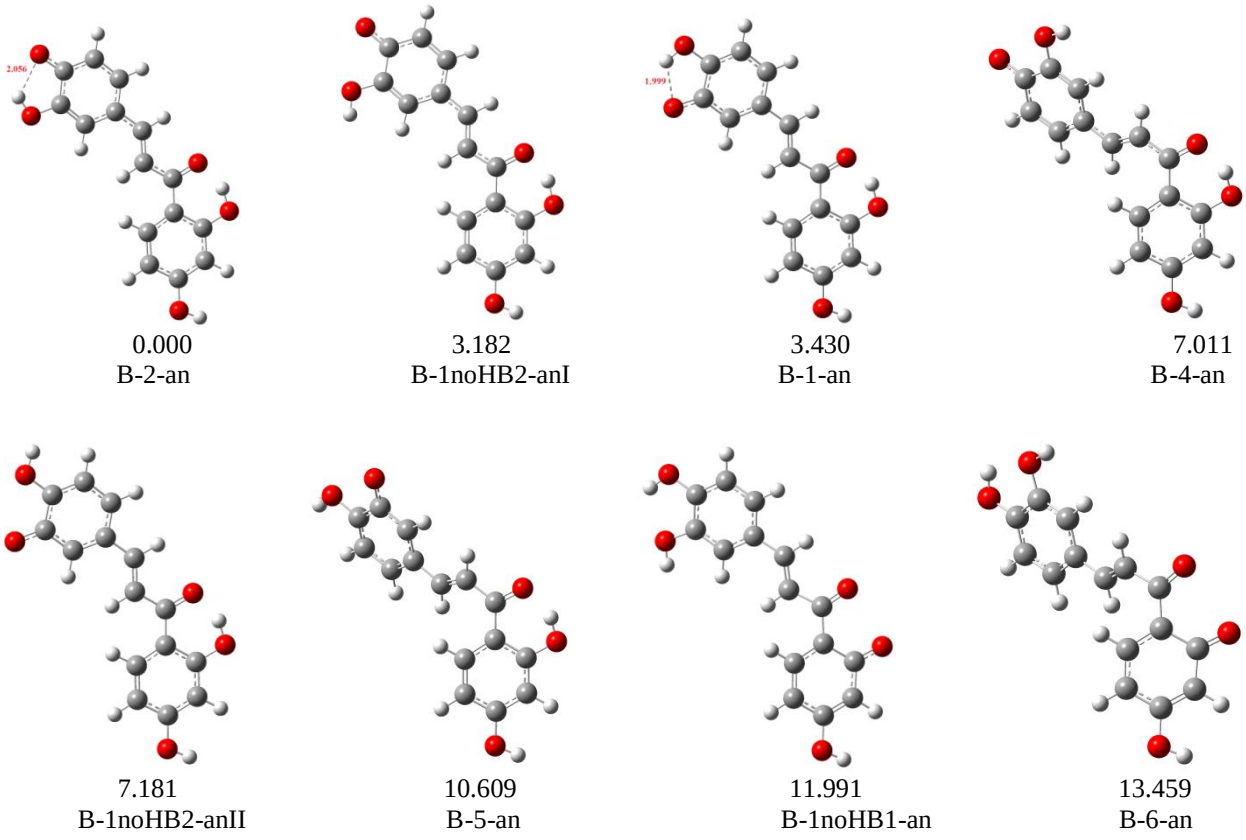

Figure 4.21 B3LYP/6-31+G(d,p) optimised conformers for deprotonated butein arranged in order of increasing relative energy (ΔE, kcal/mol), B3LYP/6-311+G(2d,p)//B3LYP/6-31+G(d,p) results in water solution. Similar geometries were obtained for the BP86/6-311+G(2d,p)//BP86/6-31+G(d,p) calculation method.

Table 4.26 Relative energy values (ΔE, kcal/mol) for the deprotonated conformers of butein in water solution

Conformer	*A*[a]		*B*[b]	
	total energy (Hartree)	ΔE (kcal/mol)	total energy (Hartree)	ΔE (kcal/mol)
DFT/B3LYP results				
B-2-an	-954.5744673	0.000	-954.8097496	0.000
B-1noHB2-anI	-954.5696683	3.011	-954.8046787	3.182
B-1-an	-954.5690459	3.402	-954.8042835	3.430
B-4-an	-954.5636276	6.802	-954.7985771	7.011
B-1noHB2-anII	-954.5633450	6.979	-954.7983062	7.181
B-5-an	-954.5579320	10.376	-954.7928430	10.609
B-1noHB1-an	-954.5558148	11.705	-954.7906406	11.991
B-6-an	-954.5535698	13.113	-954.7883014	13.459
DFT/B3LYP results				
B-2-an	-954.5866572	0.000	-954.8240070	0.000
B-1noHB2-anI	-954.5810880	3.495	-954.8180711	3.725
B-1-an	-954.5808999	3.613	-954.8182371	3.621
B-4-an	-954.5749432	7.351	-954.8118252	7.644
B-1noHB2-anII	-954.5738742	8.021	-954.8108346	8.266
B-5-an	-954.5682575	11.546	-954.8051699	11.820
B-1noHB1-an	-954.5625634	15.120	-954.7994811	15.390
B-6-an	-954.5603598	16.502	-954.7971509	16.852

[a] Results obtained using the 6-31+G(d,p) basis set
[b] Single point results using the 6-311+G(2d,p) basis set, starting from the optimised geometries

4.3.2. Relative stability and binding energies for butein···Fe^{n+} complexes formed from neutral butein and bare Fe^{n+} cations

The optimised complexes of the butein···Fe^{n+} complexes with the neutral butein and bare Fe^{n+} cations are shown in Figure 4.22 for DFT/B3LYP results and Figure 4.23 for DFT/BP86 results; the corresponding relative energy values (ΔE, kcal/mol) are reported in Table 4.27. Among the complexes of butein with the Fe(II) cation the lowest-energy complex corresponds to the coordination of the cation at the hydroxyl–*keto* reactive site. The ΔE gap between the first lowest-energy complex and the second lowest-energy complex corresponds to 2.089 kcal/mol. This result implies that the ΔE values in water solution are dampened with respect to the results *in vacuo* such that the coordination of the Fe^{n+} cation to either the hydroxyl–*keto* and hydroxyl–hydroxyl reactive sites may be considered populated in water solution. The coordination of the Fe^{n+} cation at the π system of the aromatic ring A is the least preferred complex and corresponds to relative energy of 10.000 kcal/mol. The ΔE values for the complexes with the Fe(III) cation suggests that coordination to the hydroxyl–*keto* reactive site may be the only one to be observed; the ΔE gap between the lowest-energy complex and the rest

of the complexes with the Fe(III) cation is relatively large (i.e., with a 8.027–9.491 kcal/mol range) such that these complexes may not be considered to exist.

The bond distance between the acceptor atoms on the ligand and the Fe^{n+} cations are longer than the bond distances for corresponding complexes obtained *in vacuo*, which implies that the interaction between the ligand molecule with the water molecules as well as the simultaneous interaction between the Fe^{n+} cation and the water molecules tend to weaken the bond strength between the ligand and the Fe^{n+} cation.

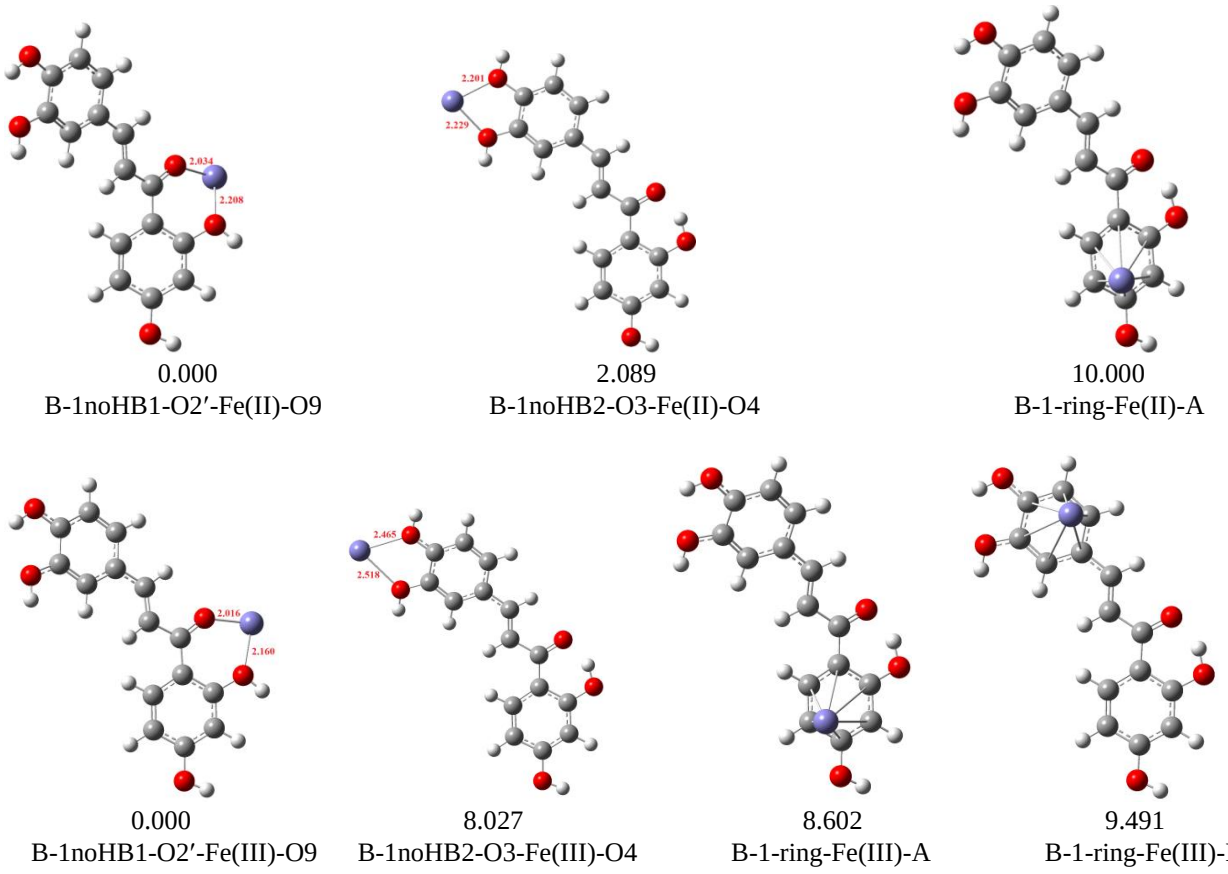

Figure 4.22 B3LYP/6-31+G(d,p) optimised complexes for butein···Fe^{n+} complexes (arranged in order of increasing relative energy (ΔE, kcal/mol)) formed from neutral butein and bare Fe^{n+} cation. B3LYP/6-311+G(2d,p)//B3LYP/6-31+G(d,p) results in water solution. The bond length between the cation and the ligand are reported in Å.

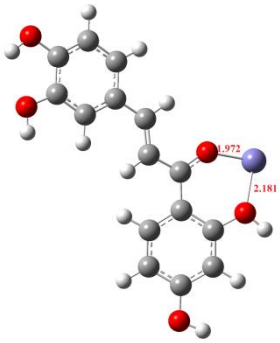

0.000
B-1noHB1-O2′-Fe(II)-O9

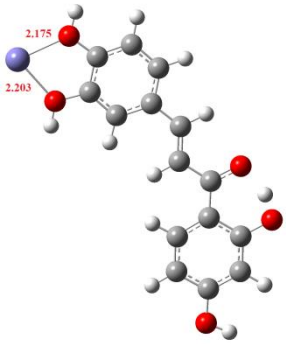

4.192
B-1noHB2-O3-Fe(II)-O4

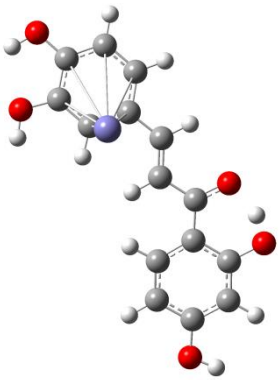

12.490
B-1-ring-Fe(II)-B

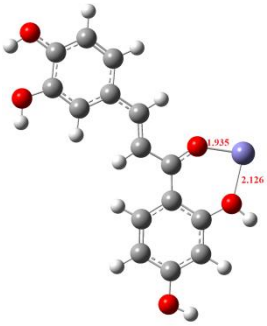

0.000
B-1noHB1-O2′-Fe(III)-O9

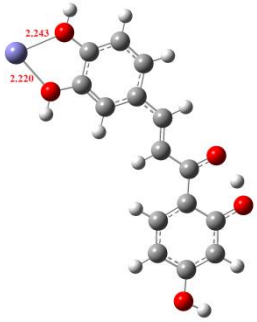

12.049
B-1noHB2-O3-Fe(III)-O4

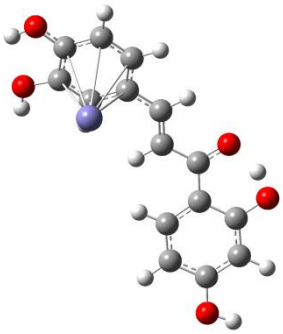

14.870
B-1-ring-Fe(III)-B

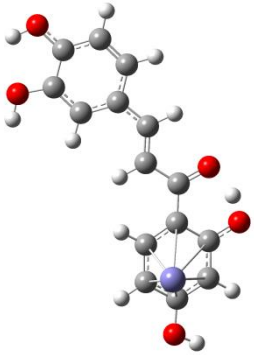

17.196
B-1-ring-Fe(III)-A

Figure 4.23 BP86/6-31+G(d,p) optimised complexes for butein···Fe^{n+} complexes (arranged in order of increasing relative energy (ΔE, kcal/mol)) formed from neutral butein and bare Fe^{n+} cation. BP86/6-311+G(2d,p) //BP86/6-31+G(d,p) results in water solution. The bond length between the cation and the ligand are reported in Å.

Table 4.27 Relative energy values (ΔE, kcal/mol) for butein···Fe^{n+} complexes formed from neutral butein and bare Fe^{n+} cations in water solution

Complex	*A*[a]		*B*[b]	
	total energy (Hartree)	ΔE (kcal/mol)	total energy (Hartree)	ΔE (kcal/mol)
DFT/B3LYP results				
B-1noHB1-O2′-Fe(II)-O9	-1078.2468414	0.000	-2218.7662074	0.000
B-1noHB2-O3-Fe(II)-O4	-1078.2454260	0.888	-2218.7628779	2.089
B-1-ring-Fe(II)-A	-1078.2336211	8.296	-2218.7502704	10.000
B-1-ring-Fe(II)-B	–[c]	–[c]	–[c]	–[c]
B-1noHB1-O2′-Fe(III)-O9	-1078.0382692	0.000	-2218.5580568	0.000
B-1noHB2-O3-Fe(III)-O4	-1078.0301093	5.120	-2218.5452648	8.027
B-1-ring-Fe(III)-B	-1078.0287351	5.983	-2218.5443495	8.602
B-1-ring-Fe(III)-A	-1078.0272204	6.933	-2218.5429324	9.491
DFT/BP86 results				
B-1noHB1-O2′-Fe(II)-O9	-1078.2955996	0.000	-2218.9104006	0.000
B-1noHB2-O3-Fe(II)-O4	-1078.2922975	2.072	-2218.9037198	4.192
B-1-ring-Fe(II)-B	-1078.2808514	9.255	-2218.8904972	12.490
B-1-ring-Fe(II)-A	–[c]	–[c]	–[c]	–[c]
B-1noHB1-O2′-Fe(III)-O9	-1078.0968660	0.000	-2218.7162723	0.000
B-1noHB2-O3-Fe(III)-O4	-1078.0839995	8.074	-2218.6970730	12.048
B-1-ring-Fe(III)-B	-1078.0838512	8.167	-2218.6925759	14.870
B-1-ring-Fe(III)-A	-1078.0789005	11.274	-2218.6888686	17.196

[a] Results obtained using the 6-31+G(d,p) basis set
[b] Single point results using the 6-311+G(2d,p) basis set, starting from optimised geometries
[c] On optimisation the calculation fails to converge

The binding energy values ($\Delta E'_{binding}$) of the butein···Fe^{n+} complexes are reported in Table 4.28. The binding energy values in water solution are significantly dampened with respect to the binding energy values for the results *in vacuo*. This result is consistent with the fact that the bond distances between butein and Fe^{n+} cation are longer in water solution than *in vacuo* (i.e., the interaction strength between the ligand and the Fe^{n+} cations is weakened in solution). Among the complexes of butein with the Fe(II) cation the strongest binding corresponds to the coordination of the Fe^{n+} cation to the hydroxyl–*keto* reactive site with $\Delta E'_{binding}$ of 18.686 kcal/mol in the B-1noHB1-O2′-Fe(II)-O9 complex. This result is in agreement with the relative energy values where coordination at the hydroxyl–*keto* reactive site is the most preferred complex. The coordination of the cation at the hydroxyl–hydroxyl reactive site corresponds to MIA value of 9.270 kcal/mol.

Among the complexes formed from the interaction of Fe(III) cation with butein, coordination of the Fe^{n+} cation at the hydroxyl–*keto* reactive site corresponding to $\Delta E'_{binding}$ of 62.304 kcal/mol and has the strongest binding. The coordination of the Fe(III) cation at the hydroxyl–hydroxyl reactive site and the π systems of the aromatic rings A and B have $\Delta E'_{binding}$ values of 45.746, 44.798 and 44.714 kcal/mol respectively, these results may imply that upon coordination of the Fe(III) cation at the above mentioned reactive sites the Fe^{n+} cation does not have a preferred site for binding which can be supported by the minute difference in their MIA values (i.e., of <1 kcal/mol). Although all the binding energy values are largely positive, which implies that interaction of the Fe^{n+} cations with butein is a thermodynamically favoured process, the large relative energy values of the complexes involving the coordination of the Fe^{n+} ion at other sites than the hydroxyl–*keto* reactive site may not exist in vivo. The $\Delta E'_{binding}$ values are much higher than those of the Fe(II) cation, what suggests that butein binds Fe(III) cation better than it binds the Fe(II) cation.

Table 4.28 Binding energy values ($\Delta E'_{binding,}$ kcal/mol) for butein···Fe^{n+} complexes formed from neutral butein and bare Fe^{n+} cations in water solution. The complexes are arranged in order of decreasing $\Delta E'_{binding}$ values

Complex	*A*[a]			*B*[b]		
	$\Delta E_{inter,}$ kcal/mol	ΔE_{def} kcal/mol	$\Delta E'_{binding,}$ kcal/mol	$\Delta E_{inter,}$ kcal/mol	ΔE_{def} kcal/mol	$\Delta E'_{binding,}$ kcal/mol
DFT/B3LYP results						
B-1noHB1-O2′-Fe(II)-O9	–5.412	1.197	6.609	–17.296	1.380	18.676
B-1noHB2-O3-Fe(II)-O4	2.204	0.687	–1.517	–8.542	0.728	9.270
B-1-ring-Fe(II)-A	10.093	0.761	–9.332	–0.088	0.844	0.932
B-1-ring-Fe(II)-B	_[c]	_[c]	_[c]	_[c]	_[c]	_[c]
B-1noHB1-O2′-Fe(III)-O9	–61.113	5.521	66.634	–56.806	5.498	62.304
B-1noHB2-O3-Fe(III)-O4	–49.264	3.712	52.976	–42.114	3.632	45.746
B-1-ring-Fe(III)-A	–46.970	4.759	51.729	–40.108	4.690	44.798
B-1-ring-Fe(III)-B	–47.920	3.848	51.768	–40.997	3.717	44.714
DFT/BP86 results						
B-1noHB1-O2′-Fe(II)-O9	–7.402	1.681	9.083	–21.538	1.846	23.384
B-1noHB2-O3-Fe(II)-O4	3.254	0.841	–2.413	–8.868	0.873	9.741
B-1-ring-Fe(II)-B	–10.935	1.019	9.916	–0.001	1.132	1.131
B-1-ring-Fe(II)-A	_[c]	_[c]	_[c]	_[c]	_[c]	_[c]
B-1noHB1-O2′-Fe(III)-O9	–75.254	4.053	79.307	–76.874	4.108	80.982
B-1noHB2-O3-Fe(III)-O4	–58.596	2.212	60.808	–56.351	2.230	58.581
B-1-ring-Fe(III)-B	–58.006	2.194	60.200	–52.947	2.193	55.140
B-1-ring-Fe(III)-A	–54.899	2.465	57.364	–50.620	3.004	53.624

[a] Results obtained using the 6-31+G(d,p) basis set
[b] Single point results using the 6-311+G(2d,p) basis set, starting from optimised geometries
[c] On optimisation the calculation fails to converge

4.3.3. Relative stability and binding energies for the butein···Fe^{n+} complexes formed from deprotonated butein and bare Fe^{n+} cations

The optimised complexes for butein with the Fe^{n+} cations are shown in Figure 4.24 for DFT/B3LYP and Figure 4.25 for DFT/BP86 results; the corresponding relative energies are reported in Table 4.29. In water solution the relative energy values are significantly dampened with respect to the results *in vacuo* such that all three complexes maybe considered populated in water solution. Among the complexes with the deprotonated butein ligand the lowest-energy complex corresponds to coordination of the Fe(II) cation at the O2′∪O9 reactive site in B-1noHB1-an-O2′-Fe(II)-O9 complex. This result is also similar to the outcome found *in vacuo*. The ΔE gap between the first lowest-energy complex and the remaining complexes for the Fe(II) cation is 1.048 and 1.631 kcal/mol for coordination at the O3H3″$O4^-$ and $O3^-$O4H4″ reactive site respectively; what suggests that in water solution there is no preference of the cation to coordinate at the $O3^-$O4H4″ reactive site or the O3H3″$O4^-$ reactive site.

Among the complexes with the Fe(III) cation only the first two complexes may be considered populated in physiological conditions (i.e., coordination at the O2′∪O9″ reactive site and the O3H3″∪$O4^-$ reactive site), which is in agreement with the results *in vacuo*, where coordination at the $O3^-$∪O4H4″ reactive site is preferred over coordination at the O3H3″∪$O4^-$ reactive site. The stability of the lowest-energy complex may be explained in similar manner as it was explained under the *in vacuo* section (i.e., the possibility of two O atoms acting as carbonyl groups with ample of electrons to donate electrons to the Fe^{n+} ions may account for the preference of the Fe^{n+} ion to bind to the O2′∪O9 than to either the O3H3″∪O4 or the O3∪O4H4″ site).

The bond distances between the Fe^{n+} ion and the deprotonated ligand are also longer with respect to the results obtained *in vacuo*. As was discussed earlier, the reason for the increase in the bond distances is related to the fact that both the ligand molecule and the Fe^{n+} cation are interacting simultaneously with solvent molecules. The lengthening of the ligand-Fe bond distances has significant implications on the interaction strength between the two species.

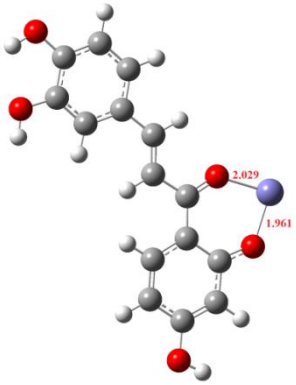

0.000
B-1noHB1-an-O2′-Fe(II)-O9

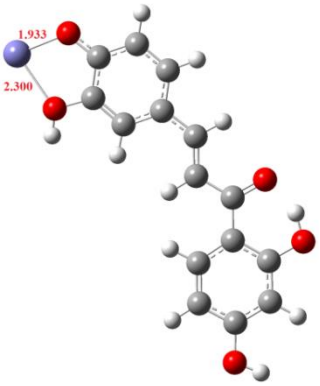

1.048
B-1noHB2-anI-O3-Fe(II)-O4

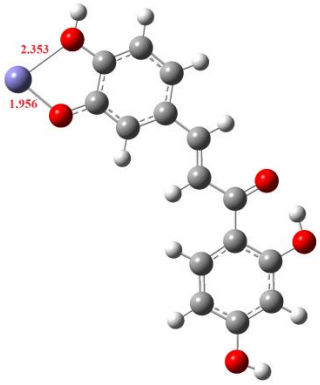

1.631
B-1noHB2-anII-O3-Fe(II)-O4

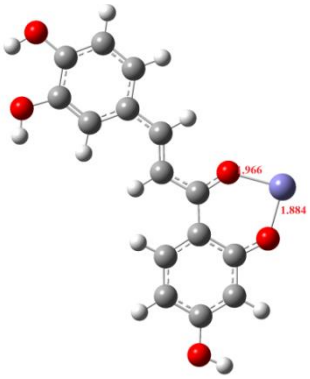

0.000
B-1noHB1-an-O2′-Fe(III)-O9

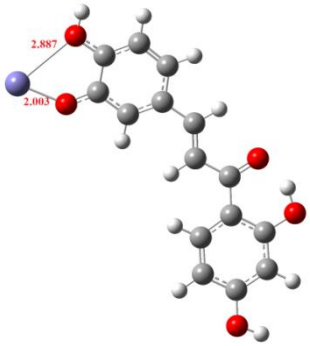

3.768
B-1noHB2-anII-O3-Fe(III)-O4

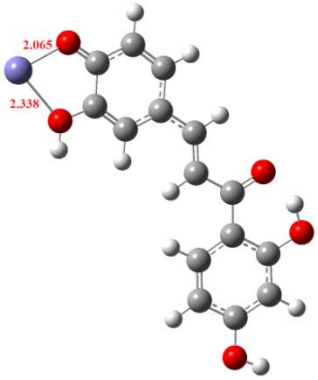

8.934
B-1noHB2-anI-O3-Fe(III)-O4

Figure 4.24 B3LYP/6-31+G(d,p) optimised complexes for butein···Fe^{n+} complexes (arranged in order of increasing relative energy (ΔE, kcal/mol)) formed from deprotonated butein and bare Fe^{n+} cation. B3LYP/6-311+G(2d,p)//B3LYP/6-31+G(d,p) results in water solution. The bond distances between the cation and the ligand are reported in Å.

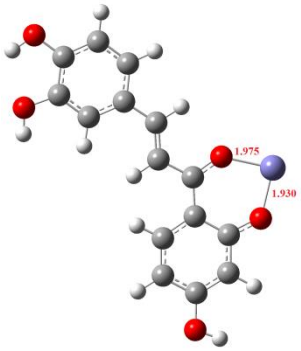

0.000
B-1noHB1-an-O2′-Fe(II)-O9

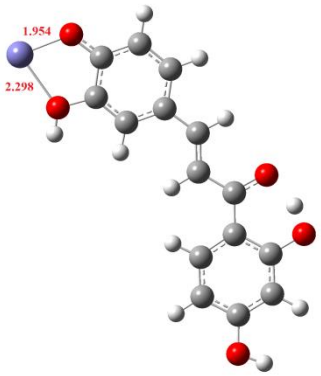

5.032
B-1noHB2-anI-O3-Fe(II)-O4

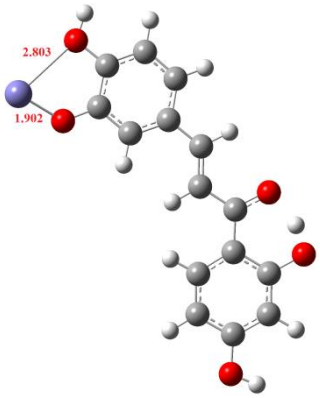

7.397
B-1noHB2-anII-O3-Fe(II)-O4

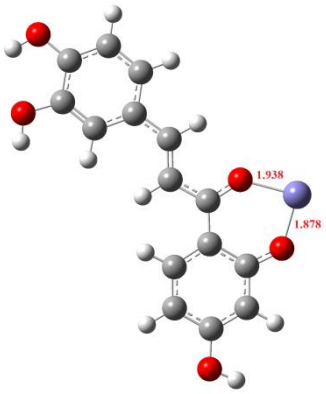

0.000
B-1noHB1-an-O2′-Fe(III)-O9

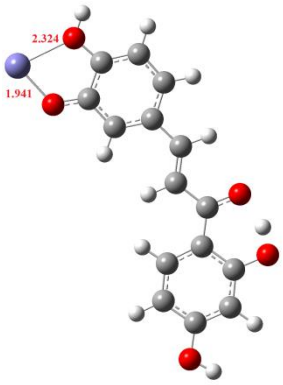

9.360
B-1noHB2-anII-O3-Fe(III)-O4

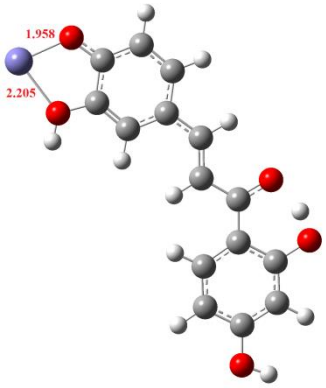

11.111
B-1noHB2-anI-O3-Fe(III)-O4

Figure 4.25 BP86/6-31+G(d,p) optimised complexes for butein···Fe^{n+} complexes (arranged in order of increasing relative energy (ΔE, kcal/mol)) formed from deprotonated butein and bare Fe^{n+} cation BP86P/6-311+G(2d,p)//BP86/6-31+G(d,p) results in water solution. The bond distances between the cation and the ligand are reported in Å.

Table 4.29 Relative energy values (ΔE, kcal/mol) for butein···Fe^{n+} complexes formed from deprotonated butein and bare Fe^{n+} cations in water solution

Complex	*A*[a]		*B*[b]	
	total energy (Hartree)	ΔE (kcal/mol)	total energy (Hartree)	ΔE (kcal/mol)
DFT/B3LYP results				
B-1noHB1-an-O2′-Fe(II)-O9	-1077.8072305	0.000	-2218.3259354	0.000
B-1noHB2-anI-O3-Fe(II)-O4	-1077.8059673	0.793	-2218.3242657	1.048
B-1noHB2-anII-O3-Fe(II)-O4	-1077.8034606	2.366	-2218.3233363	1.631
B-1noHB1-an-O2′-Fe(III)-O9	-1077.6124129	3.359	-2218.1434137	0.000
B-1noHB2-anII-O3-Fe(III)-O4	-1077.6177657	0.000	-2218.1374095	3.768
B-1noHB2-anI-O3-Fe(III)-O4	-1077.6139180	2.415	-2218.1291763	8.934
DFT/BP86 results				
B-1noHB1-an-O2′-Fe(II)-O9	-1077.8651535	0.000	-2218.4839601	0.000
B-1noHB2-anI-O3-Fe(II)-O4	-1077.8615302	2.274	-2218.4755483	5.279
B-1noHB2-anII-O3-Fe(II)-O4	-1077.8579158	4.542	-2218.4716804	7.706
B-1noHB1-an-O2′-Fe(III)-O9	-2218.4839601	0.000	-2218.3090133	0.000
B-1noHB2-anII-O3-Fe(III)-O4	-2218.4755483	5.279	-2218.2940967	9.360
B-1noHB2-anI-O3-Fe(III)-O4	-2218.4716804	7.706	-2218.2913062	11.111

[a] Results obtained using the 6-31+G(d,p) basis set
[b] Single point results using the 6-311+G(2d,p) basis set, starting from optimised geometries

The binding energy values ($\Delta E'_{binding}$, kcal/mol) are reported in Table 4.30. In water solution the binding energy values are dampened with respect to the results *in vacuo* so that it is reasonable to infer that the interactions between butein and the Fe^{n+} ion is weaker in water solution than *in vacuo*. The site of coordination that corresponds to the strongest binding is the O2′∪O9 reactive site with MIA values (kcal/mol) of 36.632 for the Fe(II) and 94.156 and for the Fe(III) cations.

Among the complexes formed through the coordination of the Fe^{n+} ion at the deprotonated catechol unit site, the coordination at the O3∪O4H4″ site is preferred over coordination at the O3H3″∪O4 site; this is true for both Fe(II) and Fe(III) complexes. However the MIA values are not significantly different and since in all cases the binding energies are positive values, the interaction between butein and Fe^{n+} cations is a favourable thermodynamic process.

It is also important to note that the binding strength for the deprotonated species is higher than that of the neutral species, a trend also observed *in vacuo*. The implication for this result is that in biological systems, where the pH of the media may be slightly acidic to neutral, both the neutral and the deprotonated species of butein may co-exist. In such cases, the deprotonated species of butein are likely to chelate the metal ions more than the neutral species.

Table 4.30 Binding energy values ($\Delta E'_{binding,}$ kcal/mol) for butein···Fe^{n+} complexes formed from deprotonated butein ligand and bare Fe^{n+} cations in water solution. The complexes are arranged in order of decreasing $\Delta E'_{binding}$ values

Complex	*A*[a]			*B*[b]		
	$\Delta E_{inter,}$ kcal/mol	ΔE_{def} kcal/mol	$\Delta E'_{binding,}$ kcal/mol	$\Delta E_{inter,}$ kcal/mol	ΔE_{def} kcal/mol	$\Delta E'_{binding,}$ kcal/mol
DFT/B3LYP results						
B-1noHB1-an-O2′-Fe(II)-O9	–23.479	1.499	24.978	–35.101	1.531	36.632
B-1noHB2-anII-O3-Fe(II)-O4	–16.388	1.039	17.427	–28.660	1.041	29.701
B-1noHB2-anI-O3-Fe(II)-O4	–13.994	1.725	15.719	–25.245	1.725	26.970
B-1noHB1-an-O2′-Fe(III)-O9	–87.811	3.437	91.248	–90.694	3.462	94.156
B-1noHB2-anII-O3-Fe(III)-O4	–82.477	2.806	85.283	–78.117	2.394	80.511
B-1noHB2-anI-O3-Fe(III)-O4	–84.030	1.197	85.227	–76.949	2.734	79.683
DFT/BP86 results						
B-1noHB1-an-O2′-Fe(II)-O9	–28.900	1.983	30.883	–45.702	2.047	47.749
B-1noHB2-anII-O3-Fe(II)-O4	–17.260	1.320	18.580	–30.872	1.270	32.142
B-1noHB2-anI-O3-Fe(II)-O4	–15.001	1.931	16.932	–28.758	1.905	30.663
B-1noHB1-an-O2′-Fe(III)-O9	–108.130	4.094	112.220	–113.080	4.092	117.172
B-1noHB2-anI-O3-Fe(III)-O4	–93.631	2.350	95.981	–94.839	2.109	96.948
B-1noHB2-anII-O3-Fe(III)-O4	–91.470	2.920	94.390	–92.050	2.674	94.724

[a] Results obtained using the 6-31+G(d,p) basis set
[b] Single point results using the 6-311+G(2d,p) basis set, starting from optimised geometries

4.3.4. AIM analysis of the bonding within the butein complexes

The BCP data of the electron density distributions ($\rho(\mathbf{r})$) and its laplacian ($\nabla^2\rho$ (r)) for the butein···Fe^{n+} complexes in water solution are reported in Table 4.31 for the DFT/B3LYP results and Table 4.32 for the DFT/BP86 results. The strongest bond among the complexes with the neutral butein ligand corresponds to the O9···Fe^{n+} bond with ρ value of 0.072 and 0.074 e/Å^3 for Fe(II) and Fe(III) cations respectively. For the coordination of the cation at the O3∪O4 reactive site (i.e., hydroxyl–hydroxyl reactive site) ρ is 0.044 for the Fe(II) cation and 0.023 e/Å^3 for the Fe(III) cation. The weakest bond corresponds to the coordination of the cation at the π system of the aromatic rings, with ρ value of 0.019 e/Å^3 for the C5′···Fe bond in B-1-Fe(III)-ring-A. Among the complexes with the deprotonated butein ligand with the Fe(II) cation, the largest value of ρ (i.e., 0.092 e/Å^3) corresponds to the O3···Fe^{2+} bond for the complexes with the Fe(II) cation, followed by the O2′···Fe^{2+} bond with ρ value of 0.090 e/Å^3, a different trend is observed for the *in vacuo* results; where the O2′···Fe bond is the strongest. For complexes with deprotonated butein ligand and Fe(III) cation the strongest bond corresponds to the O9···Fe^{3+} bond with ρ of 0.090 e/Å^3. The weakest bond corresponds to the O3···Fe^{3+} bond present in B-1noHB2-anI-Fe-O3-Fe(III)-O4 complex. From the results obtained it is reasonable to infer that

for the complexes with the neutral ligand, the strongest bond corresponds to the O9···Fe^{n+} bond, a result consistent with those obtained *in vacuo*. However, a comparison of the ρ values between the results *in vacuo* and the results in water solution clearly indicates that the ρ values are significantly small in water solution, which is an indication of the weakening of the bond strength. Therefore, the results on the electron density augment the results obtained on the MIA values in that both indicate the weakening of the interaction strength between the ligand and the Fe^{n+} ions in water solution.

The $\nabla^2\rho$ values in e/Å^5 are all positive and fall in the 0.220–0.379 and the 0.044–0.424 range for complexes of neutral butein with Fe(II) and Fe(III) cations respectively and a range 0.150–0.478 and 0.146–0.548 for the complexes with the deprotonated butein ligand with Fe(II) and Fe(III) cations respectively. These values of the $\nabla^2\rho$ are indicative of closed shell interactions between the ligand and the cation; this is further supported by the values of *H* which are negative. The |V|/G ratio has values within the 0.9–1.4 range among complexes of the Fe^{n+} cations with neutral and deprotonated butein ligand, what is also suggestive of closed shell interactions.

Table 4.31 Bond critical point data for butein···Fe^{n+} complexes, UB3LYP/6-31+G(d,p) results in water solution.

Complex	Bond type	ρ e/Å^3	$\nabla^2\rho$ e/Å^5	V (Hartree)	G (Hartree)	H (Hartree)	$\frac{\lvert V\rvert}{G}$
B-1noHB1-O2′-Fe(II)-O9	O2′···Fe	0.044	0.242	–0.056	0.058	0.002	0.961
	O9···Fe	0.072	0.379	–0.101	0.098	–0.003	1.032
B-1noHB2-O3-Fe(II)-O4	O3···Fe	0.042	0.220	–0.051	0.053	0.002	0.963
	O4···Fe	0.044	0.243	–0.056	0.058	0.002	0.962
B-1noHB1-an-O2′-Fe(II)-O9	O2′···Fe	0.090	0.478	–0.141	0.130	–0.011	1.081
	O9···Fe	0.075	0.393	–0.107	0.103	–0.004	1.042
B-1noHB2-anI-O3-Fe(II)-O4	O3···Fe	0.037	0.165	–0.040	0.041	0.001	0.981
	O4···Fe	0.083	0.432	–0.124	0.116	–0.008	1.069
B-1noHB2-anII-O3-Fe(II)-O4	O3···Fe	0.092	0.471	–0.141	0.129	–0.012	1.091
	O4···Fe	0.030	0.150	–0.035	0.036	0.001	0.964
B-1-noHB1-O2′-Fe(III)-O9	O2′···Fe	0.049	0.261	–0.060	0.063	0.002	0.962
	O9···Fe	0.074	0.424	–0.112	0.109	–0.003	1.027
B-1noHB2-O3-Fe(III)-O4	O3···Fe	0.021	0.080	–0.021	0.020	–0.000	1.022
	O4···Fe	0.023	0.095	–0.024	0.024	7.00x 10^{-5}	0.997
B-1-ring-Fe(III)-A	C5′···Fe	0.019	0.044	–0.015	0.013	–0.002	1.148
B-1noHB1-an-O2′-Fe(III)-O9	O2′···Fe	0.111	0.584	–0.191	0.169	–0.023	1.134
	O9···Fe	0.090	0.439	–0.132	0.121	–0.011	1.091
B-1noHB2-anI-O3-Fe(III)-O4	O3···Fe	0.031	0.146	–0.033	0.035	0.002	0.952
	O4···Fe	0.067	0.374	–0.097	0.095	–0.002	1.018
B-1noHB2-anII-O3-Fe(III)-O4	O3···Fe	0.077	0.414	–0.112	0.108	–0.004	1.039

Table 4.32 Bond critical point data for butein···Fe^{n+} complexes UBP86/6-31+G(d,p) results in water solution

Complex	Bond type	ρ e/Å^3	$\nabla^2\rho$ e/Å^5	V (Hartree)	G (Hartree)	H (Hartree)	$\frac{\lvert V \rvert}{G}$
B-1noHB1-O2′-Fe(II)-O9	O2′···Fe	0.049	0.246	–0.059	0.060	0.001	0.983
	O9···Fe	0.086	0.450	–0.130	0.121	–0.009	1.074
B-1noHB2-O3-Fe(II)-O4	O3···Fe	0.046	0.235	–0.056	0.057	0.001	0.982
	O4···Fe	0.049	0.258	–0.616	0.063	–0.553	9.778
B-1noHB1-an-O2′-Fe(II)-O9	O2′···Fe	0.098	0.503	–0.156	0.141	–0.015	1.106
	O9···Fe	0.085	0.465	–0.133	0.125	–0.008	1.064
B-1noHB2-anI-O3-Fe(II)-O4	O3···Fe	0.036	0.174	–0.042	0.042	0.000	1.000
	O4···Fe	0.094	0.458	–0.141	0.128	–0.013	1.102
B-1noHB2-anII-O3-Fe(II)-O4	O3···Fe	0.105	0.534	–0.170	0.152	–0.018	1.118
B-1-noHB1-O2′-Fe(III)-O9	O2′···Fe	0.056	0.281	–0.068	0.069	0.001	0.986
	O9···Fe	0.096	0.491	–0.150	0.136	–0.014	1.103
B-1noHB2-O3-Fe(III)-O4	O3···Fe	0.044	0.211	–0.049	0.051	0.002	0.961
	O4···Fe	0.041	0.201	–0.046	0.048	0.002	0.958
B-1-ring-Fe(III)-A	C5′···Fe	0.024	0.043	–0.017	0.014	–0.003	1.214
B-1-ring-Fe(III)-B	C3′···Fe	0.005	0.017	–0.003	0.004	0.001	0.750
B-1noHB1-an-O2′-Fe(III)-O9	O2′···Fe	0.114	0.580	–0.193	0.169	–0.024	1.142
	O9···Fe	0.098	0.481	–0.149	0.134	–0.015	1.112
B-1noHB2-anI-O3-Fe(III)-O4	O3···Fe	0.046	0.218	–0.052	0.053	0.001	0.981
	O4···Fe	0.094	0.470	–0.143	0.130	–0.013	1.100
B-1noHB2-anII-O3-Fe(III)-O4	O3···Fe	0.098	0.486	–0.151	0.136	–0.015	1.110
	O4···Fe	0.034	0.150	–0.035	0.036	1.00x 10^{-3}	0.972

4.3.5. NPA charges, spin density and orbital occupancies

The values of the charges and the spin density for the butein···Fe^{n+} complexes are reported in Table 4.33. For the Fe(II) cation the charge is reduced from 2 to a 1.8–1.9 *e* range and for the Fe(III) cation from 3 to a 1.9–2 *e* range, which is indicative of positive charge transfer from the Fe^{n+} cations to the butein ligand. For the complexes with neutral butein and Fe^{n+} cation, the highest amount of charge transfer corresponds to the coordination at the hydroxyl–*keto* reactive site, with values of 0.136 and 1.088 *e* for Fe (II) and Fe(III) cations respectively. The least amount of charge transferred is at the π system of the aromatic rings. Among the Fe (II) cation complexes with the deprotonated butein ligand, the highest amount of charge transfer corresponds to coordination at the O2′∪O9 site (i.e., 0.192 *e*) and for the Fe(III) cation it corresponds to coordination at the O3H3″∪O4$^-$ reactive site with a value of 1.046 *e*. The results obtained further imply that more positive charge is transferred when the Fe^{n+} cation is coordinated to the deprotonated ligand than to the neutral ligand and that charge transfer is highest for the Fe(III) complexes. A comparison with the results *in vacuo* suggests that higher charge transfer occurs *in vacuo* than in water solution.

Table 4.33 NPA charges and spin density values for the Fe^{n+} cations in complexes of butein in water solution

Complex	charge *(e)*		spin density	
	DFT/B3LYP results	DFT/BP86 results	DFT/B3LYP results	DFT/BP86 results
B-1noHB1-O2′-Fe(II)-O9	1.864	1.813	3.917	3.865
B-1noHB2-O3-Fe(II)-O4	1.922	1.885	3.956	3.925
B-1-ring-Fe(II)-A	1.979	–[a]	3.991	–[a]
B-1-ring-Fe(II)-B	–[a]	1.938	–[a]	3.941
B-1noHB1-an-O2′-Fe(II)-O9	1.808	1.738	3.863	3.809
B-1noHB2-anI-O3-Fe(II)-O4	1.826	1.744	3.896	3.823
B-1noHB2-anII-O3-Fe(II)-O4	1.813	1.748	3.886	3.819
B-1noHB1-O2′-Fe(III)-O9	1.912	2.038	3.954	4.088
B-1noHB2-O3-Fe(III)-O4	1.968	2.051	3.985	4.087
B-1-ring-Fe(III)-A	1.983	2.066	3.994	4.078
B-1-ring-Fe(III)-B	2.007	2.126	4.011	4.142
B-1noHB1-an-O2′-Fe(III)-O9	2.116	1.996	4.189	4.074
B-1noHB2-anI-O3-Fe(III)-O4	1.954	2.032	4.002	4.098
B-1noHB2-anII-O3-Fe(III)-O4	2.012	2.031	4.046	4.106

[a] On optimisation, the calculation fails to reach convergence

The spin density values for the butein···Fe^{n+} complexes are reported in Table 4.33. The spin density distributions for the complexes formed with neutral ligand and bare Fe^{n+} cation are shown in Figure 4.26 and the spin density distributions for the complexes with the deprotonated ligand and the bare Fe^{n+} cation are shown in Figure 4.27. Among the butein···Fe^{n+} complexes the Fe(II) cation has spin density values ranging from 3.863–3.991 for both the complexes with neutral and the deprotonated butein ligand, which suggest that there is minimal spin density transfer from the Fe^{n+} cation to the butein molecule; this is also observed through the analysis of the spin density distribution images shown in Figure 4.26 and Figure 4.27, which shown much of the spin density localised on the Fe(II) ion. Among the complexes with the Fe(III) cation the spin density values are within the 3.954–4.189 range. A comparison of the Fe(II) and Fe(III) complexes implies that there is greater spin density delocalisation in the Fe(III) complexes than in the Fe(II) complexes which further supports the fact that Fe(III) binds stronger to the ligand molecule than Fe(II). The reduction in the spin density suggests that the transfer of electrons from butein to the Fe^{n+} cations increases the tendency for the electrons in the *d* orbitals to be paired.

The orbital occupancies of the free Fe^{n+} cation and the complexed Fe^{n+} cation are reported in Table 4.34. The values of the 4s occupancies suggests that upon coordination of the Fe^{n+} cation to the ligand there is a transfer of electron density from the ligand to the cations such that the 4s orbital tends to be partially filled with an electron(s); it increases from 0.000 in the free Fe^{n+} cation to a range of 0.011–0.039 *e* for Fe (II) cation and a range of 0.002–0.036 *e* for the Fe(III) cation when coordinating to the neutral ligand and from 0.000 to a range of 0.046–0.056 *e* for Fe(II) cation and a range of 0.025–0.055 *e* for the Fe(III) cation when coordinated to the deprotonated ligand. Analysis of the *d* orbitals occupancies suggests that upon coordination to the butein ligand, the ligand tends to transfer electrons from itself to the Fe^{n+} cations in the d_{xz}, d_{yz}, $d_{x^2-y^2}$, and d_{z^2} orbitals such that these orbitals are partially filled. For the d_{xy} orbital the Fe^{n+} cation transfer electrons from itself to the partially filled *d* orbitals of the ligand as seen in the results reported on Table 4.34.

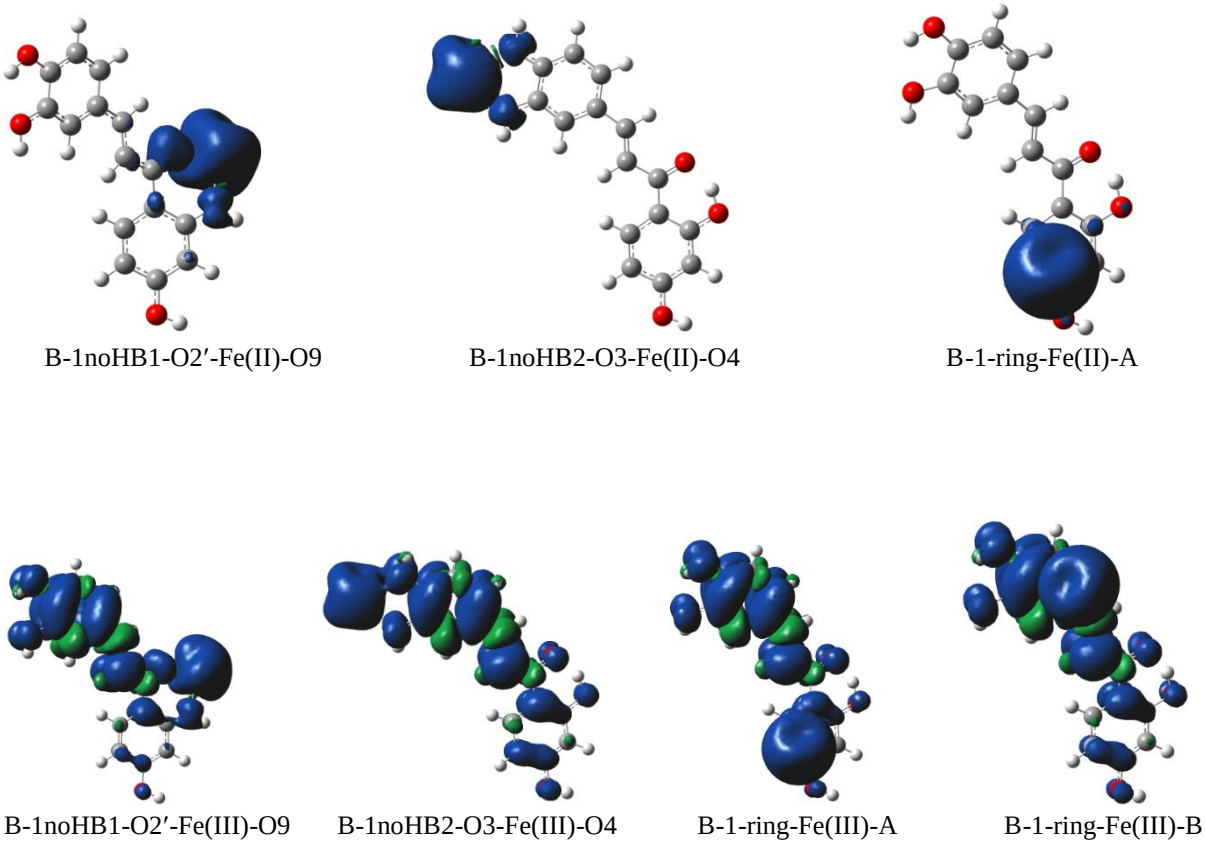

Figure 4.26 Spin density distribution for the butein···Fe^{n+} complexes formed from interactions of neutral butein and bare Fe^{n+} cations, B3LYP/6-31+G(d,p) results in water solution. The surface isovalue used is 0.0004 au. The blue colour corresponds to positive spin densities and the green colour denotes the negative spin density.

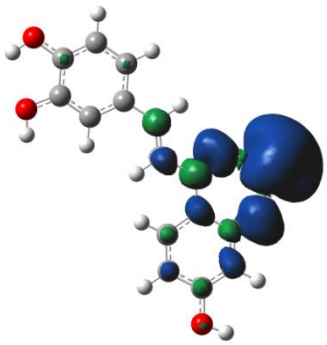

B-1noHB1-an-O2′-Fe(II)-O9

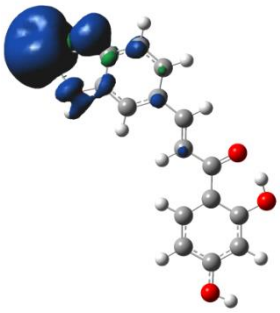

B-1noHB2-anI-O3-Fe(II)-O4

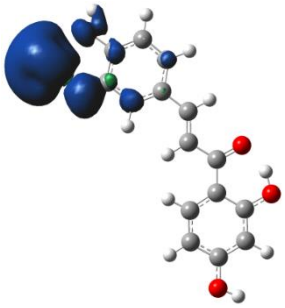

B-1noHB2-anII-O3-Fe(II)-O4

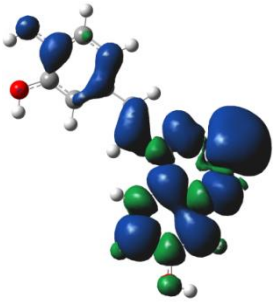

B-1noHB1-an-O2′-Fe(III)-O9

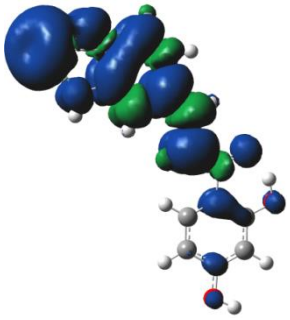

B-1noHB2-anI-O3-Fe(III)-O4

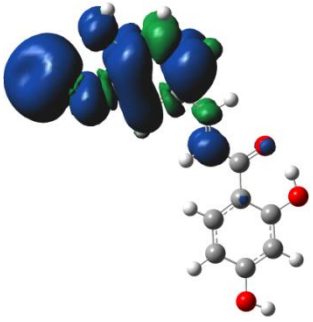

B-1noHB2-anII-O3-Fe(III)-O4

Figure 4.27 Spin density distribution for the butein···Fe^{n+} complexes formed from interactions of deprotonated butein and bare Fe^{n+} cations, B3LYP/6-31+G(d,p) results in water solution. The surface isovalue used is 0.0004 au. The blue colour corresponds to positive spin densities and the green colour denotes the negative spin density.

Table 4.34 Natural atomic orbital occupancies for some valence orbitals in the isolated Fe^{n+} cations and in complexes with butein results in water solution with different methods

Isolated and Fe complex	Orbitals and the corresponding natural atomic orbital occupancies					
DFT/B3LYP results						
	s (4s)	d_{xy} (3d)	d_{xz} (3d)	d_{yz} (3d)	$d_{x^2-y^2}$ (3d)	d_{z^2} (3d)
Fe(II)	0.000	1.998	1.000	1.000	1.000	1.000
B-1noHB1-O2′-Fe(II)-O9	0.039	1.138	1.232	1.092	1.161	1.447
B-1noHB2-O3-Fe(II)-O4	0.025	1.091	1.21	1.062	1.362	1.305
B-1-ring-Fe(II)-A	0.011	1.695	1.283	1.015	1.003	1.004
B-1-ring-Fe(II)-B	_[a]	_[a]	_[a]	_[a]	_[a]	_[a]
B-1noHB1-an-O2′-Fe(II)-O9	0.056	1.078	1.897	1.090	1.020	1.008
B-1noHB2-anI-O3-Fe(II)-O4	0.046	1.445	1.526	1.040	1.025	1.059
B-1noHB2-anII-O3-Fe(II)-O4	0.048	1.020	1.059	1.968	1.045	1.014
Fe(III)	0.000	1.000	1.000	1.000	1.000	1.000
B-1noHB1-O2′-Fe(III)-O9	0.036	1.583	1.264	1.029	1.077	1.071
B-1noHB2-O3-Fe(III)-O4	0.013	1.074	1.266	1.134	1.209	1.322
B-1-ring-Fe(III)-A	0.010	1.669	1.284	1.028	1.009	1.007
B-1-ring-Fe(III)-B	0.002	1.291	1.118	1.135	1.127	1.313
B-1noHB1-an-O2′-Fe(III)-O9	0.055	1.167	1.248	1.264	1.045	1.062
B-1noHB2-anI-O3-Fe(III)-O4	0.034	1.031	1.026	1.312	1.163	1.454
B-1noHB2-anII-O3-Fe(III)-O4	0.025	1.004	1.067	1.206	1.358	1.309
DFT/BP86 results						
Fe(II)						
B-1noHB1-O2′-Fe(II)-O9	0.047	1.498	1.107	1.128	1.295	1.084
B-1noHB2-O3-Fe(II)-O4	0.029	1.069	1.201	1.065	1.404	1.324
B-1-ring-Fe(II)-A	_[a]	_[a]	_[a]	_[a]	_[a]	_[a]
B-1-ring-Fe(II)-B	0.008	1.49	1.14	1.075	1.04	1.296
B-1noHB1-an-Fe-O2′-Fe(II)-O9	0.066	1.146	1.846	1.09	1.045	1.022
B-1noHB2-anI-Fe-O3-Fe(II)-O4	0.055	1.534	1.425	1.076	1.051	1.082
B-1noHB2-anII-Fe-O3-Fe(II)-O4	0.052	1.452	1.079	1.464	1.051	1.129
Fe(III)						
B-1noHB1-O2′-Fe(III)-O9	0.043	1.387	1.200	1.044	1.113	1.147
B-1noHB2-O3-Fe(III)-O4	0.024	1.183	1.160	1.059	1.481	1.022
B-1-ring-Fe(III)-A	0.009	1.703	1.081	1.011	1.083	1.035
B-1-ring-Fe(III)-B	0.004	1.223	1.030	1.044	1.034	1.529
B-1noHB1-an-Fe-O2′-Fe(III)-O9	0.061	1.231	1.367	1.160	1.078	1.064
B-1noHB2-anI-Fe-O3-Fe(III)-O4	0.046	1.022	1.033	1.141	1.213	1.484
B-1noHB2-anII-Fe-O3-Fe(III)-O4	0.044	1.062	1.200	1.113	1.118	1.395

[a] On optimisation the calculation fails to converge

4.3.6. Conformational stability and geometries for the homobutein conformers

The optimised conformers of homobutein in water solution are shown in Figure 4.28 and the corresponding ΔE values (kcal/mol) are reported in Table 4.35. The energy gap between the conformers is significantly decreased in comparison to the results obtained *in vacuo*. The lowest-energy conformer possesses both the first intramolecular bond and the second intramolecular hydrogen bond, indicating that both intramolecular hydrogen bonds are vital for the stabilisation of the conformers in solution, a similar result was obtained *in vacuo*. The ΔE gap between the first three lowest-energy conformers of homobutein is significantly small (i.e., < 1 kcal/mol), which implies that they can be considered to be iso-energetic. Conformers in which the first intramolecular hydrogen bond is removed result in very high relative energy values compared to the removal of the second intramolecular hydrogen bond, what may suggest that the first intramolecular hydrogen bond plays a greater role in conformational stability more than the presence of the second intramolecular hydrogen bond, a similar trend was also identified *in vacuo*. Although there is a significant reduction in the energy gap between conformers, it is still reasonable to state that the conformers that do not have the first intramolecular hydrogen bond may not exist in vivo, mainly because of their high relative energy values.

Conformers that differ in terms of the rotation of the C7–C8 bond show similar trend as was observed *in vacuo*; for instance, the energy gap between the hB-1 and hB-4 pair is 6.414kcal/mol while the hB-1noHB2 and hB-5 pair of conformers have an energy gap of 6.918 kcal/mol; the ΔE gap between the hB-1noHB1 and hB-6 pair (i.e., conformers in which the first intramolecular hydrogen bond is absent) is 0.809kcal/mol.

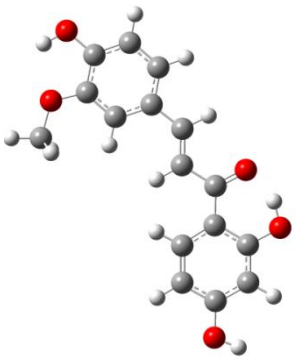

0.000
hB-1

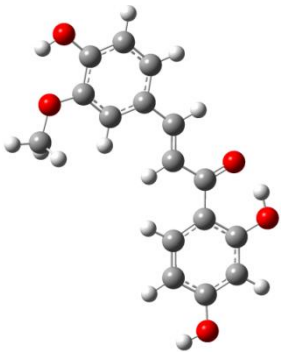

0.098
hB-2

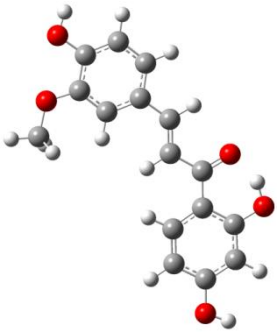

0.918
hB-1noHB2

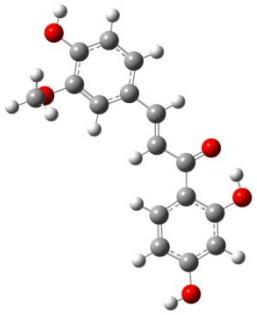

3.614
hB-3

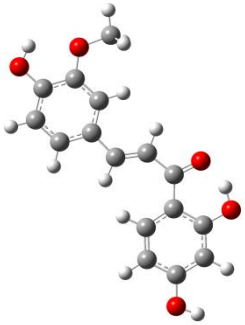

6.414
hB-4

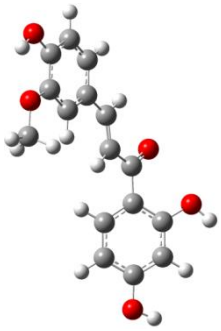

7.213
hB-1noHB1

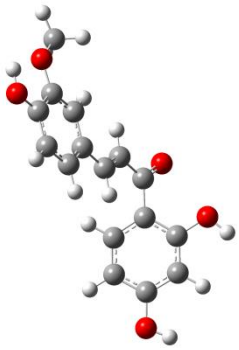

7.386
hB-5

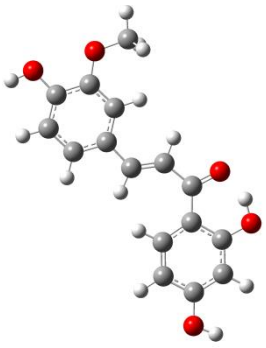

8.005
hB-6

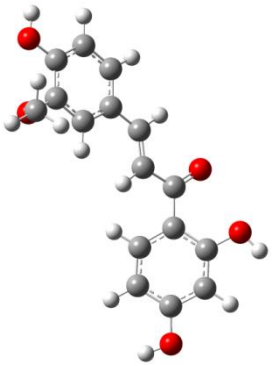

10.670
hB-3noHB1

Figure 4.28 B3LYP/6-31+G(d,p) optimised conformers for neutral homobutein arranged in order of increasing relative energy (ΔE, kcal/mol), B3LYP/6-311+G(2d,p)//B3LYP/6-31+G(d,p) results in water solution. Similar geometries were obtained for the B86/6-311+G(2d,p)//B86/6-31+G(d,p) calculation method.

Table 4.35 Relative energies (ΔE, kcal/mol) for the neutral conformers of homobutein in water solution

Conformer	*A*[a]		*B*[b]	
	total energy (Hartree)	ΔE (kcal/mol)	total energy (Hartree)	ΔE (kcal/mol)
DFT/B3LYP results				
hB-1	-994.3340834	0.000	-994.5762566	0.000
hB-2	-994.3338835	0.125	-994.5761004	0.098
hB-1noHB2	-994.3327208	0.855	-994.5747945	0.918
hB-3	-994.3283238	3.614	-994.5705000	3.612
hB-4	-994.3238487	6.422	-994.5660349	6.414
hB-1noHB1	-994.3225885	7.213	-994.5647889	7.196
hB-5	-994.3223887	7.339	-994.5644839	7.386
hB-6	-994.3212891	8.029	-994.5634991	8.005
hB-3noHB1	-994.3170763	10.672	-994.5592034	10.701
DFT/BP86 results				
hB-1	-994.3364647	0.000	-994.5808738	0.000
hB-2	-994.3362498	0.135	-994.5793824	0.936
hB-1noHB2	-994.3351273	0.839	-994.5793803	0.937
hB-3	-994.3290137	4.676	-994.5733965	4.692
hB-4	-994.3271451	5.848	-994.5714716	5.900
hB-1noHB1	-994.3256701	6.774	-994.5698570	6.913
hB-5	-994.3220259	9.061	-994.5664685	9.040
hB-6	-994.3207460	9.863	-994.5651552	9.864
hB-3noHB1	-994.3149546	13.498	-994.5593645	13.497

The optimised deprotonated conformers obtained in water solution are shown in Figure 4.29 and the corresponding ΔE (kcal/mol) are reported in Table 4.36. Among the deprotonated conformers of homobutein in water solution the lowest-energy conformer corresponds to the removal of the H4″ proton and the presence of the first intramolecular hydrogen bond, a result which is consistent with the results obtained for the butein conformers. The ΔE gap between the lowest-energy complex and the second lowest-energy complex corresponds to 3.890 kcal/mol which implies that this conformer (second lowest-energy conformer) may exist in water solution. Although the relative energy in water solution is dampened with respect to the energy obtained *in vacuo* only these two conformers (i.e., hB-1noHB2-an and hB-4-an) may be considered to exist in physiological conditions. The least preferred deprotonation site is the removal of the H2′ proton for both bent and non-bent aliphatic chain arrangement, a result in agreement with those obtained *in vacuo*.

The removal of the H4″ and H2′ protons in the hB-4 and hB-6 conformers to from the hB-4-an and hB-6-an conformers respectively results in energy increase of 2.524 kcal/mol for the removal of the H4″ proton and 1.115 kcal/mol for the removal of the H2′ proton.

The results obtained suggests that for both bent and non-bent aliphatic chain arrangement the removal of the H2′ proton (i.e., corresponding to the removal of the first intramolecular hydrogen bond) results in high relative energy values what suggests that the removal of the H4″ proton is preferred, a result that is in agreement with those obtained for butein.

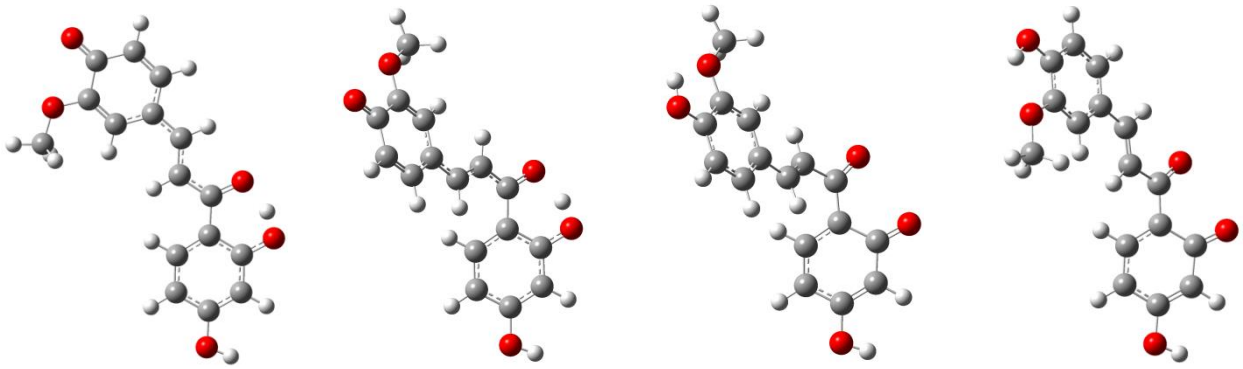

Figure 4.29 B3LYP/6-31+G(d,p) optimised conformers for deprotonated homobutein arranged in order of increasing relative energy (ΔE, kcal/mol), B3LYP/6-311+G(2d,p)//B3LYP/6-31+G(d,p) results in water solution. Similar geometries were obtained for the BP86/6-311+G(2d,p)//BP86/6-31+G(d,p) calculation method.

Table 4.36 Relative energy values (ΔE, kcal/mol) for the deprotonated conformers of homobutein in water solution

Conformer	*A*[a]		*B*[b]	
	total energy (Hartree)	ΔE (kcal/mol)	total energy (Hartree)	ΔE (kcal/mol)
DFT/B3LYP results				
hB-1noHB2-an	-993.8676617	0.000	-994.1097679	0.000
hB-4-an	-993.8614837	3.877	-994.1035693	3.890
hB-6-an	-993.8518623	9.914	-994.0987876	6.890
hB-1noHB1-an	-993.8540681	8.530	-994.0960117	8.632
DFT/BP86 results				
hB-1noHB2-an	-993.8755716	0.000	-994.1198024	0.000
hB-4-an	-993.8693020	3.934	-994.1134598	3.980
hB-1noHB1-an	-993.8571798	11.541	-994.1013676	11.568
hB-6-an	-993.8550346	12.887	-994.0990862	13.000

[a] Results obtained using the 6-31+G(d,p) basis set
[b] Single point results using the 6-311+G(2d,p) basis set, starting from optimised geometries

4.3.7. Relative stability and binding energies for homobutein···Fe^{n+} complexes formed from neutral homobutein and bare Fe^{n+} cations

The optimised homobutein···Fe^{n+} complexes are shown in Figure 4.30 for the DFT/B3LYP results and Figure 4.31 for the DFT/BP86 results; the corresponding ΔE (kcal/mol) are reported Table 4.37. The most preferred complexes correspond to the coordination of the cations at the hydroxyl–*keto* reactive site. The ΔE gap between the lowest-energy complex and the second lowest-energy complex correspond to 2.174 kcal/mol for the Fe(II) cation which is significantly decreased in comparison with the results obtained *in vacuo*. The ΔE energy gap between the lowest-energy complex and the hB-1-ring-Fe(II)-A complex corresponds to 10.054 kcal/mol which suggests that coordination at ring A may not be preferred, and therefore, such complexes may not exist in nature. Among the complexes with the Fe(III) cation the ΔE energy gap between lowest-energy complex and the all other complexes corresponds to ΔE value greater than 3.5kcal/mol (i.e., with a 7.727–8.567 kcal/mol range), what may suggest that only the coordination of the Fe(III) cation at the hydroxyl–*keto* reactive site is the most probable to observe *in vivo*.

The bond distance values between the ligand donor atoms and the Fe^{n+} cation also suggests that they are longer in water solution than *in vacuo*, which is an indication of the weakening of the binding between homobutein and Fe^{n+} cations.

The $\Delta E'_{binding}$ values (kcal/mol) are reported in Table 4.38. They are significantly dampened with respect to the results *in vacuo*, which is suggestive of the fact that in water solution the interactions between the ligand and the Fe^{n+} cations are weaker. For the complexes with the Fe^{n+} cations the strongest binding corresponds to the coordination of the cations to the hydroxyl–*keto* reactive site, a result which is similar to that obtained *in vacuo*. Coordination at the methoxy–hydroxyl site results in the second strongest binding with values of 9.719 kcal/mol and 47.422 kcal/mol for the Fe(II) and Fe(III) cations respectively. The weakest binding energy corresponds to the coordination of the Fe^{n+} cations at the π system of aromatic ring A for coordination with the Fe(II) cation and coordination at the π system of aromatic ring B for coordination of the Fe(III) cation. A comparison of the $\Delta E'_{binding}$ values suggests that homobutein may tend to act as better antioxidant when chelating the Fe(III) cation than the Fe(II) cation; a similar result are observed for the coordination of the cations to the butein ligand, both *in vacuo* and in water solution.

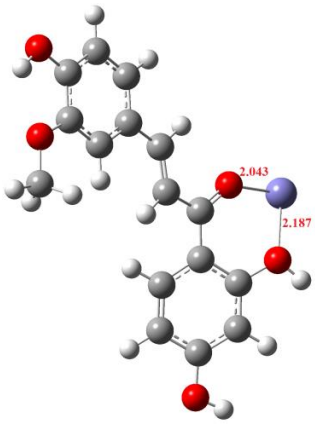

0.000
hB-1noHB1-O2′-Fe(II)-O9

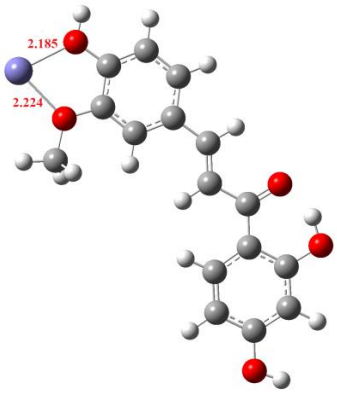

2.174
hB-1noHB2-O3-Fe(II)-O4

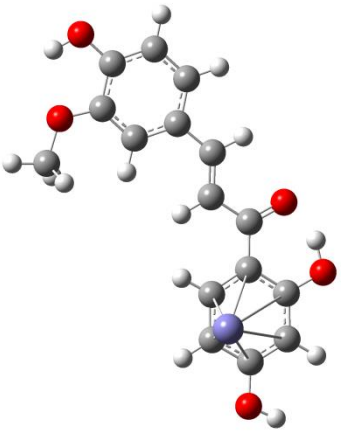

10.054
hB-1-ring-Fe(II)-A

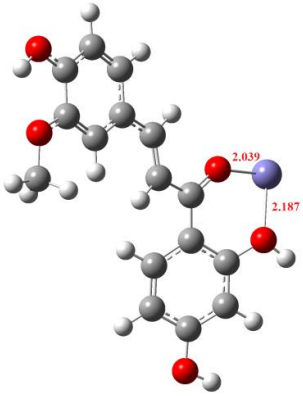

0.000
hB-1noHB1-O2′-Fe(III)-O9

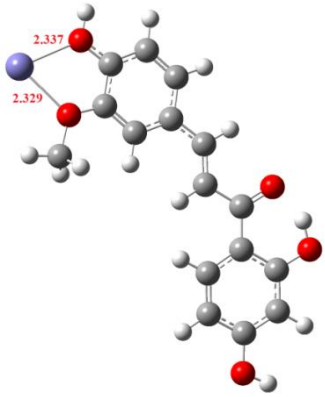

7.727
hB-1noHB2-O3-Fe(III)-O4

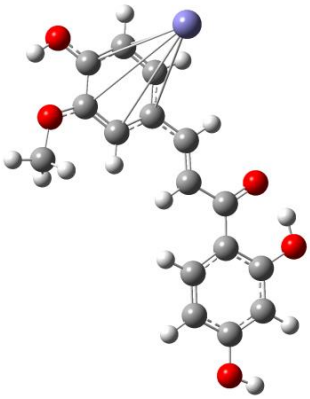

8.567
hB-1-ring-Fe(III)-B

Figure 4.30 B3LYP/6-31+G(d,p) optimised homobutein···Fe^{n+} complexes (arranged in order of increasing relative energy (ΔE, kcal/mol)) formed from neutral homobutein and bare Fe^{n+} cation B3LYP/6-311+G(2d,p)//B3LYP/6-31+G(d,p) results in water solution. The bond length between the cation and the ligand are reported in Å.

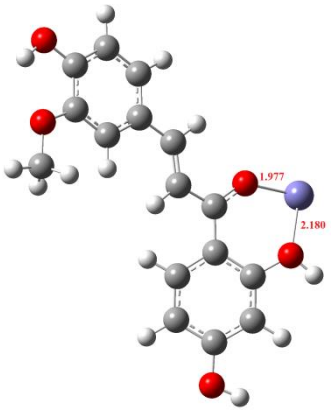

0.000
hB-1noHB1-O2′-Fe(II)-O9

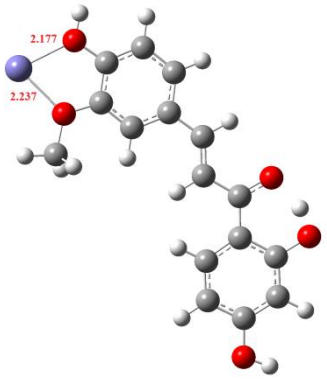

4.467
hB-1noHB2-O3-Fe(II)-O4

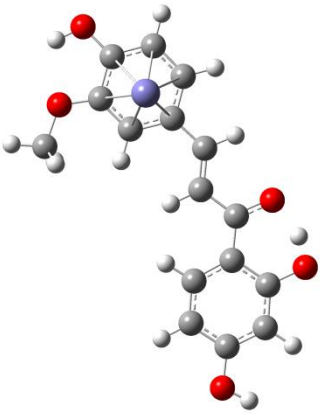

11.232
hB-1-ring-Fe(II)-B

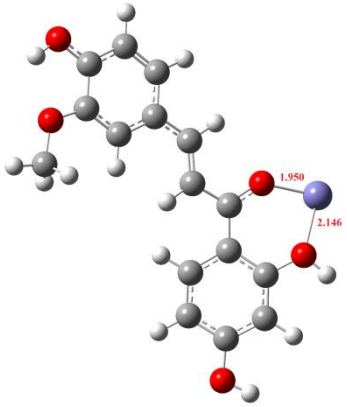

0.000
hB-1noHB1-O2′-Fe(III)-O9

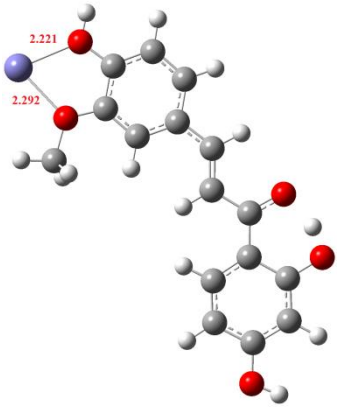

12.112
hB-1noHB2-O3-Fe(III)-O4

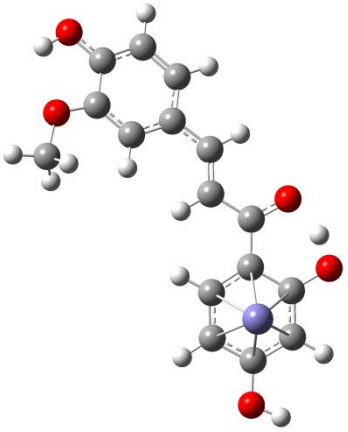

14.883
hB-1-ring-Fe(III)-A

Figure 4.31 BP86/6-31+G(d,p) optimised homobutein···Fe^{n+} complexes (arranged in order of increasing relative energy (ΔE, kcal/mol)) formed from neutral homobutein and bare Fe^{n+} cation BP86/6-311+G(2d,p)//BP86/6-31+G(d,p) results in water solution. The bond length between the cation and the ligand are reported in Å.

Table 4.37 Relative energy values (ΔE, kcal/mol) for the homobutein···Fe^{n+} complexes formed from neutral homobutein ligand and bare Fe^{n+} cations, results in water solution

Complex	*A*[a]		*B*[b]	
	total energy (Hartree)	ΔE (kcal/mol)	total energy (Hartree)	ΔE (kcal/mol)
DFT/B3LYP results				
hB-1noHB1-O2′-Fe(II)-O9	-1117.5433309	0.000	-2258.0719461	0.000
hB-1noHB2-O3-Fe(II)-O4	-1117.5431658	0.104	-2258.0684812	2.174
hB-1-ring-Fe(II)-A	-1117.5311633	7.635	-2258.0559247	10.054
hB-1-ring-Fe(II)-B	–[c]	–[c]	–[c]	–[c]
hB-1noHB1-O2′-Fe(III)-O9	-1117.3382836	0.000	-2257.8653333	0.000
hB-1noHB2-O3-Fe(III)-O4	-1117.3297429	5.359	-2257.8530198	7.727
hB-1-ring-Fe(III)-B	-1117.3283437	6.238	-2257.8516811	8.567
hB-1-ring-Fe(III)-A	–[c]	–[c]	–[c]	–[c]
DFT/BP86 results				
hB-1noHB1-O2′-Fe(II)-O9	-1117.5904054	0.000	-2258.2128655	0.000
hB-1noHB2-O3-Fe(II)-O4	-1117.5868370	2.239	-2258.2057471	4.467
hB-1-ring-Fe(II)-B	-1117.5800179	6.158	-2258.1949661	11.232
hB-1-ring-Fe(II)-A	–[c]	–[c]	–[c]	–[c]
hB-1noHB1-O2′-Fe(III)-O9	-1117.3921390	0.000	-2258.0195684	0.000
hB-1noHB2-O3-Fe(III)-O4	-1117.3800234	7.603	-2258.0002660	12.112
hB-1-ring-Fe(III)-A	-1117.3794266	7.977	-2257.9959304	14.833
hB-1-ring-Fe(III)-B	–[c]	–[c]	–[c]	–[c]

[a] Results obtained using the 6-31+G(d,p) basis set
[b] Single point results using the 6-311+G(2d,p) basis set, starting from optimised geometries
[c] On optimisation the calculation fails to converge

Table 4.38 Binding energy values ($\Delta E'_{binding}$, kcal/mol) for homobutein···Fe^{n+} complexes formed from neutral homobutein ligand and bare Fe^{n+} cations results in water solution. The complexes are arranged in order of decreasing $\Delta E'_{binding}$ values

Complex	*A*[a]			*B*[b]		
	ΔE_{inter}, kcal/mol	ΔE_{def} kcal/mol	$\Delta E'_{binding}$, kcal/mol	ΔE_{inter}, kcal/mol	ΔE_{def} kcal/mol	$\Delta E'_{binding}$, kcal/mol
DFT/B3LYP results						
hB-1noHB1-O2′-Fe(II)-O9	–28.518	1.177	29.695	–17.445	1.372	18.817
hB-1noHB2-O3-Fe(II)-O4	–17.586	0.696	18.282	–8.992	0.727	9.719
hB-1-ring-Fe(II)-A	–5.455	0.477	5.932	–0.195	0.558	0.753
hB-1-ring-Fe(II)-B	–[c]	–[c]	–[c]	–[c]	–[c]	–[c]
hB-1noHB1-O2′-Fe(III)-O9	–86.431	5.062	91.493	–57.919	5.053	62.972
hB-1noHB2-O3-Fe(III)-O4	–70.244	3.613	73.857	–43.914	3.508	47.422
hB-1-ring-Fe(III)-B	–64.766	3.818	68.584	–42.157	3.637	45.794
hB-1-ring-Fe(III)-A	–[c]	–[c]	–[c]	–[c]	–[c]	–[c]
DFT/BP86 results						
hB-1noHB1-O2′-Fe(II)-O9	–7.432	1.588	9.020	–21.806	1.789	23.595
hB-1noHB2-O3-Fe(II)-O4	3.028	0.748	–2.280	–9.236	0.760	9.996
hB-1-ring-Fe(II)-B	8.146	0.068	–8.078	–1.534	0.142	1.676
hB-1-ring-Fe(II)-A	–[c]	–[c]	–[c]	–[c]	–[c]	–[c]
hB-1noHB1-O2′-Fe(III)-O9	–75.578	3.616	79.194	–77.663	3.697	81.360
hB-1-ring-Fe(III)-A	–58.540	2.084	60.624	–57.701	2.054	59.755
hB-1noHB2-O3-Fe(III)-O4	–59.734	1.962	61.696	–57.449	1.916	59.365
hB-1-ring-Fe(III)-B	–[c]	–[c]	–[c]	–[c]	–[c]	–[c]

[a] Results obtained using the 6-31+G(d,p) basis set
[b] Single point results using the 6-311+G(2d,p) basis set, starting from optimised geometries
[c] On optimisation the calculation does not converge

4.3.8. Relative stability and binding energies for homobutein···Fe^{n+} complexes formed from deprotonated homobutein and bare Fe^{n+} cations

The optimised homobutein···Fe^{n+} complexes formed with deprotonated homobutein ligand are shown in Figure 4.32; the corresponding ΔE values (kcal/mol) are reported in Table 4.39. The lowest-energy complex corresponds to the coordination of the cations to the O2′∪O9 reactive site, which is a similar result to the outcome obtained *in vacuo*. The ΔE gap between the first lowest-energy complexes and the second-lowest energy complexes is 1.310 kcal/mol for Fe(II) cation and 3.246 kcal/mol for Fe(III) cation. These values suggest that both coordination at the O2′∪O9 reactive site and the O3CH3∪O4 reactive site are preferred in water solution, a trend different to that observed *in vacuo*.

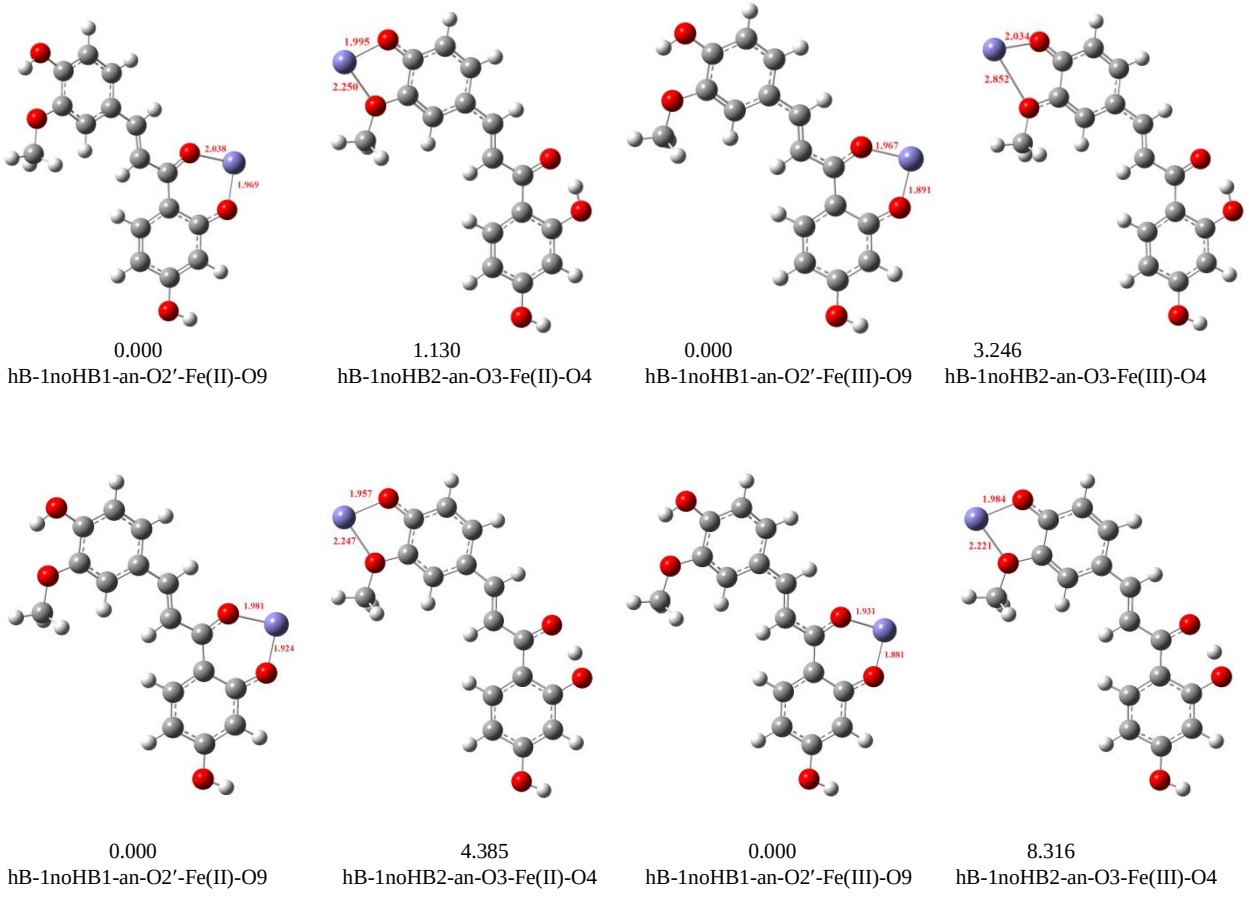

Figure 4.32 Optimised homobutein···Fe^{n+} complexes (arranged in order of increasing relative energy (ΔE, kcal/mol)) formed from deprotonated homobutein ligand and bare Fe^{n+} cations. The first row shows the B3LYP/6-31+G(d,p) results and the second row of structures corresponds to the BP86/6-31+G(d,p) results. The bond length between the cation and the ligand are reported in Å.

Table 4.39 Relative energy values (ΔE, kcal/mol) for the homobutein···Fe^{n+} complexes formed from deprotonated homobutein ligand and bare Fe^{n+} cations in water solution

Complex	*A*[a]		*B*[b]	
	total energy (Hartree)	ΔE (kcal/mol)	total energy (Hartree)	ΔE (kcal/mol)
DFT/B3LYP results				
hB-1noHB1-an-O2′-Fe(II)-O9	-1117.1046216	0.000	-2257.6341921	0.000
hB-1noHB2-an-O3-Fe(II)-O4	-1117.1045741	0.030	-2257.6321037	1.310
hB-1noHB1-an-O2′-Fe(III)-O9	-1116.9101734	3.866	-2257.4486408	0.000
hB-1noHB2-an-O3-Fe(III)-O4	-1116.9163348	0.000	-2257.4434674	3.246
DFT/BP86 results				
hB-1noHB1-an-O2′-Fe(II)-O9	-1117.1590316	0.000	-2257.7860349	0.000
hB-1noHB2-an-O3-Fe(II)-O4	-1117.1565328	1.568	-2257.7790466	4.385
hB-1noHB1-an-O2′-Fe(III)-O9	-1116.9789384	0.000	-2257.6115854	0.000
hB-1noHB2-an-O3-Fe(III)-O4	-1116.9728971	3.791	-2257.5983334	8.316

[a] Results obtained using the 6-31+G(d,p) basis set
[b] Single point results using the 6-311+G(2d,p) basis set, starting from optimised geometries

The $\Delta E'_{binding}$ values (kcal/mol) are reported in Table 4.40. The coordination of the Fe^{n+} cations at the O2′∪O9 site corresponds to the strongest binding, with MIA values of 38.249 kcal/mol for the Fe(II) cation and 94.160 kcal/mol for the Fe(III) cation. The MIA values for the coordination of the cation to the O3CH3∪O4 reactive site is slightly weaker, being nearly 10 kcal/mol (for the Fe(II) results) and 13 kcal/mol (for the Fe(III) results) less than the MIA values for the coordination at the O2′∪O9 reactive site. A comparison of the Fe(II) and Fe(III) results obtained here further confirm the fact that the chalcone derivatives (i.e., butein and homobutein) may act as a better antioxidant when chelating the Fe(III) cation than the Fe(II) cation.

Table 4.40 Binding energy values ($\Delta E'_{binding}$, kcal/mol) for the homobutein···Fe^{n+} complexes formed from deprotonated homobutein and bare Fe^{n+} cations in water solution. The complexes are arranged in order of decreasing $\Delta E'_{binding}$ values

Complex	*A*[a]			*B*[b]		
	ΔE_{inter}, kcal/mol	ΔE_{def} kcal/mol	$\Delta E'_{binding}$, kcal/mol	ΔE_{inter}, kcal/mol	ΔE_{def} kcal/mol	$\Delta E'_{binding}$, kcal/mol
DFT/B3LYP results						
hB-1noHB1-an-O2′-Fe(II)-O9	–22.938	1.260	24.198	–36.912	1.337	38.249
hB-1noHB2-an-O3-Fe(II)-O4	–14.378	1.423	15.810	–26.970	1.438	28.408
hB-1noHB1-an-O2′-Fe(III)-O9	–87.502	3.560	91.062	–90.603	3.557	94.160
hB-1noHB2-an-O3-Fe(III)-O4	–82.838	2.634	85.472	–78.724	2.151	80.875
DFT/BP86 results						
hB-1noHB1-an-O2′-Fe(II)-O9	–28.437	1.941	30.378	–45.821	1.998	47.819
hB-1noHB2-an-O3-Fe(II)-O4	–15.327	1.710	17.037	–29.867	1.686	31.553
hB-1noHB1-an-O2′-Fe(III)-O9	–107.986	4.198	112.184	–113.505	2.078	117.67
hB-1noHB2-an-O3-Fe(III)-O4	–92.654	2.358	95.012	–93.622	5.798	95.700

[a] Results obtained using the 6-31+G(d,p) basis set
[b] Single point results using the 6-311+G(2d,p) basis set, starting from optimised geometries

4.3.9. AIM analysis of the bonding within the homobutein complexes

The bond critical point (BCP) data of the electron density distributions $\rho(\mathbf{r})$ and its second derivative ($\nabla^2\rho$ (r)) for the homobutein···Fe^{n+} complexes are reported in Table 4.41 for the DFT/B3LYP results and Table 4.42 for the DFT/BP86 results. The strongest bond among the complexes formed with neutral homobutein ligand and the bare Fe^{n+} cation corresponds to the O9···Fe^{n+} bond with ρ values of 0.120 and 0.130 e/Å^3 for the Fe(II) and Fe(III) cations respectively, what is in agreement with the binding energy. The weakest bond corresponds to the coordination of the Fe^{n+} cations at the C2′···Fe^{n+} with ρ value of 0.042 e/Å^3 for the Fe(II) cation and 0.061 e/Å^3 for the Fe(III) cation. Among the complexes with the deprotonated homobutein ligand the largest value of ρ corresponds to the coordination of the Fe^{n+} cation at the O2′···Fe^{2+} bond with values of ρ 0.124 e/Å^3 and O4···Fe^{3+} bond with ρ value of at the 0.133 e/Å^3 for coordination with the Fe(II) and the Fe(III) cation respectively.

Analysis of the values of the $\nabla^2\rho$ (e/Å^5) shows a range of 0.120–0.673 and 0.107–0.687 e/Å^5 for the complexes of neutral homobutein ligand with the Fe(II) and Fe(III) cations respectively. Among the complexes with the deprotonated homobutein ligand for both bare and hydrated Fe^{n+} cations$\nabla^2\rho$ ranges from 0.194–0.627 e/Å^5 for Fe(II) cation and 0.163–0.740 e/Å^5 for Fe(III) cation. These values of $\nabla^2\rho$, which are positive, are suggestive of closed shell interactions; this is further supported by the negative values of *H* which approach zero. The |V|/G ratio values are within the 0.9–1.0 for complexes of the Fe^{n+} cations with both neutral or deprotonated homobutein ligand, which further supports that the type of interactions formed between the Fe^{n+} cations and the ligand are inclined towards closed-shell interactions.

Table 4.41 Bond critical point data for homobutein···Fe^{n+} complexes UB3LYP/6-31+G(d,p) results in water

Complex	Bond type	ρ e/Å^3	$\nabla^2\rho$ e/Å^5	V (Hartree)	G (Hartree)	H (Hartree)	$\frac{\lvert V \rvert}{G}$
hB-1noHB1-O2′-Fe(II)-O9	O2′···Fe	0.068	0.407	–0.105	0.103	–0.0015	1.014
	O9···Fe	0.120	0.673	–0.225	0.197	–0.0285	1.145
hB-1noHB2-O3-Fe(II)-O4	O3···Fe	0.056	0.317	–0.079	0.079	0.0001	0.999
	O4···Fe	0.058	0.339	–0.084	0.084	0.0004	0.995
hB-1-ring-Fe(II)-A	C3′···Fe	0.042	0.120	–0.044	0.037	–0.0071	1.191
	C6′···Fe	0.054	0.170	–0.062	0.052	–0.0099	1.189
hB-1-ring-Fe(II)-B	C2···Fe	0.043	0.128	–0.047	0.039	–0.0073	1.185
	C5···Fe	0.049	0.151	–0.055	0.046	–0.0086	1.185
hB-1noHB1-an-O2′-Fe(II)-O9	O2′···Fe	0.124	0.618	–0.219	0.187	–0.0323	1.173
	O9···Fe	0.122	0.621	–0.215	0.185	–0.0299	1.161
hB-1noHB2-an-O3-Fe(II)-O4	O3···Fe	0.050	0.342	–0.075	0.080	0.0053	0.934
	O4···Fe	0.110	0.674	–0.223	0.196	–0.0273	1.139
hB-1noHB1-O2′-Fe(III)-O9	O2′···Fe	0.067	0.393	–0.101	0.100	–0.0015	1.015
	O9···Fe	0.130	0.687	–0.243	0.207	–0.0357	1.172
hB-1noHB2-O3-Fe(III)-O4	O3···Fe	0.061	0.355	–0.089	0.089	–0.0003	1.004
	O4···Fe	0.061	0.379	–0.093	0.094	0.0007	0.993
hB-1-ring-Fe(III)-A	C5′···Fe	0.072	0.107	–0.067	0.047	–0.0203	1.431
hB-1-ring-Fe(III)-B	C5···Fe	0.069	0.153	–0.072	0.055	–0.017	1.308
	C6···Fe	0.069	0.137	–0.069	0.052	–0.0177	1.341
hB-1noHB1-an-O2′-Fe(III)-O9	O2′···Fe	0.128	0.740	–0.254	0.219	–0.0344	1.155
	O9···Fe	0.109	0.633	–0.201	0.179	–0.0212	1.116
hB-1noHB2-an-O3-Fe(III)-O4	O3···Fe	0.059	0.283	–0.074	0.072	–0.0018	1.024
	O4···Fe	0.133	0.675	–0.247	0.208	–0.0389	1.187

Table 4.42 Bond critical point data for homobutein···Fe^{n+} complexes UBP86/6-31+G(d,p) results in water

Complex	Bond type	ρ e/Å^3	$\nabla^2\rho$ e/Å^5	V (Hartree)	G (Hartree)	H (Hartree)	$\frac{\lvert V \rvert}{G}$
hB-1noHB1-O2′-Fe(II)-O9	O2′···Fe	0.049	0.246	–0.059	0.060	0.001	0.983
	O9···Fe	0.085	0.444	–0.127	0.119	–0.008	1.067
hB-1noHB2-O3-Fe(II)-O4	O3···Fe	0.043	0.209	–0.051	0.051	0.000	1.000
	O4···Fe	0.048	0.256	–0.611	0.063	–0.548	9.698
hB-1noHB1-an-O2′-Fe(II)-O9	O2′···Fe	0.010	0.510	–0.159	0.143	–0.016	1.112
	O9···Fe	0.084	0.457	–0.130	0.122	–0.008	1.066
hB-1noHB2-an-O3-Fe(II)-O4	O3···Fe	0.041	0.204	–0.049	0.050	0.001	0.980
	O4···Fe	0.093	0.454	–0.139	0.126	–0.013	1.103
hB-1noHB1-O2′-Fe(III)-O9	O2′···Fe	0.055	0.259	–0.635	0.064	–0.571	9.922
	O9···Fe	0.093	0.471	–0.141	0.129	–0.012	1.093
hB-1noHB2-O3-Fe(III)-O4	O3···Fe	0.037	0.162	–0.038	0.039	0.001	0.974
	O4···Fe	0.043	0.216	–0.050	0.052	0.002	0.962
hB-1noHB1-an-O2′-Fe(III)-O9	O2′···Fe	0.113	0.574	–0.191	0.167	–0.024	1.144
	O9···Fe	0.099	0.491	–0.154	0.138	–0.016	1.116
hB-1noHB2-an-O3-Fe(III)-O4	O3···Fe	0.045	0.206	–0.049	0.050	0.001	0.980
	O4···Fe	0.088	0.434	–0.129	0.119	–0.010	1.084

4.3.10. NPA charges, spin density and orbital occupancies

The NPA charges as and the spin density values are reported in Table 4.43 for the homobutein···Fe^{n+} complexes. In water solution the charge of the Fe(II) cation is reduced from 2 to a 1.7–1.9 *e* range and from 3 to a 1.9–2.0 *e* range for Fe(III) cation. Among the complexes with the neutral homobutein ligand, the largest amount of charge density transfer corresponds to the coordination of the Fe^{n+} cations at the hydroxyl–*keto* reactive site. This result implies that the strongest interaction site between the Fe^{n+} cation and the ligand is the hydroxyl–*keto* reactive site; similar inference is obtained when analysing the binding energy values, where coordination to the hydroxyl–*keto* reactive site corresponds to the strongest binding between the cation and the ligand.

For the complexes of the Fe^{n+} cations with the deprotonated homobutein ligand similar trends are observed in that coordination of the Fe^{n+} cations at the O2′∪O9 reactive site results in the highest electron density transfer. The results of the charge transfer in water solution are significantly dampened with respect to those *in vacuo*. The site of coordination with the least transfer of electron density corresponds to the π system of the aromatic ring A for both coordination with the Fe(II) and Fe(III) cation. However, an assessment of the charge density transfer at the aromatic rings is not very straightforward because the charge density of the π system does not necessary corresponds to the charge density on the individual C atoms of the aromatic rings.

Table 4.43 NPA charges and spin densities for the Fe^{n+} cations in the complexes with butein results in water solution

Complex	charge *(e)*		spin density	
	DFT/B3LYP results	DFT/BP86 results	DFT/B3LYP results	DFT/BP86 results
hB-1noHB1-O2′-Fe(II)-O9	1.874	1.769	3.922	3.862
hB-1noHB2-O3-Fe(II)-O4	1.912	1.876	3.950	3.918
hB-1-ring-Fe(II)-A	1.978	–[a]	3.989	–[a]
hB-1-ring-Fe(II)-B	–[a]	1.961	–[a]	3.820
hB-1noHB1-an-O2′-Fe(II)-O9	1.789	1.735	3.865	3.809
hB-1noHB2-an-O3-Fe(II)-O4	1.815	1.735	3.890	3.817
hB-1noHB1-O2′-Fe(III)-O9	1.900	2.036	3.942	4.088
hB-1noHB2-O3-Fe(III)-O4	1.951	2.145	3.974	4.109
hB-1-ring-Fe(III)-A	–[a]	2.101	–[a]	4.114
hB-1-ring-Fe(III)-B	2.002	–[a]	4.006	–[a]
hB-1noHB1-an-O2′-Fe(III)-O9	2.102	1.987	4.176	4.068
hB-1noHB2-an-O3-Fe(III)-O4	1.982	1.947	4.017	4.089

[a] On optimisation, the calculation fails to reach convergence

The spin density distribution for the homobutein···Fe^{n+} complexes formed with homobutein and bare Fe^{n+} cation are shown in Figure 4.33 and the spin density distributions for the homobutein···Fe^{n+} complexes formed with the deprotonated ligand and the bare Fe^{n+} cation are shown in Figure 4.34. Among the complexes with the neutral homobutein ligand the spin density for the Fe(II) cation is within the 3.865–3.992 range, indicating that there is insignificant changes in the spin density on the Fe^{n+} ion with respect to the isolated Fe(II) cation; the spin density for the complexes with Fe(III) cation has the 3.942–4.176 range. Since spin density change is a measure of the antioxidant ability of the ligand [243], it is reasonable to state that the antioxidant ability of homobutein, in water solution, is more pronounced when homobutein chelates the Fe(III) cation than when it chelates the Fe(II) cation.

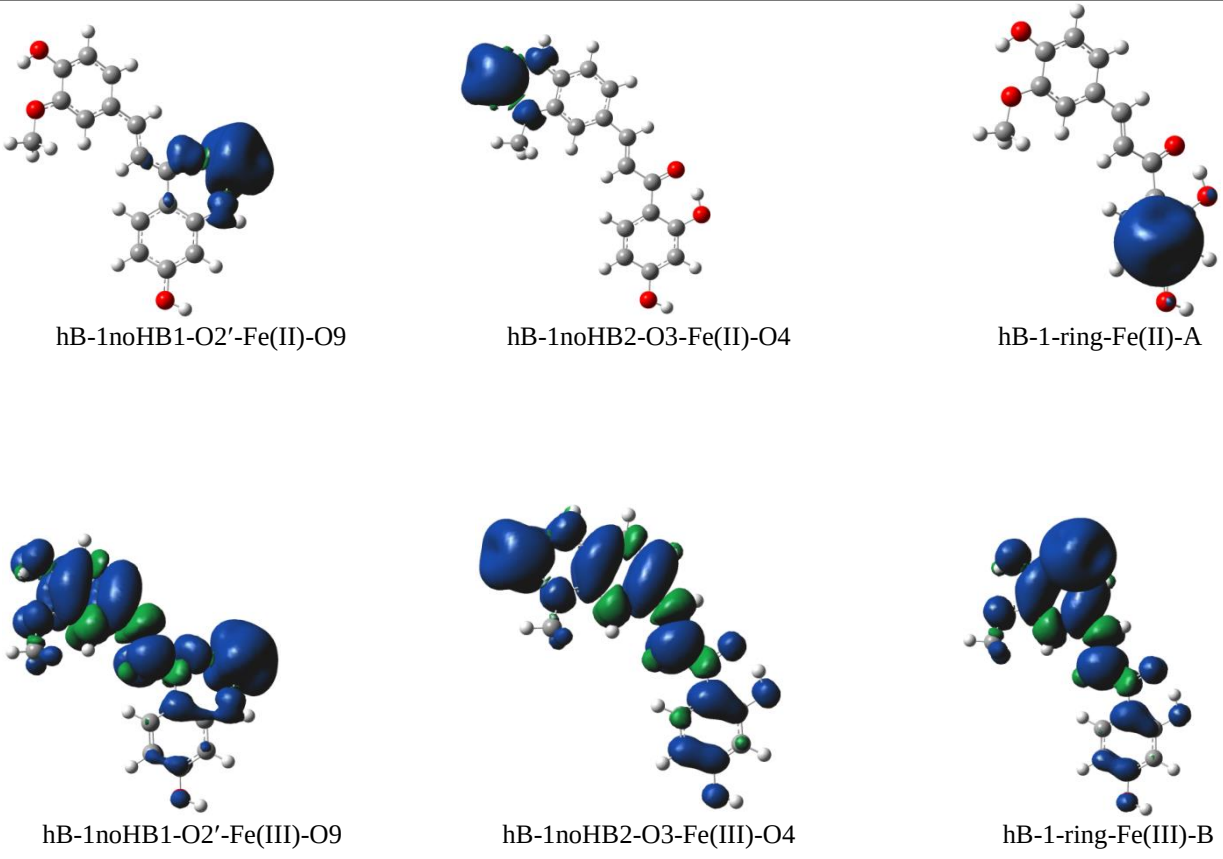

Figure 4.33 Spin density distribution for the homobutein···Fe^{n+} complexes formed from interactions of neutral homobutein and bare Fe^{n+} cations, B3LYP/6-31+G(d,p) results in water solution. The surface isovalue used is 0.0004 au. The blue colour corresponds to positive spin densities and the green colour denotes the negative spin density.

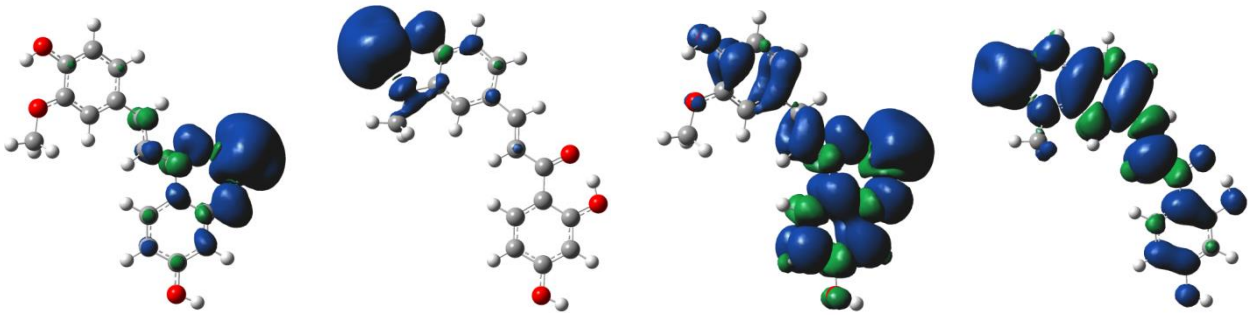

hB-1noHB1-an-O2′-Fe(II)-O9 hB-1noHB2-an-O3-Fe(II)-O4 hB-1noHB1-an-O2′-Fe(III)-O9 hB-1noHB2-an-O3-Fe(III)-O4

Figure 4.34 Spin density distribution for the homobutein···Fe^{n+} complexes formed from interactions of deprotonated homobutein and bare Fe^{n+} cations, B3LYP/6-31+G(d,p) results in water solution. The surface isovalue used is 0.0004 au. The blue colour corresponds to positive spin densities and the green colour denotes the negative spin density.

The orbital occupancies are reported in Table 4.44. Analysis of the 4s orbital suggests that upon complexation homobutein tends to donate electrons to the empty 4s orbital of the cation, for the Fe(II) cation there is minimal transfer with a range of 0.012–0.058 and 0.002–0.056 for the Fe(III) cation. The d_{xy} orbitals shows that for complexes with the Fe(II), the ligand donates electrons from itself to either the ligand or to the other *d* orbitals. The *d* orbitals occupancy suggests that there is a transfer of electrons from the Fe^{n+} cations to the ligand as seen in the d_{xz}, d_{yz}, d_x^2-y^2 and d_z^2 orbitals where there is an increase in the occupancy values of the Fe^{n+} cations before complexation and after complexation. Analysis of the d_{xy} orbital suggests that the Fe^{n+} cations tend to donate electrons from itself to the partially filled *d* orbitals of the homobutein ligand, for both complexes with neutral and deprotonated ligand.

Table 4.44 Natural atomic orbital occupancies for some valence orbitals in the isolated Fe^{n+} cations and in complexes with homobutein results in water solution with different methods

Isolated and Fe complex	Orbitals and the corresponding natural atomic orbital occupancies					
	S (4s)	d_{xy} (3d)	d_{xz} (3d)	d_{yz} (3d)	$d_{x^2-y^2}$ (3d)	d_{z^2} (3d)
Fe(II)	0.000	1.998	1.000	1.000	1.000	1.000
hB-1noHB1-O2′-Fe(II)-O9	0.039	1.053	1.164	1.044	1.771	1.028
hB-1noHB2-O3-Fe(II)-O4	0.029	1.037	1.170	1.056	1.473	1.296
hB-1-ring-Fe(II)-A	0.012	1.700	1.285	1.011	1.002	1.001
hB-1-ring-Fe(II)-B	_[a]	_[a]	_[a]	_[a]	_[a]	_[a]
hB-1noHB1-an-O2′-Fe(II)-O9	0.058	1.185	1.303	1.089	1.08	1.45
hB-1noHB2-an-O3-Fe(II)-O4	0.051	1.313	1.084	1.520	1.139	1.041
Fe(III)	0.000	1.000	1.000	1.000	1.000	1.000
hB-1noHB1-O2′-Fe(III)-O9	0.035	1.656	1.074	1.025	1.234	1.049
hB-1noHB2-O3-Fe(III)-O4	0.017	1.083	1.251	1.028	1.586	1.063
hB-1-ring-Fe(III)-A	_[a]	_[a]	_[a]	_[a]	_[a]	_[a]
hB-1-ring-Fe(III)-B	0.002	1.069	1.207	1.091	1.482	1.140
hB-1noHB1-an-O2′-Fe(III)-O9	0.056	1.360	1.136	1.122	1.091	1.090
hB-1noHB2-an-O3-Fe(III)-O4	0.026	1.192	1.059	1.011	1.068	1.642
DFT/BP86						
Fe(II)	0.000	1.998	1.000	1.000	1.000	1.000
hB-1noHB1-O2′-Fe(II)-O9	0.046	1.717	1.064	1.063	1.217	1.054
hB-1noHB2-O3-Fe(II)-O4	0.031	1.061	1.231	1.056	1.533	1.189
hB-1-ring-Fe(II)-A	_[a]	_[a]	_[a]	_[a]	_[a]	_[a]
hB-1-ring-Fe(II)-B	0.004	1.011	1.015	1.233	1.563	1.199
hB-1noHB1-an-O2′-Fe(II)-O9	0.068	1.401	1.525	1.09	1.224	1.19
hB-1noHB2-an-O3-Fe(II)-O4	0.059	1.158	1.152	1.581	1.202	1.077
Fe(III)	0.000	1.000	1.000	1.000	1.000	1.000
hB-1noHB1-O2′-Fe(III)-O9	0.043	1.309	1.084	1.078	1.298	1.125
hB-1noHB2-O3-Fe(III)-O4	0.026	1.013	1.3	1.416	1.055	1.024
hB-1-ring-Fe(III)-A	0.004	1.272	1.397	1.011	1.105	1.1
hB-1-ring-Fe(III)-B	_[a]	_[a]	_[a]	_[a]	_[a]	_[a]
hB-1noHB1-an-O2′-Fe(III)-O9	0.071	1.324	1.231	1.109	1.116	1.155
hB-1noHB2-an-O3-Fe(III)-O4	0.047	1.114	1.095	1.05	1.133	1.508

[a] On optimisation the calculation fails to converge

In summary, the results of the study on butein and homobutein suggests that both compounds are able to bind Fe^{n+} cations *in vacuo* and in water solution In water solution the relative energies as well as the binding energies are significantly dampened indicating that interactions in water solution are weaker than interactions *in vacuo*. Complexes with the hdyration in the coordinated sphere have higher binding energy than complexes without hydration in the coordiated sphere.

4.4. Comparison of the performance of the calculation methods

The section provides a comparison of the result obtained using the DFT/B3LYP method and the results obtained using the DFT/BP86 method, the two methods utilised throughout the study. A comparison of the relative energy trend across the conformers of the different species (e.g., neutral and deprotonated species of butein and homobutein) is the same for both methods, however, the magnitude of the relative energy values suggest that the energy values obtained using the DFT/B3LYP method are found to be lower than those obtained for the DFT/BP86 method.

Analysis of the binding energy (ΔE′binding, kcal/mol) values suggests that *in vacuo* the values obtained using the DFT/BP86 method tend to be overestimated with respect to the values obtained using the DFT/B3LYP method; this results is true for all complexes *in vacuo* and in water solution. The tendency for the overestimation of the binding energies between the ligand and the metal ions by the DFT/BP86 method may be related to the fact that pure functions tends to overestimate the binding energies of complexes [244, 245] with respect to hybrid functions such as B3LYP.

The result on the charges and the spin density values shows that the is no specific trend to be identified in that in some complexes the DFT/B3LYP method shows the greatest reduction in charge while for some complexes the DFT/BP86 shows the greatest reduction in charge for both Fe(II) and Fe(III) complexes *in vacuo* and in water solution.

CHAPTER 5

RESULTS AND DISCUSSION: ANTIOXIDANT PROPERTIES OF KANAKUGIOL AND PEDICELLIN

5.1. Introduction

This chapter provides results and discussions on the antioxidant property of kanakugiol and pedicellin through their Fe chelation ability. The results *in vacuo* are reported first followed by the results in water solution. The results reported in this chapter follow a similar pattern as that presented in chapter 4, namely, first the results on the isolated molecules are presented followed by the results on the ligand-Fe complexes. The naming for the conformers of kanakugiol and pedicellin is such that the letters K and P are utilised to denote kanakugiol and pedicellin respectively, followed by the Arabic number to indicate the different conformers. For instance, K-1 and P-1 represent the lowest-energy conformer of kanakugiol and pedicellin respectively. The same pattern utilised for the neutral species is adopted for the deprotonated species of kanakugiol, however, the acronym "an" is used to indicate deprotonation and an Arabic number is given in increasing order to indicate the different conformers.

The naming of the complexes is such that the name of the conformer from which it was obtained is given first followed by an acronym indicating the atoms or group at which the Fe^{n+} ion is coordinated on the ligand and the oxidation state of the Fe^{n+} cation is indicated in round brackets. For instance, the naming in the K-1-O2′-Fe(II)-O3′ complex implies that the conformer K-1 was used in preparation of this complex and that the Fe^{n+} cation of oxidation state +2 is coordinated at the O2′ and O3′ reactive site.

As was done in Chapter 4, all bond lengths, charges, spin densities and electron density properties reported in the text are obtained from DFT/B3LYP calculation results with the 6-31+G(d,p) basis set unless indicated otherwise and all the energies values reported in the text are those obtained using the B3LYP/6-311+G(2d,p)//B3LYP/6-31+G(d,p) calculation method.

5.2. Results *in vacuo*

5.2.1. Conformational stability and geometries for kanakugiol conformers

The optimised conformers of neutral kanakugiol are shown in Figure 5.1 and the corresponding relative energy values (ΔE, kcal/mol) are reported in Table 5.1. The stability of the conformers can be related to the orientation of the 2-propen-1-one aliphatic chain, orientation of the methoxy groups and the number of intramolecular hydrogen bonds present in the conformer. Non-bent orientation of the aliphatic chain is preferred over the bent orientation, for instance, the ΔE gap between a conformer with a non-bent orientation of the aliphatic chain (K-1) and a corresponding conformer with a bent orientation of the aliphatic chain (K-4) is 4.415 kcal/mol. The preferred orientation of the methoxy groups is one in which the steric effects between neighbouring methyl groups is minimised. For instance, the ΔE gap between K-1 and K-3, which differs due to the orientation of the methoxy groups, is 2.864 kcal/mol. Finally, conformers with the high number of intramolecular hydrogen bonds are preferred to conformers with fewer intramolecular hydrogen bonds. Kanakugiol can form two types of intramolecular hydrogen bonds, the O–H···O and the C–H···O. The lowest-energy conformer for kanakugiol (K-1) is one the number of intramolecular hydrogen bonds is maximised, the 2-propen-1-one aliphatic chain has a non-bent arrangement and the steric effects between methyl groups on neighbouring methoxy groups is minimised.

The first three lowest-energy conformers have the same number of intramolecular hydrogen bonds and have non-bent arrangement of the aliphatic chain; the only difference among them is the arrangement of the methoxy groups. The implication of this result is that the steric effects, due to the arrangement of the methoxy groups, may results in an energy difference of 2–3 kcal/mol. Upon removal of the first intramolecular hydrogen bond, the energy increases beyond 5 kcal/mol, indicating that conformers that do not have the first intramolecular hydrogen bond may not exist *in vacuo* (that in line with the Boltzmann's conformational distribution).

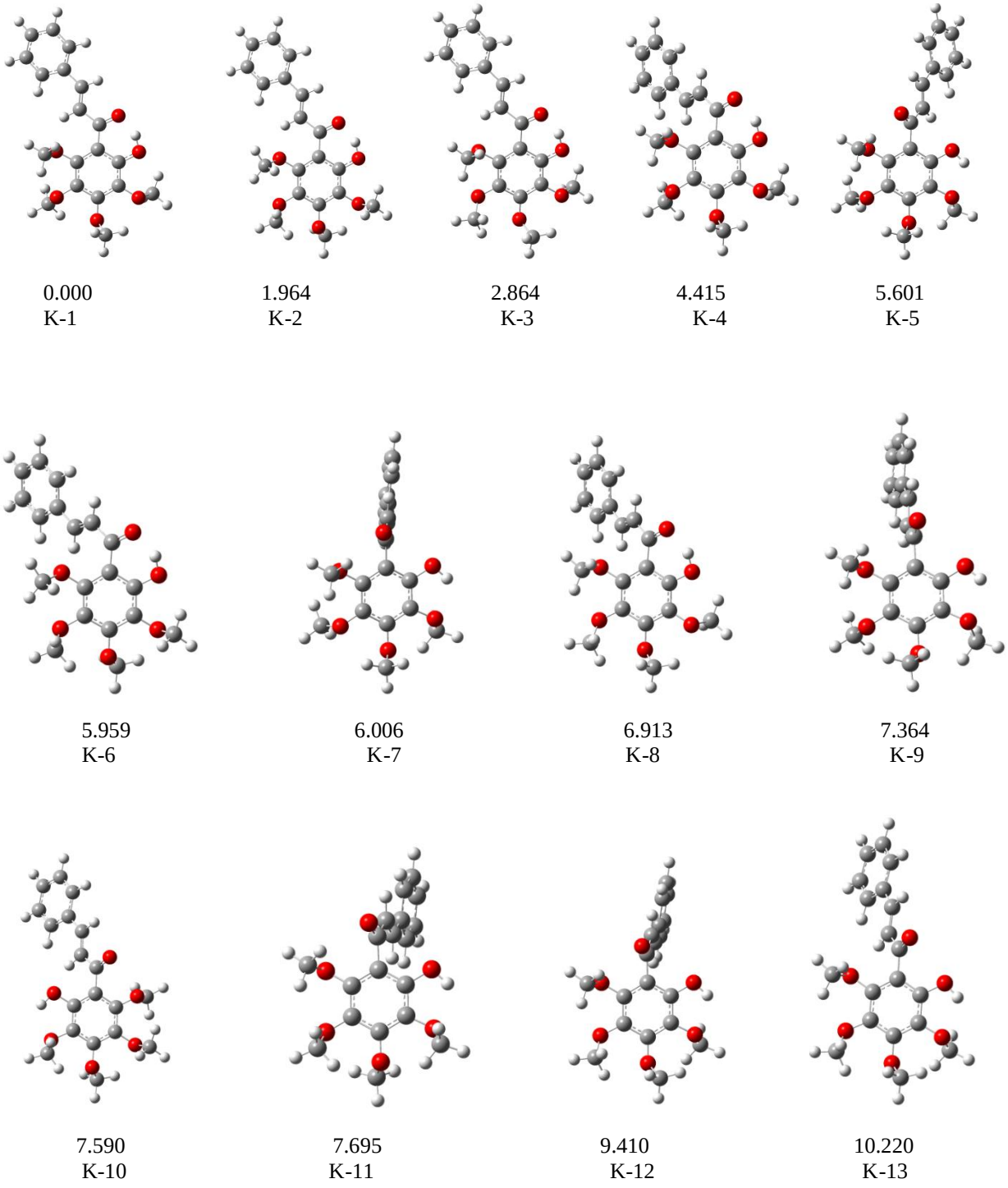

Figure 5.1 B3LYP/6-31+G(d,p) optimised conformers for the neutral kanakugiol arranged in order of increasing relative energy (ΔE, kcal/mol), B3LYP/6-311+G(d,p)// B3LYP/6-31+G(d,p) results *in vacuo*.

Table 5.1 *In vacuo* relative energy values (ΔE, kcal/mol) for neutral kanakugiol conformers

Conformer	*A*[a]		*B*[b]	
	total energy (Hartree)	ΔE (kcal/mol)	total energy (Hartree)	ΔE (kcal/mol)
DFT/B3LYP results				
K-1	-1187.4053702	0.000	-1187.6941259	0.000
K-2	-1187.4024491	1.833	-1187.6909961	1.964
K-3	-1187.4008093	2.862	-1187.6895620	2.864
K-4	-1187.3978526	4.717	-1187.6870906	4.415
K-5	-1187.3958659	5.964	-1187.6852000	5.601
K-6	-1187.3950008	6.507	-1187.6846293	5.959
K-7	-1187.3954970	6.196	-1187.6845545	6.006
K-8	-1187.3938681	7.218	-1187.6831088	6.913
K-9	-1187.3928839	7.835	-1187.6823913	7.364
K-10	-1187.3923900	8.145	-1187.6820297	7.590
K-11	-1187.3879670	10.921	-1187.6818628	7.695
K-12	-1187.3921102	8.321	-1187.6791298	9.410
K-13	-1187.3892587	10.110	-1187.6778400	10.220
DFT/BP86 results				
K-1	-1187.3979923	0.000	-1187.6893257	0.000
K-2	-1187.3957707	1.394	-1187.6869374	1.499
K-3	-1187.3942605	2.342	-1187.6856625	2.299
K-4	-1187.3900831	4.963	-1187.6818524	4.690
K-7	-1187.3884863	5.965	-1187.6801860	5.735
K-8	-1187.3869160	6.951	-1187.6788032	6.603
K-5	-1187.3846466	8.375	-1187.6766978	7.924
K-6	-1187.3836310	9.012	-1187.6758850	8.434
K-9	-1187.3821254	9.957	-1187.6743574	9.393
K-10	-1187.3816150	10.277	-1187.6738553	9.708
K-12	-1187.3809489	10.695	-1187.6733905	9.999
K-13	-1187.3786294	12.150	-1187.6710970	11.440
K-11	-1187.3778200	12.658	-1187.6702531	11.970

[a] Results obtained using the B3LYP/6-31+G(d,p) method

[b] Single point results obtained using the B3LYP/6-311+G(2d,p) method, starting from optimised geometries

5.2.2. Relative stability and binding energies for kanakugiol···Fe^{n+} complexes formed from neutral kanakugiol and Fe^{n+} cations

The optimised complexes of kanakugiol···Fe^{n+} complexes are shown in Figure 5.2 for the DFT/B3LYP results and Figure 5.3 for the DFT/BP86 results; the corresponding ΔE values (kcal/mol) are reported in Table 5.2. Among the complexes of kanakugiol with the Fe^{2+} cation, the lowest-energy complex corresponds to the coordination of the Fe^{n+} cation at the hydroxyl–methoxy site. The geometry of the ligand in the complex suggests significant conformational changes in the arrangement of the methoxy groups at C4′ and C3′. For instance (considering DFT/B3LYP results), the torsion angle of the C atom of the methoxy groups at C4′ and C3′ are 69° and −70° respectively in the isolated K-1 conformer while in the K-1-O2′-Fe(II)-O3′ complex, the two C atoms have torsion angle values of 159° and −121° respectively.

Another significant geometrical change that is observed between K-1 and the complexed K-1 is the presence of proton transfer from O2′ to O9 in the complexed K-1; the O2′–H2′ bond distance in the complex is 1.642 Å, which indicates that H2′ atom is no longer bonded to O2′; O9···H2′ bond distance is 0.983Å, which is within the O9–H2′ van der Waal bond distance. These bond distance changes indicate a complete transfer of the proton from O2′ to O9. The implication for the observed changes is the loss of aromaticity for ring A in the complex. The bond distances for the O2′···Fe^{2+} and O3′···Fe^{2+} interactions have values of 1.881 Å and 2.046 Å respectively. The effective partial atomic charge plays crucial role in assessing the chemical bonding between Fe^{2+} ion and the O atoms it interacts. The calculated effective charges (obtained from natural population analysis scheme) for Fe, O2′ and O3′ in K-1-O2′-Fe(II)-O3′ are 1.334 *e*, –0.799 *e* and –0.634 *e* respectively, what suggests significant deviations from the formal oxidation states of +2 for Fe and –2 for O atoms. These deviations are indicative of a partially covalent character of the Fe–O bonds in K-1-O2′-Fe(II)-O3′ complex. The $4s^{0.11}4p^{0.05}3d^{6.50}$ orbital occupancy of the valence shells for iron suggests that this covalent character is spread between the three orbitals.

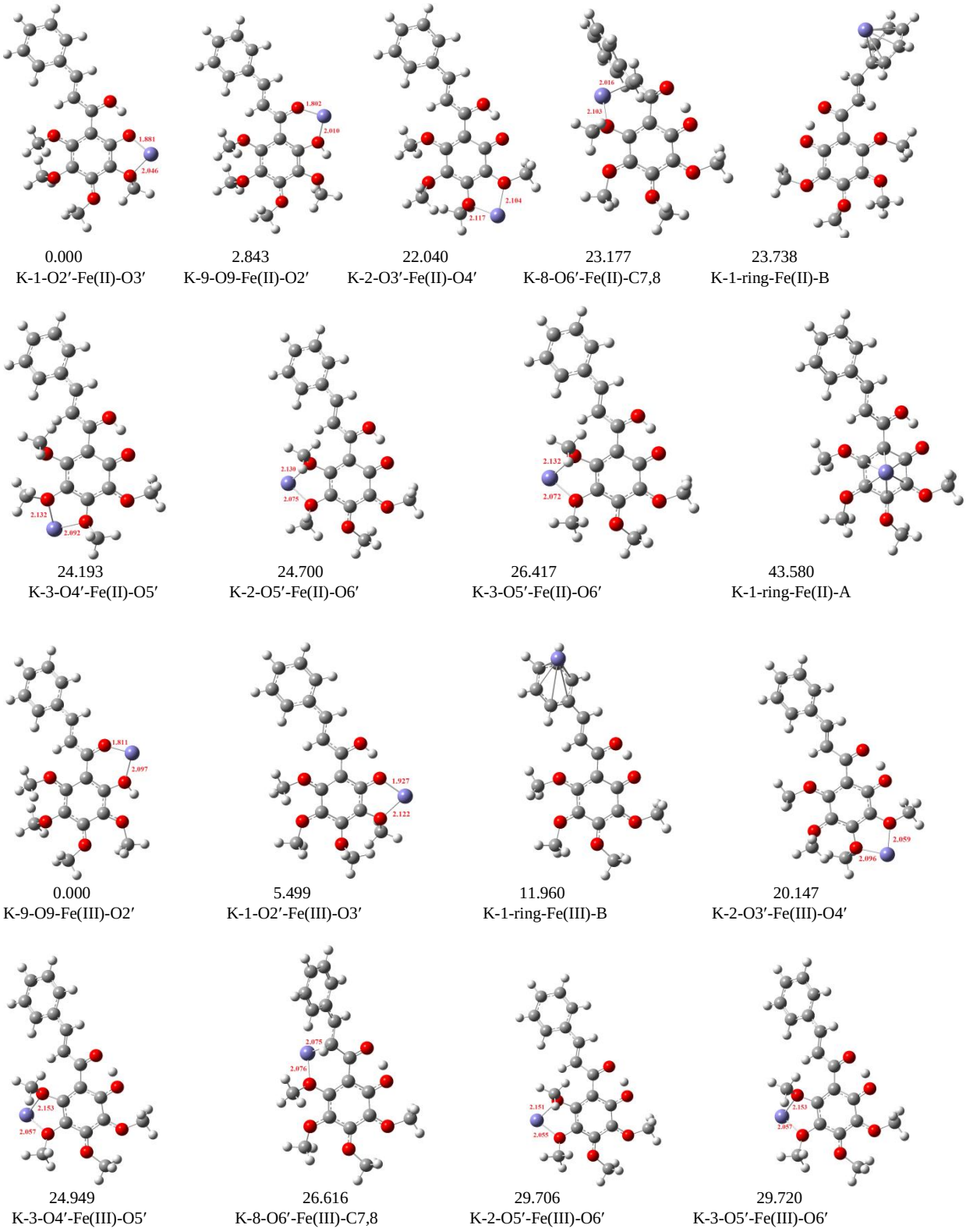

Figure 5.2 B3LYP/6-31+G(d,p) optimised kanakugiol···Fe^{n+} complexes (arranged in order of increasing relative energy (ΔE, kcal/mol)) formed from neutral kanakugiol and Fe^{n+} cations. B3LYP/6-311+G(2d,p)//B3LYP/6-31+G(d,p) results *in vacuo*. The bond length between the cation and the ligand is reported in Å.

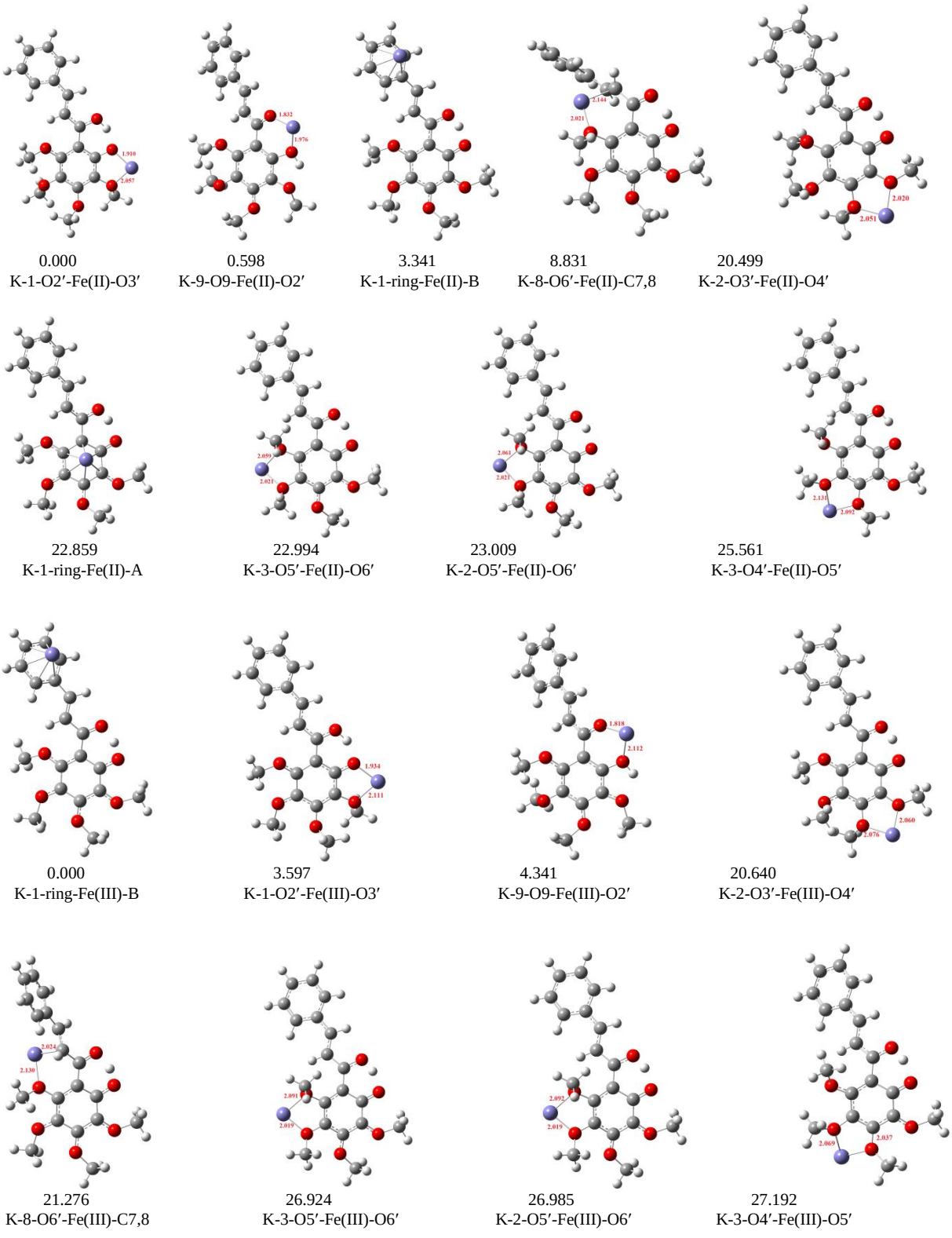

Figure 5.3 BP86/6-31+G(d,p) optimised kanakugiol···Fe^{n+} complexes (arranged in order of increasing relative energy (ΔE, kcal/mol)) formed from neutral kanakugiol and Fe^{n+} cations. BP86/6-311+G(2d,p)//BP86/6-31+G(d,p) results *in vacuo*. The bond length between the cation and the ligand is reported in Å.

Table 5.2 *In vacuo* relative energy (ΔE, kcal/mol) for kanakugiol···Fe^{n+} complexes formed from neutral kanakugiol and Fe^{n+} cations

Complex	*A*[a]		*B*[B]	
	total energy (Hartree)	ΔE (kcal/mol)	total energy (Hartree)	ΔE (kcal/mol)
DFT/B3LYP results				
K-1-O2′-Fe(II)-O3′[c]	-1310.2626801	0.000	-2450.8423844	0.000
K-3-O2′-Fe(II)-O3′[c]	–[c]	–[c]	–[c]	–[c]
K-9-O9-Fe(II)-O2'	-1310.2560058	4.188	-2450.8378532	2.843
K-2-O3′-Fe(II)-O4′	-1310.2334788	18.324	-2450.8072620	22.040
K-8-O6′-Fe(II)-C7,8	-1310.2279424	21.798	-2450.8054495	23.177
K-1-ring-Fe(II)-B	-1310.2419461	13.011	-2450.8045547	23.738
K-3-O4′-Fe(II)-O5′	-1310.2310190	19.868	-2450.8038296	24.193
K-2-O5′-Fe(II)-O6′	-1310.2287932	21.264	-2450.8030222	24.700
K-3-O5′-Fe(II)-O6′	-1310.2288317	21.240	-2450.8002866	26.417
K-1-ring-Fe(II)-A	-1310.2076487	34.533	-2450.7729345	43.580
K-9-O9-Fe(III)-O2′	-1309.7854768	0.000	-2450.3650325	0.000
K-1-O2′-Fe(III)-O3′[c]	-1309.7831798	1.441	-2450.3562695	5.499
K-3-O2′-Fe(III)-O3′[c]	–[c]	–[c]	–[c]	–[c]
K-1-ring-Fe(III)-B	-1309.7725631	8.104	-2450.3459730	11.960
K-2-O3′-Fe(III)-O4′	-1309.7592485	16.458	-2450.3329258	20.147
K-3-O4′-Fe(III)-O5′	-1309.7511529	21.539	-2450.3252254	24.979
K-8-O6′-Fe(III)-C7,8	-1309.7461185	24.698	-2450.3226174	26.616
K-2-O5′-Fe(III)-O6′	-1309.7443482	25.809	-2450.3176927	29.706
K-3-O5′-Fe(III)-O6′	-1309.7443449	25.811	-2450.3176699	29.720
K-1-ring-Fe(III)-A	–[d]	–[d]	–[d]	–[d]
DFT/BP86 results				
K-1-O2′-Fe(II)-O3′[c]	-1310.3277621	0.000	-2451.0024790	0.000
K-3-O2′-Fe(II)-O3′[c]	–[c]	–[c]	–[c]	–[c]
K-9-O9-Fe(II)-O2'	-1310.3189842	5.5082	-2450.9962020	0.598
K-1-ring-Fe(II)-B	-1310.3168430	6.8518	-2450.9971556	3.341
K-8-O6′-Fe(II)-C7,8	-1310.3096444	11.369	-2450.9884059	8.831
K-2-O3′-Fe(II)-O4′	-1310.2985519	18.330	-2450.9698119	20.499
K-1-ring-Fe(II)-A	-1310.2878001	25.077	-2450.9660503	22.859
K-3-O5′-Fe(II)-O6′	-1310.2942728	21.015	-2450.9658350	22.994
K-2-O5′-Fe(II)-O6′	-1310.2943611	20.959	-2450.9658113	23.009
K-3-O4′-Fe(II)-O5′	-1310.2310245	60.704	-2450.9617453	25.561
K-1-ring-Fe(III)-B	-1309.8497685	1.075	-2450.5296394	0.000
K-1-O2′-Fe(III)-O3′[c]	-1309.8514810	0.000	-2450.5239078	3.597
K-3-O2′-Fe(III)-O3′[c]	–[c]	–[c]	–[c]	–[c]
K-9-O9-Fe(III)-O2′	-1309.8479056	2.244	-2450.5227222	4.341
K-2-O3′-Fe(III)-O4′	-1309.8271126	15.291	-2450.4967475	20.640
K-8-O6′-Fe(III)-C7,8	-1309.8222504	18.342	-2450.4957345	21.276
K-3-O5′-Fe(III)-O6′	-1309.8162154	22.129	-2450.4867340	26.924
K-3-O4′-Fe(III)-O5′	-1309.8217658	18.648	-2450.4863066	27.192
K-2-O5′-Fe(III)-O6′	-1309.8161628	22.162	-2450.4867801	26.985
K-1-ring-Fe(III)-A	–[d]	–[d]	–[d]	–[d]

[a] Results obtained using the 6-31+G(d,p) basis set

[b] Results obtained using the 6-311+G(2d,p) basis set, starting from optimised geometries

[c] After optimisation, the two complexes have the same energy

[d] On optimisation, the Fe(III) ion drifts away from the aromatic ring and binds between O6′ and C7=C8 region

In the second lowest-energy complex (K-9-O9-Fe(II)-O2'), the Fe^{n+} ion is coordinated on the hydroxyl–*keto* reactive site; the energy gap between this complex and the lowest-energy complex is 2.844 kcal/mol. This complex also shows significant geometry changes in the conformation of K-1-noHB1 between the isolated case and the complexed case; the changes are associated with the arrangement of the methyl group at O3′ (it has torsion angle of 67° in the isolated molecule and 53° in the complex), at O4′ (it has torsion angle of 110° in the isolated molecule and 160° in the complex) as well as the arrangement of the *keto* O9 (it has torsion angle of 100° in the isolated molecule and 156° in the complex). Further comparisons of the geometries of the two complexes are limited by the fact that K-1-O2′-Fe(II)-O3′ has further geometric changes associated with the proton transfer process. The bond distances in K-1-noHB1-O9-Fe(II)-O2' for the O2′···Fe^{2+} and O9···Fe^{2+} interactions have values of 2.010 Å and 1.802 Å respectively.

Complexes in which the Fe(II) ion is coordinated simultaneously at the methoxy–methoxy site, on the aromatic ring (both ring A and ring B) and simultaneously on O6′ and the C7=C8 double bond in the aliphatic chain have very high ΔE values (22.040–43.580 kcal/mol) that they may be considered to not exist *in vivo*. The most characterising features of these geometries (with the exception of K-8-O6′-Fe(II)-C7,8 and K-1-ring-Fe(II)-B) is the existence of a proton transfer from O2′ to O9 in the geometry of the ligand.

Among the kanakugiol···Fe^{3+} complexes, the preferred one corresponds to the situation in which the cation is bidentated at the hydroxyl–*keto* site (between O9 and O2′). The energy gap between K-9-O9-Fe(III)-O2′ and the second lowest-energy complex (K-1-O2′-Fe(III)-O3′) is about 5.499kcal/mol. The geometric parameters between the ligand and the Fe(III) ion show some interesting trend; the O2′···Fe and the O9···Fe bond distances in K-9-O9-Fe(III)-O2′ have values of 2.097 Å and 1.811 Å respectively; the O2′···Fe and the O3′···Fe bond distances (Å) in K-2-O2′-Fe(III)-O3′ have values of 1.927 Å and 2.122 Å respectively. These results suggest that coordination of the Fe(III) cation to kanakugiol results in longer bond distances than Fe(II). Other significant geometric changes involve specifically the ligand. For instance, upon formation of the complex, internal proton transfer is observed for situations in which the metal ion is bidentated at the methoxy–methoxy sites as well as at the methoxy–α,β unsaturated site. The arrangement of some of the methoxy groups as well as the keto group changes significantly between the optimised kanakugiol and the kanakugiol structure in the complexes, for instance, a

comparison of the torsion angle of O9 in K-9 (100.4°) and in K-9-O9-Fe(III)-O2′ (151.3°), the lowest-energy complex suggests a distortion of ≈51°; a comparison of the torsion angle of the C atom of the methoxy group at C4′ in the isolated conformer (K-9) and in the complex (K-9-O9-Fe(III)-O2′) shows a distortion of 55°. Complexes in which the Fe^{3+} ion is coordinated at the methoxy–methoxy sites, on the aromatic ring (both ring A and ring B) and at the methoxy–α,β unsaturated site have high relative energy values (above 5 kcal/mol), suggesting that they may not exist *in vacuo*.

The binding energy ($\Delta E'_{binding}$, kcal/mol) values are reported in Table 5.3. Among the complexes of neutral kanakugiol with Fe(II) ion, it is observed that the arrangement of the Fe^{n+} ion in the hydroxyl–*keto* site and in the hydroxyl–methoxy region results in the highest MIA. The least MIA corresponds to the coordination of the Fe^{n+} ion on the aromatic ring A (230.021 kcal/mol). These results suggest that the binding energy difference for either of the lowest-energy complexes (hydroxyl–*keto* site and the hydroxyl–methoxy site) and the complexes in which the Fe^{n+} ion binds to the methoxy–methoxy site, aromatic ring or methoxy–α,β unsaturated site is greater than 20 kcal/mol. A comparison of the MIA values for kanakugiol with Fe(II) and those of kanakugiol with Cu(II) and Co(II) cations [230] shows that the trend in the binding energies is such that $Cu^{2+} > Co^{2+} > Fe^{2+}$. This trend is in agreement with the Irving William series [246].

Table 5.3 Binding energy ($\Delta E'_{binding}$, kcal/mol) values for kanakugiol···Fe^{n+} complexes formed from neutral kanakugiol and Fe^{n+} cations *in vacuo*. The complexes are arranged in order of decreasing $\Delta E'_{binding}$ values

Complex	*A*[a]			*B*[B]		
	$\Delta E_{inter,}$ kcal/mol	ΔE_{def} kcal/mol	$\Delta E'_{binding,}$ kcal/mol	$\Delta E_{inter,}$ kcal/mol	ΔE_{def} kcal/mol	$\Delta E'_{binding,}$ kcal/mol
DFT/B3LYP results						
K-9-O9-Fe(II)-O2'	–239.794	22.006	261.800	–254.072	23.430	277.502
K-1-O2′-Fe(II)-O3′[c]	–236.147	26.171	262.318	–249.552	26.836	276.388
K-3-O2′-Fe(II)-O3′[c]	–[c]	–[c]	–[c]	–[c]	–[c]	–[c]
K-8-O6′-Fe(II)-C7,8	–221.566	22.319	243.885	–233.298	23.238	256.536
K-2-O3′-Fe(II)-O4′	–219.655	20.249	239.904	–229.477	20.563	250.040
K-2-O5′-Fe(II)-O6′	–216.715	11.048	227.763	–226.816	22.370	249.186
K-3-O5′-Fe(II)-O6′	–217.768	21.724	239.492	–226.000	21.876	247.876
K-1-ring-Fe(II)-B	–223.136	19.474	242.610	–225.814	20.793	246.607
K-3-O4′-Fe(II)-O5′	–219.141	23.449	242.590	–228.223	9.552	237.775
K-1-ring-Fe(II)-A	–201.614	29.300	230.914	–205.972	24.049	230.021
K-9-O9-Fe(III)-O2′	–687.120	33.672	720.792	–685.510	47.934	733.444
K-1-ring-Fe(III)-B	–671.181	37.030	708.211	–666.187	38.317	704.504
K-8-O6′-Fe(III)-C7,8	–661.805	31.504	693.309	–658.444	32.914	691.358
K-1-O2′-Fe(III)-O3′[c]	–677.843	37.915	715.758	–672.648	14.091	686.739
K-3-O2′-Fe(III)-O3′[c]	–[c]	–[c]	–[c]	–[c]	–[c]	–[c]
K-2-O3′-Fe(III)-O4′	–664.659	17.388	682.047	–659.964	18.010	677.974
K-3-O4′-Fe(III)-O5′	–660.608	19.415	680.023	–656.031	20.027	676.058
K-2-O5′-Fe(III)-O6′	–655.309	21.161	676.470	–650.405	21.746	672.151
K-3-O5′-Fe(III)-O6′	–656.336	20.101	676.437	–651.290	20.815	672.105
K-1-ring-Fe(III)-A	–[d]	–[d]	–[d]	–[d]	–[d]	–[d]
DFT/BP86 results						
K-9-O9-Fe(II)-O2′	–259.428	17.536	276.964	–276.081	18.854	294.935
K-1-O2′-Fe(II)-O3′[c]	–254.980	20.727	275.707	–270.628	21.217	291.845
K-3-O2′-Fe(II)-O3′[c]	–[c]	–[c]	–[c]	–[c]	–[c]	–[c]
K-8-O6′-Fe(II)-C7,8	–250.561	21.259	271.820	–268.399	22.119	290.518
K-1-ring-Fe(II)-B	–248.128	19.050	267.178	–267.287	20.206	287.493
K-1-ring-Fe(II)-A	–229.903	24.735	254.638	–247.768	25.622	273.390
K-3-O4′-Fe(II)-O5′	–196.618	20.406	217.024	–247.366	18.879	266.245
K-3-O5′-Fe(II)-O6′	–236.307	15.094	251.401	–249.932	15.173	265.132
K-2-O5′-Fe(II)-O6′	–235.414	16.086	251.500	–249.117	16.015	265.105
K-2-O3′-Fe(II)-O4′	–238.044	12.703	250.747	–251.627	12.794	264.421
K-9-O9-Fe(III)-O2′	–712.296	26.868	739.164	–713.591	28.320	741.911
K-1-ring-Fe(III)-B	–703.508	26.291	729.799	–708.539	29.095	782.634
K-1-O2′-Fe(III)-O3′[c]	–704.583	30.122	734.705	–704.942	30.981	735.923
K-3-O2′-Fe(III)-O3′[c]	–[c]	–[c]	–[c]	–[c]	–[c]	–[c]
K-8-O6′-Fe(III)-C7,8	–693.191	23.241	716.432	–693.866	24.372	718.238
K-2-O3′-Fe(III)-O4′	–690.686	19.836	710.522	–689.397	20.306	709.703
K-3-O4′-Fe(III)-O5′	–688.278	23.885	712.163	–683.646	21.846	705.492
K-2-O5′-Fe(III)-O6′	–683.815	21.987	705.802	–683.143	22.180	705.323
K-3-O5′-Fe(III)-O6′	–684.795	20.954	705.749	–683.914	21.298	705.212
K-1-ring-Fe(III)-A	–[d]	–[d]	–[d]	–[d]	–[d]	–[d]

[a] Results obtained using the 6-31+G(d,p) basis set

[b] Results obtained using the 6-311+G(2d,p) basis set, starting from optimised geometries

[c] After optimisation, the two complexes have the same energy

[d] On optimisation, the Fe(III) ion drifts away from the aromatic ring and binds between O6′ and C7=C8 region

Among the complexes of neutral kanakugiol···Fe^{3+}, the highest MIA corresponds to the situation in which the Fe^{n+} ion binds to the hydroxy–*keto* reactive site (733.444 kcal/mol). Therefore for both kanakugiol···Fe^{2+} and kanakugiol···Fe^{3+}, the strongest interaction site between kanakugiol and the Fe^{n+} ion is the hydroxyl–*keto* reactive site. The preference for the hydroxyl–*keto* binding site has also been reported for other polyphenol derivatives such as flavonoids [55, 113, 247]. The cation···π interactions (for the interaction between the Fe^{n+} ion and ring B) has the second highest MIA (704.504 kcal/mol); this is significantly different from the trend observed for the Fe(II) complexes were the methoxy–methoxy reactive site has higher MIA than the cation···π interactions. The MIA difference for the hydroxyl–*keto* reactive site and the aromatic ring B site is nearly 30 kcal/mol, what suggests that hydroxyl–*keto* reactive site may be the only interaction site between the ligand and the metal ions. With the kanakugiol···Fe^{3+} complexes, the methoxy–methoxy site corresponds to the weakest binding energy (672.1–678 kcal/mol). However because the MIA in all the cases are largely positive, it is reasonable to infer that *in vacuo*, kanakugiol can strongly bind both Fe(II) and Fe(III) ions. Since the *vacuum* medium is used in this study to represent the most ideal non-polar media (where the dielectric constant, ε = 1), it is possible to infer that the interaction between kanakugiol and the Fe^{n+} ions would represent strong interaction in non-polar media. The MIA results also suggest that kanakugiol binds Fe(III) much stronger than it binds Fe(II), a result that has also been reported for other chalcone derivatives [248].

5.2.3. Binding energies for the kanakugiol···Fe^{n+} complexes formed from deprotonated kanakugiol and Fe^{n+} cations

A study on the interaction between Fe^{n+} cations and deprotonated kanakugiol was performed because experimental findings have shown that in biological systems, polyphenol derivatives may deprotonated under neutral or acidic solution [249]. There is only one possible site for deprotonation for kanakugiol (i.e., the H atom of the O2′∪H2′ hydroxyl group). After deprotonation, the Fe^{n+} cation can be coordinated at all possible reactive sites on the deprotonated kanakugiol molecule. However, for the purpose of this work, the Fe^{n+} cation has been coordinated only at the deprotonated reactive site (i.e., the O2′∪O9 site, after the removal of the H2′ proton). The optimised kanakugiol···Fe^{n+} complexes formed from deprotonated kanakugiol ligand and Fe^{n+} cations are shown in Figure 5.4. The MIA (kcal/mol) corresponding to the interaction between the Fe(II) and the Fe(III) with the deprotonated kanakugiol is 464.903 and 989.792 respectively.

Therefore, in comparison with the neutral species, the deprotonated kanakugiol has higher MIA than the neutral molecule. The implication for this is that, under physiological conditions, deprotonated kanakugiol has greater tendency to chelate free metal ions than neutral kanakugiol. This result is in agreement with the experimental findings that deprotonated polyphenol derivatives give rise to particular large metal-binding stability constants with Fe(III) than with Fe(II) [55, 250]. Another implication of this result is that since deprotonated kanakugiol have higher binding energies, they are likely to exhibit greater antioxidant properties than neutral kanakugiol.

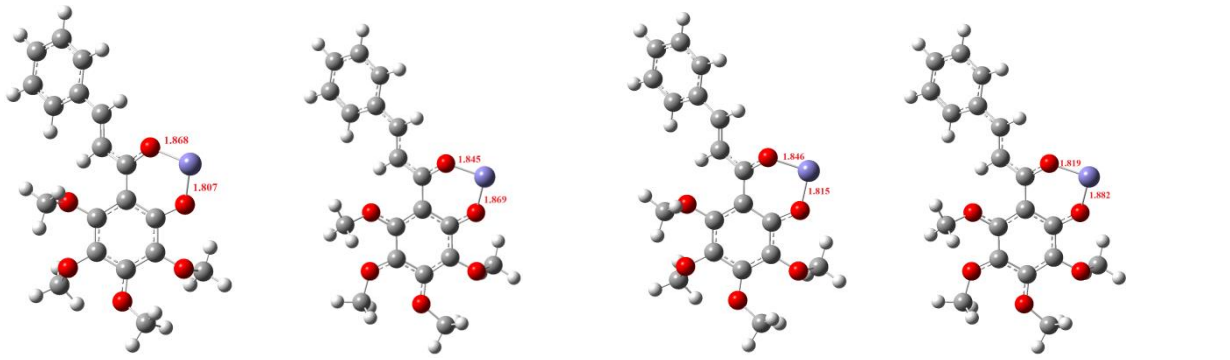

464.903	989.792	480.642	1 001.063
K-1-an-O2′-Fe(II)-O9	K-1-an-O2′-Fe(III)-O9	K-1-an-O2′-Fe(II)-O9	K-1-an-O2′-Fe(III)-O9

Figure 5.4 Optimised kanakugiol···Fe^{n+} complexes formed from deprotonated kanakugiol and Fe^{n+} cations. The first two structures were obtained using the DFT/B3LYP method and the last two structures were obtained using the DFT/BP86 method. The interaction energies reported below each structure were obtained from single point calculations using the 6-311+G(2d,p) basis set starting from the optimised geometries. The bond length between the cation and the ligand is reported in Å.

5.2.4. AIM analysis of the bonding within the kanakugiol···Fe complexes

The results obtained for the study of the bond critical properties of the electron density distribution $\rho(\mathbf{r})$, its Laplacian $\nabla^2\rho$ (r) are reported in Table 5.4 for the DFT/B3LYP results and Table 5.5 for the DFT/BP86 results. Among the complexes of kanakugiol with the Fe(II) cation the strongest bond corresponds to the O9···Fe^{2+} bond in the K-9-O9-Fe(II)-O2′ complex with ρ value of 0.136 e/Å^3. The methoxy–methoxy sites have a range of 0.055–0.065 e/Å^3 for the values of ρ while the weakest bond corresponds to C4′···Fe^{2+} bond with ρ value of 0.039 e/Å^3. These results are in agreement with the results obtained for the binding energies, where the preferred binding site is the hydroxyl–*keto* reactive site and the least preferred site for the coordination of the Fe(II) cation is the π system of aromatic ring A.

Among the complexes of neutral kanakugiol with the Fe(III) cation the largest ρ value (i.e., 0.670 e/Å^3) corresponds to the O3···Fe^{3+} bond in K-2-O3′-Fe(III)-O4′. The range of ρ among the complexes with Fe(III) is 0.055–0.068 e/Å^3. For the complexes with the deprotonated kanakugiol and either Fe(II) or Fe(III) cation the O9···Fe^{n+} bond is stronger than the O2′···Fe^{n+} bond, the ρ values are 0.140 for Fe(II) cation and 0.125 for Fe(III) cation.

Analysis of the $\nabla^2\rho$ (e/Å^5) of the electron density shows that for complexes with either neutral or deprotonated kanakugiol ligand all values are less than 1 and are positive, which is indicative of dative interactions. This is further supported by the values of *H* and the |V|/G ratio; the values of *H* are inclined more towards zero, and the |V|/G ratio values have a 1.0–1.5 range, what is indicative that the interactions are dative in nature.

Table 5.4 Bond critical point data for the kanakugiol···Fe^{n+} complexes, UB3LYP/6-31+G(d,p) results *in vacuo*

Complex	Bond type	ρ e/Å^3	$\nabla^2\rho$ e/Å^5	V (Hartree)	G (Hartree)	H (Hartree)	$\frac{\lvert V \rvert}{G}$
K-2-O3′-Fe(II)-O4′	O3′···Fe	0.059	0.342	–0.086	0.086	–4E-04	1.004
	O4′···Fe	0.059	0.327	–0.836	0.827	–0.010	1.012
K-2-O5′-Fe(II)-O6′	O5′···Fe	0.065	0.376	–0.097	0.096	–0.002	1.016
	O6′···Fe	0.057	0.317	–0.081	0.080	–7E-04	1.009
K-1-O2′-Fe(II)-O3′	O2′···Fe	0.113	0.602	–0.199	0.175	–0.024	1.138
	O3′···Fe	0.072	0.407	–0.110	0.106	–0.004	1.037
K-3-O4′-Fe(II)-O5′	O4′···Fe	0.062	0.350	–0.090	0.089	–0.001	1.013
	O5′···Fe	0.055	0.312	–0.078	0.078	1×10^{-5}	1.000
K-3-O5′-Fe(II)-O6′	O5′···Fe	0.063	0.386	–0.098	0.097	–7E-04	1.007
	O6′···Fe	0.056	0.321	–0.081	0.081	–3E-04	1.003
K-8-O6′-Fe(II)-C7,8	O6′···Fe	0.098	0.168	–0.107	0.075	–0.033	1.438
	C8···Fe	0.060	0.338	–0.086	0.085	–8E-04	1.010
K-1-ring-Fe(II)-A	C1′···Fe	0.051	0.135	–0.055	0.044	–0.010	1.236
	C4′···Fe	0.039	0.105	–0.039	0.033	–0.007	1.201
K-1-ring-Fe(II)-B	C2···Fe	0.048	0.115	–0.049	0.039	–0.010	1.258
	C3···Fe	0.043	0.145	–0.049	0.043	–0.006	1.150
	C5···Fe	0.051	0.124	–0.053	0.042	–0.011	1.257
K-9-O9-Fe(II)-O2	O2′···Fe	0.077	0.436	–0.119	0.114	–0.005	1.043
	O9···Fe	0.136	0.732	–0.265	0.224	–0.041	1.183
K-1-an-O2′-Fe(II)-O9	O2′···Fe	0.140	0.704	–0.264	0.220	–0.044	1.200
	O9···Fe	0.119	0.606	–0.208	0.180	–0.028	1.156
K-2-O3′-Fe(III)-O4′	O3′···Fe	0.670	0.396	–0.103	0.101	–0.002	1.017
	O4′···Fe	0.063	0.344	–0.090	0.088	–0.002	1.022
K-2-O5′-Fe(III)-O6′	O5′···Fe	0.068	0.396	–0.103	0.101	–0.002	1.022
	O6′···Fe	0.055	0.295	–0.075	0.075	–8E-04	1.010
K-1-O2′-Fe(III)-O3′	O2′···Fe	0.099	0.549	–0.168	0.153	–0.015	1.099
	O3′···Fe	0.063	0.300	–0.081	0.078	–0.003	1.037
K-3-O4′-Fe(III)-O5′	O4′···Fe	0.068	0.382	–0.100	0.098	–0.002	1.024
	O5′···Fe	0.064	0.371	–0.096	0.094	–0.001	1.014
K-3-O5′-Fe(III)-O6′	O5′···Fe	0.068	0.394	–0.130	0.101	–0.002	1.021
	O6′···Fe	0.055	0.293	–0.075	0.074	–8E-04	1.010
K-8-O6′-Fe(III)-C7,8	O6′···Fe	0.066	0.362	–0.096	0.093	–0.003	1.027
	C8···Fe	0.093	0.111	–0.091	0.059	–0.032	1.532
K-1-ring-Fe(III)-A	–[a]	–[a]	–[a]	–[a]	–[a]	–[a]	–[a]
K-1-ring-Fe(III)-B	C4···Fe	0.085	0.126	–0.085	0.058	–0.027	1.462
K-9-O9-Fe(III)-O2′	O2′···Fe	0.131	0.723	–0.253	0.217	–0.036	1.166
	O9···Fe	0.060	0.343	–0.086	0.086	–3E-05	1.000
K-1-an-O2′-Fe(III)-O9	O2′···Fe	0.119	0.597	–0.206	0.177	–0.028	1.159
	O9···Fe	0.125	0.642	–0.225	0.193	–0.032	1.168

[a] On optimisation the Fe(III) ion drifts away from the aromatic ring and binds between O6′ and C7=C8 region

Table 5.5 Bond critical point data for the kanakugiol···Fe^{n+} complexes, UBP86/6-31+G(d,p) results *in vacuo*

Complex	Bond type	ρ e/Å^3	$\nabla^2\rho$ e/Å^5	V (Hartree)	G (Hartree)	H (Hartree)	$\frac{\lvert V \rvert}{G}$
K-2-O3′-Fe(II)-O4′	O3′···Fe	0.075	0.427	–0.116	0.111	–0.005	1.045
	O4′···Fe	0.071	0.385	–0.104	0.100	–0.004	1.040
K-2-O5′-Fe(II)-O6′	O5′···Fe	0.076	0.424	–0.116	0.111	–0.005	1.045
	O6′···Fe	0.069	0.376	–0.101	0.097	–0.004	1.041
K-1-O2′-Fe(II)-O3′	O2′···Fe	0.104	0.554	–0.175	0.157	–0.018	1.115
	O3′···Fe	0.070	0.386	–0.104	0.100	–0.004	1.040
K-3-O4′-Fe(II)-O5′	O4′···Fe	0.064	0.338	–0.089	0.087	–0.002	1.023
	O5′···Fe	0.057	0.303	–0.078	0.076	–0.002	1.026
K-3-O5′-Fe(II)-O6′	O5′···Fe	0.076	0.423	–0.117	0.111	–0.006	1.054
	O6′···Fe	0.070	0.377	–0.102	0.098	–0.004	1.041
K-8-O6′-Fe(II)-C7,8	O6′···Fe	0.076	0.409	–0.114	0.108	–0.006	1.056
	C7···Fe	0.078	0.221	–0.095	0.075	–0.020	1.267
	C8···Fe	0.084	0.217	–0.100	0.077	–0.023	1.299
K-1-ring-Fe(II)-A	C1′···Fe	0.070	0.148	–0.074	0.055	–0.019	1.345
	C4′···Fe	0.050	0.098	–0.047	0.036	–0.011	1.306
K-1-ring-Fe(II)-B	C2···Fe	0.058	0.177	–0.068	0.056	–0.012	1.214
	C3···Fe	0.057	0.184	–0.068	0.057	–0.011	1.193
	C5···Fe	0.057	0.180	–0.067	0.056	–0.011	1.196
	C6···Fe	0.056	0.178	–0.066	0.055	–0.011	1.200
K-9-O9-Fe(II)-O2′	O2′···Fe	0.086	0.468	–0.135	0.126	–0.009	1.071
	O9···Fe	0.127	0.669	–0.236	0.201	–0.035	1.174
K-1-an-O2′-Fe(II)-O9	O2′···Fe	0.135	0.692	–0.253	0.213	–0.040	1.188
	O9···Fe	0.125	0.629	–0.222	0.189	–0.033	1.175
K-2-O3′-Fe(III)-O4′	O3′···Fe	0.068	0.382	–0.101	0.098	–0.003	1.031
	O4′···Fe	0.067	0.361	–0.096	0.093	–0.003	1.032
K-2-O5′-Fe(III)-O6′	O5′···Fe	0.077	0.429	–0.118	0.113	–0.005	1.004
	O6′···Fe	0.064	0.343	–0.091	0.088	–0.003	1.034
K-1-O2′-Fe(III)-O3′	O2′···Fe	0.097	0.523	–0.159	0.144	–0.015	1.104
	O3′···Fe	0.061	0.322	–0.084	0.082	–0.002	1.024
K-3-O4′-Fe(III)-O5′	O4′···Fe	0.075	0.414	–0.112	0.108	–0.004	1.037
	O5′···Fe	0.069	0.376	–0.101	0.097	–0.004	1.041
K-3-O5′-Fe(III)-O6′	O5′···Fe	0.076	0.424	–0.117	0.111	–0.006	1.054
	O6′···Fe	0.065	0.345	–0.092	0.089	–0.003	1.034
K-8-O6′-Fe(III)-C7,8	O6′···Fe	0.058	0.296	–0.077	0.075	–0.002	1.027
	C8···Fe	0.099	0.162	–0.106	0.073	–0.033	1.452
K-1-ring-Fe(III)-A	–[a]	–[a]	–[a]	–[a]	–[a]	–[a]	–[a]
K-1-ring-Fe(III)-B	C3···Fe	0.051	0.144	–0.056	0.045	–0.011	1.244
	C5···Fe	0.053	0.150	–0.057	0.047	–0.010	1.213
	C6···Fe	0.051	0.147	–0.055	0.046	–0.009	1.196
K-9-O9-Fe(III)-O2′	O2′···Fe	0.058	0.319	–0.080	0.080	0.000	1.000
	O9···Fe	0.128	0.701	–0.243	0.209	–0.034	1.163
K-1-an-O2′-Fe(III)-O9	O2′···Fe	0.111	0.603	–0.197	0.173	–0.024	1.139
	O9···Fe	0.132	0.688	–0.246	0.209	–0.037	1.177

[a] On optimisation the Fe(III) ion drifts away from the aromatic ring and binds between O6′ and C7=C8 region

5.2.5. NPA charges, spin density and orbital occupancies

The charges and the spin densities of the complexes are reported in Table 5.6. Among the complexes of Fe(II) with the neutral kanakugiol, the charge of the cation is reduced from 2 to a 0.9–1.4 *e* range and from 3 to a 1.1–1.4 *e* range for Fe(III) complexes, this reduction in positive charge implies that upon complexation electron density is transferred from the ligand to the cation. For complexes coordinating the Fe(II) cation the highest positive charge transfer corresponds to the methoxy–methoxy reactive sites and the π system of the aromatic rings.

Among the complexes with the Fe (III) cation similar trends are observed to those of the Fe(II) complexes in that the highest amount of charge transfer corresponds to the methoxy–methoxy reactive sites and the π system of the aromatic rings. For the complexes with the deprotonated ligand there is positive charge transfer of 0.6 *e* and 1.6 *e* for the Fe(II) and Fe(III) cations respectively. The fact that the Fe(III) cation is reduced to ≈2 suggest that Fe(III) binds stronger than Fe(II) to the kanakugiol ligand for complexes with either neutral or deprotonated kanakugiol ligand. It is reasonable to conclude, therefore, that the initial neutral ligand is oxidized to a radical cation (i.e., kanakugiol$^{\bullet+}$) while the initial deprotonated ligand is oxidized to a neutral radical species (i.e., kanakugiol$^{\bullet}$). The reduction of ferric ions (Fe(III)) to ferrous form by kanakugiol implies that the results obtained here are in agreement with what would be expected experimentally through the use of the ferric ions (Fe(III)) reducing antioxidant power assay technique [251].

The spin density distributions for the kanakugiol···Fe^{n+} complexes formed from neutral kanakugiol and Fe^{n+} cations are shown in Figure 5.5 and the spin density distributions for the kanakugiol···Fe^{n+} complexes formed from deprotonated kanakugiol and Fe^{n+} cations are shown in Figure 5.6. The spin density on the free Fe^{n+} cations are 4 and 5 respectively, however after coordination to the kanakugiol ligand, there is a decrease in the spin density of the cations with a of 2.941–3.653 range for the Fe(II) complexes and a 3.124–3.579 range for the Fe(III) complexes. This decrease in the spin density shows kanakugiol is able to act as good antioxidant when chelating both the Fe(II) and Fe(III) cations.

Table 5.6 NPA charges and spin density values for the Fe^{n+} cations in the kanakugiol complexes

Complex	charge *(e)*		spin density	
	DFT/B3LYP results	DFT/BP86 results	DFT/B3LYP results	DFT/BP86 results
K-2-O3′-Fe(II)-O4′	0.917	1.029	2.987	3.136
K-2-O5′-Fe(II)-O6′	0.933	1.014	3.008	3.127
K-1-O2′-Fe(II)-O3′	1.334	1.161	3.474	3.313
K-3-O4′-Fe(II)-O5′	0.895	0.895	2.965	3.073
K-3-O5′-Fe(II)-O6′	0.928	1.014	3.003	3.127
K-8-O6′-Fe(II)-C7,8	0.977	0.933	3.027	3.046
K-1-ring-Fe(II)-A	0.929	0.963	3.244	3.205
K-1-ring-Fe(II)-B	0.966	0.881	2.941	2.853
K-9-O9-Fe(II)-O2′	1.441	1.213	3.563	3.368
K-1-an-O2′-Fe(II)-O9	1.337	1.133	3.518	3.297
K-2-O3′-Fe(III)-O4′	1.179	1.162	3.254	3.256
K-2-O5′-Fe(III)-O6′	1.077	1.135	3.150	3.238
K-1-O2′-Fe(III)-O3′	1.341	1.243	3.445	3.365
K-3-O4′-Fe(III)-O5′	1.138	1.165	3.212	3.943
K-3-O5′-Fe(III)-O6′	1.075	1.136	3.148	3.239
K-8-O6′-Fe(III)-C7,8	1.259	1.083	3.522	3.198
K-1-ring-Fe(III)-A	–[a]	1.229	–[a]	3.360
K-1-ring-Fe(III)-B	1.055	1.074	3.124	3.116
K-9-O9-Fe(III)-O2′	1.441	1.299	3.550	3.417
K-1-an-O2′-Fe(III)-O9	1.430	1.312	3.579	3.434

[a] On optimisation the Fe^{n+} cation migrates to the electron rich O2′O3′, becoming identical to K-3-O2-Fe(III)-O3 complex

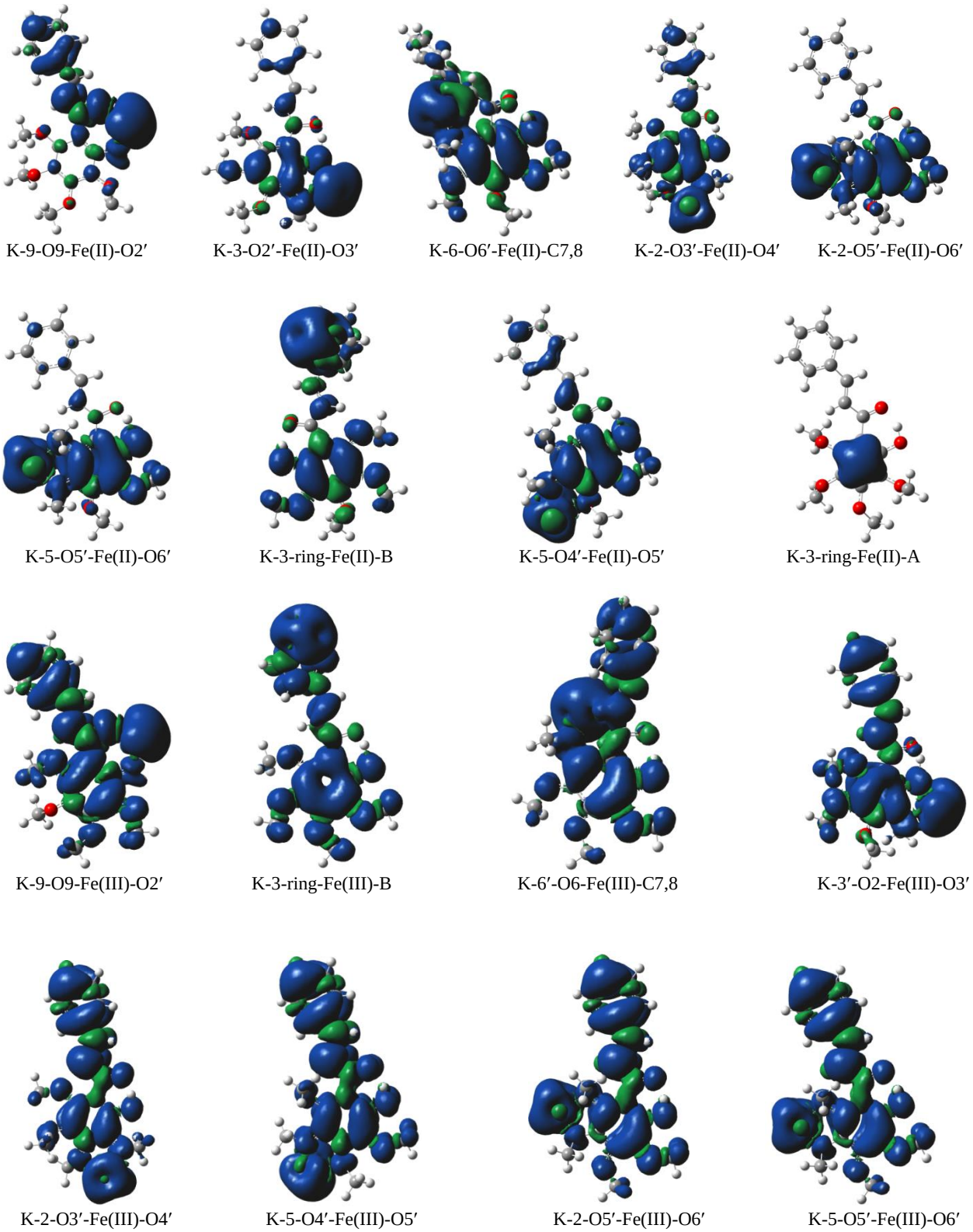

Figure 5.5 Spin density distribution for the kanakugiol···Fe^{n+} complexes formed from interactions of neutral kanakugiol and Fe^{n+} cations, B3LYP/6-31+G(d,p) results *in vacuo*. The surface isovalue used is 0.0004 au. The blue colour corresponds to positive spin densities and the green colour denotes the negative spin density.

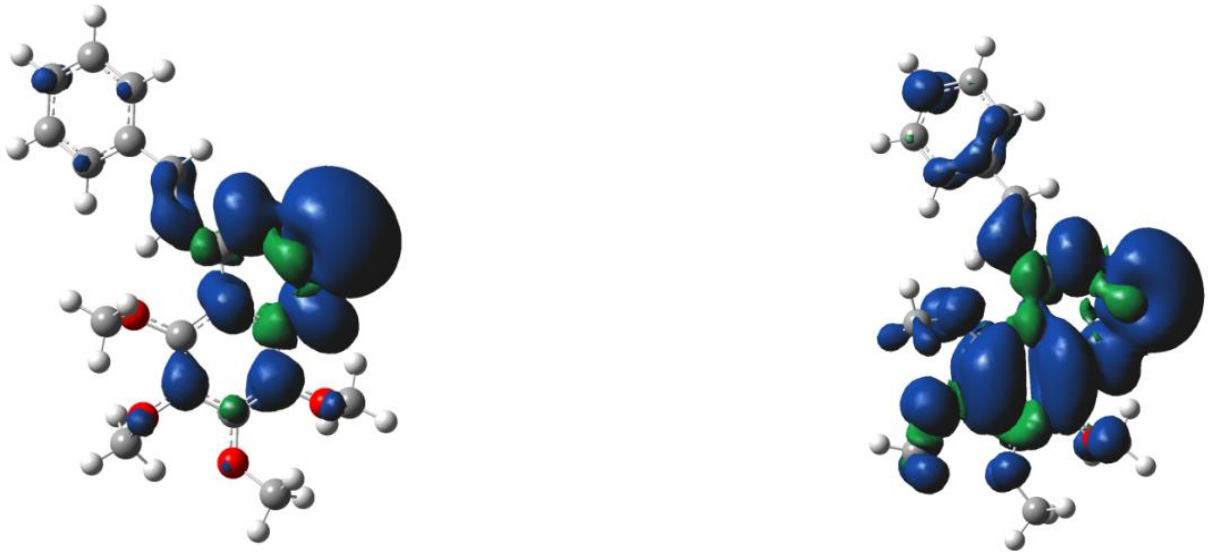

K-1-an-O2′-Fe(II)-O9 K-1-an-O2′-Fe(III)-O9

Figure 5.6 Spin density distribution for the kanakugiol···Fe^{n+} complexes formed from interactions of deprotonated kanakugiol and Fe^{n+} cations, B3LYP/6-31+G(d,p) results *in vacuo*. The surface isovalue used is 0.0004 au. The blue colour corresponds to positive spin densities and the green colour denotes the negative spin density.

The orbital occupancies for the kanakugiol···Fe^{n+} for complexes formed from either neutral kanakugiol or deprotonated kanakugiol are reported in Table 5.7. Analysis of the 4s orbital shows that upon coordination to the different reactive sites (on the kanakugiol ligand) there is a transfer of electrons from the ligand to the empty 4s orbital of the Fe^{n+} cations, this observation is supported by the increase in the number of electrons in the 4s orbital as seen in Table 5.7. Before complexation the 4s orbitals have occupancy of 0.000 and after complexation the occupancy of the 4s orbital has a range of 0.113–0.196 *e* for the Fe(II) cation and 0.088–0.215 *e* for the Fe(III) cation. The *d* orbital occupancies shows that for the d_{xy} orbital the Fe(II) cation tends to donate electrons to the central ligand with a range of 1.081–1.702 *e*. Coordination of the Fe(III) cation shows that for the d_{xy} orbital the ligand tends to donate electrons to the partially filled *d* orbitals of the cation. Analysis of the d_{xz}, d_{yz}, $d_{x^2-y^2}$, and d_{z^2} orbitals shows that upon coordination the ligand tends to donate electrons to the partially filled *d* orbitals of the Fe^{n+} cations (i.e., both Fe(II) and Fe(III) cations).

Table 5.7 Natural atomic orbital occupancies for some valence orbitals in the isolated Fe^{n+} cations and in complexes of kanakugiol, results *in vacuo*

Isolated and Fe complex	Orbitals and the corresponding natural atomic orbital occupancies					
	S (4s)	d_{xy} (3d)	d_{xz} (3d)	d_{yz} (3d)	$d_{x^2-y^2}$ (3d)	d_{z^2} (3d)
DFT/B3LYP results						
Fe(II)	0.000	1.998	1.000	1.000	1.000	1.000
K-2-O3′-Fe(II)-O4′	0.165	1.192	1.202	1.184	1.708	1.598
K-2-O5′-Fe(II)-O6′	0.155	1.339	1.116	1.293	1.547	1.582
K-1-O2′-Fe(II)-O3′	0.113	1.081	1.252	1.57	1.391	1.208
K-3-O4′-Fe(II)-O5′	0.178	1.778	1.297	1.221	1.117	1.476
K-3-O5′-Fe(II)-O6′	0.163	1.393	1.020	1.080	1.563	1.819
K-8-O6′-Fe(II)-C7,8	0.144	1.645	1.253	1.574	1.1	1.218
K-1-ring-Fe(II)-A	0.116	1.782	1.082	1.013	1.109	1.915
K-1-ring-Fe(II)-B	0.052	1.420	1.314	1.48	1.337	1.317
K-9-O9-Fe(II)-O2′	0.116	1.250	1.436	1.416	1.085	1.17
K-1-an-O2′-Fe(II)-O9	0.196	1.298	1.173	1.597	1.085	1.235
Fe(III)	0.000	1.000	1.000	1.000	1.000	1.000
K-2-O3′-Fe(III)-O4′	0.089	1.251	1.018	1.125	1.572	1.731
K-2-O5′-Fe(III)-O6′	0.105	1.243	1.096	1.140	1.566	1.741
K-1-O2′-Fe(III)-O3′	0.090	1.087	1.518	1.573	1.296	1.054
K-3-O4′-Fe(III)-O5′	0.095	1.689	1.125	1.238	1.162	1.513
K-3-O5′-Fe(III)-O6′	0.107	1.278	1.028	1.021	1.564	1.893
K-8-O6′-Fe(III)-C7,8	0.215	1.125	1.098	1.221	1.384	1.649
K-1-ring-Fe(III)-A	_[a]	_[a]	_[a]	_[a]	_[a]	_[a]
K-1-ring-Fe(III)-B	0.142	1.190	1.308	1.701	1.468	1.116
K-9-O9-Fe(III)-O2′	0.088	1.219	1.767	1.217	1.090	1.128
K-1-an-O2′-Fe(III)-O9	0.172	1.197	1.373	1.253	1.077	1.432
DFT/BP86 results						
Fe(II)						
K-2-O3′-Fe(II)-O4′	0.147	1.253	1.143	1.226	1.557	1.603
K-2-O5′-Fe(II)-O6′	0.153	1.284	1.130	1.191	1.505	1.684
K-1-O2′-Fe(II)-O3′	0.130	1.098	1.244	1.649	1.481	1.189
K-3-O4′-Fe(II)-O5′	0.178	1.779	1.298	1.225	1.116	1.472
K-3-O5′-Fe(II)-O6′	0.157	1.328	1.052	1.058	1.499	1.855
K-8-O6′-Fe(II)-C7,8	0.192	1.461	1.331	1.266	1.280	1.386
K-1-ring-Fe(II)-A	0.204	1.340	1.279	1.433	1.499	1.197
K-1-ring-Fe(II)-B	0.097	1.241	1.237	1.691	1.420	1.327
K-9-O9-Fe(II)-O2′	0.148	1.443	1.185	1.298	1.181	1.470
K-1-an-O2′-Fe(II)-O9	0.244	1.244	1.407	1.243	1.117	1.536
Fe(III)						
K-2-O3′-Fe(III)-O4′	0.093	1.218	1.062	1.085	1.654	1.691
K-2-O5′-Fe(III)-O6′	0.115	1.339	1.106	1.018	1.497	1.754
K-1-O2′-Fe(III)-O3′	0.107	1.106	1.515	1.589	1.352	1.050
K-3-O4′-Fe(III)-O5′	0.101	1.719	1.326	1.158	1.065	1.430
K-3-O5′-Fe(III)-O6′	0.114	1.303	1.173	1.117	1.459	1.662
K-8-O6′-Fe(III)-C7,8	0.200	1.156	1.336	1.605	1.480	1.076
K-1-ring-Fe(III)-A	0.116	1.127	1.210	1.206	1.516	1.558
K-1-ring-Fe(III)-B	0.091	1.258	1.390	1.489	1.422	1.189
K-9-O9-Fe(III)-O2′	0.102	1.245	1.741	1.252	1.117	1.198
K-1-an-O2′-Fe(III)-O9	0.129	1.271	1.357	1.487	1.115	1.286

[a] on optimisation the Fe^{n+} cation migrates to the electron rich O2′O3′, becoming identical to K-3-O2-Fe(III)-O3 complex

5.2.6. Conformational stability and geometries for the pedicellin conformers

The optimised conformers of pedicellin are shown in Figure 5.7 and the corresponding ΔE values (kcal/mol) are reported in Table 5.8. The energy difference among the conformers is small and remains below 3.5 kcal/mol (with the exception of P-14), therefore it is reasonable to consider that most conformers of pedicellin are populated and may co-exist *in vacuo*.

The first five conformers of pedicellin corresponds to a situation where the aliphatic chain has a bent chain arrangement; this may suggest that in this molecule bent aliphatic chain arrangement is often preferred to non-bent aliphatic chain arrangement. This result is significantly different to the trend observed for butein, homobutein and kanakugiol where the prefered conformers are those in which the aliphatic chain has non-bent arrangement. Among the pedicellin conformers, the bent aliphatic chain arrangement (i.e., an arrangement that results in the C1′–C9–C8–C7 torsion angle of nearly 0) often results in an interaction of the C7–H7 group with the π system of ring A. The resultant C–H···$\pi_{aromatic}$ interactions may account for the often preference for the conformers with the bent aliphatic chain to the conformers with the non-bent aliphatic chain (where such interactions are absent).

The major difference among the geometries of pedicellin conformers is related to the orientation of the methoxy groups in ring A, however the ΔE gap between the P-1 and P-2 conformers is <1kcal/mol, which suggests that the difference in the methoxy group orientation has minimal roles in determining conformational stability.

Since all the conformers can be considered to exist *in vacuo*, a comprehensive study on the complexes of pedicellin with Fe^{n+} cations would require that all the conformers be considered for the investigation. However, since the reactive sites are the same in all the conformers and the rigidity of the conformers suggest that no major geometric changes may be expected upon interaction with the cation (beside the changes on the orientation of the methyl groups as well as the orientation of the O9 atom), the study on the complexes considered only a selected set of conformers for interaction with the Fe^{n+} cations. The selected conformers are considered to be representative enough to cover for all the significant features of pedicellin that should be included in the study of the ligand···metal cation interaction.

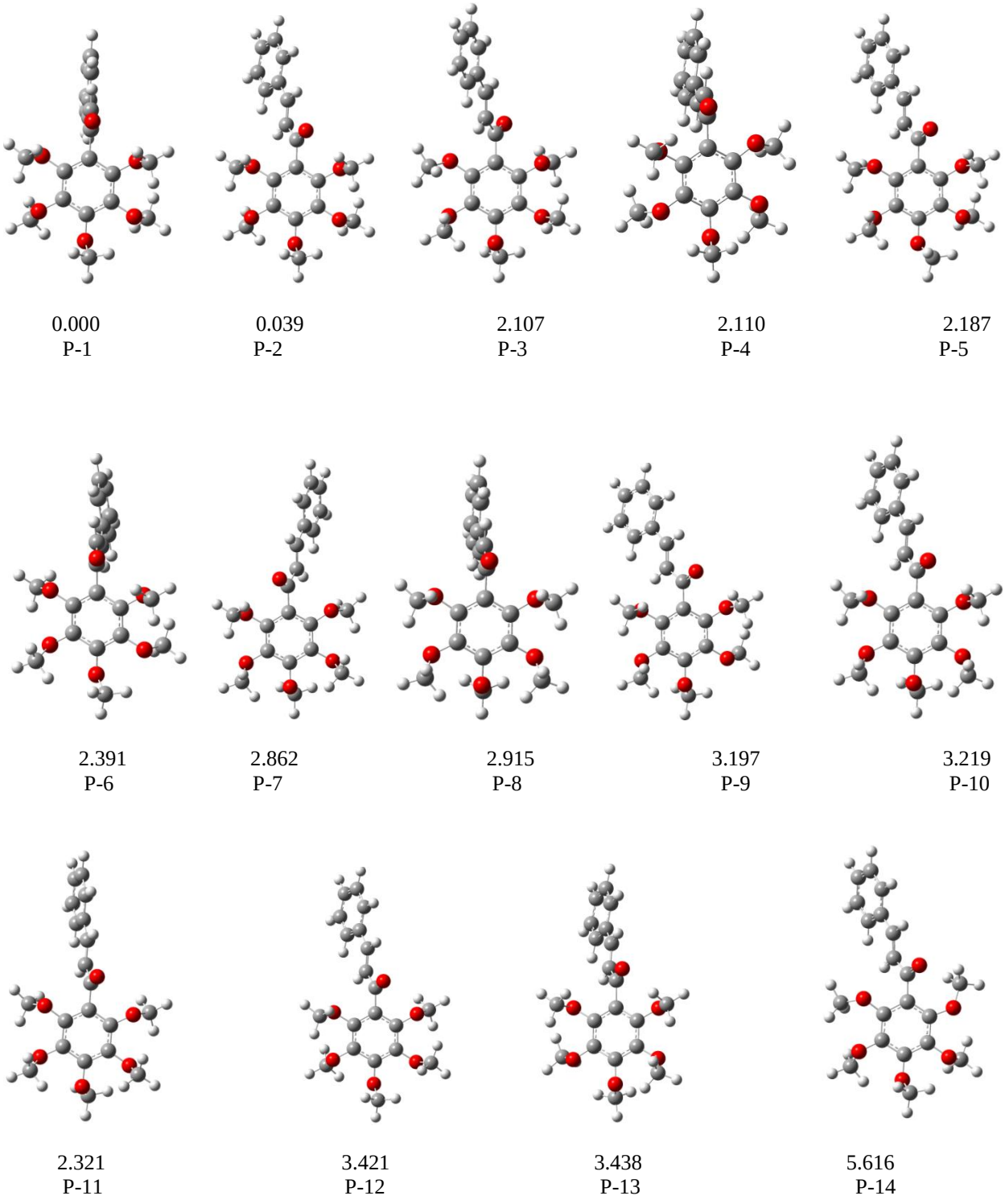

Figure 5.7 B3LYP/6-31+G(d,p) optimised conformers of the isolated pedicellin conformers arranged in order of increasing relative energy (ΔE, kcal/mol). B3LYP/6-31+G(d,p)//B3LYP/6-311+G(d,p) results *in vacuo*.

Table 5.8 *In vacuo* relative energy (ΔE, kcal/mol) values for the pedicellin conformer

Conformer	*A*[a]		*B*[b]	
	total energy (Hartree)	ΔE (kcal/mol)	total energy (Hartree)	ΔE (kcal/mol)
DFT/B3LYP results				
P-1	-1226.6898862	0.068	-1226.9869193	0.000
P-2	-1226.6899947	0.000	-1226.9868568	0.039
P-3	-1226.6868327	1.984	-1226.983562	2.107
P-4	-1226.6865849	2.140	-1226.9835562	2.110
P-5	-1226.6864611	2.217	-1226.9834346	2.187
P-6	-1226.6863234	2.304	-1226.9831087	2.391
P-7	-1226.6855166	2.810	-1226.9823583	2.862
P-8	-1226.6851366	3.049	-1226.9822742	2.915
P-9	-1226.6849702	3.153	-1226.9818253	3.197
P-10	-1226.6847920	3.265	-1226.9817891	3.219
P-11	-1226.6848175	3.249	-1226.9817711	3.231
P-12	-1226.6842964	3.576	-1226.9814681	3.421
P-13	-1226.6844140	3.502	-1226.9814409	3.438
P-14	-1226.6813677	5.414	-1226.9779690	5.616
DFT/BP86 results				
P-2	-1226.6731145	0.000	-1226.9726794	0.000
P-1	-1226.6727950	0.200	-1226.9725873	0.058
P-4	-1226.6727945	0.201	-1226.9725874	0.058
P-3	-1226.6710257	1.311	-1226.9705258	1.351
P-5	-1226.6704787	1.654	-1226.9701585	1.582
P-6	-1226.6704598	1.666	-1226.9700018	1.680
P-9	-1226.6695361	2.245	-1226.9690392	2.284
P-8	-1226.6691317	2.499	-1226.9689535	2.338
P-10	-1226.6688229	2.693	-1226.9685719	2.576
P-12	-1226.6686205	2.820	-1226.9683475	2.718
P-13	-1226.6689074	2.640	-1226.9685529	2.589
P-11	-1226.6683239	3.006	-1226.9680549	2.902
P-7	-1226.6668058	3.959	-1226.9662350	4.044
P-14	-1226.6552676	11.200	-1226.9552834	10.916

[a] Results obtained using the B3LYP/6-31+G(d,p) method
[b] Results obtained using the B3LYP/6-311+G(2d,p) method, starting from optimised geometries

5.2.7. Relative stability and binding energies for the pedicellin···Fe^{n+} complexes from neutral pedicellin and Fe^{n+} cations

The optimised pedicellin···Fe^{n+} complexes are shown in Figure 5.8 and Figure 5.9 for DFT/B3LYP and DFT/BP86 method respectively; the corresponding ΔE (kcal/mol) values are reported in Table 5.9. The lowest-energy complex corresponds to coordination of the Fe^{n+} ion at the methoxyl–*keto* reactive site, which indicates that the methoxyl–*keto* site is the preferred site for the coordination of the metal ion. The ΔE gap between the first lowest-energy complex and the second lowest-energy complex is 8.411 kcal/mol for Fe(II) cation and 24.069 kcal/mol for Fe(III), this energy gap is too high such that the second lowest-energy complexes may be considered not populated *in vacuo*. The implication of this result is that for pedicellin, there is only one site for interaction with the Fe^{n+} cation, (i.e., the methoxyl–*keto* reactive site). The coordination of the Fe^{n+} ion at the π system of the aromatic rings is preferred over the coordination to the methoxy–methoxy reactive sites.

The major geometric change between the isolated pedicellin and the complexed pedicellin is the arrangement of the methoxy group at the C5′ position. For instance, the torsion angle for the C atom of the methoxy group at the C5′ position varies by 47° in P-2-O2′-Fe(II)-O9 (it is 103° in the isolated conformer and 150° in the complex) and by 56° in P-2-O2′-Fe(III)-O9 (it is 159° in the complex). The torsion angle of O9 also changes significantly between the isolated pedicellin (where it has a value of −54°) and the complexed pedicellin (where it has a value of 36° in P-2-O2′-Fe(II)-O9 and 41° in P-2-O2′-Fe(III)-O9).

The bond distances between the Fe^{n+} cation and the site to which it is coordinated have values of 1.952 Å and 2.044 Å for the O2′···Fe^{2+} and O2′···Fe^{3+} respectively; O9···Fe^{n+} bond distance has a value of 1.825 Å and 1.824 Å for O9···Fe^{2+} and O9···Fe^{3+} respectively. These bond distance parameters suggests that the coordination of the Fe^{n+} cation onto the pedicellin ligand does not show specific preference for either Fe(II) or Fe(III) cation.

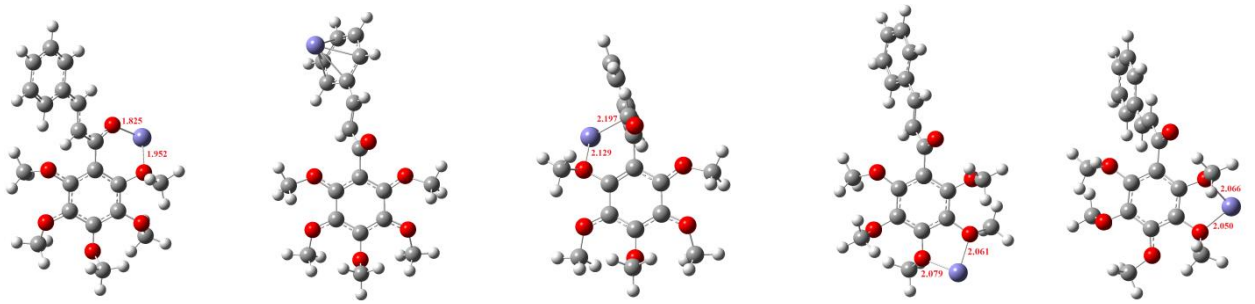

0.000
P-2-O2′-Fe(II)-O9

8.411
P-2-ring-Fe(II)-B

11.124
P-1-O6′-Fe-(II)-C7,8

21.953
P-9-O3′-Fe(II)-O4′

26.297
P-1-O2′-Fe(II)-O3′

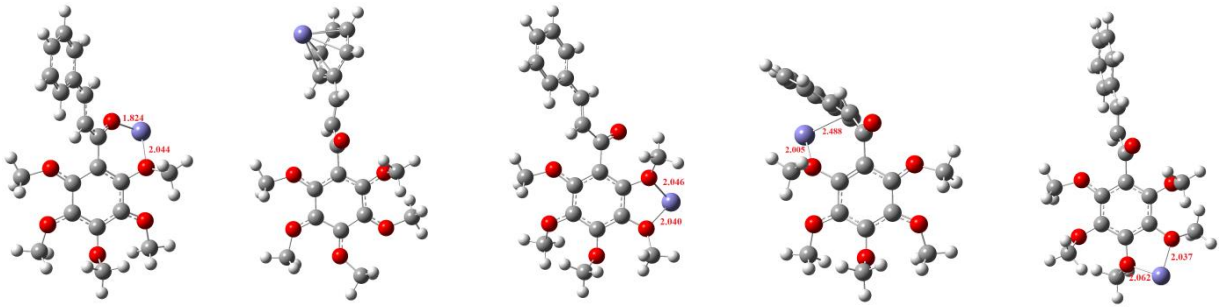

0.000
P-2-O2′-Fe(III)-O9

24.069
P-1-ring-Fe(III)-B

28.579
P-1-O2′-Fe(III)-O3′

29.798
P-1-O6′-Fe-(III)-C7,8

30.752
P-9-O3′-Fe(III)-O4′

Figure 5.8 B3LYP/6-31+G(d,p) optimised pedicellin···Fe^{n+} complexes arranged in order of increasing relative energy (ΔE, kcal/mol). B3LYP/6-311+G(2d,p)//B3LYP/6-31+G(d,p) results *in vacuo*. The bond length between the cation and the ligand are reported in Å.

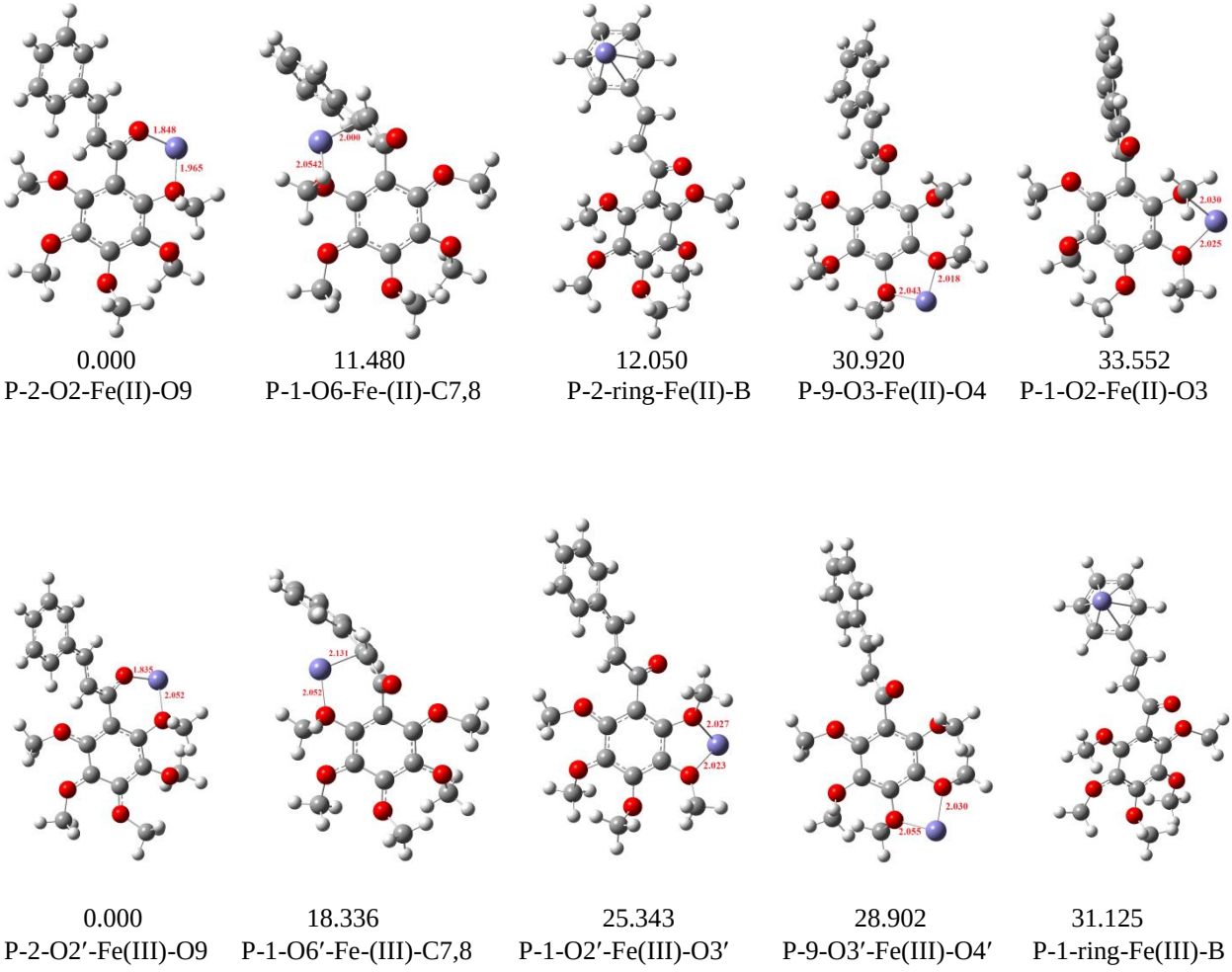

0.000
P-2-O2-Fe(II)-O9

11.480
P-1-O6-Fe-(II)-C7,8

12.050
P-2-ring-Fe(II)-B

30.920
P-9-O3-Fe(II)-O4

33.552
P-1-O2-Fe(II)-O3

0.000
P-2-O2′-Fe(III)-O9

18.336
P-1-O6′-Fe-(III)-C7,8

25.343
P-1-O2′-Fe(III)-O3′

28.902
P-9-O3′-Fe(III)-O4′

31.125
P-1-ring-Fe(III)-B

Figure 5.9 BP86/6-31+G(d,p) optimised pedicellin···Fe^{n+} complexes arranged in order of increasing relative energy (ΔE, kcal/mol). BP86/6-311+G(2d,p)//BP86/6-31+G(d,p) results *in vacuo*. The bond length between the cation and the ligand are reported in Å.

Table 5.9 *In vacuo* relative energy (ΔE, kcal/mol) for pedicellin···Fe^{n+} complexes formed from neutral pedicellin and Fe^{n+} cations

Complex	*A*[a]		*B*[B]	
	total energy (Hartree)	ΔE (kcal/mol)	total energy (Hartree)	ΔE (kcal/mol)
DFT/B3LYP results				
P-2-O2′-Fe(II)-O9[c]	-1349.5537290	0.000	-2490.1291140	0.000
P-2-ring-Fe(II)-A[c]	–[c]	–[c]	–[c]	–[c]
P-2-ring-Fe(II)-B	-1349.5265803	17.036	-2490.1157097	8.411
P-1-O6′-Fe-(II)-C7,8	-1349.5263864	17.158	-2490.1113875	11.124
P-9-O3′-Fe(II)-O4′	-1349.5107523	26.968	-2490.0941303	21.953
P-1-O2′-Fe(II)-O3′	-1349.5030850	31.780	-2490.0872073	26.297
P-1-O2′-Fe(III)-O9[c]	-1349.0886924	0.000	-2489.6765141	0.000
P-1-ring-Fe(III)-A[c]	–[c]	–[c]	–[c]	–[c]
P-2-ring-Fe(III)-B	-1349.0510219	23.639	-2489.6381576	24.069
P-1-O2′-Fe(III)-O3′	-1349.0479296	25.579	-2489.6309698	28.579
P-1-O6′-Fe-(III)-C7,8	-1349.0393814	30.943	-2489.6290282	29.798
P-9-O3′-Fe(III)-O4′	-1349.0442703	27.875	-2489.6275073	30.752
DFT/BP86 results				
P-2-O2′-Fe(II)-O9[c]	-1349.6144857	0.000	-2490.2991001	0.000
P-2-ring-Fe(II)-A[c]	–[c]	–[c]	–[c]	–[c]
P-1-O6′-Fe-(II)-C7,8	-1349.5962397	11.450	-2490.2808028	11.480
P-2-ring-Fe(II)-B	-1349.5907329	14.905	-2490.2799018	12.050
P-9-O3′-Fe(II)-O4′	-1349.5692203	28.404	-2490.2498193	30.920
P-1-O2′-Fe(II)-O3′	-1349.5645813	31.315	-2490.2456315	33.552
P-2-O2′-Fe(III)-O9[c]	-1349.1433180	0.000	-2489.8255866	0.000
P-2-ring-Fe(III)-A[c]	–[c]	–[c]	–[c]	–[c]
P-1-O6′-Fe-(III)-C7,8	-1349.1088953	21.601	-2489.7963666	18.336
P-1-O2′-Fe(III)-O3′	-1349.1059171	23.469	-2489.7852000	25.343
P-9-O3′-Fe(III)-O4′	-1349.1004661	26.890	-2489.7795282	28.902
P-2-ring-Fe(III)-B	-1349.0953012	30.131	-2489.7759857	31.125

[a] Results obtained using the 6-31+G(d,p) basis set

[b] Results obtained using the 6-311+G(2d,p) basis set, starting from optimised geometries

[c] On optimisation, the Fe^{n+} cation drifts away from the aromatic ring and the two complexes become identical

The binding energy ($\Delta E'_{binding}$, kcal/mol) values for the pedicellin···Fe^{n+} complexes are reported in Table 5.10. Among the complexes with the Fe^{n+} cations the strongest binding corresponds to the coordination of the cations to the methoxy–*keto* site with MIA values of 271.079 kcal/mol for Fe(II) cation and 731.600 kcal/mol for Fe(III) cation, what is in agreement with the relative energy results where coordination to the methoxy–*keto* reactive site is the most preferred. However, since the binding energies are positive for all the complexes, it is envisaged that the interaction between pedicellin with the Fe^{n+} cations is a favourable thermodynamic process *in vacuo*. Among the complexes with the Fe(II) cation, there is no preference of coordination to the π system on aromatic ring B over coordination at the methoxy–α,β-unsaturated reactive site (i.e., the binding energy difference between the two complexes is less than 1 kcal/mol). The weakest binding corresponds to the coordination of the Fe^{n+} cation to the methoxy–methoxy reactive site. Therefore, coordinating the metal ions at the methoxy–methoxy reactive site results in the least preferred geometry and the weakest binding energy. The implication of this result is that the Fe^{n+} cation probably does not at all interact with this site

A comparison of the $\Delta E'_{binding}$ values between complexes formed with Fe(II) and complexes formed with Fe(III) cation suggest that pedicellin acts as a better antioxidant when chelating the Fe(III) cation than the Fe(II) cation. This result is also consistent with the results obtained for butein, homobutein and kanakugiol where in all cases, Fe(III) cation tends to bind stronger to the ligand than Fe(II) cation. The preference for the stronger interaction of the Fe(III) cation with the ligand is related to its high positive charge.

Table 5.10 Binding energy ($\Delta E'_{binding}$, kcal/mol) values for pedicellin···Fe^{n+} complexes *in vacuo*. The complexes are arranged in order of decreasing $\Delta E'_{binding}$ values

Complex	*A*[a]			*B*[B]		
	$\Delta E_{inter,}$ kcal/mol	ΔE_{def} kcal/mol	$\Delta E'_{binding,}$ kcal/mol	$\Delta E_{inter,}$ kcal/mol	ΔE_{def} kcal/mol	$\Delta E'_{binding,}$ kcal/mol
DFT/B3LYP results						
P-2-O2′-Fe(II)-O9[c]	–240.178	23.888	264.066	–245.786	25.293	271.079
P-2-ring-Fe(II)-A[c]	–[c]	–[c]	–[c]	–[c]	–[c]	–[c]
P-1-O6′-Fe-(II)-C7,8	–223.088	24.587	247.675	–234.623	25.634	260.257
P-2-ring-Fe(II)-B	–223.142	21.731	244.873	–237.375	22.847	260.222
P-9-O3′-Fe(II)-O4′	–216.363	6.4862	222.849	–226.991	7.0113	234.002
P-1-O2′-Fe(II)-O3′	–208.667	13.760	222.427	–219.450	14.453	233.903
P-2-O2′-Fe(III)-O9[c]	–690.951	40.110	731.061	–689.913	41.687	731.600
P-2-ring-Fe(III)-A[c]	–[c]	–[c]	–[c]	–[c]	–[c]	–[c]
P-2-ring-Fe(III)-B	–667.312	35.736	703.048	–665.844	37.209	703.053
P-1-O6′-Fe-(III)-C7,8	–660.076	35.405	695.481	–660.076	36.490	696.566
P-1-O2′-Fe(III)-O3′	–665.440	27.029	692.469	–661.294	28.013	689.307
P-9-O3′-Fe(III)-O4′	–666.228	15.501	681.729	–662.318	16.479	678.797
DFT/BP86 results						
P-2-O2′-Fe(II)-O9[c]	–262.260	19.929	282.189	–278.953	21.075	300.028
P-2-ring-Fe(II)-A[c]	–[c]	–[c]	–[c]	–[c]	–[c]	–[c]
P-1-O6′-Fe-(II)-C7,8	–251.011	21.206	272.217	–267.529	22.222	289.751
P-2-ring-Fe(II)-B	–247.355	19.654	267.009	–266.906	20.680	287.586
P-1-O2′-Fe(II)-O3′	–231.145	13.561	247.706	–245.549	14.006	259.465
P-9-O3′-Fe(II)-O4′	–236.101	6.862	242.963	–250.313	7.175	257.488
			0			
P-2-O2′-Fe(III)-O9[c]	–715.072	29.157	744.229	–716.441	30.690	747.131
P-2-ring-Fe(III)-A[c]	–[c]	–[c]	–[c]	–[c]	–[c]	–[c]
P-1-O6′-Fe-(III)-C7,8	–693.672	34.013	727.685	–698.163	35.109	733.272
P-9-O3′-Fe(III)-O4′	–620.427	13.805	704.232	–689.823	21.613	711.436
P-1-O2′-Fe(III)-O3′	–691.803	23.032	714.835	–691.156	16.723	707.879
P-2-ring-Fe(III)-B	–689.423	30.126	719.048	–695.823	27.335	723.158

[a] Results obtained using the 6-31+G(d,p) basis set

[b] Results obtained using the 6-311+G(2d,p) basis set, starting from optimised geometries

[c] On optimisation, the Fe^{n+} cation drifts away from the aromatic ring and the two complexes become identical

5.2.8. AIM analysis of the bonding within the pedicellin···Fe^{n+} complexes

The BCP values for the electron density distribution ρ(**r**), its Laplacian $\nabla^2\rho$ (r) are reported in Table 5.11 for the DFT/B3LYP results and Table 5.12 for the DFT/BP86 results. Among the complexes of pedicellin with the Fe^{n+} cation the largest value of ρ corresponds to the O9···Fe^{n+} bond with a value of 0.130 e/Å^3 for both Fe(II) and Fe(III) cation, which is agreement with the results obtained for the binding energy values (i.e., both values indicates that O9 is the strongest interaction site with the metal ion). The values of ρ among complexes with either Fe(II) or Fe(III) cations has a 0.046–0.130 e/Å^3 range. The values of $\nabla^2\rho$ are all less than 1 e/Å^{5}and are all positive; positive values of $\nabla^2\rho$ are indicative of dative character between the cation and the central ligand. Analysis of the values of total energy density (*H*), which are negative and close to zero, is also indicative of dative character shell interactions. The |V|/*G* ratio has a range of 1.00–1.43, which a further indication of the dative nature for the type of bonding between pedicellin and the Fe^{n+} ions (i.e., a type of bonding reflecting both ionic and covalent nature).

Table 5.11 Bond critical point data for the studied pedicellin···Fe^{n+} complexes, UB3LYP/6-31+G(d,p) results *in vacuo*

Complex	Bond type	ρ e/Å^3	$\nabla^2\rho$ e/Å^5	V (Hartree)	G (Hartree)	H (Hartree)	$\frac{\lvert V\rvert}{G}$
P-2-O2′-Fe(II)-O9	O2′···Fe	0.092	0.490	–0.146	0.134	–0.012	1.088
	O9···Fe	0.130	0.710	–0.251	0.214	–0.037	1.171
P-2-ring-Fe(II)-B	C1···Fe	0.046	0.144	–0.051	0.043	–0.007	1.170
	C2···Fe	0.046	0.147	–0.052	0.044	–0.007	1.167
	C4···Fe	0.048	0.152	–0.054	0.046	–0.008	1.173
	C5···Fe	0.047	0.152	–0.053	0.045	–0.007	1.164
P-1-O2′-Fe(II)-O3′	O2′···Fe	0.069	0.380	–0.102	0.099	–0.004	1.036
	O3′···Fe	0.070	0.400	–0.106	0.103	–0.003	1.029
P-9-O3′-Fe(II)-O4′	O3′···Fe	0.065	0.369	–0.096	0.094	–0.002	1.020
	O4′···Fe	0.068	0.390	–0.103	0.100	–0.003	1.025
P-1-O6′-Fe-(II)-C7,8	O6′···Fe	0.056	0.312	–0.079	0.079	0.000	1.008
	C7···Fe	0.091	0.152	–0.097	0.067	–0.029	1.434
P-2-O2′-Fe(III)-O9	O2′···Fe	0.071	0.407	–0.108	0.105	–0.003	1.032
	O9···Fe	0.130	0.682	–0.242	0.206	–0.036	1.173
P-2-ring-Fe(III)-B	C4···Fe	0.053	0.151	–0.058	0.048	–0.010	1.216
P-1-O2′-Fe(III)-O3′	O2′···Fe	0.070	0.404	–0.107	0.104	–0.003	1.029
	O3′···Fe	0.072	0.411	–0.109	0.106	–0.003	1.031
P-9-O3′-Fe(III)-O4′	O3′···Fe	0.072	0.415	–0.111	0.107	–0.004	1.034
	O4′···Fe	0.069	0.380	–0.101	0.099	–0.003	1.026
P-1-O6′-Fe-(III)-C7,8	O6′···Fe	0.081	0.416	–0.119	0.111	–0.007	1.065
	C2···Fe	0.050	0.114	–0.047	0.038	–0.009	1.249
	C7···Fe	0.053	0.140	–0.057	0.046	–0.011	1.235

Table 5.12 Bond critical point data for the studied pedicellin···Fe^{n+} complexes, UBP86/6-31+G(d,p) results *in vacuo*

Complex	Bond type	ρ e/Å^3	$\nabla^2\rho$ e/Å^5	V (Hartree)	G (Hartree)	H (Hartree)	$\frac{\lvert V\rvert}{G}$
P-2-O2′-Fe(II)-O9	O2′···Fe	0.052	0.290	–0.069	0.071	0.002	0.972
	O9···Fe	0.005	0.020	–0.004	0.005	0.001	0.800
P-2-ring-Fe(II)-B	C1···Fe	0.048	0.256	–0.061	0.063	0.002	0.968
	C2···Fe	0.035	0.155	–0.038	0.038	0.000	1.000
	C4···Fe	0.052	0.289	–0.069	0.07	0.001	0.986
	C5···Fe	0.037	0.181	–0.435	0.044	–0.391	9.886
P-1-O2′-Fe(II)-O3′	O2′···Fe	0.051	0.291	–0.069	0.071	0.002	0.972
	O3′···Fe	0.011	0.036	–0.010	0.009	–0.001	1.111
P-9-O3′-Fe(II)-O4′	O3′···Fe	0.048	0.254	– 0.061	0.062	0.001	0.984
	O4′···Fe	0.040	0.195	– 0.047	0.048	0.001	0.979
P-1-O6′-Fe-(II)-C7,8	O6′···Fe	0.005	0.017	–0.003	0.004	0.001	0.750
	C7···Fe	0.053	0.309	–0.070	0.075	0.005	0.933
P-2-O2′-Fe(III)-O9	O2′···Fe	0.004	0.017	–0.003	0.004	0.001	0.750
	O9···Fe	0.005	0.018	–0.004	0.004	0.000	1.000
P-2-ring-Fe(III)-B	C4···Fe	0.043	0.233	–0.054	0.056	0.002	0.964
P-1-O2′-Fe(III)-O3′	O2′···Fe	0.067	0.354	–0.092	0.090	–0.002	1.022
	O3′···Fe	0.092	0.485	–0.144	0.133	–0.011	1.083
P-9-O3′-Fe(III)-O4′	O3′···Fe	0.060	0.298	–0.077	0.755	0.678	0.102
	O4′···Fe	0.088	0.467	–0.136	0.126	–0.010	1.079
P-1-O6′-Fe-(III)-C7,8	O6′···Fe	0.065	0.364	–0.093	0.092	–0.001	1.011
	C2···Fe	0.045	0.255	–0.059	0.061	0.002	0.967
	C7···Fe	0.048	0.256	–0.061	0.063	0.002	0.968

5.2.9. NPA charges, spin density and orbital occupancies

The NPA charges and the spin density values are reported in Table 5.13 for the pedicellin···Fe^{n+} complexes. Among the complexes with the Fe(II) cation the charge is reduced from +2 to a 0.911–1.398 *e* range and from +3 to a 1.003–1.444 *e* range for the Fe(II) and Fe(III) cation respectively. The largest amount of charge transfer corresponds to the coordination of the Fe^{n+} cations to the π system of aromatic ring B, this phenomenon may be explained in terms of the electron cloud of the benzene ring; the benzene ring has ample of electrons to donate to the Fe^{n+} cations therefore more electron density is transferred from the ligand to the cation. Coordination at the methoxy–*keto* site shows the least amount of charge transfer (i.e., 0.602 *e* and 1.556 *e* for Fe(II) and Fe(III) cations respectively). From the results obtained it is reasonable to infer that the electron cloud of the benzene ring has high electron density to donate to the metal cation than the lone pairs on O9. The coordination at the methoxy–methoxy reactive sites has values of 0.837 *e* and 0.964 *e* for the Fe(II) cation and 1.786 *e* and 1.752 *e* for the Fe(III) cation.

Table 5.13 NPA charges and spin density values for the Fe^{n+} cations in the pedicellin···Fe complexes

Complex	charge *(e)*		spin density	
	DFT/B3LYP results	DFT/BP86 results	DFT/B3LYP results	DFT/BP86 results
P-2-O2′-Fe(II)-O9[a]	1.398	1.159	3.558	3.323
P-2-ring-Fe(II)-A[a]	–[a]	–[a]	–[a]	–[a]
P-2-ring-Fe(II)-B	0.911	0.877	2.940	2.856
P-1-O2′-Fe(II)-O3′	1.163	1.082	3.221	3.166
P-9-O3′-Fe(II)-O4′	1.036	1.057	3.123	3.171
P-1-O6′-Fe-(II)-C7,8	1.022	0.955	3.038	3.008
P-2-O2′-Fe(III)-O9[a]	1.444	1.263	3.574	3.395
P-2-ring-Fe(III)-A[a]	–[a]	–[a]	–[a]	–[a]
P-2-ring-Fe(III)-B	1.003	1.112	3.043	3.381
P-1-O2′-Fe(III)-O3′	1.214	1.176	3.292	3.361
P-9-O3′-Fe(III)-O4′	1.248	1.178	3.330	3.279
P-1-O6′-Fe-(III)-C7,8	1.321	1.077	3.576	3.245

[a] On optimisation the cation migrates from the ring and the two complexes become identical

The spin density distributions for the pedicellin···Fe^{n+} complexes are shown in Figure 5.10. The spin density values of the Fe^{n+} cations have a range of 2.940–3.558 for the Fe(II) cation and 3.043–3.576 for the Fe(III) cation which is indicative of a transfer of electros from the ligand to the partially filled *d* orbitals of the Fe^{n+} cation. This reduction in the spin density value of the cations implies that pedicellin has the ability to act as a good antioxidant agent. The reduction is the spin density is more significant for the Fe(III) cation than for the Fe(II) cation.

Analysis of the spin density distribution indicates that the spin density is distributed throughout the ligand and the Fe^{n+} cation, however, it is also clear that for the spin density is more distributed to the ligand in the case of the ligand···Fe(III) complexes than in the case of ligand···Fe(II). An implication of the broad delocalisation of the spin density, between the ligand the Fe^{n+} ion, is that the interaction between pedicellin and Fe^{n+} cation is likely to be a mixture of ionic and covalent character (i.e., a dative type of bonding), because if it was entirely ionic in nature, the spin density would be localised entirely on the Fe^{n+} cation. This information is therefore in agreement with the conclusion reached in section 5.2.8, that the type of bonding in the complexes of pedicellin with the Fe^{n+} cations is dative in nature.

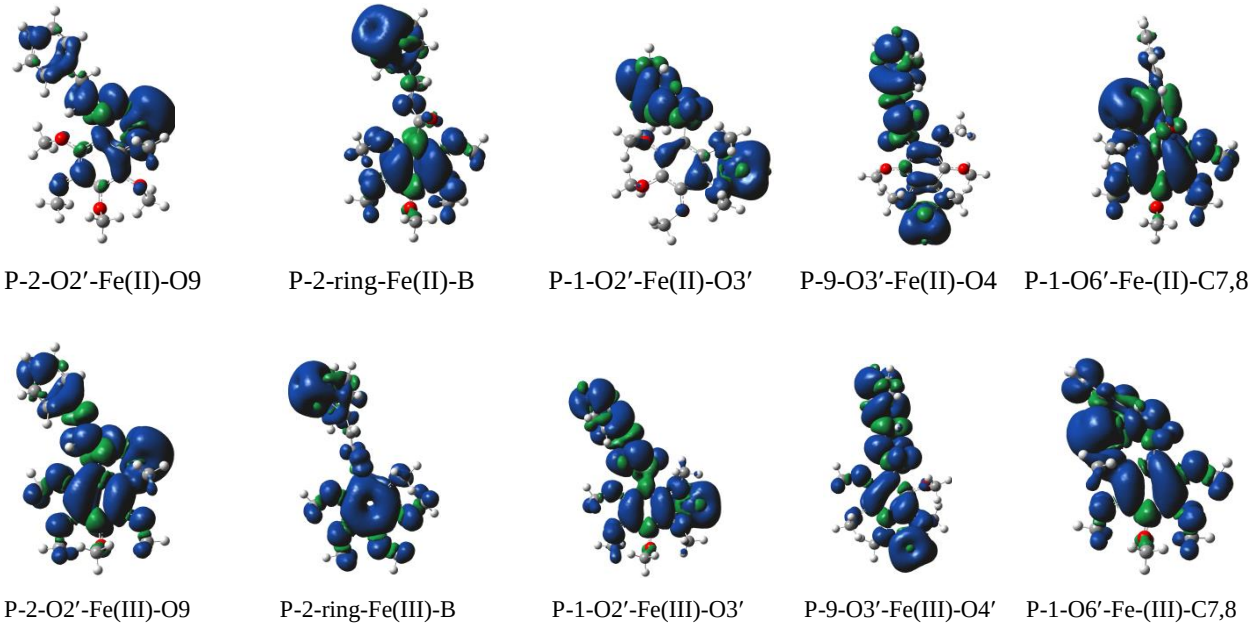

Figure 5.10 Spin density distribution for the pedicellin···Fe^{n+} complexes formed from interactions of neutral pedicellin and Fe^{n+} cations B3LYP/6-31+G(d,p) results *in vacuo*. The surface isovalue used is 0.0004 au. The blue colour corresponds to positive spin densities and the green colour denotes the negative spin density.

The natural orbital occupancies are reported in Table 5.14 for the pedicellin···Fe^{n+} complexes. Analysis of the 4s orbitals shows that upon complexation the ligand tends to donate electrons to the Fe^{n+} cations, which is seen by the increase from 0.000 to a 0.075–0.187 *e* range for the Fe(II) cation and from 0.000 to a 0.076– 0.176 *e* range for the Fe(III) cation. For the *d* orbitals among the complexes with the Fe(II) cation, the occupancy of the d_{xy} orbital decreases when it is complexes with the ligand(i.e., there is less number of electrons within it as compared to when it is isolated). The decrease in the occupancy of the d_{xy} orbital may mean that it has either donated some of its electrons to the ligand (i.e., back-donation mechanism) or it has distributed some of its electrons to other *d* orbitals of the metal ion. Among the complexes with the Fe(III) cation, the occupancy of the d_{xy} orbital tends to increases, which also imply that the orbital has received electrons density from the ligand or from other *d* orbitals of the metal ion. Analysis of the d_{xz}, d_{yz}, $d_{x^2-y^2}$, and the d_{z^2} orbital shows that upon complexation the ligand tends to donate electrons to the partially filled *d* orbitals of the Fe^{n+} cations. This can be seen by the increase in the occupancies of these orbitals (Table 5.14).

Table 5.14 Natural atomic orbital occupancies for some valence orbitals of the isolated Fe^{n+} cations and in pedicellin···Fe^{n+} complexes, results *in vacuo*

Isolated and Fe complex	Orbitals and the corresponding natural atomic orbital occupancies					
	S (4s)	d_{xy} (3d)	d_{xz} (3d)	d_{yz} (3d)	$d_{x^2-y^2}$ (3d)	d_{z^2} (3d)
DFT/B3LYP results						
Fe(II)	0.000	1.998	1.000	1.000	1.000	1.000
P-2-O2′-Fe(II)-O9[a]	0.130	1.342	1.113	1.473	1.108	1.365
P-2-ring-Fe(II)-A[a]	–[a]	–[a]	–[a]	–[a]	–[a]	–[a]
P-2-ring-Fe(II)-B	0.075	1.588	1.317	1.601	1.104	1.313
P-1-O2′-Fe(II)-O3′	0.133	1.482	1.545	1.221	1.159	1.253
P-9-O3′-Fe(II)-O4′	0.142	1.218	1.14	1.044	1.609	1.773
P-1-O6′-Fe-(II)-C7,8	0.141	1.303	1.623	1.424	1.229	1.18
Fe(III)	0.000	1.000	1.000	1.000	1.000	1.000
P-2-O2′-Fe(III)-O9[a]	0.103	1.552	1.198	1.176	1.094	1.379
P-2-ring-Fe(III)-A[a]	–[a]	–[a]	–[a]	–[a]	–[a]	–[a]
P-2-ring-Fe(III)-B	0.076	1.290	1.707	1.344	1.352	1.156
P-1-O2′-Fe(III)-O3′	0.097	1.219	1.148	1.856	1.299	1.13
P-9-O3′-Fe(III)-O4′	0.095	1.283	1.132	1.034	1.415	1.758
P-1-O6′-Fe-(III)-C7,8	0.176	1.149	1.214	1.659	1.251	1.092
DFT/BP86 results						
Fe(II)						
P-2-O2′-Fe(II)-O9[a]	0.168	1.327	1.138	1.522	1.215	1.404
P-2-ring-Fe(II)-A[a]	–[a]	–[a]	–[a]	–[a]	–[a]	–[a]
P-2-ring-Fe(II)-B	0.098	1.544	1.328	1.609	1.115	1.321
P-1-O2′-Fe(II)-O3′	0.149	1.434	1.369	1.688	1.159	1.079
P-9-O3′-Fe(II)-O4′	0.153	1.246	1.203	1.072	1.498	1.734
P-1-O6′-Fe-(II)-C7,8	0.180	1.359	1.545	1.582	1.182	1.076
Fe(III)						
P-2-O2′-Fe(III)-O9[a]	0.121	1.641	1.294	1.124	1.114	1.392
P-2-ring-Fe(III)-A[a]	–[a]	–[a]	–[a]	–[a]	–[a]	–[a]
P-2-ring-Fe(III)-B	0.101	1.211	1.288	1.069	1.331	1.178
P-1-O2′-Fe(III)-O3′	0.111	1.234	1.151	1.813	1.298	1.181
P-9-O3′-Fe(III)-O4′	0.113	1.289	1.203	1.047	1.429	1.709
P-1-O6′-Fe-(III)-C7,8	0.183	1.349	1.329	1.361	1.245	1.312

[a] On optimisation, the Fe^{n+} cation drifts away from the aromatic ring and the two complexes become identical

5.3. Results in water solution

5.3.1. Conformational stability and geometries of isolated kanakugiol

The optimised conformers of kanakugiol in water solution are shown in Figure 5.11 and the relative energy (ΔE, kcal/mol) are reported in Table 5.15. The lowest energy conformer in water solution is the same as that obtained *in vacuo*. However, the energy gap among conformers is significantly reduced such that all conformers have relative energies less than 3.5 kcal/mol, what suggests that they may all be considered to co-exist under physiological conditions. In this way, it is reasonable to infer that beside the usual factors contributing to conformational stability (i.e., the presence of intramolecular hydrogen bonds, the orientation of the aliphatic chain and the methoxy groups) solvent effects may also be considered as another factor that play significant role in determining conformational stability. The ΔE gap between K-1 and K-3 is 0.232 kcal/mol, which suggests that, in water solution, the orientations of the methoxy groups have minimal role in determine the conformational preference.

It also important to note the relative energy order obtained *in vacuo* is not maintained in solution; in some instance, some conformers that had high energy *in vacuo* have lower energy in water solution. One reason for the preference of some conformers in water solution to have lower energy than other conformers is that the solvent effects may have greater contribution on specific conformers than on other conformers, a factor that is determined by the ability of the solvent molecules to interact with the various functional groups within a given conformer. Since the solvent molecules considered here are water molecules, the likely interaction between the kanakugiol ligand and the solvent molecules is the intermolecular hydrogen bonds involving the hydrogen bond donor and acceptor groups within the ligand. Therefore, the accessibility of these donor and acceptor groups to the water molecules highly influences the stability of the resultant conformers in water solution; conformers that will form stronger intermolecular hydrogen bonds with water molecules are likely to be greatly stabilised than conformers that have minimal interaction with solvent molecules.

As discussed in the previous sections, the fact that all the conformers are likely to exist in solution implies that a thorough investigation of the kanakugiol···Fe complexes should consider all the possible conformers. However, for simplicity sake, representative conformers were selected for utilisation for the study of the kanakugiol···Fe complexes in water solution.

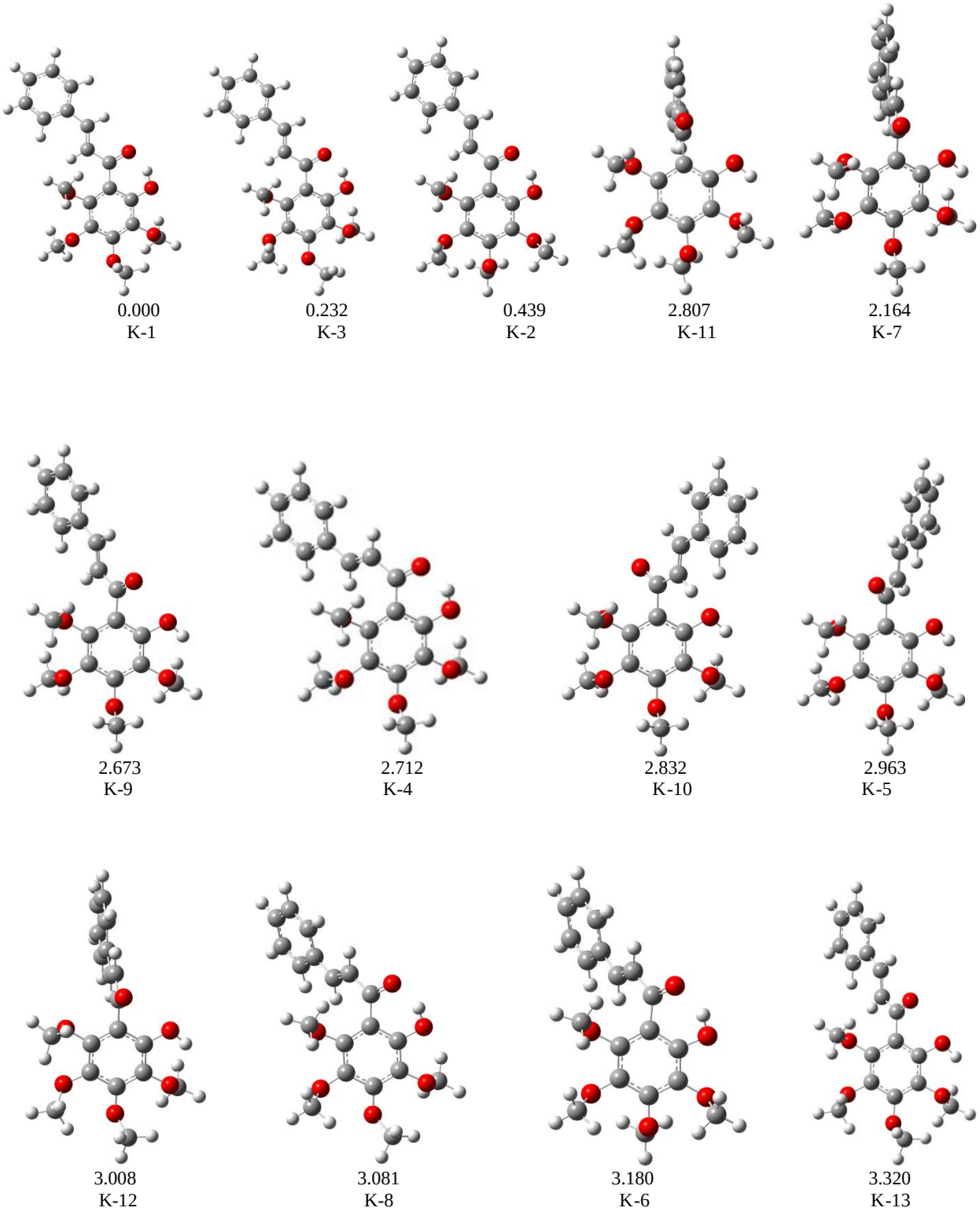

Figure 5.11 B3LYP/6-31+G(d,p) optimised conformers for the neutral kanakugiol (arranged in order of increasing relative energy (ΔE, kcal/mol)), B3LYP/6-31+G(d,p)//B3LYP/6-311+G(2d,p) results in water solution.

Table 5.15 Relative energy (ΔE, kcal/mol) values for neutral kanakugiol conformers in water solution

Conformer	A^a		B^B	
	total energy (Hartree)	ΔE (kcal/mol)	total energy (Hartree)	ΔE (kcal/mol)
DFT/B3LYP results				
K-1	-1187.4178308	0.000	-1187.7043528	0.000
K-3	-1187.4174926	0.212	-1187.7039828	0.232
K-2	-1187.4170281	0.504	-1187.7036540	0.439
K-11	-1187.4123026	3.469	-1187.6998803	2.807
K-7	-1187.4124282	3.390	-1187.7009038	2.164
K-9	-1187.4131207	2.956	-1187.7000936	2.673
K-4	-1187.4129892	3.038	-1187.7000308	2.712
K-10	-1187.4128404	3.132	-1187.6998403	2.832
K-5	-1187.4127615	3.181	-1187.6996317	2.963
K-12	-1187.4129833	3.042	-1187.6995591	3.008
K-8	-1187.4125346	3.323	-1187.6994425	3.081
K-6	-1187.4137720	2.547	-1187.6992850	3.180
K-13	-1187.4126232	3.268	-1187.6990615	3.320
DFT/BP86 results				
K-1	-1187.4103116	0.000	-1187.6995110	0.000
K-2	-1187.4094855	0.518	-1187.6986607	0.534
K-3	-1187.4093998	0.572	-1187.6985713	0.590
K-8	-1187.4039582	3.987	-1187.6936012	3.708
K-4	-1187.4030057	4.585	-1187.6927108	4.267
K-7	-1187.4023893	4.971	-1187.6919304	4.757
K-5	-1187.4010761	5.795	-1187.6907266	5.512
K-11	-1187.4011455	5.752	-1187.6908283	5.448
K-6	-1187.4007519	5.999	-1187.6906163	5.582
K-12	-1187.4005570	6.121	-1187.6903381	5.756
K-9	-1187.4005020	6.156	-1187.6902403	5.817
K-13	-1187.4004853	6.166	-1187.6901881	5.850
K-10	-1187.4001691	6.365	-1187.6899468	6.002

[a] Results obtained using the B3LYP/6-31+G(d,p) method
[b] Results obtained using the B3LYP/6-311+G(2d,p) method, starting from optimised geometries

5.3.2. Relative stability and binding energies for the kanakugiol···Fe^{n+} complexes formed from neutral kanakugiol and Fe^{n+} cations

The optimised kanakugiol···Fe^{n+} complexes formed from neutral kanakugiol and bare Fe^{n+} cations are shown in Figure 5.12 and Figure 5.13 for the DFT/B3LYP and DFT/BP86 methods respectively; the corresponding ΔE (kcal/mol) are reported in Table 5.16. Among the complexes with the Fe(II) cation, the lowest-energy complex corresponds to the coordination of the Fe^{n+} cation to the hydroxyl–*keto* reactive site (K-9-O9-Fe(II)-O2). The ΔE gap between the first lowest-energy complex and the second lowest-energy complex is 0.784 kcal/mol, which suggests that the two complexes may co-exist *in vivo*. The coordination of the Fe(II) cation at the different methoxy–methoxy reactive sites have ΔE range of 1.612–5.069 kcal/mol, what suggests that complexes where the Fe^{n+} cation is coordinated to the different methoxy–methoxy reactive sites may also be considered to exist *in vivo*, this result differs from those obtained *in vacuo* where coordination to the different methoxy–methoxy reactive sites is not preferred. The least preferred coordination of the Fe^{2+} cation is at the π systems of aromatic ring A and B, and the methoxy–α,β-unsaturated sites; these sites have ΔE values of 10.300, 9.909 and 9.146 kcal/mol respectively and therefore may be considered not to exist *in vivo*. Among the complexes formed from the interaction between kanakugiol and the Fe(III) cation, the lowest-energy complex corresponds to the coordination of the Fe^{3+} cation at the hydroxyl–methoxy reactive site. The second lowest-energy complex corresponds to the coordination of the cation at the hydroxyl–*keto* and has ΔE of 4.526 kcal/mol. The ΔE gap between the first-lowest energy complex and the remaining complexes is > 5 kcal/mol, what suggests that in water solution the complexes may not be populated. The least preferred coordination site is at the methoxy–α,β–unsaturated reactive site.

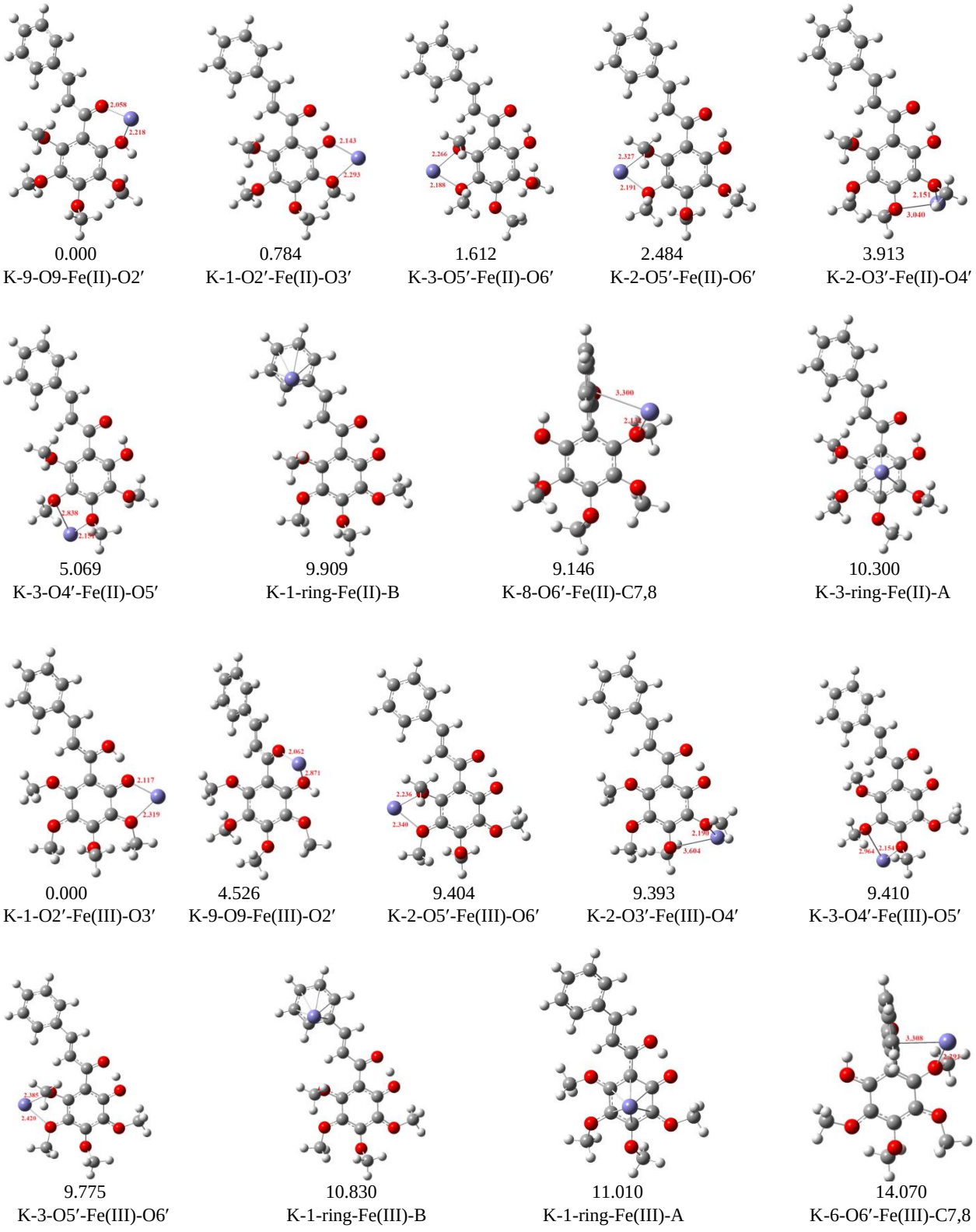

Figure 5.12 B3LYP/6-31+G(d,p) optimised kanakugiol···Fe^{n+} (arranged in order of increasing relative energy (ΔE, kcal/mol)) formed from neutral kanakugiol and Fe^{n+} cations, B3LYP/6-311+G(2d,p)//B3LYP/6-31+G(d,p) results in water solution. The bond length between the cation and the ligand are reported in Å.

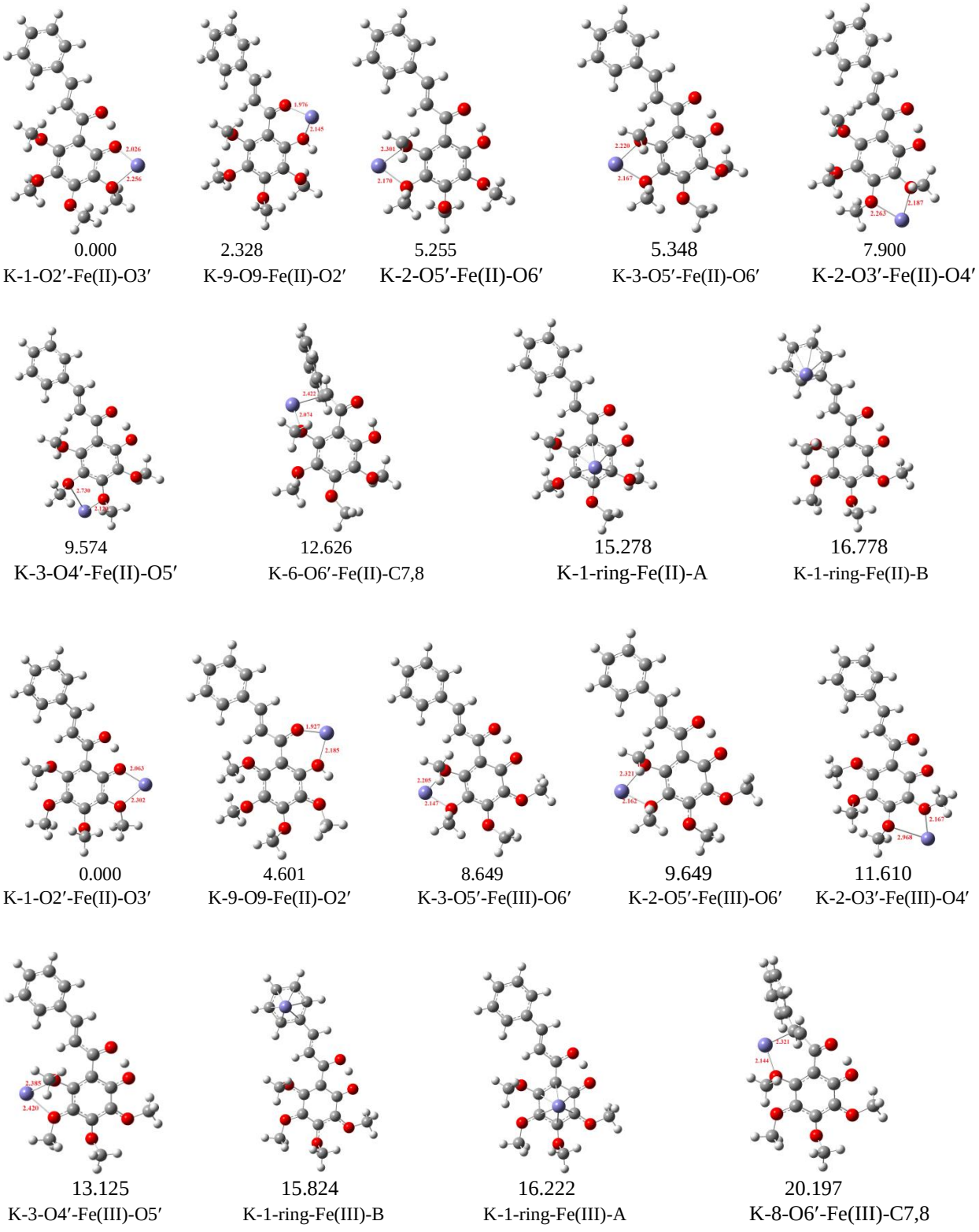

Figure 5.13 BP86/6-31+G(d,p) optimised kanakugiol···Fe^{n+} (arranged in order of increasing relative energy (ΔE, kcal/mol)) formed from neutral kanakugiol and Fe^{n+} cations, BP86/6-311+G(2d,p)//BP86/6-31+G(d,p) results in water solution. The bond length between the cation and the ligand are reported in Å.

Table 5.16 Relative energy (ΔE, kcal/mol) values for kanakugiol···Fe^{n+} complexes formed from neutral kanakugiol and Fe^{n+} cations in water solution

Complex	*A*[a]		*B*[B]	
	total energy (Hartree)	ΔE (kcal/mol)	total energy (Hartree)	ΔE (kcal/mol)
DFT/B3LYP results				
K-9-O9-Fe(II)-O2′	-1310.6282163	0.091	-2451.2020306	0.000
K-1-O2′-Fe(II)-O3′[c]	-1310.6283613	0.000	-2451.2007805	0.784
K-3-O2′-Fe(II)-O3′[c]	–[c]	–[c]	–[c]	–[c]
K-3-O5′-Fe(II)-O6′	-1310.6270602	0.816	-2451.1994620	1.612
K-2-O5′-Fe(II)-O6′	-1310.6262258	1.344	-2451.1980716	2.484
K-2-O3′-Fe(II)-O4′	-1310.6241302	2.655	-2451.1957941	3.913
K-3-O4′-Fe(II)-O5′	-1310.6226706	3.571	-2451.1939520	5.069
K-1-ring-Fe(II)-B	-1310.6147297	8.554	-2451.1862397	9.909
K-8-O6′-Fe(II)-C7,8	-1310.6149049	8.444	-2451.1874548	9.146
K-1-ring-Fe(II)-A	-1310.6148368	10.299	-2451.1856178	10.300
K-1-O2′-Fe(III)-O3′[c]	-1310.4320406	0.000	-2451.0032298	0.000
K-3-O2′-Fe(III)-O3′[c]	–[c]	–[c]	–[c]	–[c]
K-9-O9-Fe(III)-O2′	-1310.4231151	5.601	-2450.9960168	4.526
K-2-O5′-Fe(III)-O6′	-1310.4182048	8.682	-2450.9882440	9.404
K-2-O3′-Fe(III)-O4′	-1310.4178337	8.915	-2450.9882608	9.393
K-3-O4′-Fe(III)-O5′	-1310.4174799	9.137	-2450.9882342	9.410
K-3-O5′-Fe(III)-O6′	-1310.4170137	9.430	-2450.9876836	9.755
K-1-ring-Fe(III)-B	-1310.4152803	10.517	-2450.9859720	10.830
K-1-ring-Fe(III)-A	-1310.4158746	10.144	-2450.9856913	11.010
K-8-O6-Fe(III)-C7,8	-1310.4097082	14.014	-2450.9808122	14.070
DFT/BP86 results				
K-1-O2′-Fe(II)-O3′[c]	-1310.6691419	0.000	-2451.3382943	0.000
K-3-O2′-Fe(II)-O3′[c]	–[c]	–[c]	–[c]	–[c]
K-9-O9-Fe(II)-O2′	-1310.6629163	3.907	-2451.3345838	2.328
K-2-O5′-Fe(II)-O6′	-1310.6625920	4.110	-2451.3299201	5.255
K-3-O5′-Fe(II)-O6′	-1310.6626567	4.070	-2451.3297713	5.348
K-2-O3′-Fe(II)-O4′	-1310.6583355	6.781	-2451.3257067	7.900
K-3-O4′-Fe(II)-O5′	-1310.6564525	7.963	-2451.3230374	9.574
K-8-O6′-Fe(II)-C7,8	-1310.6465822	14.156	-2451.3181730	12.626
K-1-ring-Fe(II)-A	-1310.6505117	11.691	-2451.3139470	15.278
K-1-ring-Fe(II)-B	-1310.6485510	12.921	-2451.3115572	16.778
K-1-O2′-Fe(III)-O3′[c]	-1310.4726061	0.000	-2451.1438458	0.000
K-3-O2′-Fe(III)-O3′[c]	–[c]	–[c]	–[c]	–[c]
K-9-O9-Fe(III)-O2′	-1310.4626066	6.275	-2451.1365132	4.601
K-3-O5′-Fe(III)-O6′	-1310.4615675	6.927	-2451.1300625	8.649
K-2-O5′-Fe(III)-O6′	-1310.4609964	7.285	-2451.1284689	9.649
K-2-O3′-Fe(III)-O4′	-1310.4588484	8.633	-2451.1253433	11.610
K-3-O4′-Fe(III)-O5′	-1310.4571274	9.713	-2451.1229298	13.125
K-1-ring-Fe(III)-B	-1310.4557125	10.601	-2451.1186294	15.824
K-1-ring-Fe(III)-A	-1310.4551960	10.920	-2451.1179946	16.222
K-8-O6′-Fe(III)-C7,8	-1310.4400724	20.420	-2451.1116603	20.197

[a] Results obtained using the 6-31+G(d,p) basis set
[b] Results obtained using the 6-311+G(2d,p) basis set, starting from optimised geometries
[c] After optimisation, the two complexes have the same energy

The $\Delta E'_{binding}$ (kcal/mol) values are reported in Table 5.17. Among the complexes formed from the interaction between kanakugiol and the Fe(II) cation, the strongest binding corresponds to the coordination of the cation to the methoxy–methoxy site with MIA value of 19.777 kcal/mol in K-2-O5′-Fe(II)-O6′ complex. This result is different to the result obtained for the relative energy results and the results reported for the binding energies *in vacuo*, this difference in the trend of binding energies may be related to the extent of deformation of the conformer used in the preparation of the complexes. *In vacuo*, the coordination of the Fe^{2+} ions at the hydroxyl-*keto* reactive site and the hydroxyl–methoxy reactive site results in the highest ΔE_{def} value while in water solution, the coordination of the Fe^{2+} ion at the methoxy–methoxy reactive sites results in the highest ΔE_{def} value. The coordination of the cation to the π system of the aromatic rings corresponds to the weakest binding. Among the Fe(III) complexes the strongest binding corresponds to coordination at the hydroxyl–methoxy site with MIA value of 77.410 kcal/mol. The coordination at the methoxy–methoxy reactive sites shows a difference of less than 1 kcal/mol what is suggests that there in water solution there is no preference of the Fe(III) cation to coordinate at one methoxy site over the other. The weakest binding corresponds to the coordination at the π system of the aromatic ring B, which is in agreement with the result obtained for the Fe(II) cation.

From the result obtained it is reasonable to infer that in water solution kanakugiol binds the Fe(III) cation better than the Fe(II) cation, similar trends were observed for the results *in vacuo*. Furthermore, it is reasonable to infer that in water solution the binding energy values are significantly dampened with respect to the result *in vacuo*, what may suggest that the presence of solvent molecules reduces the strength of interactions between the cations and the ligand. The weakening in the interactions can also be realised through the analysis of the Fe···ligand bond distances *in vacuo* and in water solution; the bond distances are shorter *in vacuo* than the bond distances in water solution (Figure 5.2 and Figure 5.12).

Table 5.17 The binding energy ($\Delta E'_{binding}$, kcal/mol) values for kanakugiol···Fe^{n+} complexes formed from neutral kanakugiol and Fe^{n+} cations in water solution. The complexes are arranged in order of decreasing $\Delta E'_{binding}$ values

Complex	*A*[a]			*B*[B]		
	ΔE_{inter}, kcal/mol	ΔE_{def} kcal/mol	$\Delta E'_{binding}$, kcal/mol	ΔE_{inter}, kcal/mol	ΔE_{def} kcal/mol	$\Delta E'_{binding}$, kcal/mol
DFT/B3LYP results						
K-2-O5′-Fe(II)-O6′	3.013	0.622	–2.391	–9.541	10.236	19.777
K-2-O3′-Fe(II)-O4′	4.328	0.214	–4.114	–8.021	10.392	18.413
K-9-O9-Fe(II)-O2'	–0.688	1.588	2.276	–14.169	1.857	16.026
K-1-O2′-Fe(II)-O3′[c]	2.177	1.679	–0.498	–10.712	1.891	12.603
K-3-O2′-Fe(II)-O3′[c]	–[c]	–[c]	–[c]	–[c]	–[c]	–[c]
K-3-O5′-Fe(II)-O6′	2.781	1.028	–1.753	–10.117	1.005	11.122
K-8-O6′-Fe(II)-C7,8	7.297	3.008	–4.289	–5.432	2.970	8.402
K-3-O4′-Fe(II)-O5′	5.536	0.982	–4.554	–6.659	1.029	7.688
K-1-ring-Fe(II)-B	10.730	0.247	–10.483	–1.587	0.235	1.822
K-1-ring-Fe(II)-A	10.663	0.393	–10.270	–1.197	0.543	1.740
K-1-O2′-Fe(III)-O3′[c]	–61.212	20.380	81.592	–56.874	20.536	77.410
K-3-O2′-Fe(III)-O3′[c]	–[c]	–[c]	–[c]	–[c]	–[c]	–[c]
K-9-O9-Fe(III)-O2′	–58.567	13.509	72.076	–55.020	13.775	68.795
K-1-ring-Fe(III)-A	–51.068	20.901	71.969	–45.868	20.935	66.803
K-2-O3′-Fe(III)-O4′	–52.801	15.412	68.213	–47.918	15.629	63.547
K-2-O5′-Fe(III)-O6′	–53.034	14.828	67.862	–47.908	14.973	62.881
K-3-O5′-Fe(III)-O6′	–52.288	15.020	67.308	–47.350	15.136	62.486
K-3-O4′-Fe(III)-O5′	–51.995	14.658	66.653	–47.696	14.522	62.218
K-8-O6′-Fe(III)-C7,8	–50.522	15.399	65.921	–45.887	15.446	61.333
K-1-ring-Fe(III)-B	–50.695	14.780	65.475	–46.044	15.021	61.065
DFT/BP86 results						
K-9-O9-Fe(II)-O2'	–3.689	1.831	5.520	–20.517	2.244	22.761
K-1-O2′-Fe(II)-O3′[c]	–1.440	4.747	6.187	–17.028	4.814	21.842
K-3-O2′-Fe(II)-O3′[c]	–[c]	–[c]	–[c]	–[c]	–[c]	–[c]
K-8-O6′-Fe(II)-C7,8	8.730	6.238	–2.492	–8.110	6.281	14.391
K-3-O5′-Fe(II)-O6′	2.057	1.067	–0.990	–12.269	1.010	13.279
K-2-O5′-Fe(II)-O6′	2.152	0.692	–1.460	–12.307	0.651	12.958
K-2-O3′-Fe(II)-O4′	4.823	2.040	–2.783	–9.663	2.017	11.680
K-3-O4′-Fe(II)-O5′	5.950	1.644	–4.306	–8.044	1.602	9.646
K-1-ring-Fe(II)-A	10.251	0.143	–10.108	–1.750	0.224	1.974
K-1-ring-Fe(II)-B	11.481	1.175	–10.306	–0.250	1.208	1.458
K-1-O2′-Fe(III)-O3′[c]	–70.671	13.724	84.395	–72.163	13.891	86.054
K-3-O2′-Fe(III)-O3′[c]	–[c]	–[c]	–[c]	–[c]	–[c]	–[c]
K-9-O9-Fe(III)-O2′	–70.552	11.396	81.948	–73.380	11.862	85.242
K-3-O5′-Fe(III)-O6′	–64.317	12.522	76.839	–64.104	12.247	76.351
K-2-O5′-Fe(III)-O6′	–63.905	12.837	76.742	–63.048	12.616	75.664
K-2-O3′-Fe(III)-O4	–62.557	13.900	76.457	–61.086	13.736	74.822
K-8-O6′-Fe(III)-C7,8	–54.243	16.379	70.622	–55.675	16.531	72.206
K-3-O4′-Fe(III)-O5′	–62.996	13.525	76.521	–58.333	12.840	71.173
K-1-ring-Fe(III)-A	–59.746	14.344	74.090	–55.942	14.499	70.441
K-1-ring-Fe(III)-B	–60.070	14.388	74.548	–56.340	14.554	68.894

[a] Results obtained using the 6-31+G(d,p) basis set

[b] Results obtained using the 6-311+G(2d,p) basis set, starting from optimised geometries

[c] After optimisation, the two complexes have the same energy

5.3.3. Binding energies for the kanakugiol···Fe^{n+} complexes formed from deprotonated kanakugiol and Fe^{n+} cations

The optimised kanakugiol···Fe^{n+} complexes formed from deprotonated ligand and Fe^{n+} cation are shown in Figure 5.14. The values of the binding energies for the deprotonated complexes of kanakugiol with the Fe(II) and the Fe(III) are 35.584 kcal/mol and 96.454 kcal/mol respectively. This result suggests that in solution, the interaction between the Fe^{n+} ion and the selected chalcone derivatives is a favourable thermodynamic process. A comparison of the MIA values for the ligand···Fe^{n+} complexes involving the neutral and deprotonated species of kanakugiol suggests that it is greater for deprotonated kanakugiol than for neutral kanakugiol, which suggests that under physiological conditions (where the aqueous media play an important role), deprotonated kanakugiol would have greater tendency to chelate the free metal ions than neutral kanakugiol. It is therefore meaningful to conclude that the antioxidant properties of kanakugiol in physiological conditions are more related to their deprotonated species than to their neutral species.

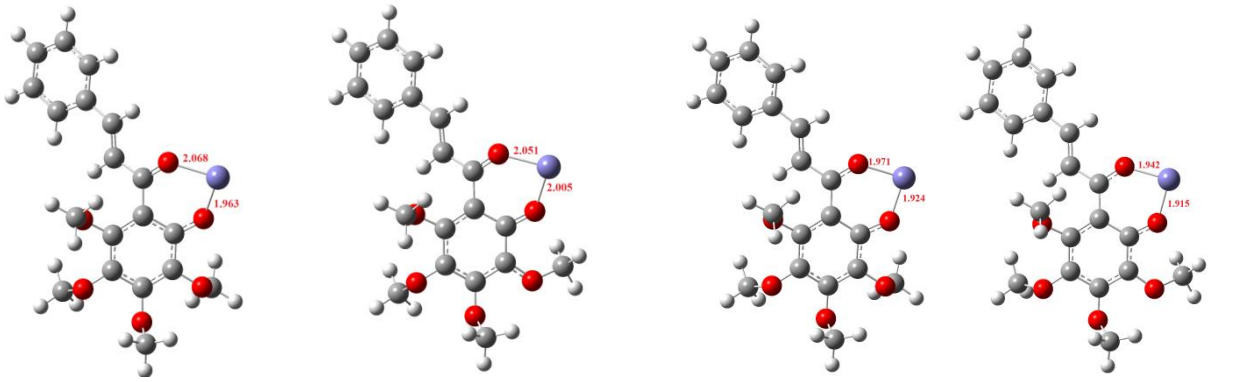

35.584
K-1-an-O2′-Fe(II)-O9

96.454
K-1-an-O2′-Fe(III)-O9

45.808
K-1-an-O2′-Fe(II)-O9

117.04
K-1-an-O2′-Fe(III)-O9

Figure 5.14 Optimised kanakugiol···Fe^{n+} complexes formed from deprotonated kanakugiol and Fe^{n+} cations. The first two structures were obtained using the DFT/B3LYP method and the last two structures were obtained using the DFT/BP86 method. The interaction energies reported below each structure were obtained from single point calculations using the 6-311+G(2d,p) basis set starting from the optimised geometries. The bond length between the cation and the ligand is reported in Å.

5.3.4. AIM analysis of the bonding within the kanakugiol···Fe^{n+} complexes

The bond critical points (BCP) values for the electron density, ρ, and its second derivative (the Laplacian, $\nabla^2\rho$) are reported in Table 5.18 for the DFT/B3LYP results and Table 5.19 for the DFT/BP86 results. Among the complexes with the neutral kanakugiol ligand, the strongest bond corresponds to the O9···Fe bond, with ρ value of 0.062 e/Å^3 for the Fe(II) cation and 0.067 e/Å^3 for the Fe(III) cation. For the complexes with the deprotonated kanakugiol ligand the strongest bond corresponds to the O2′···Fe bond with ρ values of 0.092 and 0.077 e/Å^3 for the Fe(II) and Fe(III) cations respectively. These results are in agreement with the results obtained for both the binding energy values in that coordination of the Fe^{n+} cation at the hydroxyl–*keto* is the most preferred. The weakest bond among the complexes formed from the neutral kanakugiol ligand corresponds to the coordination of the cation to the π system of the aromatic rings. The results obtained here are also consistent with the results obtained *in vacuo*.

Analysis of the values of the Laplacian implies that the interactions between the ligand and the cation are closed-shell interactions; this is evident from the positive values of the Laplacian which are inclined more towards zero. The values of *H* which are inclined more towards zero are also suggestive of the interactions between the cation and the Fe^{n+} cation being closed-shell interactions. This observation is further supported by the V|/G ratio values with a range of 0.8–1.0. The results obtained in water solution are consistent to those obtained *in vacuo*, in that the interactions between the cation and the ligand are considered to be closed-shell interactions, a trend what is different from that reported *in vacuo*, where the type of bonding is largely dative in nature.

Table 5.18 Bond critical point data for the studied kanakugiol···Fe^{n+} complexes, UB3LYP/6-31+G(d,p) results in water solution

Complex	Bond type	ρ e/Å^3	$\nabla^2\rho$ e/Å^5	V (Hartree)	G (Hartree)	H (Hartree)	$\frac{\lvert V \rvert}{G}$
K-2-O3′-Fe(II)-O4′	O3′···Fe	0.052	0.290	–0.069	0.071	0.002	0.972
	H···Fe	0.005	0.020	–0.004	0.005	0.001	0.800
K-2-O5′-Fe(II)-O6′	O5′···Fe	0.048	0.256	–0.061	0.063	0.002	0.968
	O6′···Fe	0.035	0.155	–0.038	0.038	0.000	1.000
K-1-O2′-Fe(II)-O3′	O2′···Fe	0.052	0.289	–0.069	0.07	0.001	0.986
	O3′···Fe	0.037	0.181	–0.435	0.044	–0.391	9.886
K-3-O4′-Fe(II)-O5′	O4′···Fe	0.051	0.291	–0.069	0.071	0.002	0.972
	O5′···Fe	0.011	0.036	–0.010	0.009	–0.001	1.111
K-3-O5′-Fe(II)-O6′	O5′···Fe	0.048	0.254	– 0.061	0.062	0.001	0.984
	O6′···Fe	0.040	0.195	– 0.047	0.048	0.001	0.979
K-8-O6′-Fe(II)-C7,8	C8···Fe	0.005	0.017	–0.003	0.004	0.001	0.750
	O6′···Fe	0.053	0.309	–0.070	0.075	0.005	0.933
K-1-ring-Fe(II)-A	C1···Fe	0.004	0.017	–0.003	0.004	0.001	0.750
K-1-ring-Fe(II)-B	C5···Fe	0.005	0.018	–0.004	0.004	0.000	1.000
K-9-O9-Fe(II)-O2'	O2′···Fe	0.043	0.233	–0.054	0.056	0.002	0.964
	O9′···Fe	0.067	0.354	–0.092	0.090	–0.002	1.022
K-1-an-O2′-Fe(II)-O9	O2′···Fe	0.088	0.467	–0.136	0.126	–0.010	1.079
	O9′···Fe	0.065	0.364	–0.093	0.092	–0.001	1.011
K-2-O3′-Fe(III)-O4′	O3′···Fe	0.045	0.255	–0.059	0.061	0.002	0.967
	H···Fe	0.006	0.021	–0.005	0.005	0.000	1.000
K-2-O5′-Fe(III)-O6′	O5′···Fe	0.032	0.150	–0.035	0.036	0.001	0.972
	O6′···Fe	0.042	0.216	–0.051	0.053	0.002	0.962
K-1-O2′-Fe(III)-O3′	O2′···Fe	0.057	0.312	–0.077	0.077	0.000	1.000
	O3′···Fe	0.034	0.164	–0.038	0.040	0.002	0.950
K-3-O4′-Fe(III)-O5′	O4′···Fe	0.050	0.289	–0.068	0.070	0.002	0.971
K-3-O5′-Fe(III)-O6′	O5′···Fe	0.026	0.113	–0.028	0.028	0.000	1.000
	O6′···Fe	0.029	0.130	–0.319	0.032	–0.287	9.969
K-8-O6′-Fe(III)-C7,8	C8···Fe	0.035	0.182	–0.042	0.044	0.002	0.955
	O6′···Fe	0.061	0.018	–0.004	0.004	0.000	1.000
K-1-ring-Fe(III)-A	C4···Fe	0.005	0.018	–0.002	0.004	–0.301	1.000
K-1-ring-Fe(III)-B	C6···Fe	0.005	0.017	–0.003	0.004	0.001	0.750
K-9-O9-Fe(III)-O2′	O2′···Fe	0.043	0.233	–0.054	0.056	0.002	0.964
	O9···Fe	0.067	0.354	–0.092	0.090	–0.002	1.022
K-1-an-O2′-Fe(III)-O9	O2′···Fe	0.077	0.446	–0.120	0.116	–0.004	1.034
	O9···Fe	0.069	0.353	–0.093	0.091	–0.002	1.022

Table 5.19 Bond critical point data for the studied kanakugiol···Fe^{n+} complexes UBP86/6-31+G(d,p) results in water solution

Complex	Bond type	ρ e/Å^3	$\nabla^2\rho$ e/Å^5	V (Hartree)	G (Hartree)	H (Hartree)	$\frac{\lvert V\rvert}{G}$
K-2-O3′-Fe(II)-O4′	O3′···Fe	0.050	0.247	–0.061	0.061	0.002	0.967
	O4′···Fe	0.041	0.191	–0.047	0.047	0.000	1.000
K-2-O5′-Fe(II)-O6′	O5′···Fe	0.052	0.261	–0.065	0.065	0.001	0.972
	O6′···Fe	0.038	0.163	–0.042	0.041	0.002	0.962
K-1-O2′-Fe(II)-O3′	O2′···Fe	0.076	0.379	–0.105	0.010	0.000	1.000
	O3′···Fe	0.043	0.201	–0.050	0.050	0.002	0.950
K-3-O4′-Fe(II)-O5′	O4′···Fe	0.056	0.311	–0.076	0.077	0.002	0.971
	O5′···Fe	0.015	0.043	–0.013	0.012	0.000	1.000
K-3-O5′-Fe(II)-O6′	O5′···Fe	0.052	0.263	–0.065	0.066	0.000	1.000
	O6′···Fe	0.046	0.219	–0.055	0.055	0.000	1.000
K-8-O6′-Fe(II)-C7,8	O6′···Fe	0.066	0.324	–0.086	0.083	–0.001	1.024
	C8···Fe	0.048	0.097	–0.043	0.033	–0.095	1.050
K-1-ring-Fe(II)-A	C3′···Fe	0.005	0.017	–0.004	0.004	0.000	1.000
	C5′···Fe	0.005	0.018	–0.004	0.004	0.001	0.987
K-9-O9-Fe(II)-O2′	O2′···Fe	0.054	0.271	–0.066	0.067	–0.001	1.083
	O9···Fe	0.084	0.454	–0.129	0.121	0.001	0.985
K-1-an-O2′-Fe(II)-O9	O2′···Fe	0.099	0.512	–0.159	0.144	0.000	1.000
	O9···Fe	0.087	0.467	–0.135	0.125	–0.003	1.036
K-2-O3′-Fe(III)-O4′	O3′···Fe	0.050	0.258	–0.062	0.063	–0.010	1.303
K-2-O5′-Fe(III)-O6′	O5′···Fe	0.054	0.257	–0.064	0.064	0.000	1.000
	O6′···Fe	0.037	0.150	–0.038	0.038	0.000	1.000
K-1-O2′-Fe(III)-O3′	O2′···Fe	0.069	0.349	–0.092	0.090	0.001	0.985
	O3′···Fe	0.037	0.158	–0.038	0.039	–0.008	1.066
K-3-O4′-Fe(III)-O5′	O4′···Fe	0.051	0.309	–0.074	0.070	–0.004	1.056
	O5′···Fe	0.012	0.042	–0.010	0.011	0.001	0.909
K-3-O5′-Fe(III)-O6′	O5′···Fe	0.056	0.269	–0.067	0.067	0.001	0.984
	O6′···Fe	0.048	0.223	–0.056	0.056	0.000	1.000
K-8-O6′-Fe(III)-C7,8	O6′···Fe	0.055	0.257	–0.065	0.064	0.000	1.000
	C8···Fe	0.054	0.113	–0.050	0.039	–0.002	1.022
K-1-ring-Fe(III)-A	C3′···Fe	0.006	0.018	–0.003	0.004	0.001	0.974
	C5′···Fe	0.006	0.018	–0.003	0.004	0.001	0.750
K-9-O9-Fe(III)-O2′	O2′···Fe	0.047	0.240	–0.056	0.058	0.002	0.966
	O9···Fe	0.096	0.498	–0.151	0.138	0.000	1.000
K-1-an-O2′-Fe(III)-O9	O2′···Fe	0.010	0.541	–0.168	0.151	0.000	1.000
	O9···Fe	0.096	0.471	–0.145	0.131	–0.001	1.016

5.3.5. NPA charges, spin density and orbital occupancies

The NPA charges and the spin density of the Fe^{n+} cations after complexation are reported in Table 5.20. Among the kanakugiol···Fe^{n+} complexes with neutral kanakugiol ligand the positive charge decreases from 2 to a 1.8–1.9 *e* range for the Fe(II) cation and from 3 to a 1.9–2 *e* range for Fe(III) cations. This result implies that there is minimal positive charge transfer from the Fe(II) cation to the ligand (conversely one can say there is minimal electron density transfer from the ligand to the metal ion).

The implication of this finding is that in water solution, and indeed in biological systems, the Fe(II) cation is not reduced by kanakugiol (both the neutral and the deprotonated species). Since similar results were obtained for butein and homobutein (section 4.3.5 and 4.3.10, Chapter 4) in water solution, it is reasonable to infer that in general, the Fe(II) chelation antioxidant properties of chalcone derivatives is relatives to their ability to coordinate the Fe(II) ions and not on their ability to reduce the Fe(II) ions.

Among the complexes for which kanakugiol coordinates the Fe(III) cation, the highest amount of positive charge transfer corresponds to the coordination of the cation at the hydroxyl–*keto* reactive site. The ability of kanakugiol (both neutral and deprotonated species) to reduce the Fe(III) cation to nearly +2 and the fact that the highest MIA values corresponds to the coordination of the Fe(III) cation rather than the Fe(II) cation suggests that kanakugiol acts as a better antioxidant when chelating the Fe(III) cation than the Fe(II) cation.

The coordination of Fe(III) cation to kanakugiol in water solution implies that the overall charge of the complex is three. However, since the charge on the metal cation is found to be ≈2+ in most cases, this implies that the charge on the kanakugiol ligand in the complex is +1. Thus, in the process of reducing the metal ion from a charge of 3+ to a charge of 2+, kanakugiol is oxidised to a positively charged radical cation species. Therefore the complex formed from the interaction of kanakugiol and Fe(III) cation is actually an interaction between positively charged radical kanakugiol species (i.e., kanakugiol$^{\bullet+}$ species) and an Fe(II) cation.

Table 5.20 NPA charges and spin density values for the Fe^{n+} cations in the complexes of kanakugiol obtained in water solution

Complex	charge *(e)*		spin density	
	DFT/B3LYP results	DFT/BP86 results	DFT/B3LYP results	DFT/BP86 results
K-2-O3′-Fe(II)-O4′	1.953	1.878	3.965	3.915
K-2-O5′-Fe(II)-O6′	1.922	1.878	3.944	3.907
K-1-O2′-Fe(II)-O3′	1.904	1.804	3.945	3.863
K-3-O4′-Fe(II)-O5′	1.906	1.914	3.963	3.935
K-3-O5′-Fe(II)-O6′	1.918	1.871	3.942	3.903
K-8-O6′-Fe(II)-C7,8	1.946	1.854	3.963	3.869
K-1-ring-Fe(II)-A	1.964	1.954	3.991	3.979
K-1-ring-Fe(II)-B	1.987	1.978	3.993	3.985
K-9-O9-Fe(II)-O2'	1.876	1.831	3.922	3.879
K-1-an-O2′-Fe(II)-O9	1.800	1.757	3.868	3.821
K-2-O3′-Fe(III)-O4′	1.970	2.010	3.975	4.025
K-2-O5′-Fe(III)-O6′	1.951	1.994	3.963	4.021
K-1-O2′-Fe(III)-O3′	1.932	2.034	3.970	4.079
K-3-O4′-Fe(III)-O5′	1.958	1.975	3.968	4.003
K-3-O5′-Fe(III)-O6′	1.963	1.995	3.972	4.024
K-8-O6′-Fe(III)-C7,8	1.964	1.893	3.978	3.895
K-1-ring-Fe(III)-A	1.985	2.041	4.009	4.069
K-1-ring-Fe(III)-B	1.989	1.999	3.994	4.002
K-9-O9-Fe(III)-O2'	1.923	1.998	3.950	4.041
K-1-an-O2′-Fe(III)-O9	1.910	1.956	3.966	4.026

The spin density values are largely unchanged with respect to the isolated Fe(II) cation while they decrease from 5 to a 3.930–4.009 range for Fe(III) cation. A decrease in the spin density for the complexes formed with the Fe(III) cation is an indication of the electron density transfer from the ligand to the metal cation. The spin density distributions for the kanakugiol···Fe^{n+} complexes formed from neutral and deprotonated kanakugiol are shown in Figure 5.15 and Figure 5.16 respectively. The spin density distribution of the Fe(II) complexes shows that in water solution it is largely localised on the Fe(II) cation and minimally delocalised across the ligand, what is in agreement with the results obtained for the charge transfer, where in water solution the Fe(II) cation is undergoes minimal reduction compared to the results *in vacuo*. This results also implies that the type of bonding between the ligand the Fe(II) cation is largely ionic in nature, which is in agreement with the assessment of the Laplacian ($\nabla^2\rho$) and the V|/G ratio values obtained from AIM analysis.

Among the kanakugiol···Fe^{n+} complexes formed from the interaction between kanakugiol and Fe(III) cation, the spin density distribution shows that there is a significant spin density on the ligand, specifically localised on ring A. In this way, the spin density distribution also highlights the fact that there is electron density transfer from the ligand to the Fe(III) cation.

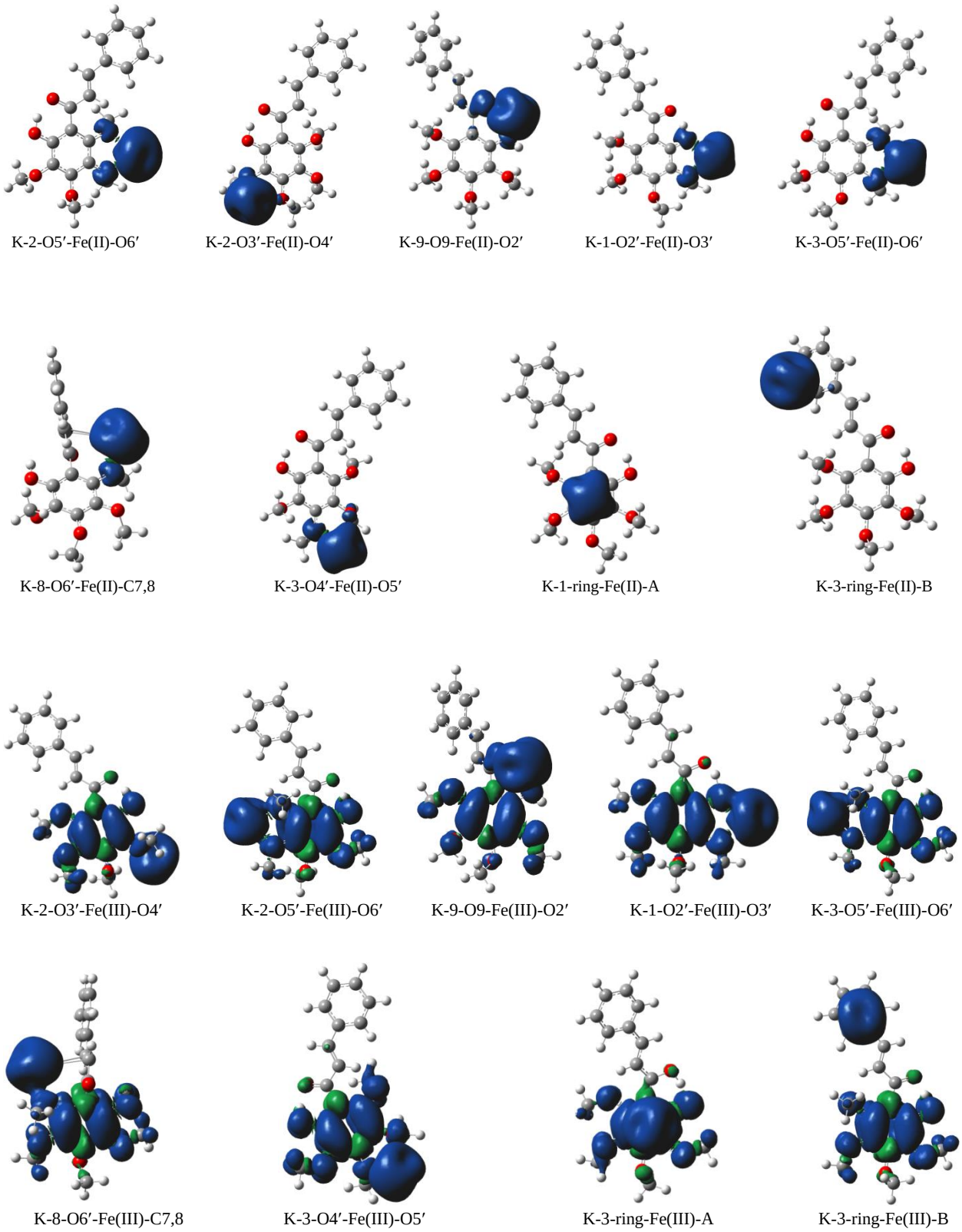

Figure 5.15 Spin density distribution for the kanakugiol···Fe^{n+} complexes formed from interactions of neutral kanakugiol and Fe^{n+} cations B3LYP/6-31+G(d,p) results in water solution. The surface isovalue used is 0.0004 au. The blue colour corresponds to positive spin densities and the green colour denotes the negative spin density.

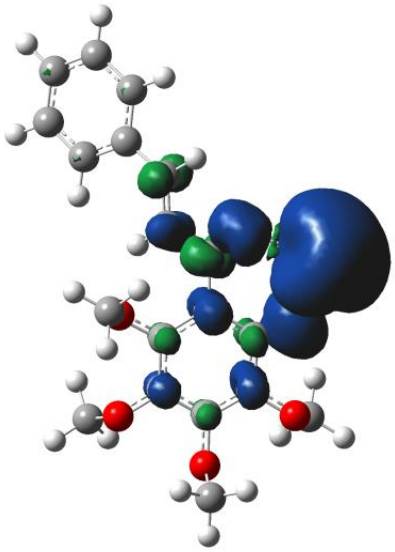

K-1-O2′-Fe(II)-O9-an

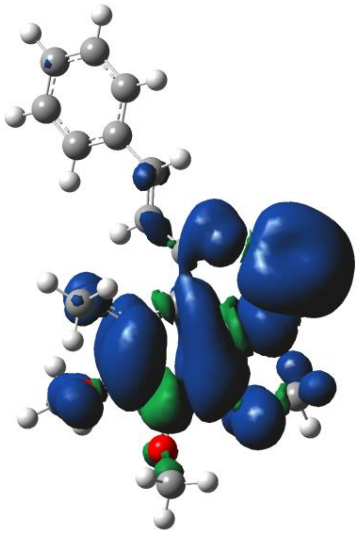

K-1-O2′-Fe(III)-O9-an

Figure 5.16 Spin density distribution for the kanakugiol···Fe^{n+} complexes formed from interactions of deprotonated kanakugiol and Fe^{n+} cations B3LYP/6-31+G(d,p) results in water solution. The surface isovalue used is 0.0004 au. The blue colour corresponds to positive spin densities and the green colour denotes the negative spin density.

The orbital occupancies for the 4*s* and 3*d* orbitals of the metal cations are reported in Table 4.24. Analysis of the 4*s* indicates that there is an increase in the occupancy in comparison to the isolated Fe^{n+} cation. The increase in the occupancy of the 4*s* may be interpreted to mean that the ligand tends to donate electrons to the 4s orbital of the Fe^{n+} cation. Analysis of the *d* orbitals shows that the occupancy of the d_{xy} orbital among the Fe(II) complexes tends to decrease with respect to the isolated Fe(II) cation; a decrease in the occupancy of this orbital may imply that it tends to donate electrons to the orbitals of the ligand (i.e., there is back-donation process from the metal ion to the ligand). The extent of decrease in the occupancy of this orbital is however dependent on the reactive site to which the metal ion is coordinated. In all other *d* orbitals of Fe(II), and indeed in all *d* orbitals of Fe(III) cation, the occupancy tends to increase; the increase in the orbital occupancy may be understood to imply that the ligand tends to donate elections to the partially filled *d* orbitals of the Fe^{n+} cations, a result that is consistent with the *in vacuo* results (section 5.2.5).

Table 5.21 Natural atomic orbital occupancies for some valence orbitals of the isolated Fe^{n+} cations in a number of complexes with kanakugiol in water solution

isolated and Fe complex	orbitals and the corresponding natural atomic orbital occupancies					
	S (4s)	d_{xy} (3d)	d_{xz} (3d)	d_{yz} (3d)	$d_{x^2-y^2}$ (3d)	d_{z^2} (3d)
DFT/B3LYP result						
Isolated Fe(II)	0.000	1.998	1.000	1.000	1.000	1.000
K-2-O3′-Fe(II)-O4′	0.009	1.063	1.114	1.232	1.235	1.377
K-2-O5′-Fe(II)-O6′	0.020	1.032	1.011	1.158	1.297	1.541
K-1-O2′-Fe(II)-O3′	0.032	1.140	1.084	1.193	1.616	1.007
K-3-O4′-Fe(II)-O5′	0.012	1.743	1.127	1.088	1.012	1.051
K-3-O5′-Fe(II)-O6′	0.020	1.346	1.013	1.117	1.560	1.005
K-8-O6′-Fe(II)-C7,8	0.011	1.316	1.519	1.004	1.022	1.161
K-1-ring-Fe(II)-A	0.008	1.039	1.004	1.186	0.002	1.057
K-1-ring-Fe(II)-B	0.003	1.051	1.325	1.528	1.037	1.060
K-9-O9-Fe(II)-O2'	0.036	1.466	1.298	1.068	1.219	1.010
K-1-an-O2′-Fe(II)-O9	0.054	1.063	1.190	1.384	1.286	1.180
Isolated Fe(III)	0.000	1.000	1.000	1.000	1.000	1.000
K-2-O3′-Fe(III)-O4′	0.007	1.264	1.014	1.361	1.034	1.339
K-2-O5′-Fe(III)-O6′	0.013	1.345	1.077	1.082	1.502	1.015
K-1-O2′-Fe(III)-O3′	0.029	1.035	1.020	1.924	1.010	1.026
K-3-O4′-Fe(III)-O5′	0.011	1.645	1.203	1.057	1.023	1.090
K-3-O5′-Fe(III)-O6′	0.010	1.461	1.003	1.110	1.437	1.003
K-8-O6′-Fe(III)-C7,8	0.009	1.287	1.686	1.001	1.012	1.022
K-1-ring-Fe(III)-A	0.006	1.007	1.161	1.651	1.097	1.068
K-1-ring-Fe(III)-B	0.002	1.002	1.007	1.106	1.252	1.633
K-9-O9-Fe(III)-O2'	0.023	1.062	1.076	1.211	1.198	1.489
K-1-an-O2′-Fe(III)-O9	0.046	1.167	1.057	1.043	1.092	1.649
DFT/BP86 result						
Isolated Fe(II)	0.000	1.998	1.000	1.000	1.000	1.000
K-2-O3′-Fe(II)-O4′	0.024	1.079	1.115	1.047	1.814	1.019
K-2-O5′-Fe(II)-O6′	0.022	1.041	1.020	1.176	1.279	1.564
K-1-O2′-Fe(II)-O3′	0.047	1.050	1.288	1.349	1.355	1.081
K-3-O4′-Fe(II)-O5′	0.016	1.772	1.101	1.107	1.024	1.048
K-3-O5′-Fe(II)-O6′	0.025	1.242	1.035	1.199	1.595	1.012
K-8-O6′-Fe(II)-C7,8	0.045	1.041	1.022	1.700	1.136	1.163
K-1-ring-Fe(II)-A	0.008	1.001	1.159	1.027	1.250	1.578
K-1-ring-Fe(II)-B	0.003	1.753	1.084	1.010	1.161	1.004
K-9-O9-Fe(II)-O2'	0.045	1.200	1.349	1.177	1.149	1.220
K-1-an-O2′-Fe(II)-O9	0.065	1.132	1.482	1.228	1.126	1.165
Isolated Fe(III)	0.000	1.000	1.000	1.000	1.000	1.000
K-2-O3′-Fe(III)-O4′	0.009	1.718	1.036	1.096	1.100	1.015
K-2-O5′-Fe(III)-O6′	0.019	1.212	1.032	1.091	1.624	1.009
K-1-O2′-Fe(III)-O3′	0.033	1.077	1.150	1.636	1.021	1.026
K-3-O4′-Fe(III)-O5′	0.036	1.078	1.458	1.209	1.067	1.085
K-3-O5′-Fe(III)-O6′	0.022	1.329	1.019	1.143	1.457	1.014
K-8-O6′-Fe(III)-C7,8	0.045	1.088	1.011	1.415	1.161	1.348
K-1-ring-Fe(III)-A	0.008	1.026	1.058	1.764	1.008	1.075
K-1-ring-Fe(III)-B	0.002	1.015	1.124	1.025	1.224	1.603
K-9-O9-Fe(III)-O2'	0.039	1.121	1.421	1.122	1.103	1.171
K-1-an-O2′-Fe(III)-O9	0.058	1.214	1.033	1.091	1.094	1.525

5.3.6. Conformational stability and geometries for the pedicellin conformers

The optimised conformers of pedicellin in water solution are shown in Figure 5.17 and the corresponding relative energy (ΔE, kcal/mol) values are reported in Table 5.22. The ΔE gap in water solution among the conformers is significantly dampened with respect to the *in vacuo* results, a trend that has been observed with all the studied chalcone derivatives. In water solution the energy difference between conformers remains below 2.5 kcal/mol (with the exception of the P-11 conformer for the DFT/B3LYP results), implies that all conformers may be considered to co-exist.

The lowest energy conformers are those stabilised by the presence of intramolecular hydrogen bonds (which includes the O-H···O and a number of C-H···O). The results obtained also suggest the bent aliphatic chain arrangement is preferred over the non-bent aliphatic chain arrangement, these results are consistent with the *in vacuo* geometries. The results further imply that in water solution the orientation of the methoxy groups has minimal effect on conformational stability as seen by the infinitesimal difference in the ΔE gap among the conformers (i.e., less than 1kcal/mol). Since a similar result was obtained for kanakugiol in water solution, it is reasonable to generalised that for chalcone derivatives with methoxy substituents, the orientation of such groups have minimal effects in determining conformational stability, as long as solvent effects are taken into consideration.

Beside the fact that the energy gap between the conformers has significantly decreased when comparing the results *in vacuo* with the results in solution, it is also worth noting that the energy trend among the conformers (i.e., the relative energy order) is significantly different from that obtained *in vacuo*. The alteration of the energy order among conformers may be explain in the same manner as it was described for the conformers of kanakugiol in water solution, namely that the solvent effects may stabilise different conformers differently, depending on the ability of individual conformers to form intermolecular interactions with the solvent molecules.

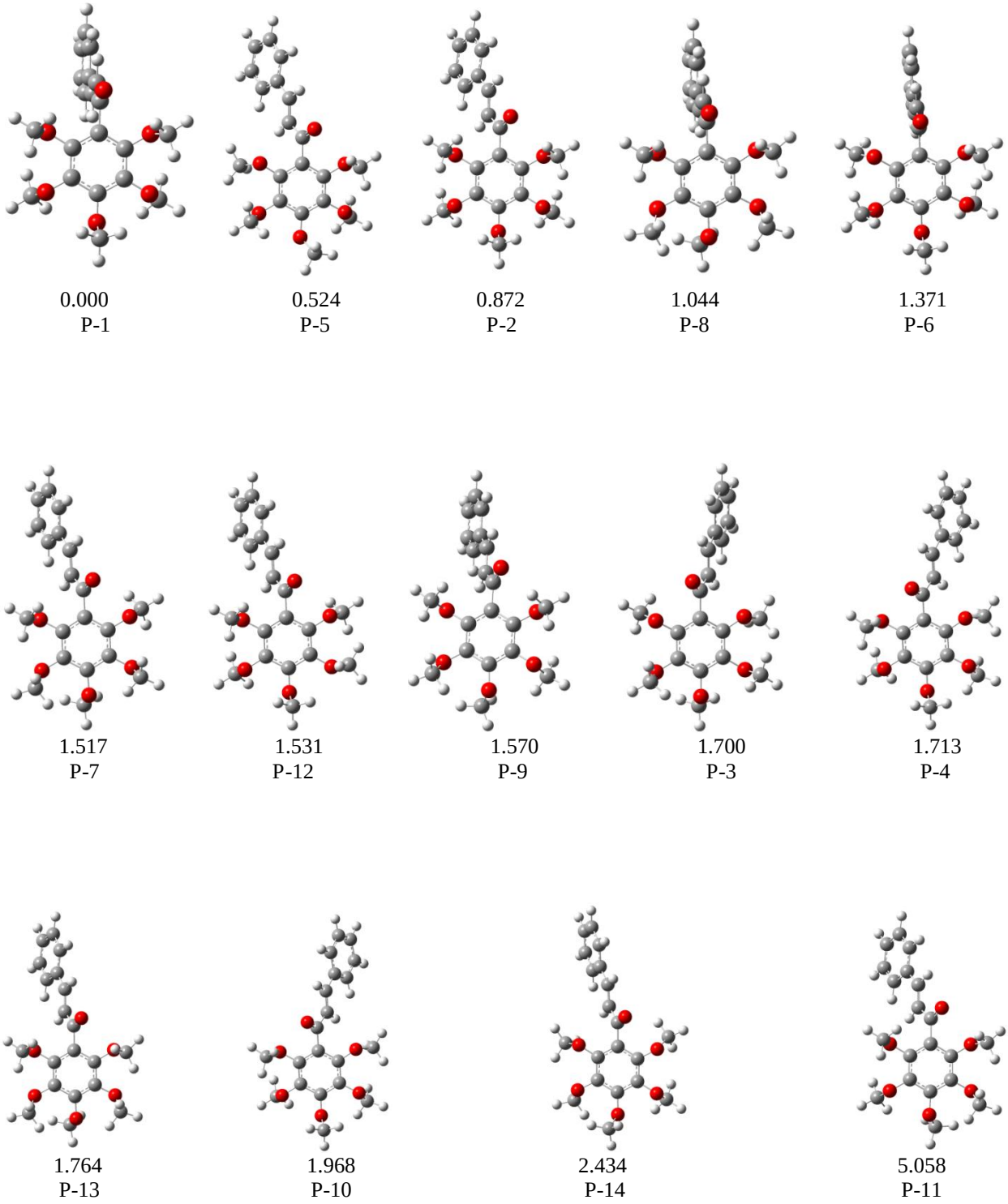

Figure 5.17 B3LYP/6-31+G(d,p) optimised conformers of the isolated pedicellin arranged in order of increasing relative energy (ΔE, kcal/mol), B3LYP/6-311+G(2d,p)//B3LYP/6-31+G(d,p) results in water solution.

Table 5.22 Relative energy (ΔE, kcal/mol) values for the pedicellin conformer in water solution

Conformer	*A*[a]		*B*[b]	
	total energy (Hartree)	ΔE (kcal/mol)	total energy (Hartree)	ΔE (kcal/mol)
DFT/B3LYP results				
P-1	-1226.7051282	0.000	-1226.9996859	0.000
P-5	-1226.7044199	0.444	-1226.9988501	0.524
P-2	-1226.7038580	0.797	-1226.9982955	0.872
P-8	-1226.7037152	0.887	-1226.9980214	1.044
P-6	-1226.7031583	1.236	-1226.9975006	1.371
P-7	-1226.7030342	1.314	-1226.9972689	1.517
P-12	-1226.7029698	1.354	-1226.9972459	1.531
P-9	-1226.7028667	1.419	-1226.9972001	1.570
P-3	-1226.7026558	1.551	-1226.9969760	1.700
P-4	-1226.7027308	1.504	-1226.9969562	1.713
P-13	-1226.7025670	1.607	-1226.9968752	1.764
P-10	-1226.7023005	1.774	-1226.9965499	1.968
P-14	-1226.7016324	2.194	-1226.9958063	2.434
P-11	-1226.7034598	1.047	-1226.9916249	5.058
DFT/BP86 results				
P-1	-1226.6867457	0.018	-1226.9841367	0.000
P-5	-1226.6867736	0.000	-1226.9839969	0.088
P-6	-1226.6865535	0.138	-1226.9837525	0.241
P-8	-1226.6863433	0.270	-1226.9834988	0.400
P-11	-1226.6859671	0.506	-1226.9831773	0.602
P-2	-1226.6857276	0.656	-1226.9830104	0.707
P-9	-1226.6856260	0.720	-1226.9828556	0.804
P-4	-1226.6856283	0.719	-1226.9826967	0.904
P-3	-1226.6853130	0.917	-1226.9825168	1.017
P-12	-1226.6854506	0.830	-1226.9822884	1.160
P-7	-1226.6848361	1.216	-1226.9819730	1.358
P-10	-1226.6845743	1.380	-1226.9817780	1.480
P-13	-1226.6845950	1.367	-1226.9817603	1.491
P-14	-1226.6844996	1.427	-1226.9815990	1.592

[a] Results obtained using the B3LYP/6-31+G(d,p) method
[b] Results obtained using the B3LYP/6-311+G(2d,p) method, starting from optimised geometries

5.3.7. Relative stability and binding energies for the pedicellin···Fe^{n+} complexes

The optimised pedicellin···Fe^{n+} complexes are shown in Figure 5.18 for the DFT/B3LYP method and Figure 5.19 for the DFT/BP86 method; the corresponding ΔE (kcal/mol) values are reported in Table 5.23. Among the complexes of pedicellin with the Fe(II) cation the lowest-energy complex corresponds to coordination at the methoxy–*keto* reactive site, which is a result similar to that found *in vacuo*. Although the ΔE gap in water solution is significantly dampened with respect to that *in vacuo*, it is reasonable to state that since all other conformers have relative energies above 5 kcal/mol, the coordination at the methoxy–*keto* reactive site is the most probable to observe in water solution. The least preferred coordination site is the π system of the aromatic ring B.

Among the Fe(III) complexes, the ΔE gap is significantly decreased with respect to the results *in vacuo*. However, most of the complexes of pedicellin with Fe(III) cation have large relative energy values, so that they may not be considered to exist *in vivo*. The results also show that the Fe^{n+} ion does not prefer to coordinate to the π system of ring B, what is consistent with the results observed *in vacuo*.

The bond distances in for the O2′···Fe^{2+} interactions in P-2-O2′-Fe(II)-O9 and in P-2-O2′-Fe(III)-O9 complex have values of 2.185 Å and 2.235 Å respectively, while the O9···Fe^{2+} bond distance has values of 2.079 Å and 2.096 Å respectively. These values suggest elongation of the bond distances in water solution with respect to the results *in vacuo*. The elongation in the bond distances are in agreement with the fact that both the ligand molecule and the Fe^{n+} cations are interacting not only with each other but also with the solvent molecules within their vicinity.

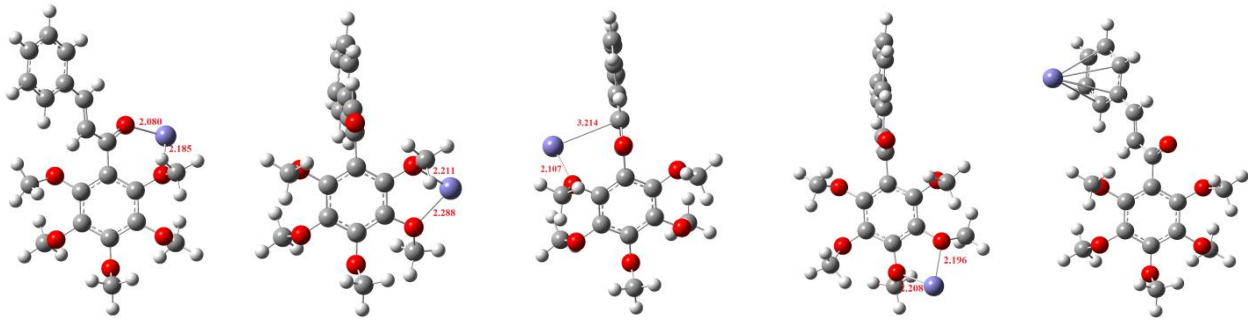

0.000	6.267	7.531	8.979	14.020
P-2-O2′-Fe(II)-O9	P-1-O2′-Fe(II)-O3′	P-1-O6′-Fe-(II)-C7,8	P-9-O3′-Fe(II)-O4′	P-2-ring-Fe(II)-B

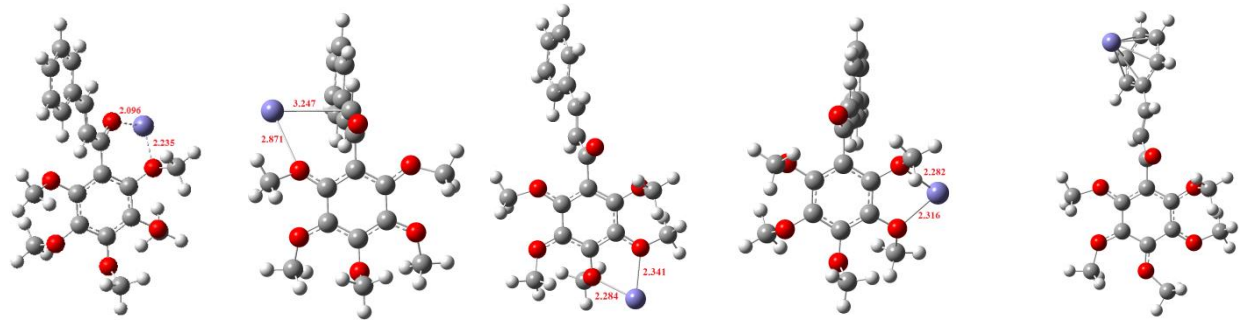

0.000	3.901	5.125	19.410	25.870
P-2-O2′-Fe(III)-O9	P-1-O6′-Fe-(III)-C7,8	P-9-O3′-Fe(III)-O4′	P-1-O2′-Fe(III)-O3′	P-2-ring-Fe(III)-B

Figure 5.18 B3LYP/6-31+G(d,p) optimised pedicellin···Fe^{n+} complexes arranged in order of increasing relative energy (ΔE, kcal/mol). B3LYP/6-311+G(2d,p)//B3LYP/6-31+G(d,p) results in water solution. The bond length between the cation and the ligand are reported in Å.

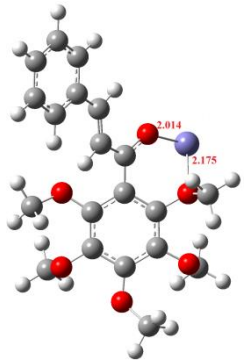

0.000
P-2-O2′-Fe(II)-O9

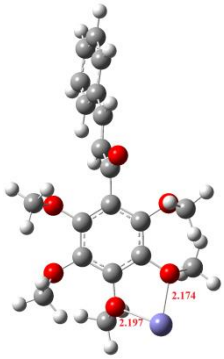

7.900
P-9-O3′-Fe(II)-O4′

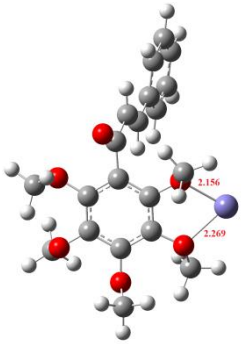

11.011
P-1-O2′-Fe(II)-O3′

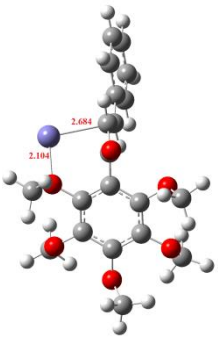

11.377
P-1-O6′-Fe-(II)-C7,8

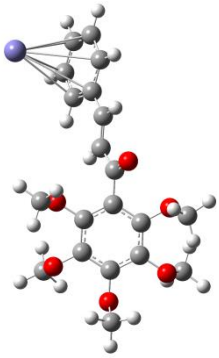

20.440
P-2-ring-Fe(II)-B

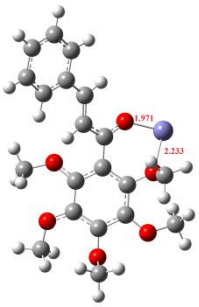

0.000
P-2-O2′-Fe(III)-O9

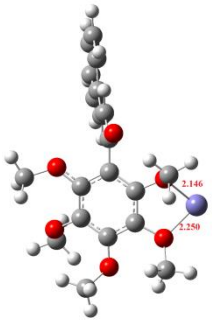

8.894
P-1-O2′-Fe(III)-O3′

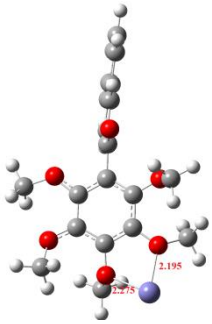

10.772
P-9-O3′-Fe(III)-O4′

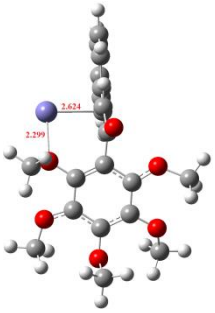

13.027
P-1-O6′-Fe-(III)-C7,8

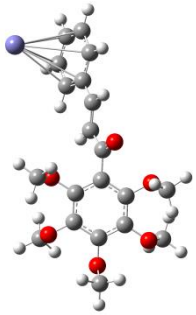

18.321
P-1-ring-Fe(III)-B

Figure 5.19 BP86/6-31+G(d,p) optimised pedicellin···Fe^{n+} complexes arranged in order of increasing relative energy (ΔE, kcal/mol). BP86/6-311+G(2d,p)//BP86/6-31+G(d,p) results in water solution. The bond length between the cation and the ligand are reported in Å.

Table 5.23 Relative energy (ΔE, kcal/mol) values for pedicellin···Fe^{n+} complexes formed from neutral pedicellin and Fe^{n+} cations in water solution

Complex	*A*[a]		*B*[B]	
	total energy (Hartree)	ΔE (kcal/mol)	total energy (Hartree)	ΔE (kcal/mol)
DFT/B3LYP results				
P-2-O2′-Fe(II)-O9[c]	-1349.9200337	0.000	-2490.5024865	0.000
P-2-ring-Fe(II)-A[c]	–[c]	–[c]	–[c]	–[c]
P-1-O2′-Fe(II)-O3′	-1349.9078188	7.665	-2490.4924995	6.267
P-1-O6′-Fe-(II)-C7,8	-1349.9104170	6.035	-2490.4904843	7.531
P-9-O3′-Fe(II)-O4′	-1349.9117427	5.203	-2490.4881777	8.979
P-2-ring-Fe(II)-B	-1349.9004202	12.308	-2490.4801380	14.020
P-1-O2′-Fe(III)-O9[c]	-1349.7122635		-2490.2962266	0.000
P-1-ring-Fe(III)-A[c]	–[c]	–[c]	–[c]	–[c]
P-1-O6′-Fe-(III)-C7,8	-1349.7020600	6.403	-2490.2900106	3.901
P-9-O3′-Fe(III)-O4′	-1349.7008398	7.168	-2490.2880595	5.125
P-1-O2′-Fe(III)-O3′	-1349.6757134	22.94	-2490.2652881	19.410
P-2-ring-Fe(III)-B	-1349.7006059	7.315	-2490.2549995	25.870
DFT/BP86 results				
P-2-O2′-Fe(II)-O9[c]	-1349.9497026	0.000	-2490.6261296	0.000
P-2-ring-Fe(II)-A[c]	–[c]	–[c]	–[c]	–[c]
P-9-O3′-Fe(II)-O4′	-1349.9376421	7.568	-2490.6135409	7.900
P-1-O2′-Fe(II)-O3′	-1349.9341213	9.777	-2490.6085821	11.011
P-1-O6′-Fe-(II)-C7,8	-1349.9325548	10.760	-2490.6079989	11.377
P-2-ring-Fe(II)-B	-1349.9213428	17.796	-2490.5935562	20.440
P-2-O2′-Fe(III)-O9[c]	-1349.7461459	0.000	-2490.4272431	0.000
P-2-ring-Fe(III)-A[c]	–[c]	–[c]	–[c]	–[c]
P-1-O2′-Fe(III)-O3′	-1349.7357788	6.505	-2490.4130700	8.894
P-9-O3′-Fe(III)-O4′	-1349.7323328	8.668	-2490.4100765	10.772
P-1-O6′-Fe-(III)-C7,8	-1349.7303668	9.902	-2490.4064840	13.027
p-2-ring-Fe(III)-B	-1349.7293461	10.542	-2490.3980467	18.321

[a] Results obtained using the 6-31+G(d,p) basis set

[b] Results obtained using the 6-311+G(2d,p) basis set, starting from optimised geometries

[c] On optimisation, the Fe^{n+} cation drifts away from the aromatic ring and the two complexes become identical

The binding energy ($\Delta E'_{binding}$, kcal/mol) values for the pedicellin···Fe^{n+} complexes are reported in Table 5.24. All the binding energies are positive, indicative that the interaction between pedicellin and the Fe^{n+} cations leads to favourable thermodynamic reaction. In water solution the binding energy values are significantly dampened with respect to the result *in vacuo*. Among the complexes with the Fe^{n+} cations the strongest binding corresponds to the coordination of the cations to the methoxy–*keto* reactive site, with MIA values of 18.082 kcal/mol for Fe(II) cation and 75.499 kcal/mol for Fe(III) cation. Coordination of the Fe^{n+} cation to the methoxy–methoxy reactive site gives a MIA value of 11.296 kcal/mol. The weakest binding corresponds to the coordination of the Fe(II) cation to the π system of the aromatic ring B.

Among the complexes with the Fe(III) cation, coordination to the methoxy–α,β–unsaturated reactive site corresponds to the second highest binding energy of 62.681 kcal/mol, a trend different to that observed for the coordination of the Fe(II) cation. The weakest binding energy corresponds to the coordination of the cation to the methoxy–methoxy reactive site, with MIA value of 36.780 kcal/mol, this trend is different to that observed for the Fe(II) complexes.

A comparison of the $\Delta E'_{binding}$ values of the complex with pedicellin suggest that pedicellin acts as a better antioxidant when chelating the Fe(III) cation than the Fe(II) cation. A trend also observed for the complexes with kanakugiol both *in vacuo* and in water solution.

Overall, it is reasonable to state that both kanakugiol and pedicellin have high metal ion affinity and the formation of their complexes with Fe^{n+} ions is a thermodynamically favored process. However, their $\Delta E'_{binding}$ values are lower than those of flavonoids such as quercetin [113] and oxovitisin [242], indicating that chalcone derivatives may be weaker metal chelators than flavonoid derivatives.

Table 5.24 Binding energy values for pedicellin···Fe^{n+} complexes in water solution. The complexes are arranged in order of decreasing $\Delta E'_{binding}$ values

Complex	*A*[a]			*B*[B]		
	$\Delta E_{inter,}$ kcal/mol	ΔE_{def} kcal/mol	$\Delta E'_{binding,}$ kcal/mol	$\Delta E_{inter,}$ kcal/mol	ΔE_{def} kcal/mol	$\Delta E'_{binding,}$ kcal/mol
DFT/B3LYP results						
P-2-O2′-Fe(II)-O9[c]	–1.366	2.151	3.517	–15.583	2.499	18.082
P-2-ring-Fe(II)-A[c]	_[a]	_[a]	_[a]	_[a]	_[a]	_[a]
P-9-O3′-Fe(II)-O4′	3.215	1.298	–1.917	–10.003	1.2925	11.296
P-1-O2′-Fe(II)-O3′	7.096	3.700	–3.396	–5.7321	3.8419	9.574
P-1-O6′-Fe-(II)-C7,8	5.466	0.401	–5.065	–7.180	0.468	7.648
P-2-ring-Fe(II)-B	–10.942	0.091	11.033	–1.556	0.184	1.743
P-2-O2′-Fe(III)-O9[c]	–45.020	7.227	52.247	–43.730	31.719	75.499
P-2-ring-Fe(III)-A[c]	_[a]	_[a]	_[a]	_[a]	_[a]	_[a]
P-1-O6′-Fe-(III)-C7,8	–50.370	17.139	67.509	–45.321	17.450	62.681
P-2-ring-Fe(III)-B	47.036	15.215	62.246	–11.584	37.055	48.639
P-9-O3′-Fe(III)-O4′	–51.023	13.591	64.614	–47.158	13.586	60.744
P-1-O2′-Fe(III)-O3′	–33.837	6.781	40.618	–46.132	17.648	63.780
DFT/BP86 results						
P-2-O2′-Fe(II)-O9[c]	–4.668	2.383	7.051	–19.749	2.734	22.483
P-2-ring-Fe(II)-A[c]	_[a]	_[a]	_[a]	_[a]	_[a]	_[a]
P-9-O3′-Fe(II)-O4′	2.836	1.333	–1.503	–11.946	1.347	13.293
P-1-O2′-Fe(II)-O3′	5.748	2.871	–2.877	–8.031	3.020	11.051
P-1-O6′-Fe-(II)-C7,8	6.731	1.506	–5.225	–7.665	1.754	9.419
P-2-ring-Fe(II)-B	13.128	0.217	–12.911	0.691	0.311	–0.380
P-2-O2′-Fe(III)-O9[c]	–69.494	10.430	79.924	–72.100	10.871	82.971
P-1-O2′-Fe(III)-O3′[c]	–62.350	12.410	74.760	–62.499	12.632	72.131
P-2-ring-Fe(III)-A	_[a]	_[a]	_[a]	_[a]	_[a]	_[a]
P-1-O6′-Fe-(III)-C7,8	–58.954	11.57	70.524	–58.366	11.855	70.221
P-9-O3′-Fe(III)-O4′	–60.890	9.189	70.079	–61.424	9.116	70.540
P-2-ring-Fe(III)-B	–61.125	8.010	69.135	–60.759	10.364	71.123

[a] Results obtained using the 6-31+G(d,p) basis set
[b] Results obtained using the 6-311+G(2d,p) basis set, starting from optimised geometries
[c] On optimisation, the Fe^{n+} cation drifts away from the aromatic ring and the two complexes become identical

5.3.8. AIM analysis of the bonding within the pedicellin···Fe^{n+} complexes

The bond critical point values for the analysis of the electron density ρ(**r**) and its Laplacian $\nabla^2\rho(r)$ of the electron density are reported in Table 5.25 for the DFT/B3LYP results and Table 5.26 for the DFT/BP86 results. Among the complexes of the Fe(II) cation the strongest bond corresponds to the O9···Fe bond with ρ value of 0.064 e/Å^3 and 0.075 e/Å^3 for the Fe(III) cation. These results are consistent with the results *in vacuo* and the trend in the binding energies. The weakest bond corresponds to the coordination of the Fe^{n+} cation to C7 with ρ value of 0.006 e/Å^3 for both the Fe(II) and Fe(III) cation.

The positive values of the Laplacian are indicative of closed-shell interactions between the cation and the ligand molecule. This observation if further supported by the values of *H* which are closer to zero. The |V|/G ratio is however largely ≤ 1, which suggests that the interactions are inclined towards ionic character. Therefore, with all the investigated chalcone derivatives, interactions in water solution are significantly weak as compared to the interactions *in vacuo*.

Table 5.25 Bond critical point data and spin density for the studied pedicellin···Fe^{n+} complexes, UB3LYP/6-31+G(d,p) results in water solution

Complex	Bond type	ρ e/Å^3	$\nabla^2\rho$ e/Å^5	V (Hartree)	G (Hartree)	H (Hartree)	$\frac{\lvert V\rvert}{G}$
P-2-O2′-Fe(II)-O9	O2′···Fe	0.048	0.263	–0.063	0.064	0.001	0.984
	O9···Fe	0.064	0.327	–0.084	0.083	–0.001	1.012
P-1-O2'-Fe(II)-O3'	O2′···Fe	0.046	0.238	–0.058	0.059	0.001	0.983
	O3′···Fe	0.038	0.179	–0.043	0.044	0.001	0.977
P-9-O3'-Fe(II)-O4'	O3′···Fe	0.047	0.247	–0.059	0.060	0.001	0.983
	O4′···Fe	0.046	0.238	–0.057	0.058	0.001	0.983
P-1-O6′-Fe-(II)-C7,8	O6′···Fe	0.057	0.316	–0.077	0.078	0.001	0.987
	C7···Fe	0.006	0.018	–0.004	0.004	0.000	1.000
P-2-O2′-Fe(III)-O9	O2′···Fe	0.045	0.200	–0.048	0.049	0.001	0.980
	O9···Fe	0.075	0.420	–0.112	0.108	–0.004	1.037
P-1-O2'-Fe(III)-O3'	O2′···Fe	0.039	0.184	–0.044	0.045	0.001	0.978
	O3′···Fe	0.035	0.164	–0.039	0.040	0.001	0.975
P-9-O3'-Fe(III)-O4'	O3′···Fe	0.032	0.146	–0.034	0.035	0.001	0.971
	O4′···Fe	0.038	0.189	–0.045	0.046	0.001	0.978
P-1-O6′-Fe-(III)-C7,8	O6′···Fe	0.009	0.030	–0.008	0.008	0.000	1.000
	C7···Fe	0.006	0.017	–0.004	0.004	0.000	1.000

Table 5.26 Bond critical point data and spin density for the studied pedicellin···Fe^{n+} complexes, UB3LYP/6-31+G(d,p) results in water solution

Complex	Bond type	ρ e/Å^3	$\nabla^2\rho$ e/Å^5	V (Hartree)	G (Hartree)	H (Hartree)	$\frac{\lvert V \rvert}{G}$
P-2-O2′-Fe(II)-O9	O2′···Fe	0.092	0.490	–0.146	0.134	–0.012	1.088
	O9···Fe	0.130	0.710	–0.251	0.214	–0.037	1.171
P-2-ring-Fe(II)-B	C1···Fe	0.046	0.144	–0.051	0.043	–0.007	1.170
	C2···Fe	0.046	0.147	–0.052	0.044	–0.007	1.167
	C4···Fe	0.048	0.152	–0.054	0.046	–0.008	1.173
	C5···Fe	0.047	0.152	–0.053	0.045	–0.007	1.164
P-1-O2'-Fe(II)-O3'	O2′···Fe	0.069	0.380	–0.102	0.099	–0.004	1.036
	O3′···Fe	0.070	0.400	–0.106	0.103	–0.003	1.029
P-9-O3'-Fe(II)-O4'	O3′···Fe	0.065	0.369	–0.096	0.094	–0.002	1.020
	O4′···Fe	0.068	0.390	–0.103	0.100	–0.003	1.025
P-1-O6′-Fe-(II)-C7,8	O6′···Fe	0.056	0.312	–0.079	0.079	0.000	1.008
	C7···Fe	0.091	0.152	–0.097	0.067	–0.029	1.434
P-2-O2′-Fe(III)-O9	O2′···Fe	0.071	0.407	–0.108	0.105	–0.003	1.032
	O9···Fe	0.130	0.682	–0.242	0.206	–0.036	1.173
P-2-ring-Fe(III)-B	C4···Fe	0.053	0.151	–0.058	0.048	–0.010	1.216
P-1-O2'-Fe(III)-O3'	O2′···Fe	0.070	0.404	–0.107	0.104	–0.003	1.029
	O3′···Fe	0.072	0.411	–0.109	0.106	–0.003	1.031
P-9-O3'-Fe(III)-O4'	O3′···Fe	0.072	0.415	–0.111	0.107	–0.004	1.034
	O4′···Fe	0.069	0.380	–0.101	0.099	–0.003	1.026
P-1-O6′-Fe-(III)-C7,8	O6′···Fe	0.081	0.416	–0.119	0.111	–0.007	1.065
	C2···Fe	0.050	0.114	–0.047	0.038	–0.009	1.249
	C7···Fe	0.053	0.140	–0.057	0.046	–0.011	1.235

5.3.9. NPA charges, spin density and orbital occupancies

The NPA charges and the spin density values are reported in Table 5.27 for the pedicellin···Fe^{n+} complexes. Among the complexes with the Fe(II) cation the charge is reduced from +2 to a 1.867–1.988 *e* range and from +3 to a 1.652–2.016 *e* range for the Fe(II) and Fe(III) cation respectively. Therefore in water solution, the Fe(II) cation undergoes minimal reduction compared to the *in vacuo* results, a results which was also found for butein, homobutein and kanakugiol. The largest amount of charge transfer corresponds to the coordination of the Fe^{n+} cations to the methoxy–*keto* reactive site for the Fe(II) cation and to the methoxy–α,β–unsaturated reactive site for the Fe(III) cation. Coordination of the Fe(II) cation to the π system of aromatic ring B shows that at this site there is less charge transfer, a different trend is observed for the *in vacuo* study. For the Fe(III) cation the least amount of charge is transferred at the coordination to the methoxy–methoxy site shows.

Table 5.27 NPA charges and spin density values for the Fe^{n+} cations in complexes with pedicellin results in water solution

Complex	charge *(e)*		spin density	
	DFT/B3LYP results	DFT/BP86 results	DFT/B3LYP results	DFT/BP86 results
P-2-O2′-Fe(II)-O9[a]	1.869	1.804	3.914	3.857
P-2-ring-Fe(II)-A[a]	–[a]	–[a]	–[a]	–[a]
P-2-ring-Fe(II)-B	1.988	1.985	3.994	3.989
P-1-O2′-Fe(II)-O3′	1.961	1.876	3.947	3.909
P-9-O3′-Fe(II)-O4′	1.915	1.872	3.939	3.903
P-1-O6′-Fe-(II)-C7,8	1.942	1.894	3.960	3.918
P-2-O2′-Fe(III)-O9[a]	2.016	1.996	3.896	4.154
P-2-ring-Fe(III)-A[a]	–[a]	–[a]	–[a]	–[a]
P-2-ring-Fe(III)-B	1.867		3.889	4.021
P-1-O2′-Fe(III)-O3′	1.935	2.015	3.955	4.044
P-9-O3′-Fe(III)-O4′	1.946	2.026	3.961	4.051
P-1-O6′-Fe-(III)-C7,8	1.979	1.927	3.993	3.940

[a] On optimisation the Fe^{n+} cations migrates from the ring and the two complexes become identical

Analysis of the spin density values suggests that there is a decrease in the spin density values with a 3.914–3.994 range for the Fe(II) which indicates minimal transfer, similar results are obtained for the charge transfer, where is water solution Fe(II) is minimally reduced and a 3.955–3.993 range for the Fe(III) cation. This reduction in the spin density implies that pedicellin has the ability to act as a good antioxidant in both media. The spin density distributions for the pedicellin···Fe^{n+} complexes are shown in Figure 5.20. The trend in the spin density distribution is similar to that reported for kanakugiol, namely, for the pedicellin···Fe^{2+}, the spin density is largely localised on the Fe^{n+} cation while for the pedicellin···Fe^{3+} complexes, the spin density is also delocalised towards the neighbouring rings of the pedicellin molecule.

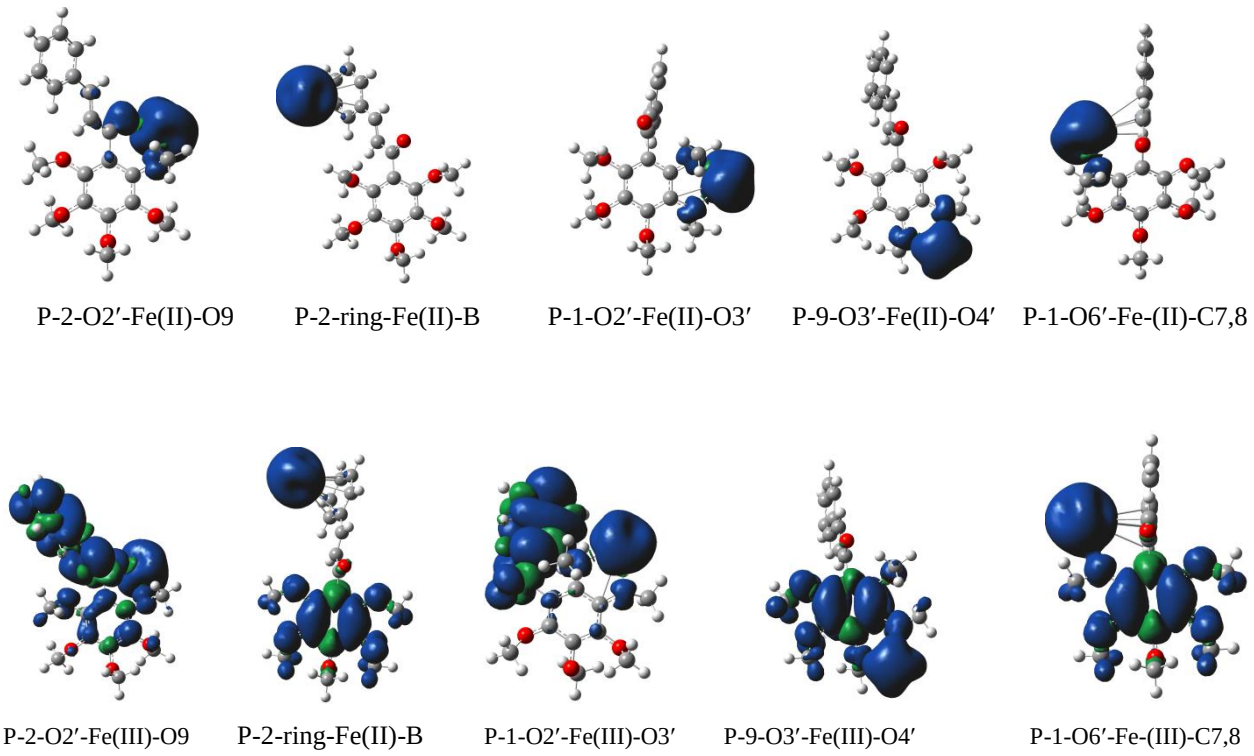

Figure 5.20 Spin density distribution for the pedicellin···Fe^{n+} complexes formed from interactions of neutral pedicellin B3LYP/6-31+G(d,p) results in water solution. The surface isovalue used is 0.0004 au. The blue colour corresponds to positive spin densities and the green colour denotes the negative spin density.

The natural orbital occupancies are reported in Table 5.28 for the pedicellin···Fe^{n+} complexes. Analysis of the 4s orbitals shows that upon coordination to the ligand to from metal···ligand complexes the ligand tends to donate electrons to the Fe^{n+} cations, which is seen by the increase in the occupancy from 0.000 to a 0.002–0.078 *e* range for the Fe(II) cation and from 0.000 to a 0.014–0.126 *e* range for the Fe(III) cation. Analysis of the occupancy of the *d* orbitals among the complexes with the Fe(II) cation suggests that the d_{xy} may have a tendence to donate electrons to the pedicellin ligand while among the complexes with the Fe(III) cation the ligand donates electrons to the partially filled d_{xy} orbital of Fe^{n+} cation. Analysis of the d_{xz}, d_{yz}, $d_{x^2-y^2}$, and the d_{z^2} orbital shows that upon complexation the ligand tends to transfer electron density to the partially filled d_{xz}, d_{yz}, $d_{x^2-y^2}$, and d_{z^2} orbitals of the Fe^{n+} cations. Similar results were obtained for other chalcone derivatives investigated in this work.

Table 5.28 Natural atomic orbital occupancies for some valence orbitals in the isolated Fe^{n+} cations pedicellin···Fe^{n+} complexes in water solution

Isolated and Fe complex	Orbitals and the corresponding natural atomic orbital occupancies					
	S (4s)	d_{xy} (3d)	d_{xz} (3d)	d_{yz} (3d)	$d_{x^2-y^2}$ (3d)	d_{z^2} (3d)
DFT/B3LYP results						
Fe(II)	0.000	1.998	1.000	1.000	1.000	1.000
P-2-O2′-Fe(II)-O9	0.037	1.454	1.102	1.140	1.025	1.345
P-2-ring-Fe(II)-A	–[a]	–[a]	–[a]	–[a]	–[a]	–[a]
P-2-ring-Fe(II)-B	0.002	1.023	1.244	1.681	1.051	1.003
P-1-O2′-Fe(II)-O3′	0.018	1.330	1.075	1.378	1.113	1.141
P-9-O3′-Fe(II)-O4′	0.022	1.233	1.278	1.047	1.411	1.075
P-1-O6′-Fe-(II)-C7,8	0.012	1.149	1.824	1.011	1.017	1.022
Fe(III)	0.000	1.000	1.000	1.000	1.000	1.000
P-2-O2′-Fe(III)-O9	0.036	1.140	1.088	1.095	1.060	1.537
P-2-ring-Fe(III)-A	–[a]	–[a]	–[a]	–[a]	–[a]	–[a]
P-2-ring-Fe(III)-B	0.118	1.165	1.233	1.274	1.117	1.161
P-1-O2′-Fe(III)-O3′	0.015	1.300	1.091	1.396	1.145	1.096
P-9-O3′-Fe(III)-O4′	0.014	1.094	1.257	1.021	1.525	1.126
P-1-O6′-Fe-(III)-C7,8	0.126	1.084	1.120	1.496	1.277	1.168
DFT/BP86 results						
Fe(II)	0.000	1.998	1.000	1.000	1.000	1.000
P-2-O2′-Fe(II)-O9	0.168	1.327	1.138	1.522	1.215	1.404
P-2-ring-Fe(II)-A	–[a]	–[a]	–[a]	–[a]	–[a]	–[a]
P-2-ring-Fe(II)-B	0.098	1.544	1.328	1.609	1.115	1.321
P-1-O2′-Fe(II)-O3′	0.149	1.434	1.369	1.688	1.159	1.079
P-9-O3′-Fe(II)-O4′	0.153	1.246	1.203	1.072	1.498	1.734
P-1-O6′-Fe-(II)-C7,8	0.180	1.359	1.545	1.582	1.182	1.076
Fe(III)	0.000	1.000	1.000	1.000	1.000	1.000
P-2-O2′-Fe(III)-O9	0.121	1.641	1.294	1.124	1.114	1.392
P-2-ring-Fe(III)-A	–[a]	–[a]	–[a]	–[a]	–[a]	–[a]
P-2-ring-Fe(III)-B	0.118	1.165	1.233	1.274	1.117	1.161
P-1-O2′-Fe(III)-O3′	0.111	1.234	1.151	1.813	1.298	1.181
P-9-O3′-Fe(III)-O4′	0.113	1.289	1.203	1.047	1.429	1.709
P-1-O6′-Fe-(III)-C7,8	0.183	1.349	1.329	1.361	1.245	1.312

[a] On optimisation, the Fe^{n+} cation drifts away from the aromatic ring and the two complexes become identical

The results of the study presented in this chapter can be summarised in terms of the prefered binding site, the spin density distribution as well as charge distribution. The prefered binding site is the hydroxy-keto site for kanakugiol and the methoxy-keto site for pedicellin. There is a decrease in the charge as well as the spin density on the Fe^{n+} ions upon coordiation to the ligand. Analysis of the metal orbial occupancies suggests that the 4s orbital occupancy tends to increase, while the occupancy of the d orbitals is variant and non-univocal.

5.4. Comparison of the results obtained with different calculation methods

This section gives a comparison of the results obtained using the DFT/B3LYP method and the DFT/BP86 method. Analysis of the relative stability of the conformers shows that for the conformers of kanakugiol in vacuo, the first four conformers remain the same among the different calculation methods, for the remaining conformers, different trends are observed. Analysis of the conformers of pedicellin shows different trends in the relative stability of the conformers with DFT/B3LYP and the DFT/BP86 method. In water solution, a comparison of the kanakugiol conformers across the different methods shows that only the lowest-energy conformer remains the same, the remaining conformers show different trends. The conformers of pedicellin show similar trends to those of kanakugiol that in water solution. However the relative energy values shows that the DFT/BP86 method gives higher values than the DFT/B3LYP method. The same trend is observed for the relative energy values of the complexes of the Fe^{n+} cations with either kanakugiol or pedicellin (i.e., values are higher with DFT/BP86 than with DFT/B3LYP).

Analysis of the binding energy values suggest that in both media, the DFT/BP86 method tends to overestimate the binding energy with respect to the values obtained using the DFT/B3LYP method. The extent of overestimation is dependent on the site at which the metal ion is coordinated. The tendency for BP86 functional to overestimate the binding energy has also been reported for the butein and homobutein complexes (Chapter 4).

The result of the charges and the spin density values shows that the is no specific trend to be identified that in some complexes the DFT/B3LYP method shows the greatest reduction in charge while for some complexes the DFT/BP86 shows the greatest reduction in charge for both Fe(II) and Fe(III) complexes *in vacuo* and in water solution. A similar conclusion was arrived at when comparing the performance of these methods on the determining the charges and spin density values for butein and homobutein.

CHAPTER 6

SUMMARY, CONCLUSIONS AND RECOMMENDATIONS

The iron chelation ability of four chalcone derivatives namely, butein, homobutein, kanakugiol and pedicellin has been investigated with the aim of elucidating their antioxidant properties, *in vacuo* and in water solution. Three parameters, which provide information on the antioxidant properties, which were investigated, are the metal ion affinity, spin density and partial charges on the metal cations. The study has been performed using the DFT/B3LYP and DFT/BP86 methods; the 6-31+G(d,p) basis set has been selected for the description of the C, H and O atoms while the LANL2DZ basis set has been selected for the Fe^{n+} cations. Single point calculations, using the 6-311+G(2d,p) basis set, have been performed to refine the energies.

The initial study for each of the chalcone derivative involved the investigation of the preferred conformation. The results show that conformational stability is influenced by an interplay between intramolecular hydrogen bonds, arrangement of the 2-propen-1-one aliphatic chain, orientation of the methoxy groups (i.e., in the kanakugiol and pedicellin ligands) and in water solution, the solvent effects. The presence of the intramolecular hydrogen bonds plays the greatest role in conformational stability. The influence of the aliphatic chain arrangement is such that the conformers with the non-bent chain are preferred for butein, homobutein and kanakugiol and conformers with the bent chain are preferred for pedicellin. In water solution the relative energies of the conformers is dampened with respect to the results *in vacuo* such that some of the conformers that are considered not populated *in vacuo* are populated in water solution. The preference of such conformers is related to their ability to interact with solvent molecules.

Analysis of the relative energy results obtained for the ligand···Fe^{n+} complexes shows that for both the results *in vacuo* and in water solution the most preferred coordination are at the hydroxyl–*keto* reactive site for butein and homobutein, while for pedicellin it is the methoxy–*keto* reactive site. Among the complexes of kanakugiol, the preferred binding sites include the hydroxyl–*keto* and the hydroxyl–methoxy reactive sites. Complexes formed by coordinating the Fe^{n+} ion at all other possible reactive sites can be considered not to exist *in vacuo*. However, in water solution, the relative energy among the different complexes are significantly decreased such that coordination at other reactive sites, such as the methoxy-

methoxy, may be observed *in vivo*. The implication for the results reported here is that the metal chelation antioxidant activity of the studied chalcone derivatives may be related to the coordination of the Fe^{n+} cations at the hydroxyl–*keto* reactive site for butein, homobutein and kanakugiol and at the methoxy–*keto* reactive site for pedicellin.

The metal ion affinity values for all the metal-ligand complexes investigated have positive values, which suggest that the selected chalcone derivatives are able to bind the Fe^{n+} cations *in vacuo* and in water solution. In water solution the binding energies are significantly dampened indicating that interactions in water solution are weaker than interactions *in vacuo*. However, with all the calculation methods and in all the media, the strongest interaction between the ligand and the Fe^{n+} cations involves the hydroxyl–*keto* reactive site for butein, homobutein and kanakugiol, and involves the methoxy–*keto* reactive site for pedicellin. The implication for these findings is that the Fe^{n+} cation rarely binds at the methoxy-methoxy reactive sites present in both kanakugiol and pedicellin, which in turn implies that the antioxidant properties of the studied compounds is most probably related to their ability to interact with the Fe^{n+} ions at the hydroxyl–*keto* reactive site for butein, homobutein and kanakugiol, and at the methoxy–*keto* reactive site for pedicellin. The deprotonated species of butein, homobutein and kanakugiol give higher Fe^{n+} ion affinity than the corresponding neutral species, which may be related to the high electron density of the deprotonated anion species. This result implies that deprotonated species of chalcone derivatives are likely to exhibit greater antioxidant properties than the corresponding neutral species.

The metal ion affinity ordering among the ligand species often corresponds to their antioxidant activity. A comparison of the Fe^{n+} ion affinity for kanakugiol and pedicellin with that of butein and homobutein indicates that the former are better Fe chelators than the latter. The results obtained also show that the selected chalcone derivatives tend to bind the Fe(III) cation better than they do the Fe(II) cation. The ability of the Fe(III) to bind all chalcone derivatives much stronger than Fe(II) cation; Fe(III) is considered as a hard Lewis acid while Fe(II) is a borderline Lewis acid, and does not bind as strongly to the hard O atoms of polyphenols as does Fe(III). In comparison with other groups of polyphenols, the binding energies values for butein, homobutein, kanakugiol and pedicellin suggests that they are lower than those of flavonoids such as quercetin, which implies that chalcone derivatives may be weaker metal chelators than flavonoids.

The atom in molecule (AIM) analysis scheme was also utilised to investigate the nature of the bonding between the metal ion and the ligand molecules. The results suggest that the strongest bond corresponds to the coordination of the cation to the *keto* O atom, and that *in vacuo*, the in interactions between the cation and the ligands tend to be dative in character while in water solution, the interaction between the cation and the ligand tend to be pure ionic in nature.

An appraisal of the reducing ability of the selected chalcone derivatives was performed through analysis of the partial atomic charge on the Fe^{n+} ions when coordinated at a particular site on the ligand. *In vacuo*, there is significant positive charge transfer for both the Fe(II) and the Fe(III) cations while in water solution there is minimal charge transfer for the Fe(II) cation. This result may imply that in water solution the chalcone derivatives only chelate the Fe(II) cation without necessarily reducing it while the Fe(III) cation is both chelated and reduced to Fe(II). The ability of the selected chalcone derivatives to reduce Fe(III) ion to Fe(II) ion is another indication of the possible antioxidant effectiveness of the selected chalcone derivatives. This observation is further supported by the reduction in the spin density of the Fe^{n+} cations.

The results reported in this work provide a reasonable starting basis for understanding the metal chelation antioxidant properties of chalcone derivatives. However, it is worth considering that there can be further improvements on various level of this study in order to enhance the simulation of the antioxidant activities of chalcone derivatives, and indeed other groups of compounds that exhibit antioxidant properties. For instance, a recommendation is made that further studies on the antioxidant properties of chalcone derivatives should consider inclusion of the polarisation functions for the description of the Fe^{n+} cations – in order to improve the description of the geometries of the resultant complexes. Future studies could also consider investigating the antioxidant properties of chalcone derivatives in non-polar media, since the biological media consist of aqueous medium and non-aqueous medium; therefore, it would be meaningful to also simulate the metal chelation mechanism in non-polar medium. Another recommendation that is of high importance, is related to the stoichiometry ratio between the ligand and the metal ion. Polyphenol derivatives are known to chelate transition metal ions with a variety of stoichiometries. Complexes with a metal:polyphenol ratio of 1:1, 1:2, 2:2 and 2:3 stoichiometries have been reported. The current study investigated only the 1:1 stoichiometry ratio. It is therefore recommended that future studies could consider investigation of at least the 1:2 stoichiometry ratio, whenever computational affordability allows for such studies.

REFERENCES

1. I. M. Møller, P. E. Jensen, A. Hansson, Oxidative modifications to cellular components in plants, *Annual Review* of *Plant Biology*, 58 (2007) 459–481.
2. M. Valko, C. J. Rhodes, J. Moncol, M. Izakovic, M. Mazur, Free radicals, metals and antioxidants in oxidative stress-induced cancer, *Chemico-Biological Interactions*, 160 (2006) 1–40.
3. P. Amunaa, F. B. Zotora, Epidemiological and nutrition transition in developing countries: impact on human health and development, *Proceedings of the Nutrition Society*, 67 (2008) 82–90.
4. S-F. Barbuceanu, D. C. Ilies, G. Saramet, V. Uivarosi, C. Draghici, V. Radulescu, Synthesis and antioxidant activity evaluation of new compounds from hydrazinecarbothioamide and 1,2,4-triazole class containing diarylsulfone and 2,4-difluorophenyl moieties, *International Journal of Molecular Sciences*, 15 (2014) 10908–10925.
5. B. Dimitrios, Sources of natural phenolic antioxidants, *Trends in Food Science & Technology*, 17 (2006) 505–512.
6. M. S. Brewer, Natural antioxidants: sources, compounds, mechanisms of action, and potential applications, *Comprehensive Reviews in Food Science and Food Safety*, 10 (2011) 221–247.
7. C. Delgado-Andrade, J. A. Rufiaán-Henares, F. J. Morales, Assessing the antioxidant activity of melanoidins from coffee brews by different antioxidant methods, *Journal of Agricultural Food Chemistry*, 53 (2005) 7832–7836.
8. H. J. Suh, M. S. Chung, Y. H. Cho, J. W. Kim, D. H. Kim, K. W. Han, J. Kim, Estimated daily intakes of butylated hydroxyanisole (BHA), butylated hydroxytoluene (BHT) and *tert*butyl hydroquinone (TBHQ) antioxidants in Korea, *Food Additives & Contaminants*, 22 (2005) 1176–1188.
9. G. M. Williams, M. Latropoulos, J. Whysner, safety assessment of butylated hydroxyanisole and butylated hydroxytoluene as antioxidant food additives, *Food Chemical Toxicology*, 37 (1999) 1027–1038.
10. B. Sun, M. Fukuhara, Effects of co-administration of butylated hydroxytoluene, butylated hydroxyanisole and flavonoids on the activation of mutagens and drug-metabolizing enzyme in mice, *Toxicology*, 122 (1997) 61–72.

11. V. Chobot, Simultaneous detection of pro- and antioxidative effects in the variants of the deoxyribose degradation assay, *Journal of Agricultural and Food Chemistry*, 58 (2010**)** 2088–2094.
12. E. Hernandez-Marin, A. Galano, A. Martínez, *Cis* carotenoids: colorful molecules and free radical quenchers, *The Journal of Physical Chemistry B*, 117 (2013**)** 4050–4061.
13. A. Galano, N. A. Macías-Ruvalcaba, O. N. M. Campos, J. Pedraza-Chaverri, Mechanism of the OH radical scavenging activity of nordihydroguaiaretic acid: a combined theoretical and experimental study, *Journal of Physical Chemistry B*, 114 (2010) 6625–6635.
14. S. Signorelli, E. L. Coitiño, O. Borsani, J. Monza, Molecular mechanisms for the reaction between •OH radicals and proline: insights on the role as reactive oxygen species scavenger in plant stress, *Journal of Physical Chemistry B*, 118 (2014) 37–47.
15. N. Agnihotri, P. C. Mishra, Mechanism of scavenging action of n-acetylcysteine for the OH radical: a quantum computational study, *Journal of Physical Chemistry B*, 113 (2009) 12096–12104.
16. J. Ren, S. Meng, Ch. E. Lekka, E. Kaxiras, Complexation of flavonoids with iron: structure and optical signature, *Journal of Physical Chemistry B*, 112 (2008) 1845–1850.
17. A. Primikyri, G. Mazzone, C. Lekka, A. G. Tzakos, N. Russo, I. P. Gerothanassis, Understanding Zinc(II) chelation with quercetin and luteolin: a combined NMR and theoretical study, *The Journal of Physical Chemistry B*, 119 (2015**)** 83–95.
18. M. Francisco-Marquez, M. Aguilar-Fernández, A. Galano, Anthranilic acid as a secondary antioxidant: implications to the inhibition of OH production and the associated oxidative stress, *Computational and Theoretical Chemistry*, 1077 (2016) 18–24.
19. T. Enoki, H. Ohnogi, K. Nagamine, Y. Kudo, K. Sugiyama, M. Tanabe, E. Kobayashi, H. Sagawa, I. Kato, Antidiabetic activities of chalcones isolated from a Japanese herb *Angelica keiskei*, *Journal of Agricultural and Food Chemistry*, 55 (2007) 6013–6017.
20. M. Rajendran, M. T. Devi, Antioxidant and metal chelation efficiency of chalcone derivatives, *Journal of Chemical Biological and Physical Sciences*, 4 (2013) 38–52.
21. H. Iqbal, V. Prabhakar, A. Sangith, B. Chandrika, R. Balasubramanian, Synthesis, anti-inflammatory and antioxidant activity of ring-A-monosubstituted chalcone derivatives, *Medicinal Chemistry Research*, 23 (2014) 4383–4394.
22. V. R. Yadav, S. Prasad, B. Sung, B. B. Aggarwal, The role of chalcones in suppression of NF-κB-mediated inflammation and cancer, *International Immunopharmacology*, 11 (2011) 295–309.

23. Z. Rozmer, P. Perjési, Naturally occurring chalcones and their biological activities, *Phytochemistry Reviews*, 10 (2014) 11101–11014.
24. Z. Nowakowska, A review of anti-infective and anti-inflammatory chalcones, *European Journal of Medicinal Chemistry*, 42 (2007) 125–137.
25. T-D. Tran, T-T-N. Nguyen, T-H. Do, T-N-P. Huynh, C-D. Tran, K-M. Thai, Synthesis and antibacterial activity of some heterocyclic chalcone analogues alone and in combination with antibiotics, *Molecules*, 17 (2012) 6684–6696.
26. L. E. Alcaraz, S. E Blanco, O. N. Puig, F. Tomas, F. H. Ferretti, Antibacterial activity of flavonoids against methicillin- resistant *Staphylococcus Aureus* strains, *Journal of Theoretical Biology*, 205 (2000) 231–240.
27. R. Li, G. L. Kenyon, F. E. Cohen, X. Chen, B. Gong, J. N. Dominguez, E. Davidson, G. Kurzban, R. E. Miller, E. O. Nuzum, P. J. Rosenthal, J. H. McKerrowis, In vitro antimalarial activity of chalcones and their derivatives, *Journal of Medicinal Chemistry*, 38 (1995) 5031–5037.
28. K. L. Lahtchev, D. I. Batovska, St. P. Parushev, V. M. Ubiyvovk, A. A. Sibirny, Antifungal activity of chalcones: a mechanistic study using various yeast strains, *European Journal of Medicinal Chemistry*, 43 (2008) 2220–2228.
29. D. P. Belsare, S. C. Pal, A. A. Kazi, R. S. Kankate, S. S. Vanjari, Evaluation of antioxidant activity of chalcones and flavonoids, *International Journal of ChemTech Research*, 2 (2010) 1080–1089.
30. S. Singh, P. K. Sharma, N. Kumar, R. Dudhe, Antioxidant activity of 2-hydroxyacetophenone chalcone, *Journal of Advances Scientific Research*, 2 (2011) 37–41.
31. J. C. Trivedi, J. B. Bariwal, K. D. Upadhyay, Y. T. Naliapara, S. K. Joshi, C. C. Pannecouque, E. De Clercq, A. K. Shah, Improved and rapid synthesis of new coumarinyl chalcone derivatives and their antiviral activity, *Tetrahedron Letters*, 48 (2007) 8472–8474.
32. H. Fan, T. Zheng, Y. Chen, G. Yang, Chemical constituents with free-radical-scavenging activities from the stem of *Fissistigma Polyanthum*, *Pharmacognosy Magazine*, 30 (2012) 98–102.
33. C-T. Hsieh, T-J. Hsieh, M. El-Shazly, D-W. Chuang, Y-H. Tsai, C-T. Yen, S-F. Wu, Y-C. Wu, F-R. Chang, Synthesis of chalcone derivatives as potential anti-diabetic agents, *Bioorganic and Medicinal Chemistry Letters*, (2012), DOIi.org/10.1016/j.bmcl.2012.04.108.

34. M. Andjelković, J. V. Camp, B. De Meulenaer, G. Depaemelaere, C. Socaciu, M. Verloo, R. Verhe Iron-chelation properties of phenolic acids bearing catechol and galloyl groups, *Food Chemistry*, 98 (2006) 23–31.
35. D. Maydt, S. De Spirt, C. Muschelknautz, W. Stahl, T. J. J. Muller, Chemical reactivity and biological activity of chalcones and other α, β-unsaturated carbonyl compounds, *Xenobiotica*, 43 (2013) 711–718.
36. C. A. C. Araújo, L. L. Leon, Biological activities of *curcuma longa L*. *Memórias do Instituto Oswaldo Cruz*, 96 (2001) 723–728.
37. N. R. Perron, H. C. Wang, S. N. DeGuire, M. Jenkins, M. Lawson, J. L. Brumaghim, Kinetics of iron oxidation upon polyphenol binding, *Dalton Transactions*, (2010) 9982–9987.
38. S. Shenvi, K. Kumar, K. S. Hatti, K. Rijesh, L. Diwakar, G. C. Reddy, Synthesis, anticancer and antioxidant activities of 2,4,5-trimethoxy chalcones and analogues from asaronaldehyde: structure–activity relationship, *European Journal* of *Medicinal Chemistry*, 62 (2013) 435–442.
39. H. S. Kareem, A. Ariffin, N. Nordin, T. Heidelberg, A. Abdul-Aziz, K. W. Kong, W. A. Yehye, Correlation of antioxidant activities with theoretical studies for new hydrazone compounds bearing a 3,4,5-trimethoxy benzyl moiety, *European Journal* of *Medicinal Chemistry*, 103 (2015) 497–505.
40. M. Salih, A. Gırtas, B. Cabir, S. Ozdemir, Novel metal (II) phthalocyanines with 3,4,5-trimethoxybenzyloxy-substituents: synthesis, characterization, aggregation behaviour and antioxidant activity, *Dyes Pigments*, 96 (2013) 152–157.
41. S. A. B. E. Van Acker, G. P. Balen, Influence of iron chelation on the antioxidant activity of flavonoids, *Biochemical Pharmacology*, 56 (1998) 935–943.
42. S. C. Chan, Y. S. Chang, J. P. Wang, S. C. Chen, S. C. Kuo, Three new flavonoids and antiallergic, anti-inflammatory constituents from the heartwood of *Dalbergia odorifera*, *Planta Medica*, 64 (1998) 53–158.
43. A. G. F. R. S. Perkin, J. J. Hummel, The colouring principle of the flowers of the *Butea frondosa*, *Journal* of the *Chemical Society Transactions*, 85 (1904) 1459–1472.
44. A. Yenesew, S. Derese, B. Irungu, J. O. Midiwo, N. C. Waters, P. Liyala, H. Akala, M. Heydenreich, M. G. Peter, Flavonoids and isoflavonoids with antiplasmodial activities from the root bark of *Erythrina abyssinica*. *Planta Medica*, 69 (2003) 658–661.
45. J. C. La Duke, Flavonoid chemistry and systematics of tithinia (composiate), *American Journal of Botany*, 5 (1982) 784–792.

46. M. E. L. Almeida, R. de Braz Filho, M. V. Bulow, J. J. L. Correa, O. R. Gottlieb, J. G. S. Maia, M. S. da Silva, Diarylpropanoids from *Iryanthera polyneura*, *Phytochemistry*, 18 (1979) 1015–1016.
47. S. M. S. Lee, H. C. Baek, H. Lee, H. B. Lee, Y. H. Kho, Cytotoxicity of lignans from *Lindera erytherocarpa* Makino, *Natural Product Sciences*, 8 (2002) 100−102.
48. Y-W. Leong, L. J. Harrison, G. J. Bennett, A. A. Kadir, J. D. Connolly, A dihydrochalcone from *Lindera lucida*, *Phytochemistry*, 47 (1998) 891–894.
49. W. Ahmad, A. M. A. Zaidi, S. Ahmad, Quality control analysis of *Didymocarpus Pedicellatus* R. Br, *Indian Journal of Traditional Knowledge*, 13 (2014) 175–180.
50. J. S. Rathore, S. K. Garg, S. R. Gupta, A chalcone and flavanones from *Didymocarpus Pedicellata*, *Phytochemistry*, 20 (1981) 1755–1756.
51. V. Sharma, Siddiqui, The constituents of *Didymocarpus pedicellata* part II. Comparative studies in the constitution of pedicin, isopedicin, pedicinin and pedicellin, *Journal of Indian Chemical Society*, 16 (1939) 1–8.
52. G. Cioffi, L. M. Escobar, A. Braca, N. De Tommasi, Antioxidant chalcone glycosides and flavanones from Maclura (Chlorophora) tinctoria, *Journal of Natural Products*, 66 (2003) 1061−1064.
53. H. Braham, Z. Mighri, H. B. Jannet, S. Matthew, P. M. Abreu, Antioxidant phenolic glycosides from *Moricandia arvensis*, *Journal of Natural Products*, 68 (2005) 517–522.
54. M. Akhavan, A. Shafaghat, F. Salimi, Novel acetylated chalcone and biflavonoid glycosides from *Trigonosciadium brachytaenium (Boiss.) Alava*, *Natural Product Research*, 27 (2013) 2111–2117.
55. N. R. Perron, J. L. Brumaghim, A review of the antioxidant mechanisms of polyphenol compounds related to iron binding, *Cell Biochemistry and Biophysics*, 53 (2009) 75–100.
56. B. Halliwell, J. M. C. Gutteridge, Biologically relevant metal ion-dependent hydroxyl radical generation, *FEBS Letters*, 307 (1992) 108–112.
57. M. Guo, C. Perez, Y. Wei, E. Rapoza, G. Su, F. Bou-Abdallah, N. D. Chasteen, Iron-binding properties of plant phenolics and cranberry's bio-effects, *Dalton Transactions*, (2007) 4951–4961.
58. Z-J. Cheng, S-C. Kuo, S-C. Chan, F-N. Ko, C-M. Teng, Antioxidant properties of butein isolated from *Dalbergia odorifera*, *Biochimica et Biophysica Acta* 1392 (1998) 291–299.
59. P. Guo, W. Chen, J. Song, W. Cao, C. Tian, DFT study of the interaction between butein anion and metal cations (M = Mg^{2+}, Cr^{2+}, Fe^{2+}, and Cu^{2+}): taking an insight into its chelating property, *Journal of Molecular Structure* (*theochem*), 849 (2008) 33–36.

60. W. J. Hehre, *A guide to molecular mechanics and quantum chemical calculations*, 1st edition, Wavefunction Inc., United States of America, 2003.
61. E. G. Lewars, *Computaional chemistry*: *introduction to the theory and applications of molecular and quantum mechanics*, 1st edition, Kluwer Academic Publishers, United States of America, 2004.
62. E. G. Lewars, *Computaional chemistry*: *introduction to the theory and applications of molecular and quantum mechanics*, 2nd edition, Kluwer Academic Publishers, United States of America, 2011.
63. J. D. Cutnell, K. W. Johnson, *Physics*, 7th edition, John Wiley & Sons Inc., United States of America, 2007.
64. P. W. Atkins, *Physical Chemistry*, 4th edition, Oxford University Press, United States, 1990.
65. P. W. Atkins, J. De Paula, *Physical chemistry*, 8th edition, Oxford University Press, United States, 2006.
66. P. W. Atkins, J. De Paula, *Physical chemistry*, 9th edition, Oxford University Press, United States, 2010.
67. F. Jensen, *Introduction to computational Chemistry*, John Wiley & Sons, Chichester, United States of America, 1999.
68. F. Jensen, *Introduction to computational*, 2nd edition, John Wiley and Sons, Ltd, United States of America, 2007.
69. T. Engel, P. Reid, *Physical Chemistry*, 2nd edition, Pearson education, Inc., United States of America, 2006.
70. I. Jones, T. J. Rainsford, B. M. Fischer, D. Abbott, Calculation of low-frequency vibrational modes of biologically important isomers, *Proceedings of SPIE*, 6416 (2006) 641607–641611.
71. P. W. Abegg, T. K. Ha, *Ab initio* calculation of spin-orbit-coupling constant from Gaussian lobe SCF molecular wavefunctions, *Molecular Physics*, 27 (1974) 763–67.
72. E. R. Davidson, D. Feller, Basis set selection for molecular calculations, *Chemical Reviews*, 86 (1988) 661–696.
73. D. A. McQuarrie, J. D. Simon, *Physical Chemistry: a molecular approach*, 1st edition, University Science Books, Sausalito California, United States of America, 1997.
74. X. Xu, D. G. Truhlar, Performance of effective core potentials for density functional calculations on 3d transition metals, *Journal Chemical Theory Computation*, 8 (2012) 80–90.

75. N. E. Schultz, D. G. Truhlar, New effective core method (effective core potential and valence basis set) for Al clusters and nanoparticles and heteronuclear Al-containing molecules, *Journal Chemical Theory Computation*, 1 (2005) 41–53.
76. X. Xu, D. G. Truhlar, Accuracy of effective core potentials and basis sets for density functional calculations, including relativistic effects, as illustrated by calculations on arsenic compounds, *Journal Chemical Theory Computation*, 7 (2011) 2766–2779.
77. Y. Yang, M. N. Weaver, K. M. Merz Jr, Assessment of the '6–31+G** + LANL2DZ mixed basis set coupled with density functional theory methods and effective core potential: prediction of heats of formation and ionization potentials for first row transition metal complexes, *Journal of Physical Chemistry*, 113 (2009) 9843–9851.
78. P. W. Atkins, R. S. Friedman, *Molecular quantum mechanics*, 3rd edition, Oxford University Press, New York, 1997.
79. S. Hammes-Schiffer, H. C. Andersen, The advantages of the general Hartree-Fock method for future computer simulation of materials, *Journal of Chemical Physics*, 99 (1993) 1901–1913.
80. D. C. Young, *Computational chemistry: a practical guide for applying techniques to real-world problems*, 1st edition John Wiley & Sons, Inc., New York, 2001.
81. M. J. S. Dewar, E. G. Zoebisch, E. F. Healy, AM1: a new general purpose quantum mechanical molecular model, *Journal of the American Chemical Society*, 107 (1985) 3902–3909.
82. J. J. P. Stewart, Optimization of parameters for semi-empirical methods I. method, *Journal of Computational Chemistry*, 10 (1989) 209–220.
83. R. C. Bingham, M. J. S. Dewar, D. H. Lo, Ground states of molecules. XXV. MINDO/3. Improved version of the MINDO semi-empirical SCF-MO method, *Journal of the American Chemical Society*, 97 (1975) 1285–1293.
84. M. C. Zerner, G. H. Loew, R. F. Kirchner, U. T. Mueller-Westerhoff, An intermediate neglect of differential overlap technique for spectroscopy of transition-metal complexes ferrocene, *Journal of the American Chemical Society*, 102 (1980) 589–599.
85. A. Hinchliffe, *Molecular modelling for beginners*, 2nd edition, John Wiley & Sons Ltd, West Sussex, United Kingdom, 2008.
86. W. Koch, M. C. Holthausen, *A chemist's guide to density functional theory*, 2nd edition, John Wiley and Sons Ltd., New York, 2001.

87. D. N. Laikov, Fast evaluation of density functional exchange-correlation terms using the expansion of the electron density in auxiliary basis sets, *Chemical Physics Letters*, 281 (1997) 151–156.
88. I. Jones, T. J. Rainsford, B. M. Fischer, D. Abbott, Calculation of low-frequency vibrational modes of biologically important isomers, *Proceedings of SPIE*, 6416 (2006) 641607–641611.
89. C. Adamo, V. Barone, Toward reliable density functional methods without adjustable parameters: the PBE0 model, *Journal of Physics and Chemistry*, 110 (1999) 6158–69.
90. G. D. Mahan, *Many-particle physics*, 3rd edition, Kluwer Academic/Plenum Publishers, New York, 2000.
91. A. I. Liechtenstein, M. I. Katsnelson, V. P. Antropoy, V. A. Gubanov, Local spin density functional approach to the theory of exchange interactions in ferromagnetic metals and alloys, *Journal of Magnetism and Magnetic Materials*, 67 (1987) 65–74.
92. A. D. Becke, Density-functional exchange-energy approximation with correct asymptotic-behavior, *Physical Review A*, 38 (1988) 3098–3100.
93. J. P. Perdew, K. Burke, Y. Wang, Generalized gradient approximation for the exchange-correlation hole of a many-electron system, *Physical Review B*, 54 (1996) 16533–16539.
94. C. J. Cramer, *Essentials of computational chemistry: theories and models*, 2nd edition, John Wiley and Sons Ltd., United States of America, 2004.
95. J. P. Perdew, K. Burke, M. Ernzerhof, Generalized gradient approximation made simple, *Physical Reviews Letters*, 77 (1996) 3865–3868.
96. C. Lee, W. Yang, R. G. Parr, Development of the Colle-Salvetti correlation-energy formula into a functional of the electron density, *Physical Reviews B*, 37 (1988) 785–789.
97. A. Droghetti, D. Alfé, S. Sanvito, Ground state of a spin-crossover molecule calculated by diffusion Monte Carlo, *Physical Review B*, 87 (2013) 205114–205115.
98. K. Sharkas, A. Savin, H. Jørgen, A. Jensen, J. Toulouse, A multi-configurational hybrid density functional theory, *The Journal of Chemical Physics*, 137 (2012) 044104–044110.
99. Y. Zhao, D. G. Truhlar, The M06 suite of density functionals for main group thermochemistry, thermochemical kinetics, noncovalent interactions, excited states, and transition elements: two new functionals and systematic testing of four M06-class functionals and 12 other functionals, *Theoretical Chemistry Accounts*, 120 (2008) 215–241.

100. Y. Zhao, D. G. Truhlar, Comparative DFT study of van der Waals complexes: rare-gas dimers, alkaline-earth dimers, zinc dimer, and zinc-rare-gas dimers, *Journal of Physical Chemistry*, 110 (2006) 5121−5129.
101. N. Prabhu, K. Sharp, Protein−solvent interactions, *Chemical Reviews*, 106 (2006) 1616−1623.
102. L. Mammino, M. M. Kabanda, Considering the medium when studying biologically active molecules: motivation, options and challenges, in Z. ul Haq,
103. A. V. Marenich, C. J. Cramer, D. G. Truhlar, Universal solvation model based on solute electron density and on a continuum model of the solvent defined by the bulk dielectric constant and atomic surface tensions, *Journal of Physical Chemistry B*, 113 (2009) 6378–6396.
104. D. Riccardi, G. Li, Q. Cui, Importance of van der Waals interactions in QM/MM simulations, *Journal of Physical Chemistry B*, 108 (2004) 6467–6478.
105. J. A. Rank, D. Baker, Contributions of solvent–solvent hydrogen bonding and van der Waals interactions to the attraction between methane molecules in water, *Biophysical Chemistry*, 71 (1998) 199–204.
106. J. Tomasi, B. Mennucci, E. Cancès, The IEF version of the PCM solvation method: an overview of a new method addressed to study molecular solutes at the QM ab initio level, *Journal of Molecular Structure* (*theochem*), 464 (1999) 211–226.
107. V. Barone, M. Cossi, Quantum calculation of molecular energies and energy gradients in solution by a conductor solvent model, *Journal of Physical Chemistry A*, 102 (1998) 1995–2001.
108. J. Tomasi, M. Persic, Molecular interactions in solution: an overview of methods based on continuous distributions of the solvent, *Chemical Reviews*, 94 (1994) 2027–2094.
109. W. Im, D. Beglov, B. Roux, Continuum solvation model: computation of electrostatic forces from numerical solutions to the Poisson-Boltzmann equation, *Computer Physics Communications*, 111 (1998) 59–75.
110. C. J. Cramer; D. G. Truhlar, *Continuum solvation models: classical and quantum mechanical implementations*, VCH publishers, New York, 1995.
111. C. J. Fennell, K. A. Dill, Physical modeling of aqueous solvation, *Journal of Statistical Physics*, 145 (2011) 209–226.
112. R. M. Levy, E. Gallicchio, Computer simulations with explicit solvent: recent progress in the thermodynamic decomposition of free energies and in modeling electrostatic effects, *Annual Review* of *Physical Chemistry*, 49 (1998) 531–567.

113. M. Leopoldini, Nino Russo, S. Chiodo, M Toscano, Iron chelation by the powerful antioxidant flavonoid quercetin, *Journal of Agricultural and Food Chemistry,* 54 (2006) 6343−6351.
114. L. Mammino, M. M. Kabanda, A computational study of the interactions of the phloroglucinol molecule with water, *Journal of Molecular Structure* (*theochem*), 852 (2008) 36–45.
115. P. Florová, P. Sklenovský, P. Banáš, M. Otyepka, Explicit water models affect the specific solvation and dynamics of unfolded peptides while the conformational behavior and flexibility of folded peptides remain intact, *Journal of Chemical Theory and Computations*, 6 (2010) 3569–3579.
116. P. F. B. Gončalves, H. Stassen, New approach to free energy of solvation applying continuum models to molecular dynamics simulation, *Journal of Computational Chemistry*, 23 (2002) 706–714.
117. F. Zheng, C-G. Zhan, Computational modelling of solvent effects on protein-ligand interactions using fully polarizable continuum model and rational drug design, *Communication Computer Physics*, 13 (2013) 31−60.
118. C. J. Cramer, D. G. Truhlar, *Structure and reactivity in aqueous solutions: an overview*, Washington DC, 1994.
119. J. B. Foresman, A. Frisch, *Exploring chemistry with electronic structure methods*, 2nd edition, Gaussian, Inc. Pittsburgh, PA, 1996.
120. A. Klamt, Conductor-like screening model for real solvents: a new approach to the quantitative calculation of solvation phenomena, *Journal of Physical Chemistry*, 99 (1995) 2224−2235.
121. P. Ren, J. Chun, D. G. Thomas, M. J. Schnieders, M. Marucho, J. Zhang, N. A. Baker, Biomolecular electrostatics and solvation: a computational perspective, *Quarterly Reviews of Biophysics*, 45 (2012) 427–491.
122. A. V. Marenich, C. J. Cramer, D. G. Truhlar, Performance of SM6, SM8, and SMD on the SAMPL1 test set for the prediction of small-molecule solvation free energies, *Journal of Physical Chemistry B*, 113 (2009) 4538–4543.
123. R. F. Ribeiro, A. V. Marenich, C. J. Cramer, D. G. Truhlar, Prediction of SAMPL2 aqueous solvation free energies and tautomeric ratios using the SM8, SM8AD and SMD solvation models, *Journal* of *Computer Aided Molecular*, 24 (2010) 317–333.
124. J. Tomasia, B. Mennuccia, E. Cancès, The IEF version of the PCM solvation method: an overview of a new method addressed to study molecular solutes at the QM *ab initio* level, *Journal of Molecular Structure* (*theochem*), 464 (1999) 211–226.

125. J. V. Ponomanenko, M. P. Ponomarenko, A. S. Frolov, D. G. Vorobyev, G. C. Overton, N. A. Kolchavov, Conformational and physicochemical DNA features specific for transcription factor binding sites, *Bioinformatics*, 15 (1999) 654–668.
126. J. Uthuppan, K. Soni, Conformational analysis: a review, *The Journal of Pharmaceutical Sciences and Research*, 4 (2013) 34−41.
127. S-W. Yin, C-H. Tang, Q-B. Wen, X-Q. Yang, D-B. Yuan, The relationships between physicochemical properties and conformational features of succinylated and acetylated kidney bean (*Phaseolus vulgaris* L.) protein isolates, *Food Research International*, 43 (2010) 730–738.
128. C-H. Tang, X. Sun, A comparative study of physicochemical and conformational properties in three vicilins from *Phaseolus legumes*: implications for the structure−function relationship, *Food Hydrocolloids*, 25 (2011) 315–324.
129. G. Siligardi, B. Samorì, S. Melandri, M. Visconi, A. F. Drake, Correlations between biological activities and conformational properties for human, salmon, eel, porcine calcitonins and elcatonin elucidated by CD spectroscopy, *European Journal of Biochemistry*, 221 (1994) 1117–1125.
130. R. E. Taylor, J. Zajicek. Conformational properties of epothilone, *Journal of Organic Chemistry*, 64 (1999) 7224–7228.
131. E. Wünsch, R. Scharf, E. Peggion, M. T. Foffani, J. P. Bali, Conformational properties of gastrin peptides: synthesis, biological activity, and preliminary CD characterization of the (Asp)5 analog of des-Trp1, Leu12-Minigastrin, *Biopolymer*, 25 (1986) 229–234.
132. D. G. Wallace, J. W. Donovan, P. M. Schneider, A. M. Meunier, J. L. Lundblad, Biological activity and conformational stability of the domains of plasma fibronectin, *Archives of Biochemistry and Biophysics*, 212 (1981) 515–524.
133. G-Y. Tian, X-X. Sun-Shanghai, C-Y. Shen, The relationship of conformation, stability and biological activity of *Trichosanthin* in aqueous solution, *Acta Chimica Sinica*, 50 (1992) 914–917.
134. E. Arunan, G. R. Desiraju, R. A. Klein, J. Sadlej, S. Scheiner, I. Alkorta, D. C. Clary, R. H. Crabtree, J. J. Dannenberg, P. Hobza, H. G. Kjaergaard, A. C. Legon, B. Mennucci, D. J. Nesbitt, Definition of the hydrogen bond, *Pure and Applied Chemistry*, 83 (2011) 1619–1636.
135. S. Panda, Consequences of hydrogen bonding in biosphere, *Journal of Pharmacy and Pharmaceutical Sciences*, 3 (2014) 564–573.

136. G. A. Jeffrey. The role of the hydrogen bond and water in biological processes, *Journal of Molecular Structure*, 322 (1994) 21–25.
137. S. Scheiner, T. Kar, Y. Gu, Strength of the $C^{\alpha}H\cdots O$ hydrogen bond of amino acid residues, *Journal of Biological Chemistry*, 276 (2001) 9832–9837.
138. L. Mammino, M. M. Kabanda, A computational study of the effects of different solvents on the characteristics of the intramolecular hydrogen bond in acylphloroglucinols, *Journal of Physical Chemistry A*, 113 (2009) 15064−15077.
139. T. Loftsson, M. E. Brewster, Physicochemical properties of water and its effect on drug delivery A commentary, *International Journal of Pharmaceutics*, 345 (2008) 248–254.
140. H-G. Korth, M. I. de Heer, P. Mulder, A DFT study on intramolecular hydrogen bonding in 2-substituted phenols: conformations, enthalpies, and correlation with solute parameters, *Journal of Physical Chemistry A*,106 (2002) 8779–8789.
141. E. S. Meadows, S. L. De Wall, L. J. Barbour, F. R. Fronczek, M-S. Kim, G. W. Gokel Structural and dynamic evidence for C−H···O hydrogen bonding in lariat ethers: implications for protein structure, *Journal of the American Chemical Society*, 122 (2000) 3325–3335.
142. G. R. Desiraju, *Crystal engineering. The design of organic solids*, Elsevier, Amsterdam, 1989.
143. E. Fan, S. A. Van Arman, S. Kincaid, A. D. Hamilton, Molecular recognition: hydrogen-bonding receptors that function in highly competitive solvents, *Journal of the American Chemical Society*, 115 (1993) 369–370.
144. Y. Kwon, Theoretical study on salicylic acid and its analogues: intramolecular hydrogen bonding, *Journal of Molecular Structure* (*theochem*), 532 (2000) 227–237.
145. G. Buemi, F. Zuccarello, Is the intramolecular hydrogen bonding energy valuable from internal rotation barriers?, *Journal of Molecular Structure* (*theochem*), 581 (2002) 71–85.
146. C. Chen, S-F. Shyu, Conformers and intramolecular hydrogen bonding of the salicylic acid monomer and its anions, *Journal of Molecular Structure* (*theochem*), 536 (2001) 25–39.
147. R. Amorati, M. Lucarini, V. Mugnaini, G. F. Pedulli, Antioxidant activity of *o*-bisphenols: the role of intramolecular hydrogen bonding, *The Journal of Organic Chemistry*, 68 (2003) 5198–5204.
148. M. V. Bel'kov, G. A. Ksendzova, P. V. Kuzovkov, G. I. Polozov, I. V. Skornyakov, V. L. Sorokin, G. B. Tolstorozhev, O. I. Shadyro, Intramolecular hydrogen bonds and

antioxidant activity of aminophenols, *Journal of Applied Spectroscopy*, 74 (2007) 635–641.

149. W. M. Latimer, W. H. Rodebush, Polarity and ionisation from the standpoint of the Lewis theory of valence, *Journal of the American Chemical Society*, 42 (1920) 1419–1433.
150. T. Elsaesser, Two-dimensional infrared spectroscopy of intermolecular hydrogen bonds in the condensed phase, *Accounts of Chemical Research*, 42 (2009) 1220–1228.
151. V. V. Gromak, *Ab initio* study of intra- and intermolecular H-bond energies in p-conjugated molecular systems, *Journal of Molecular Structure* (*theochem*), 726 (2005) 213–224.
152. T. Steiner, The hydrogen bond in the solid state, *Angewandte Chemie International Edition*, 41 (2002) 48–76.
153. J. Poater, X. Fradera, M. Solà, M. Duran, S. Simon, On the electron-pair of the hydrogen bond in the framework of the atoms in molecules theory, *Chemical Physics Letters*, 369 (2003) 248–255.
154. G. A. Jeffrey, *An introduction to hydrogen bonding*, Oxford University Press, New York, 1997.
155. G. N. Fujii, T. E. Patwari, N. Mikami, Vibrational spectroscopic evidence of unconventional hydrogen bonds, *International Journal of Mass Spectrometry*, 220 (2002) 289–312.
156. E. Cubero, M. Orozco, F. J. Luque, Electron density topological analysis of the C-H·····O anti-hydrogen bond in the fluoro–oxirane complex, *Chemical Physics Letters*, 310 (1999) 445–450.
157. M. C. Wahl, M. Sundaralingam, C–H···O hydrogen bonding in biology, *Trends Biochemical Science*, 22 (1997) 97–102.
158. G. Muller, M. Lutz, S. Harder, Methyl group conformation-determining intermolecular C-H···O hydrogen bonds: structure of *N*-methyl-2-pyrrolidone, *Acta Crystallographica Section B*, 52 (1996) 1014–1022.
159. M. M. Nolasco, P. J. A. Ribeiro-Claro, C–H···O hydrogen bonds in cyclohexenone reveal the spectroscopic behavior of $C_{sp}{}^3$–H and $C_{sp}{}^2$–H donors, *Chemical Physical Chemistry*, 6 (2005) 496–502.
160. G. R. Desiraju, The C-H···O hydrogen bond in crystals: what is it?, *Accounts of Chemical Research*, 24 (1991) 290–296.

161. R. K. Vasu, A. Saithalavi, S. Eringathodi, K. Nobuaki, S. C. Hariharan, Molecular recognition in an organic host–guest complex: CH···O and CH···π interactions completely control the crystal packing and the host–guest complexation, *Bulletin of the Chemical Society of Japan*, 80 (2007) 484–490.
162. F. C. Pigge, F. Ghasedi, Z. Zheng, N. P. Rath, G. Nichols, J. S. Chickos, Structural characterization of crystalline inclusion complexes formed from 1,3,5-triaroylbenzene derivatives–a new family of inclusion hosts, *Journal of the Chemical Society Perkin Transactions*, 2 (2000) 2458–2464.
163. G. R. Desiraju, T. Steiner, *The weak hydrogen bond in structural chemistry and biology*, Oxford University Press, New York, 1999.
164. S. Horowitz, R. C. Trievel, Carbon-oxygen hydrogen bonding in biological structure and function, *Journal of Biological Chemistry*, 287 (2012) 41576–41582.
165. J. Kříž, J. Dybal, J. Brus, Cooperative hydrogen bonds of macromolecules. 2. Two-dimensional cooperativity in the binding of poly(4-vinylpyridine) to poly(4-vinylphenol), *Journal of Physical Chemistry B*, 110 (2006) 18338−18346.
166. K. I. Ramachandran, D. Gopakumar, K. Namboori, *Computational chemistry and molecular modelling: principle and applications*, 1st edition, Springer Berlin Heidelberg, 2008.
167. A. E. Reed, F. Weinhold, R. Weiss, J. Macheleid, Nature of the contact ion pair $CCI_3^+Cl^-$. A theoretical study, *Journal of Physical Chemistry*, 89 (1985) 2688–2694.
168. A. V. Marenich, S. V. Jerome, C. J. Cramer, D. G. Truhlar, Charge model 5: an extension of Hirschfield population analysis for the accurate description of molecular interactions in gaseous and condensed phases, *Journal of Chemical Theory and Computation*, 8 (2012) 527−541.
169. S. Kristyan, Rapid estimation of basis set error and correlation energy based on Mulliken charges and Mulliken matrix with the small 6-31G* basis set, *Theoretical Chemistry Accounts*, 115 (2006) 298–307.
170. T. Lu, F. Chen, Multiwfn: a multifunctional wavefunction analyser, *Journal of Computational Chemistry*, 33 (2012) 580–592.
171. R. Carbo-Dorca, Quantum mechanical basis for Mulliken population analysis, *Journal of Mathematical Chemistry*, 36 (2004) 231−239.
172. J. A. Pople, D. L. Beveridge, *Approximate Molecular Orbital* Theory, Mc Graw Hill, New York 1970.

173. G. Bruhn, E. R. Davidson, I. Mayer, A. E. Clark, Löwdin population analysis with and without rotational invariance, *International Journal of Quantum Chemistry*, 106 (2006) 2065–2072.
174. A. E. Clark, J. Sonnenberg, P. J. Hay, R. L. Martin, Density and wave function analysis of actinide complexes: what can fuzzy atom, atoms in molecules, Mulliken, Löwdin, and natural population can tell us?, *Journal of Physical Chemistry*, 121 (2004) 2563−2570.
175. J. P. Foster, A. E. Reed, J. E. Carpenter, F. Weinhold, Natural hybrid orbitals, *Journal of America Chemical Society*, 102 (1980) 7211−7218.
176. A. E. Reed, L. A. Curtiss, F. Weinhold, Intermolecular interactions from a natural bond orbital, donor-acceptor viewpoint, *Chemical* Reviews, 88 (1988) 899–926.
177. A. E. Reed, R. B. Weinstock, F. Weinhold, Natural population analysis, *Journal of Chemical Physics*, 83 (1985) 735–746.
178. I. S. Bushmarinov, K. A. Lyssenke, M. Y. Antipin, Atomic energy in the "atoms in molecules" theory and its uses for solving chemical problems, *Russian Chemical Reviews*, 78 (2009) 283−302.
179. R. F. W. Bader, *Atoms in molecules: a quantum theory*, Oxford University Press, New York, 1990.
180. J. R. Lane, J. Contreras-García, J-P. Piquemal, B. J. Miller, H. G. Kjaergaard, Are bond critical points really critical for hydrogen bonding?, *Journal of Chemical Theory and Computation*, 9 (2013) 3263−3266.
181. E. L. Smith, D. Sadowsky, J. A. Phillips, C. J. Cramer, D. J. Giesen, A short yet very weak dative bond: structure, bonding, and energetic properties of N_2-BH_3, *Journal of Physical Chemistry A*, 114 (2010) 2628–2636.
182. N. V. Alekseev, S. P. Knyazev, I. A. Chernyshev, Ge–N bonds in germatranes. Topological analysis, *Journal of Structural Chemistry*, 46 (2005) 387−392.
183. S. Dinda, A. G. Samuelson, The nature of bond critical points in dinuclear copper(I) complexes, *Chemistry - A European Journal*, 18 (2012) 3032−3042.
184. G. Frenking, M. Solà, S. F. Vyboishchikov, Chemical bonding in transition metal carbene complexes, *Journal of Organometallic Chemistry*, 690 (2005) 6178–6204.
185. A. Otero-de-la-Roza, M. A. Blanco, A. M. Pendás, V. Luaña, Critic: a new program for the topological analysis of solid-state electron densities, *Computer Physics Communications*, 180 (2009) 157–166.
186. P. Papelier, *Atoms in molecule: an introduction*, Prentice Hall, United Kingdom, 2000.

187. J. Poater, M. Duran, M. Solà, B. Silvi, Theoretical evaluation of electron delocalization in aromatic molecules by means of atoms in molecules (aim) and electron localization function (ELF) topological approaches, *Chemical Reviews*, 105 (2005) 3911−3947.
188. E. Espinosa, E. Molins, C. Lecomte, Hydrogen bond strengths revealed by topological analyses of experimentally observed electron densities, *Chemical Physics Letters*, 285 (1998) 170−173.
189. C. F. Matta R. J. Boyd, *The quantum theory of atoms in molecules*, Wiley-VCH Verlag GMBH & Co, Darmstadt, 2007.
190. L. Feng, F-Q. Bai, Y. Wu, H-X. Zhang, Dihydrogen bond in $C_2H_{4-n}Cl_n\cdots NaH$ (n=0, 1, 2, 3) complexes, *ab initio*, AIM and NBO studies, *Molecular Physics*, 109 (2011) 645–653.
191. P. R. Varadwj, A. Varadwj, H. M. Marques, DFT-B3LYP, NOPA-, and QTAIM-based study of the physical properties of [M(II) $(H_2O_2)_2$ (15-crow-5)] (M= Mn, Fe, Co, Ni, Cu, Zn) complexes, *Journal of Physical Chemistry*, 115 (2011) 5592−5601.
192. D. Cremer, E. Kraka, Chemical bonds without bonding electron density-does the difference electron-density analysis suffice for a description of the chemical bond?, *Angewandte Chemie International Edition*, 23 (1984) 627–628.
193. U. Gogoi, A. K. Guha, A. K. Phukan, Nature of intramolecular metal−metal interactions in supported group 4−group 9 and group 6−Ggroup 9 heterobimetallic complexes: a combined density functional theory and topological study, *Organometallics*. 30 (2011) 5991–6002.
194. G. Gervasio, R. Bianchi, D. Marabello, About the topological classification of the metal–metal bond, *Chemical Physics Letters*, 387 (2004) 481–484.
195. R. F. W. Bader, C. F. Matta, Bonding to titanium, *Inorganic Chemistry*, 40 (2001) 5603–5611.
196. V. Lobo, A. Patil, A. Phatak, N. Chandra, Free radicals, antioxidants and functional foods: Impact on human health, *Pharmacognosy Reviews*,4 (2010) 118–126.
197. F. Rautenbach, M. Faber, S. Laurie, R. Laurie, Antioxidant capacity and antioxidant content in roots of 4 sweetpotato varieties, *Journal of Food Science*, 75 (2010) C400–C405.
198. A. Srivastava, S. R. Harish, T. Shivanandappa Antioxidant activity of the roots of *Decalepis hamiltonii* (Wight & Arn.), *LWT- Food Science and Technology*, 39 (2006) 1059–1065.

199. A. Matkowski, S. Zielińska, J. Oszmiański, E. Lamer-Zarawska, Antioxidant activity of extracts from leaves and roots of *Salvia miltiorrhiza* Bunge, *S. przewalskii* Maxim., and *S. verticillata* L, *Bioresource Technology*, 99 (2008) 7892–7896.
200. Y. S. Kwon, C. M. Kim, Antioxidant constituents from the stem of Sorghum bicolor, *Archives of Pharmaceutical Research*, 26 (2003) 535−539.
201. M. J. Jung, H. Y. Chung, S. S. Kang, J. H. Choi, K. S. Bae, J. S. Choi. Antioxidant activity from the stem bark of Albizzia julibrissin, *Archives of Pharmaceutical Research*, 26 (2003) 458−462.
202. H. A. Jung, M. J. Jung, J. Y. Kim, H. Y. Chung, J. S. Choi, Inhibitory activity of flavonoids from Prunus davidiana and other flavonoids on total ROS and hydroxyl radical generation, *Archives of Pharmaceutical Research*, 26 (2003) 809−815.
203. B. Tepe, Antioxidant potentials and rosmarinic acid levels of the methanolic extracts of Salvia virgata (Jacq), Salvia staminea (Montbret & Aucher ex Bentham) and Salvia verbenaca (L.) from Turkey, *Bioresource Technology*, 99 (2008) 1584–1588.
204. Y. Zhang, X. Li, Z. Wang, Antioxidant activities of leaf extract of Salvia miltiorrhiza Bunge and related phenolic constituents, *Food and Chemical Toxicology*, 48 (2010) 2656–2662.
205. E. W. C. Chan, Y. Y. Lim, M. Omar. Antioxidant and antibacterial activity of leaves of *Etlingera*species (Zingiberaceae) in Peninsular Malaysia, *Food Chemistry*, 104 (2007) 1586–1593.
206. A. A. Hamid, O. O. Aiyelaagbe, L. A. Usman, O. M. Ameen, A. Lawal, Antioxidants: its medicinal and pharmacological applications, *African Journal of Pure and Applied Chemistry*, 4 (2010) 142−151.
207. S. J. S. Flora, M. Mittal, A. Mehta, Heavy metal induced oxidative stress & its possible reversal by chelation therapy, *Indian Journal of Medical Research*, 128 (2008) 501−523.
208. S. J. S. Flora, V. Pachauri, Chelation in metal intoxication, *International Journal of Environmental Research and Public Health*, 7 (2010) 2745−2788.
209. C. Fraga, B. Leibovitz, A. Tappel, Lipid peroxidation measured as thiobarbituric acid-reactive substances in tissue slices: characterization and comparison with homogenates and microsomes, *Free Radicals in Biology and Medicine*, 4 (1988) 155−161.
210. B. Zhao, Q. Guo, W. Xin, Free radical scavenging by green tea polyphenols, *Methods in Enzymology*, 335 (2001) 217–231.

211. M. Leopoldini, I. P. Pitarch, N. Russo, M. Toscano, Structure, conformation and electronic properties of apigenin, luteolin and taxifolin antioxidants. A first principle theoretical study, *Journal of Physical Chemistry A*, 108 (2004) 92–96.
212. M. Leopoldini, T. Marino, N. Russo, M. Toscano, Antioxidant properties of phenolic compounds. H-atom versus electron transfer mechanism, *Journal of Physical Chemistry A*, 108 (2004) 4916–4922.
213. M. Leopoldini, T. Marino, N. Russo, M. Toscano, Density functional computations of the energetic and spectroscopic parameters of quercetin and its radicals in the gas phase and in solvent, *Theoretical Chemistry Account*, 111 (2004) 210–216.
214. K. Sadasivam, R. Kumaresan, A comparative DFT study on the antioxidant activity of apigenin and scutellarein flavonoid compounds, *Molecular Physics*, 109 (2011) 839–852.
215. E. Klein, V. Lukeš, DFT/B3LYP study of the substituent effect on the reaction enthalpies of the individual steps of sequential proton loss electron transfer mechanism of phenols antioxidant action: correlation with phenolic C–O bond length, *Journal of Molecular Structure* (*theochem*), 805 (2007) 153–160.
216. M. Musialik, G. Litwinienko, Scavenging of dpph• radicals by vitamin E is accelerated by its partial ionization: the role of sequential proton loss electron transfer, *Organic Letters*, 7 (2005) 4951−4954.
217. D. Huang, B. Ou, R. L. Prior, The chemistry behind antioxidant capacity assays, *Journal of Agricultural and Food Chemistry*, 53 (2005) 1841−1856.
218. R. L. Prior, X. Wu, K. Schaich, Standardized methods for the determination of antioxidant capacity and phenolics in foods and dietary supplements, *Journal of Agricultural Food Chemistry*, 53 (2005) 4290–4302.
219. K. S. Kumar, R. Kumaresan, Theoretical investigation of the conformational, electronic and antioxidant properties of azaleatin, isorhamnetin and quercetagetin, *Molecular Simulation*, 39 (2013) 72–83.
220. M. Dianzani, G. Barrera, Pathology and physiology of lipid peroxidation and its carbonyl products, *Free Radical Pathophysiology*, 38 (2008) 19−38.
221. A. Navarro, A. Boveris, M. J. Bández, M. J. Sánchez-Pino, C. Gómez, G. Muntane, I. Ferrer, Human brain cortex: mitochondrial oxidative damage and adaptive response in Parkinson's disease and in dementia with Lewy bodies, *Free Radicals in Biology and Medicine*, 46 (2009) 1574–1580.

222. M. Guo, C. Perez, Y. Wei, E. Rapoza, G. Su, F. Bou-Abdallah, N. D. Chasteen, Iron-binding properties of plant phenolics and cranberry's bio-effects, *Dalton Transactions*, (2007) 4951–4961.
223. J. P. Kehrer, The Haber–Weiss reaction and mechanisms of toxicity, *Toxicology*, 149 (2000) 43–50.
224. D. L. Gilbert, C. A. Colton, *Reactive oxygen species in biological systems*, 1st edition, Plenum Publishers, New York, 1999.
225. S. I. Liochev, The mechanism of 'Fenton-like' reactions and their importance for biological systems. A biologist's view, *Metal Ions in Biological Systems*, 36 (1999) 1–39.
226. G. Alagona, C. Ghio, Antioxidant properties of pterocarpans through their copper(II) coordination ability. A DFT study *in vacuo* and in aqueous solution, *Journal of Physical Chemistry A*, 113 (2009) 15206–15216.
227. M. M. Kabanda, Antioxidant activity of rooperol investigated through Cu (I and II) chelation ability and the hydrogen transfer mechanism: a DFT study, *Chemical research in toxicology*, 25 (2012) 2153–2166.
228. M. R. Loizzo, R. Tundis, M. Bonesi, F. Menichini, V. Mastellone, L. Avallone, F. Menichini, Radical scavenging, antioxidant and metal chelating activities of Annona cherimola Mill. (cherimoya) peel and pulp in relation to their total phenolic and total flavonoid contents, *Journal of Food Composition and Analysis*, 25 (2012) 179–184.
229. L. Mammino, Investigation of the antioxidant properties of hyperjovinol A through its Cu(II) coordination ability, *Journal of Molecular Modeling*, 19 (2013) 2127−2142.
230. T. J. Tsiepe, M. M. Kabanda, K. R. N. Serobatse, Antioxidant properties of kanakugiol revealed through the hydrogen atom transfer, electron transfer and M^{2+} (M^{2+} = Cu(II) or Co(II) Ion) coordination ability mechanisms. A DFT study *in vacuo* and in solution, *Food* Biophysics, 10 (2015) 342–359.
231. N. J. Mills, ChemDraw Ultra 10.0; CambridgeSoft: Cambridge, MA; www.cambridgesoft.com, *American Chemical Society*, 128 (2006) 13649−13650.
232. J. Gräfenstein, D. Cremer, Can density functional theory describe multi-reference systems? Investigation of carbenes and organic biradicals, *Physical Chemistry Chemical Physics*, 2 (2000) 2091−2103.
233. S. Ketrat, S. Müller, M. Dolg, A quantum chemical study of the haptotropic rearrangements of $Cr(co)_3$ on naphthalene and phenanthrene systems, *Journal of Physical Chemistry A*, 111 (2007) 6094–6102.

234. H. Hirao, Which DFT Functional performs well in the calculation of methylcobalamin? comparison of the B3LYP and BP86 functionals and evaluation of the impact of empirical dispersion correction, *Journal of Physical Chemistry A*, 115 (2011) 9308–9313.
235. S. F. Vyboishchikov, M. Bühl, W. Thiel, Mechanism of olefin methathesis with catalysis by ruthenium carbene complexes: density functional studies on model systems, *Chemistry European Journal*, 8 (2002) 3962–3967.
236. M. J. Frisch, G. W. Trucks, H. B. Schlegel, G. E. Scuseria, M. A. Robb, J. R. Cheeseman, G. Scalmani, V. Barone, B. Mennucci, G. A. Petersson, H. Nakatsuji, M. Caricato, X. Li, H. P. Hratchian, A. F. Izmaylov, J. Bloino, G. Zheng, J. L. Sonnenberg, M. Hada, M. Ehara, K. Toyota, R. Fukuda, J. Hasegawa, M. Ishida, T. Nakajima, Y. Honda, O. Kitao, H. Nakai, T. Vreven, J. A. Montgomery Jr., J. E. Peralta, F. Ogliaro, M. Bearpark, J. J. Heyd, E. Brothers, K. N. Kudin, V. N. Staroverov, R. Kobayashi, J. Normand, K. Raghavachari, A. Rendell, J. C. Burant, S. S. Iyengar, J. Tomasi, M. Cossi, N. Rega, J. M. Millam, M. Klene, J. E. Knox, J. B. Cross, V. Bakken, C. Adamo, J. Jaramillo, R. Gomperts, R. E. Stratmann, O. Yazyev, A. J. Austin, R. Cammi, C. Pomelli, J. W. Ochterski, R. L. Martin, K. Morokuma, V. G. Zakrzewski, G. A. Voth, P. Salvador, J. J. Dannenberg, S. Dapprich, A. D. Daniels, O. Farkas, J. B. Foresman, J. V. Ortiz, J. Cioslowski, D. J. Fox, Gaussian 09, Revision C.01 Gaussian, Inc, Wallingford CT, 2009.
237. P. D. Luna, E. A. C. Bushnell, J. W. Gauld, A density functional theory investigation into the binding of the antioxidants ergothioneine and ovothiol to copper, *Journal of Physical Chemistry A*, 117 (2013) 4057−4065.
238. G. Alagona, C. Ghio, Plicatin B conformational landscape and affinity to copper (I and II) metal cations. A DFT study, *Physical Chemistry Chemical Physics*, 11 (2009) 776–790.
239. T. A. Keith, AIMAll (Version 14.06.21), TK Gristmill Software, Overland Park KS, USA, 2014.
240. R. P. Hanzlik, *Inorganic aspects of biological and organic chemistry*, Academic Press, INC, New York, 1976.
241. M. E. Bodini, G. Copia, R. Tapia, F. Leighton, L. Herrera, Iron complexes of quercetin in aprotic medium. Redox chemistry and interaction with superoxide anion radical, *Polyhedron*, 18 (1999) 2233–2239.
242. S. Alcaro, S. G. Chiodo, M. Leopoldini, F. Ortuso, Antioxidant efficiency of oxovitisin, a new class of red wine pyranoanthocyanins, revealed through quantum mechanical investigations, *Journal of* Chemical Information *and Modeling*, 53 (2013) 66–75.

243. A. B. E. S. Van Acker, M. J. de Groot, D-J. Van den Berg, M. N. J. L. Tromp, G-O. den Kelder, W. J. F. van der Vijgh, A. Bast, A quantum chemical explanation of the antioxidant activity of flavonoids, Chemical Research Toxicology, 9 (1996) 1305–1312.
244. L. Wa Chung, X. Li, K. Morokuma, Modeling enzymatic reactions in metalloenzymes and photobiology by quantum mechanics (QM) and quantum mechanics/molecular mechanics (QM/MM) calculations in C. F. Matta (Ed.), *Quantum Biochemistry*, Wiley-VCH publishers, Weinheim, German, 2010.
245. A. Bauzá, I. Alkorta, A. Frontera, J. Elguero, On the reliability of pure and hybrid DFT methods for the evaluation of halogen, chalcogen, and pnicogen bonds involving anionic and neutral electron donors, *Journal of Chemical Theory and Computation*, 9 (2013) 5201−5210.
246. P. R. Varadwaj, A. Varadwaj, H. M.Marques, DFT-B3LYP, NPA-, and QTAIM-based study of the physical properties of [M(II)(H_2O)$_2$(15-crown-5)] (M = Mn, Fe, Co, Ni, Cu, Zn) complexes. *Journal of Physical Chemistry A* 115 (2011) 5592–5601.
247. M. D. Engelmann, R. Hutcheson, I.F. Cheng, Stability of ferric complexes with 3-hydroxyflavone (flavonol), 5,7-dihydroxyflavone (chrysin), and 3′,4′-dihydroxyflavone, *Journal of Agricultural Food Chemistry*, 53 (2005) 2953–2960.
248. K. R. N. Serobatse, M. M. Kabanda, Antioxidant and antimalarial properties of butein and homobutein based on their ability to chelate iron (II and III) cations: a DFT study *in vacuo* and in solution, *European Food Research*, 242 (2016) 71–90.
249. A. T. Iffat, Z. T. Maqsoos, N. Fatima, Study of complex formation of Fe(III) with tannic acid, *Journal of the Chemical Society of Pakistan*, 27 (2005) 174–177.
250. R. G. Pearson, Hard and soft acid and basis, *Journal of American Chemical Society*, 85 (1964) 3533–3539.
251. I. F. F. Benzie, J. J. Strain, The ferric reducing ability of plasma as a measure of ‘antioxidant power’: the FRAP assay. *Anal Biochemistry*, 239 (1996) 70–76.